RISER GAS BEHAVIOR IN DEEPWATER WELLS – AN EXPERIMENTAL STUDY OF TAYLOR BUBBLE RISING IN A STAGNANT COLUMN OF LIQUID WITH DRILLING MUD PROPERTIES

by

Veerabhadra Sasikanth Denduluri

A thesis/dissertation submitted to the Department of
Petroleum Engineering,

Cullen College of Engineering

in partial fulfillment of the requirements for the degree of

Mater of Science in Petroleum Engineering

Chair of Committee: Dr. George K. Wong

Committee member: Dr. Mohamed Soliman

Committee member: Dr. Konstantinos Kostarelos

UNIVERSITY OF HOUSTON

ACKNOWLEDGMENTS

Firstly, I would like to express my sincere appreciation and gratitude to my supervisor, Professor George K. Wong, for his invaluable help, support and advice throughout the work.

I would also like to thank Carlos Ortiz for his guidance and help in the laboratory.

I am very thankful to National Academies Gulf Research Program for supporting the research work.

ABSTRACT

The severe effects of the free-bubble gas formation in deep water drilling riser is a major concern for offshore Oil and Gas industry. Understanding the comprehensive assessment of risks and consequences of the hydrocarbons entering the drilling riser is very important to control and prevent future well related accidents.

This study designed and conducted a series of experiments with air slug or Taylor bubble rising in a vertical tube and in a stagnant column of different liquids open to atmospheric pressure. The objective was to (a) gain insights on the mechanisms of gas slug rising and expanding near the top of the drilling riser, (b) develop a method to calculate slug rising velocity and slug length as a function of positions using pressure data, and (c) provide experimental data to help calibrate computational models with liquid properties similar to drilling muds.

The bubble rising test apparatus consists of 3 acrylic tubes for a total of 18 ft of height and 6.5 inches of internal diameter. We generated a Taylor bubble by pressurizing a fixed volume of air trapped in the lower 6 ft section of the apparatus. This bubble is then introduced into the bottom of the upper 12 ft section of the column by opening and closing a ball-valve. We record, track, and calculate the bubble rising velocity and bubble length using twelve pressure transducers and cameras placed 1 ft apart and two movable cameras traveling along the height of the riser. We completed tests with Taylor air bubble in three different fluids: (a) water, (b) viscous shear-thinning gel made with 0.75% (by weight) concentration of Xanthan Gum, and (c) slurry of ceramic proppant with Xanthan Gum gel.

We selected Xanthan Gum gel and the proppant slurry to emulate the shear thinning fluid properties and effects of solids in drilling mud, respectively.

Experimental results showed, as the bubble rises in the riser tube, the bubble expands due to the gradually decreasing hydrostatic pressure in the column. Air bubble-water tests showed the bubble rising velocity and length expansion were comparable to open literature data. Values interpreted from video cameras and pressure data, measured along the height of the riser tube, were consistent and complementary. Based on air bubble-water results, we established and verified a method to calculate bubble rising velocity and bubble expansion using only pressure data and without video camera data. Air bubble-viscous gel tests calculated slower bubble rising velocity and longer bubble length because of the higher gel viscosity and the thicker liquid film, respectively. Air bubble-slurry tests calculated slower bubble rising velocity and similar bubble length to that of air bubble-water case. We did not find data of Taylor bubble in slurry fluids in the literature for comparison. Results from this experimental program provided new insights on the mechanisms of slug or Taylor bubble movement in drilling riser with comparable drilling mud rheology.

TABLE OF CONTENTS

LIST OF TABLES

LIST OF FIGURES

1. Introduction

1.1 Background

The drilling crew in an oil and gas organization faces many operational problems such as lost circulation, stuck drill pipe and most importantly well control. The well control problem occurs when the pressure within the drilled rock is greater than the mud hydrostatic pressure. This induces a kick or a flow of hydrocarbon fluids into the wellbore. The scale of the kick depends on the magnitude of the differential pressure or the influx hydrocarbon volume and other factors such as rock's permeability and porosity. For a given differential pressure, a rock with higher permeability and porosity has a greater potential for larger influx volume or more severe kick than a rock with lower permeability and porosity.

When gas enters the borehole, the kick is called a gas kick. If this flow has been controlled, the kick has been killed. If not controlled or killed, the hydrocarbon moves to the surface because of the lighter hydrocarbon's density than the drilling mud. The hydrocarbon can also be displaced to the surface from the mud circulation operations. As the hydrocarbon moves up to the surface, the gas kick volume increases with decreasing pressure and increasing gas dissolution. This leads to the creation of increasing larger and faster moving gas bubble near the surface. Possible kick indicators observed at the surface include mud pit volume increase, flow rate increase, pump stroke increase, and pump pressure decrease (Neal Adams and Larry Kuhlman, 1994).

The dynamic effects of traveling free bubble from a kick are more challenging for deepwater wells. They are drilled using drilling risers. A drilling riser is a pipe that connects and extends between the subsea blowout preventer (BOP) and the drilling rig. The riser contains the drill string and isolates the drilling mud from the surrounding sea. In deepwater fields, water depths between 1500 ft and 5000 ft are not uncommon. A typical riser has an outside and inside diameter of 21 in and 19 in, respectively (Yong Bai and Qiang Bai, 2019). The combination of long and large riser dimensions results in a large drilling mud volume and makes kicks detection more difficult. When the presence of gas kick in the riser is not controlled, hydrocarbons will be discharged from top of the riser very rapidly and an extremely powerful gas blowout event can take place (Zhou and Prosperetti, 2019). If these hydrocarbons, which are flammable, spill into an environment that contains ignition sources, then a destructive explosion would follow. Such a sequence of events is considered to have been the cause of the disastrous Deepwater Horizon accident in the Gulf of Mexico in 2010 (Investigation Report 2010-10-I-OS, U.S. Chemical Safety and Hazard Investigation Board, 2016). Similarly, there are few limitations in the ability of existing well control models to represent specific conditions in the upper portion of the drilling riser. Although newer risers are designed with gas handling equipment installed at the top of the riser, operations can only improve if more is known about the behavior of gas entering the drilling muds and what happens when gas reaches the top of the riser. Hence further understanding of development and movement of large gas bubble in drilling mud and riser is essential for economical, technical, safety and environmental benefits.

1.2 Multiphase Flow

Multiphase flow addresses two or more immiscible fluids flowing simultaneously through a medium. A gas kick involves gas traveling in a liquid medium in a drill string or drilling riser. This section briefly reviews the different multiphase flow regimes in a vertical riser.

Once the free gas is in the drilling riser, Figure 1 depicts the different flow regimes (Ambrose, 2015 and Wallis, 1969) that gas can flow in liquid and travel up the riser. There are several ways in which gas and liquid phases can interact in a vertical pipe as the gas rate increases at a given liquid rate.

1. Bubbly flow – This flow occurs when the gas rate is relatively small compared to the liquid rate. There are few and small bubbles in the liquid medium. The number of gas bubbles increases with the gas rate.

2. Slug flow – As the gas rate increases a slug flow develops. This has large "bullet shaped" gas bubbles or slugs which are also known as 'Taylor bubbles.' These large bubbles have a liquid film around them as they flow through the liquid.

3. Churn flow – When gas rate increases above the slug flow slugs become unstable. The flow has more turbulences and slugs begin to break apart.

4. Annular flow – As the gas rate increases beyond the churn flow, the annular flow is formed. This consists of high gas flowing in the middle of the pipe with liquid moving around the surface of the pipe or in the annulus region.

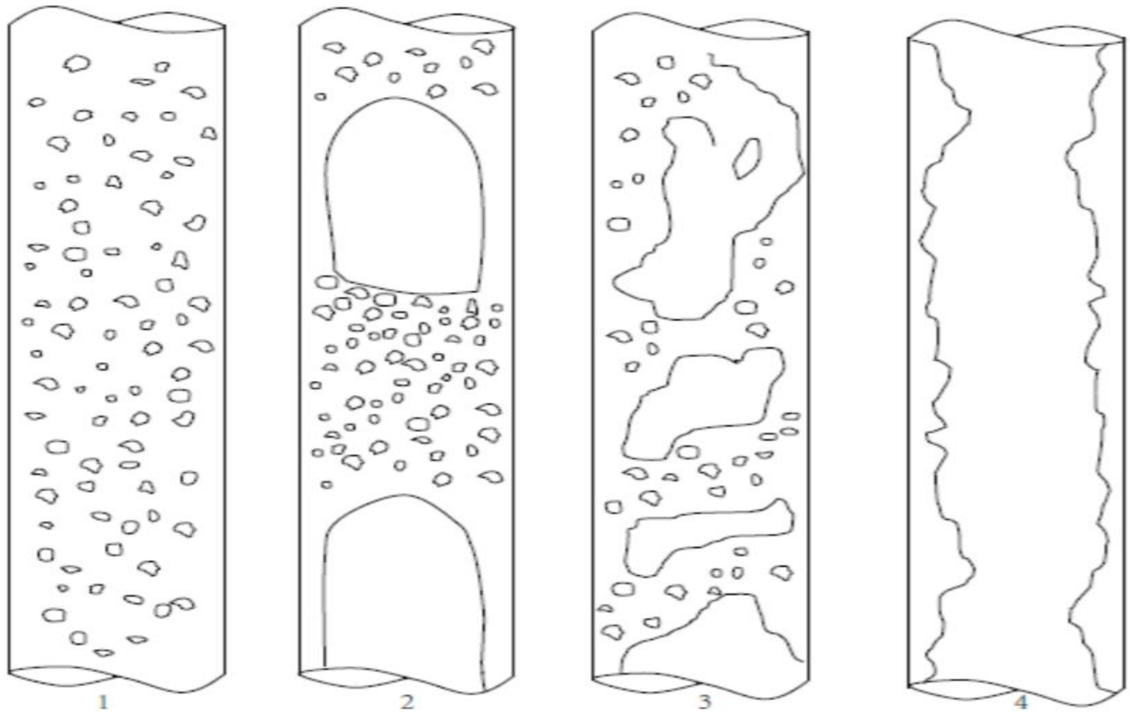

Figure 1: Different flow regimes in gas/liquid vertical upward flow by Yeoh and Tu, 2010 (1 - Bubble, 2 - Slug, 3 - Churn, 4- Annular)

In this thesis, the flow of Taylor bubbles, a characteristic part of slug flow regime, in a vertical pipe was studied. Slug flow is encountered both in research and industry, mainly in production and transportation of hydrocarbons in the oil and gas industry (Sousa, Pinto, and Campos, 2006). Chapter 2.1 briefly reviews theory and experimental data of slug flow in the literature.

1.3 Research Scope and Objectives

The objective is to gain insights on the mechanisms of gas slug rising and expanding near the top of the drilling riser and provide experimental data to help calibrate computational models with liquid properties similar to drilling muds. Also, develop a methodology to calculate bubble rising velocity and bubble length based on pressure.

We performed the experiments on a vertical tube apparatus representing a drilling riser. The tube has a total height of 18 ft and an inside diameter of 6.5 in. We used three liquid media: water, viscous gel made with 0.75 % Xanthan Gum, and solids slurry composed of ceramic proppant mixed with the Xanthan Gum's viscous gel. The ceramic proppant was 16-20 U.S. Mesh Carbolite with a median diameter of 1000 microns (Carbo Ceramics Inc, Carbolite Technical Specification Sheet, 2014) and the slurry density was 1.23 g/ml. Xanthan Gum and slurry were used to imitate the shear thinning rheology and weighting solids in the drilling mud. The slug was made of air.

The slug was created by pressuring a volume of air trapped in the lower 6 ft section of the apparatus. By opening and closing a ball-valve, this bubble was introduced into the bottom of the upper 12 ft section of the column. Twelve pressure transducers and twelve video cameras were placed 1 ft apart along the drilling riser and two movable cameras were placed beside the apparatus to track and record the bubble rising in the riser.

Figure 2 shows a slug from the water - air slug tests. The bubble has a nose region followed by a transition region ending with a tail. Figures 3 and 4 show pictures of air slug in viscous gel and slurry, respectively. For both of these cases the slug was not discernible from the video cameras.

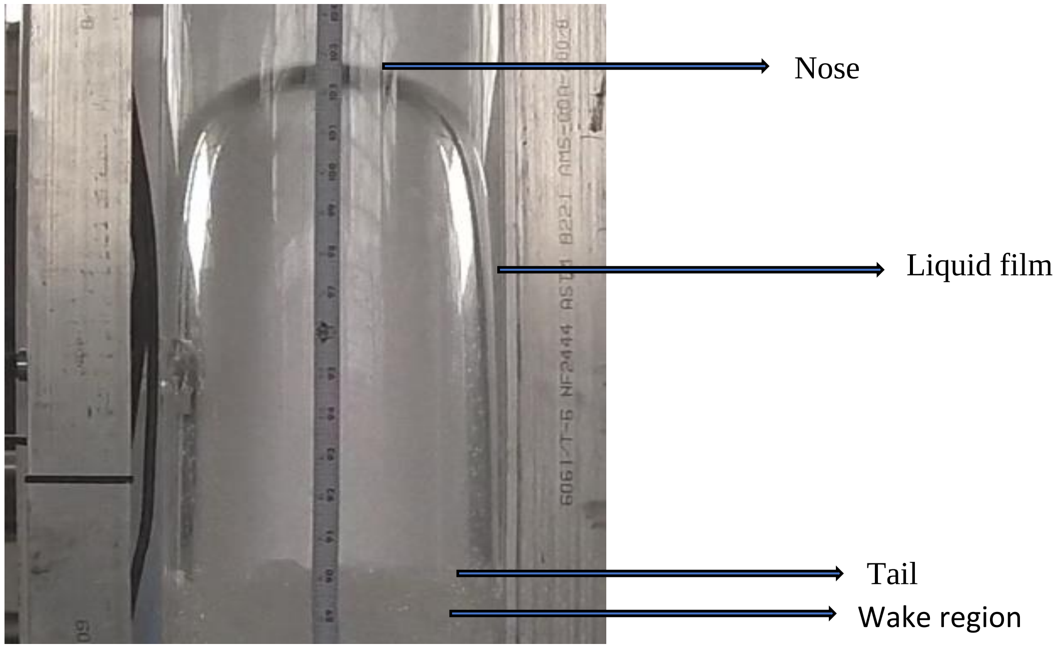

Figure 2 – Taylor bubble in water

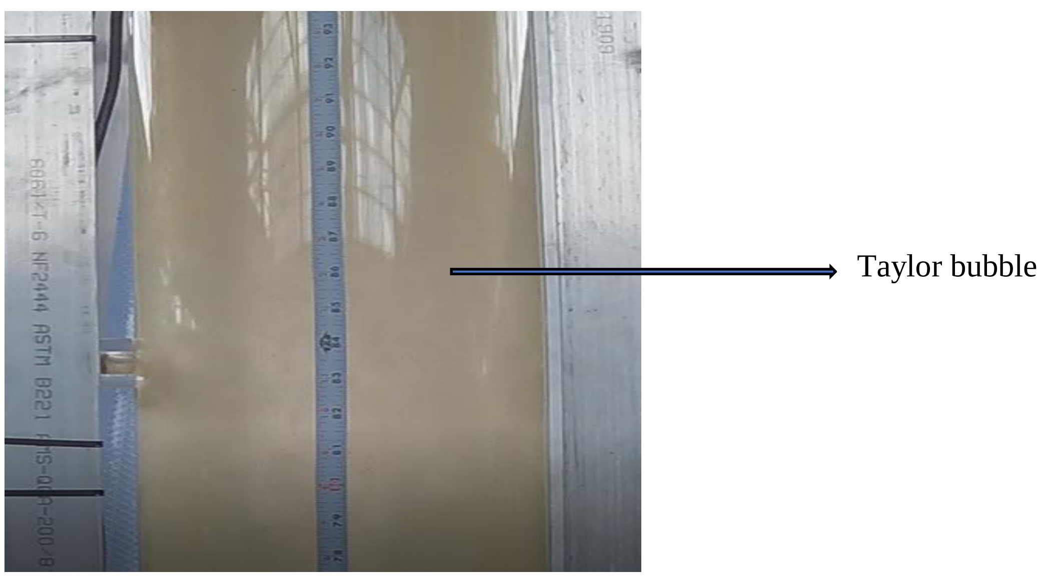

Figure 3 – Taylor bubble in viscous gel

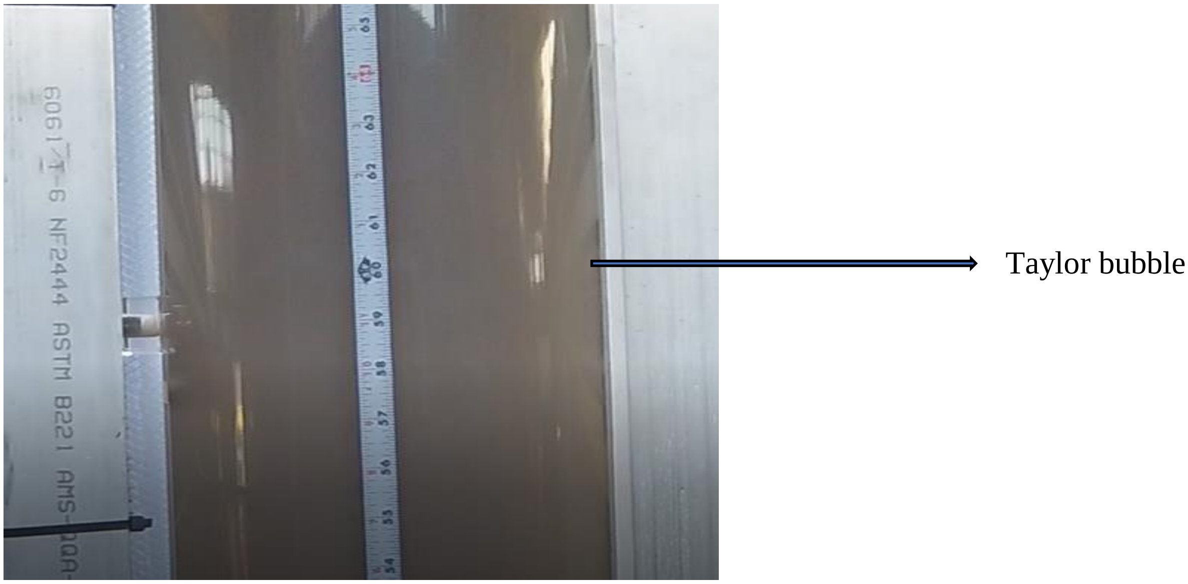

Figure 4 – Taylor bubble in slurry made of ceramic proppant

The liquid film thickness around the bubble was calculated using a standard correlation (Brown, 1965). The bubble rising velocity that will be discussed throughout this work is translational bubble rising velocity, which is calculated with the top of the column open to atmosphere.

1.4 Thesis Outline

Chapter 1 introduces the thesis work by presenting background of the topic, the motivation behind the study and summarizing the main results.

Chapter 2 reviews literature of Slug flow, Taylor bubble rise velocity in Newtonian and Non- Newtonian fluids.

Chapter 3 presents the experimental design and instrumentation used throughout the work.

Chapter 4 discusses experiment results performed using water – air slug.

Chapter 5 deals with experiments of viscous gel – air slug their results.

Chapter 6 presents experiments and results for slurry – air slug.

Chapter 7 and Chapter 8 outline conclusions and recommendations respectively.

The list of references used for this thesis work and Appendix are shown at the end.

2 Literature Review

This chapter reviews and summarizes the mechanisms and theories behind the rise of single Taylor bubble in a vertical stagnant column of liquid.

2.1 Slug Flow

Slug flow is a two-phase flow regime with long, bullet shaped bubbles known as gas slugs or Taylor bubbles **(**Ghobadi and Muzychka, 2015). Each slug almost fills the tube cross-section and has a falling film between the pipe's wall and the bubble. The slug has a rounded nose and wake region behind an irregular tail. With increase liquid viscosity, the wake region tends to decrease. Figure 5 depicts the representation of a Taylor bubble in a vertical pipe. The slug flow pattern can be found in oil and gas producing wells. For a gas kick in drilling riser, the rise of a gas slug in the riser is a slug flow.

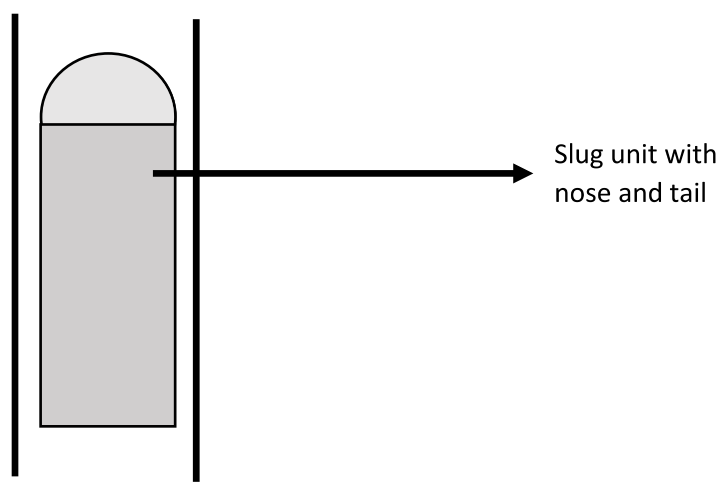

Figure 5 – Representation of gas slug in a vertical column

The pressure drop of a Taylor bubble rising can be divided into three parts: (Wallis, 1969)

1) Pressure drop in the liquid slug
2) Pressure drop around the ends of the bubble
3) Pressure drop along the body of the bubble

The gas in the bubble tends to be at constant pressure. The bubble is cylindrical in shape and has a constant curvature. Therefore, there is no pressure drop along the body of the bubble. The pressure drop in the liquid slug can be calculated by single component flow techniques. The pressure drop around the ends of the bubble can be predicted in terms of fundamental quantities.

The liquid ahead of the rising Taylor bubble is displaced upwards, such that a thin falling liquid film is formed around the bubble under gravity force. The liquid film flows downward past the tail of the Taylor bubble and penetrates into the liquid slug. Due to penetration of liquid flowing around the film and into the wake region, mixing vortices occur (Wallis, 1969). The frictional forces and interfacial tension effects are neglected in this thesis.

2.2 Rise Velocity of the Taylor Bubble

Research on Taylor bubbles dates back as far as 1913 to that by Gibson. The studies of bubbles rising through stagnant liquids as two-phase fluids are extensive (Griffith and Wallis (1961) and Nicklin (1962)).

According to R.A.S. Brown (1965), the effect of liquid viscosity on the rise velocity of bubble through stagnant liquid in a vertical tube is limited by the liquid film flow past the bubble on the tube wall. Dumitrescu (1943) assumed the bubble would have a spherical nose and plug flow in the film flow region and obtained the bubble velocity and radius of curvature of the frontal area by solving the flow around spherical nose and asymptotic film flow simultaneously. The bubble rising velocity was given by

$$U_{BR} = 0.496\sqrt{gR}\ .$$

Davies and Taylor (1950) solved the flow equations by truncating method and the bubble rising velocity was given by $U_{BR} = 0.464\sqrt{gR}$. These equations have some limitations such as the radial component of the velocity in Dumitrescu's equation was assumed to be negligible. Nicklin (1962) showed that velocity solution was not unique and corrected the equation to $U_{BR} = 0.503\sqrt{gR}$. Although there are several approximations made in obtaining these above equations, prediction of the velocities of air bubbles rising through liquids of low viscosities were very close. Both Dumitrescu and Davies and Taylor equations suggested that the rise velocity of the bubble depends on square root of pipe diameter. With this Froude number came in to existence and it is defined by $Fr = \frac{U}{\sqrt{gD(\rho_L - \rho_G)/\rho_L}}$,where U is the rise velocity of the bubble, g is gravity acceleration, ρ_L is the liquid density and ρ_G is the gas density. The Froude number is constant for inviscid flow in a regime which is independent of surface tension.

When the viscous or surface tension forces become significant, the Froude number will vary. To describe the effects of viscosity or surface tension, two dimensionless number called Eotvos number (ratio of buoyant forces to surface forces) and Morton number (the ratio of viscous to surface forces) were introduced.

Bubble in a stagnant liquid column rises through denser liquid because of its buoyancy. The bubble rising velocity through stagnant liquid is governed by the interaction between buoyancy and the other forces acting on the bubble. If the viscosity of gas or vapor in the bubble is negligible, the only three forces besides buoyancy which are important are those from liquid inertia, liquid viscosity and surface tension. The balance between buoyancy and these forces can be represented in terms of the below three dimensionless groups and their dependency on rise velocity of the bubble is shown.

Dimensionless numbers and relation with Bubble rise velocity: Wallis (1969)

$$N_f = \frac{\sqrt{gD^3(\rho_f - \rho_g)\rho_f}}{\mu_f} \qquad N_{Eo} = \frac{gD^2(\rho_f - \rho_g)}{\sigma} \qquad N_{Ar} = \frac{\sigma^{3/2}\rho_f}{\mu_f^2\sqrt{g(\rho_f - \rho_g)}}$$

$$U_{BR} = k_1 N_f \frac{\mu_f}{D\rho_f} = k_1\sqrt{gD\left(1 - \frac{\rho_g}{\rho_f}\right)}$$

N_f is the Inverse viscosity number, $N_{Eö}$ is the Eötvös number, N_{Ar} is the Archimedes number, D is the diameter of the riser tube, ρ_f is the density of the fluid, ρ_g is density of the gas, μ_f is viscosity of the fluid and g is gravity acceleration.

<u>Inertia dominant</u> takes place for $N_f > 300$ and $N_{Eö} > 100$.

Approximate analytical solutions to this problem for a cylindrical tube have been obtained by Dumitrescu (1943) and by Davies and Taylor (1950). Values of the constant k_1 are:

Dumitrescu: $k_1 = 0.35$

Davies and Taylor: $k_1 = 0.328$

The experiments conducted by Dumitrescu gave a slightly different value k_1=0.346.

Through additional experiments, the k_1 is close to 0.345 (White and Beardmore, 1962).

So, the preferred and widely used value of k_1 is 0.345.

Viscosity dominant takes place for $N_f < 2$ and $N_{Eö} > 100$. Experimental observations by Wallis, 1969 confirm the value of $k_1 = 0.01\ N_f$.

Surface tension dominant takes place for $N_{Eö} = 3.37$, $N_f^2 = 6.2 N_{Ar}$

Viana, Pardo, Yánez, Trallero, & Joseph (2003) gives universal correlation of rise velocity of long gas bubbles in round pipe for different liquids. The rise velocity that was referred in most of the literature is absolute veloicty, when the top end of the pipe is closed to atmosphere. Santos, Sena Esteves & Coelho Pinheiro (2008) gives effect of gas expansion on the velocity of individual Taylor bubbles rising in vertical columns with water open to atmosphere.

2.3 Film Thickness

As Taylor bubble rises along the vertical column of liquid, there is a film region around a bubble in which the liquid ahead of the bubble falls through. Film thickness is important to calculate bubble length and bubble expansion.

R.A.S. Brown (1965) derived an equation to calculate the equilibrium film thickness and is given by $\delta = \frac{-1+\sqrt{1+2NR}}{N}$ where $N = \sqrt[3]{14.5\ \frac{\rho_l^2 g}{\mu^2}}$

where R = frontal radius of the bubble, ρ_l = density of the liquid and μ = viscosity of the liquid.

This equation does not make the thin-film assumption. Brown recognizes that the assumption of constant Froude number is not valid when viscosity is important, as this violates Dumitrescu's assumption of potential flow.

Llewellin, Del Bello, Taddeucci, Scarlato and Lane (2012) summarizes liquid film thickness equations. It has presented Nusseldt (1916) theoretical analysis of forces acting on a viscous liquid, falling under gravity, in which fluid flow is laminar. He derived the solution for liquid film thickness which was given by $\lambda = Re_f \ \frac{3\mu}{4\rho^2 g}^{2}$, where the films Reynolds number is given by Dukler & Bergelin (1952) $Re_f = 4\frac{\tau}{\mu}$; τ is the mass flux of liquid per unit breadth of the flow. In this thesis the Brown's equation was used to calculate the liquid film thickness around the bubble for water - air, viscous gel – air and slurry – air experiments respectively. Brown's equation is widely used in the research to estimate film thickness and doesn't make thin film assumption and hence used in viscous gel and slurry experiments where liquid film is thick, along with the water – air experiments where liquid film is thin.

2.4 Viscous Gel and Slurry

The bubble rise velocity depends on the properties of the liquid and the gas slug apart from size of pipe's diameter. Taylor bubble dynamics in Newtonian liquids is well understood, whereas the study of Taylor bubbles rising in non- Newtonian fluid is limited. Due to complex liquid rheology, the flow pattern and the bubble rising have different characteristics. There is need to extend the research of Taylor bubbles in Non- Newtonian fluids. The bubble rising velocity in non-Newtonian liquids have been studied by R.G. Sousa (2005), Astarita and Apuzzo (1965). R.G.Sousa (2005) studied flow of Taylor bubbles rising in stagnant CMC solutions of different concentration using PIV measurements. CMC solution is a shear thinning fluids and visible such that an optical method was used to characterize the velocity and shape of the bubble. Hassan, Khan and

Rasul (2010) measured small or non-Taylor bubble velocity in Xanthan Gum fluids. As discussed in the Chapter 2.3, when the system is viscosity dominant, the bubble velocity can be calculated using the equation given by Wallis using fluid properties.

The literature related to rise of Taylor bubble in solids slurry is limited. Vandu, Koop, and Krishna (2004) has presented bubble rise velocities in a bubble column slurry reactor, where the bubble are small or non Taylor bubbles. This thesis will attempt to gain some understanding of Taylor bubble rise velocity in liquid slurry.

The absolute bubble rising velocity discussed in Chapter 2.2 was used to compare with the experimental results obtained in this thesis work. The liquid film thickness formula given in Chapter 2.3 was used to calculate air slug film thickness in water, viscous gel, and slurry.

3. Experimental Design and Instrumentation

The bubble drilling riser test apparatus consists of 3 vertical acrylic tubes with a total height 18 ft (5.486 m) and an internal diameter of 6.5 inch (0.165 m). The top end of the tube can exert a vacuum, be open, or closed. Newtonian, Non-Newtonian, and drilling mud (with weighting solids) can be used for liquids and air for slug bubbles. A Taylor bubble is generated by pressurizing a fixed volume of air trapped in the lower 6 ft (1.829 m) section of the apparatus and introduced into the bottom of the upper 12 ft (3.658 m) section of the liquid column by opening and closing a main ball-valve. There are twelve pressure transducers placed 1 ft (0.305 m) apart along the height of the bubble riser. There are also twelve stationary Lorex high frequency cameras placed in line with the pressure gauges with two movable cameras to track and record the bubble expansion. Figure 6 shows the design drawing of the bubble riser and Figure 7 presents a picture of the actual equipment. The double diaphragm pump used to pump viscous gel and slurry in to the riser column is shown in Figure 8.

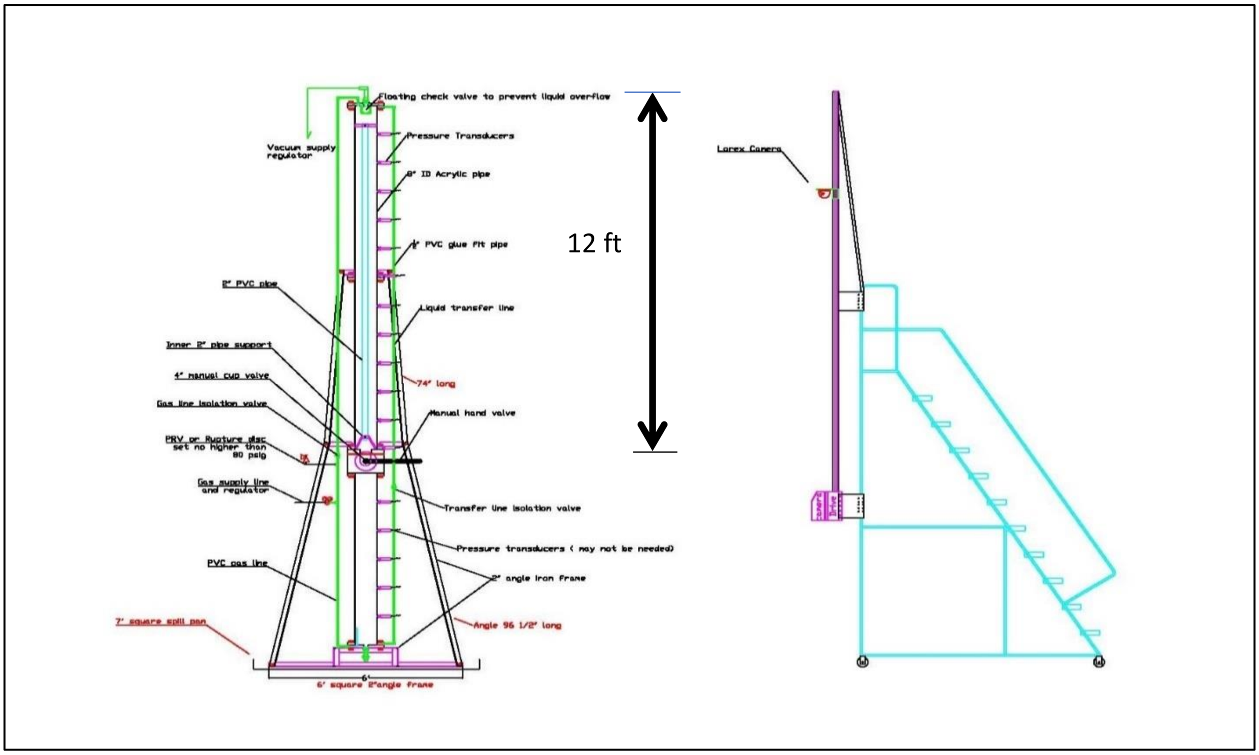

Figure 6: Design drawing of drilling riser-tube apparatus

Figure 7: Picture of the bubble riser with pressure transducers and cameras

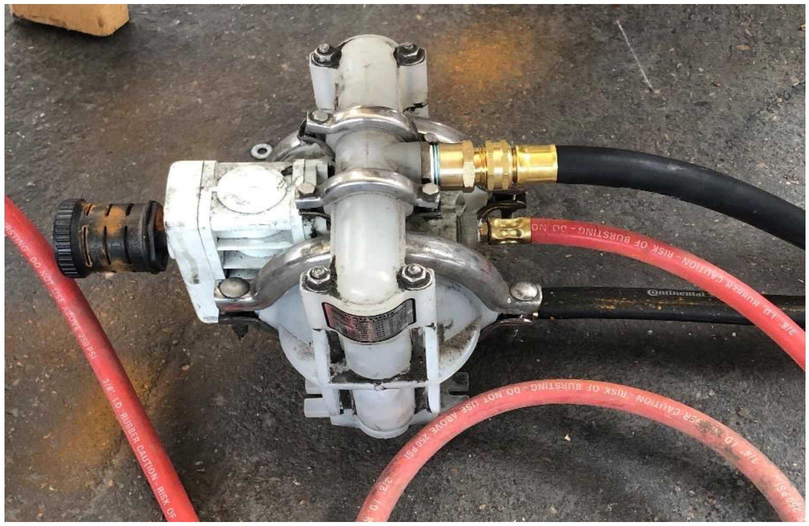

Figure 8: Double diaphragm pump used to pump viscous gel, slurry

To fill the drilling riser with water, open fill port valve by connecting water hose, with drain valve in closed and main valve in open position respectively. Once it fills the lower 6 ft of riser, close the main valve and fill port valve. Open fill port valve again to fill upper 12 ft section with water. While filling or draining the riser, vent valve should always be open to atmosphere so that the compressed air will not enter in the riser. To drain the riser, connect the pipe to bottom drain valve and open it. For finetuning volume inside the riser, close the main valve and open liquid transfer valve by pressurizing riser with air compressor and by opening air regulator valve. Once the desired level is reached, close liquid transfer valve and air regulator valve respectively. The position of different gauges (in inches) on the riser with respect to main valve are:

Channel 2: 11”

Channel 3: 23”

Channel 4: 35”

Channel 5: 47”

Channel 6: 59.5”

Channel 7: 71”

Channel 8: 83”

Channel 9: 95”

Channel 10:107”

Channel 11: 119”

Channel 12: 131”

Experimental procedure

Before starting a test, the Lorex cameras were set up in front of drilling riser tube. The DAQ PRO software by Omega Engineering was used during experimental run to record voltage and time data for all the channels respectively. Once the test was started, the following data/signals were obtained simultaneously:

(1) High speed videos of elongated bubble passing through the observation channels at different heights.

(2) Voltage vs Time data from DAQ DATA PRO software.

The recorded data and images were analyzed offline. To generate a bubble, fill up the riser with water and note down reading of the water level in inches. The bottom part of the riser tube has air pocket of certain inches which will be pressurized. Main valve is closed, and vent valve is open to atmosphere. The pressure was supplied to the bottom part of the tube with a Husky air compressor by turning on the air regulator valve. Once the test desired pressure is reached, the regulator valve is turned off. The main valve is opened in a rapid manner to create a stable taylor bubble which travels all the way through top of the riser before bursting out at the top. The moving camera control switch is turned on and start the data collection through DAQ DATA PRO software just before opening the main valve. During our research, all experiments were carried out at constant temperature and surface tension was not considered. Procedure for calibration is shown in Appendix A.

Lorex Cameras

Twelve stationary cameras and two movable Lorex cameras placed in front of drilling riser were used during this research work to record and track bubble expansion along the riser. NVR can record video in real-time (30 frames per second) on all twelve channels. Continuous, scheduled, and motion recording can be enabled respectively. In our research work, 20 frames per second was selected for camera recording to complement with 40 HZ frequency used in the strip chart recording. Twelve Omega Engineering pressure transducers were used with a range of 0 to 30 psig. These transducers are tested to meet published specifications traceable to the United States National Institute of Standards Technology.

4. Water - Air Slug Experiments

4.1 Overview

Water – Taylor Air bubble experiments have been performed in the first phase of the research to understand the physics behind the Taylor bubble rising in a vertical tube. Water and air slug experiments are easier to perform and there are sufficient results available in the literature for comparison. Movements of air slug in water are visible with the video camera. Recorded slug movements and sizes with time provide independent and complementary data to help validate results interpreted from pressure. As shown in Figures 3 and 4, air slugs in viscous gel and slurry media are not optically discernible. A major objective of this thesis is to establish a method to predict the slug rising velocity and bubble length in gel and slurry media using pressure versus time data only. Results from water with air slug experiments are instrumental in helping meet this objective.

4.2 Experiment 1 and Data Analysis

Calibration or pressure transducers was performed before the main experimental run. The main ball-valve is opened throughout the calibration procedure. All 12 transducers in the tube were calibrated with the riser filled with water and pressurized with 0, 1, 2, 3 and 4 psig respectively. The voltage data from these 12 channels were collected at corresponding pressure. The output voltage was then plotted against input gauge pressure to establish a relation between voltage and pressure for each of the channels. These calibration plots are shown in Appendix B. The test conditions used for the experiment after calibration are tabulated below in Table 1.

Figure 9 : Water level in the riser tube

Table 1 : Test conditions for water experiment 1

S. No	Parameters	
1	Water level in the riser	132.5 inches
2	Pressure applied to the air pocket	12 psig
3	Length of the air pocket	9.4375 inches

The air pocket of 9.4375 inches in length was created in the bottom section of the drilling riser tube and the air pocket was pressurized to 12 psig. The video camera and pressure collection systems were turned on to start the data collection. The main valve was then opened to release a stable Taylor bubble into the upper 12 ft of the riser tube. The video camera and pressure data were collected and analyzed after each test. Figure 10 shows the pressure versus time data for Channels 2 to 12 in the riser tube.

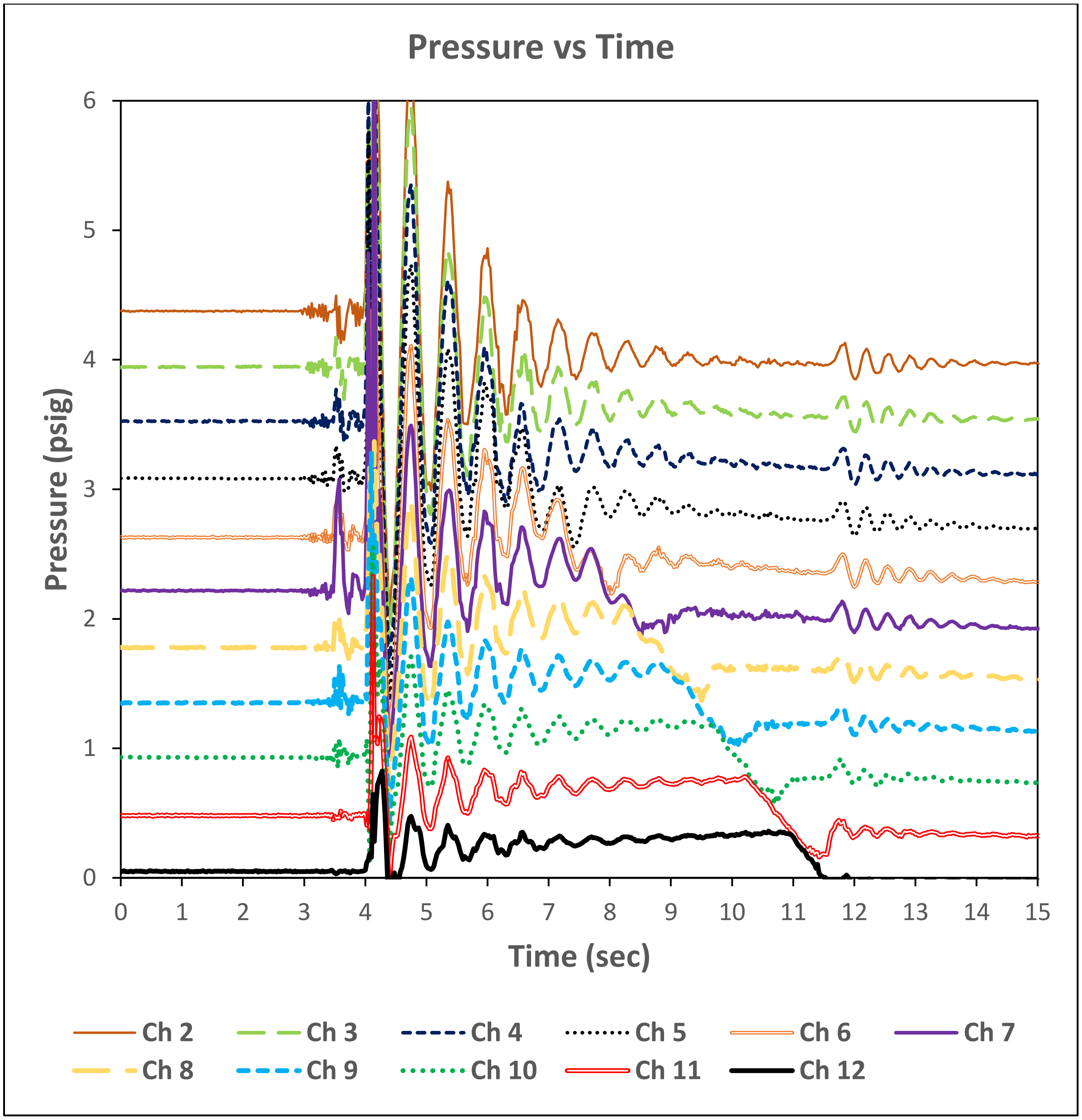

Figure 10: Pressure as a function of time for water experiment 1

From the pressure plot, before the introduction of the air slug, the difference between successive pressure readings of Channels 2 to 12 is the expected water pressure gradient of

0.433 psi/ft. The distance between Channel 6 and 7 is not 1 foot apart and the pressure gradient is not 0.433 psi/ft. These results confirm the pressure gauges are calibrated.

The pressure spikes at about 3.5 sec signaled the start of the opening of the ball-valve and the introduction of the air slug into the riser tube. This event created pressure oscillations observed in all transducers that affected the pressure responses throughout the test and the data analyses. The magnitude of the pressure oscillations was damped out proportionally as a distance away from the bottom channel. The closest and the farthest channels from the ball-valve (Channel 2 and Channel 12) had the largest and smallest oscillation pressure amplitude, respectively. The pressure oscillations for every channel occurred at the same time or at the same frequency. Therefore, they are not related or induced by the gas slug passing each transducer while travelling along the height of the riser tube.

The pressure reading for every channel starts increasing as the water level increases with the rise of the Taylor bubble along the tube. The mechanism is as the bubble rises, it displaces some liquid ahead of bubble’s nose and raises the liquid level. At the same time a partial amount of liquid is travelling down through the film region around the bubble. Therefore, the liquid level rise is not a piston displacement moving all liquid ahead of the slug. The relative proportion of liquid displaced ahead of the bubble’s nose and flowing around the liquid films would depend on the fluid viscosity and the liquid film thickness. For channel 12, at around 11 sec, the water level stops rising and the pressure versus time slope turns from a positive to negative value and follows with a continuous and constant negative value. In general, the change of the pressure slope from positive to negative represents the bubble’s nose entering the position of the pressure gauge. The following portion of the constant negative pressure slope represents the bubble passing through the gauge location. The lowest pressure drop corresponds to the bubble’s tail exiting. Figure 10 shows pressure readings after the bubble leaves each channel is less than the pressure at the start of the experiment. This pressure drop is due to the loss of water level corresponding to the volume of the air slug introduced to the riser. The final pressure recorded in Channel 12 is negative after the air slug exited the top of the tube and the water level is below Channel 12.

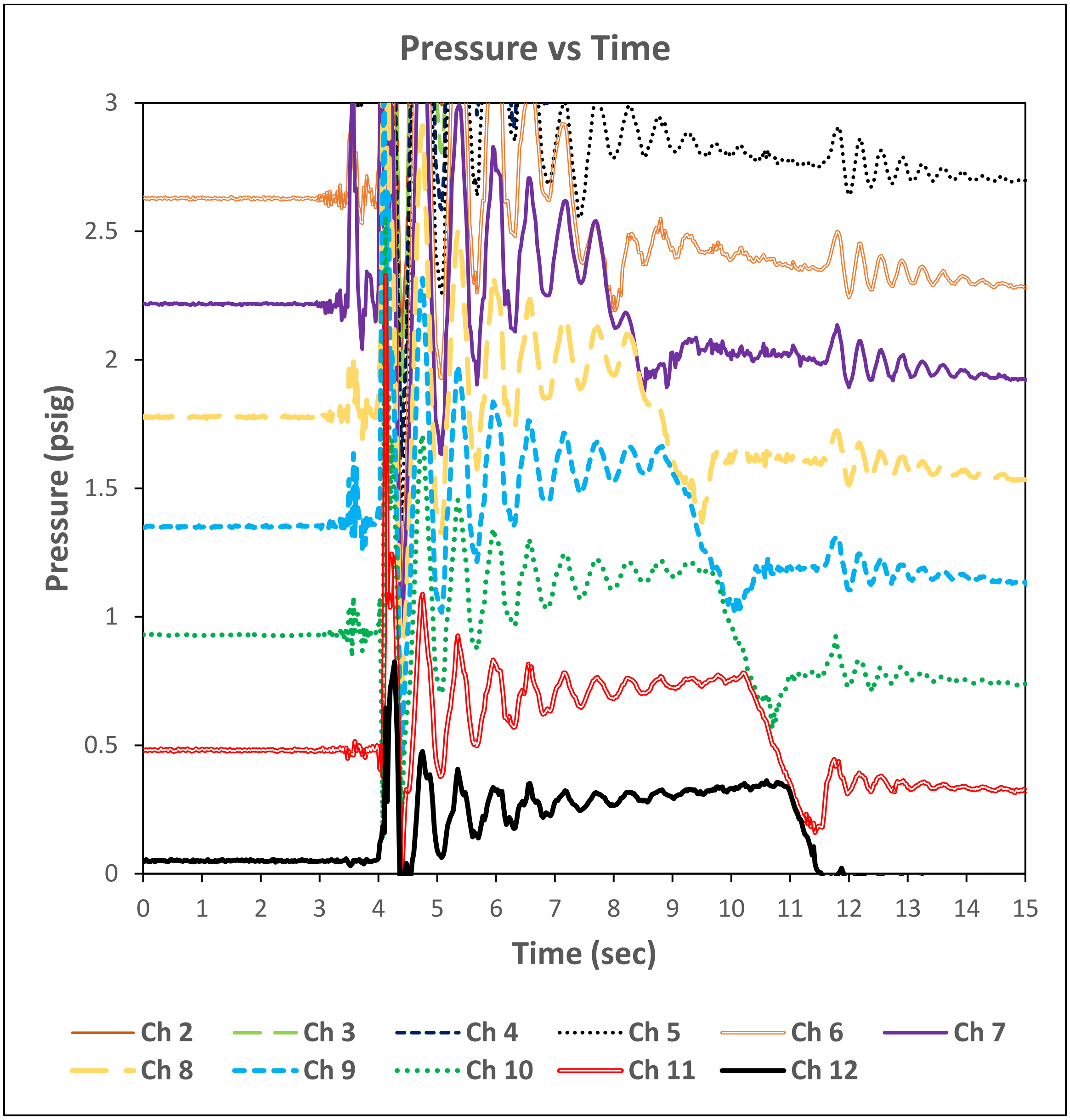

Figure 11: Pressure drop region for water experiment 1 – channels 7 to 12

The average absolute bubble rising velocity (see Chapter 2.2) can be calculated by subtracting the water level rising velocity from the bubble rising velocity. The level rising velocity is the pressure versus time slope before the bubble's nose enters Channel 12. The bubble rising velocity is the negative slope of pressure versus time when the bubble is passing through Channel 12. For this experiment the absolute velocity is 1.487 - 0.0621 =

1.425 ft/sec. The conditions in this experiment are inertia dominant and the bubble velocity can be calculated using the equation discussed in Chapter 2.2. Using $k_1 = 0.345$, the absolute velocity is 1.439 ft/sec. This absolute velocity is not a function of position. The calculation of bubble rising velocity with position is discussed below.

Method to Calculate Bubble Length

From the pressure plot, we cannot predict length of the bubble directly. We need a method or model to calculate the bubble rising velocity and length as a function of time and position. In this section we will present a method to calculate bubble rising velocity, bubble length and its rate of expansion. This method assumes the following:

- Any drop in hydrostatic pressure (at a given gauge) is due to reduction of density caused by the air slug above the gauge.
- Dynamic effects of liquid above and around the Taylor bubble are not considered.
- The bubble is assumed to be a cylinder.

However, to calculate the bubble length this method needs the input of the liquid film thickness. This film thickness is assumed to be constant. The above assumptions do not affect the calculation of the bubble rising velocity. This velocity is determined by the time interval needed for the slug to travel between 2 channels with a known separation distance.

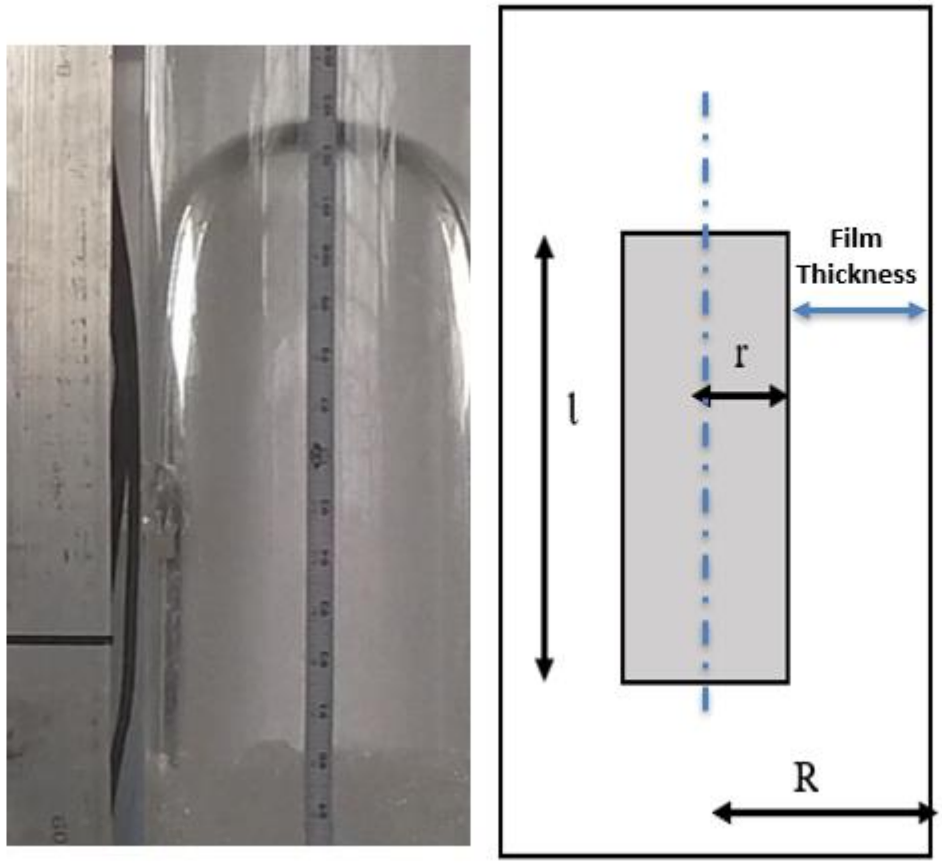

Figure 12: Taylor bubble with dimensions

Derivation of the bubble length:

Equation (1) defines the hydrostatic pressure of a column of liquid above a given gauge.

Pressure = density of the liquid * height of liquid above the gauge. ------- (1)

However, when the bubble start passing a gauge's position, there will be a change in the hydrostatic pressure because of the air slug volume affecting the fluid density. For a cylindrical air slug with radius r and length l, inside of a riser tube with radius R and a liquid level H, as shown in Figure 12, the length of the bubble is given in Equation (4).

The derivation of Equation (4) can be shown below. The forces acting on a bubble are weight of the total liquid above each channel and the air slug together.

Volume of air = $\pi r^2 l$,

Volume of water = $(\pi R^2 H - \pi r^2 l)$,

Force acting on the bubble due to air = $\rho_a \pi r^2 l$,

Force acting on the bubble due to water = $\rho_w (\pi R^2 H - \pi r^2 l)$,

Total force acting on the bubble = $\rho_a \pi r^2 l + \rho_w (\pi R^2 H - \pi r^2 l)$, ------ (2)

Total pressure acting on the bubble at channel i = $\frac{r^2 l\,(\rho_a - \rho_w) + \rho_w R^2 H}{R^2}$,

If the above equation is rewritten with respect to pressure of Channel 12,

$$P_i = \frac{r^2 l\,(\rho_a - \rho_w) + \rho_w R^2 h}{R^2} + P_{12} \qquad \text{------} \quad (3)$$

The length of air bubble, l is given by the Equation (4) as:

$$l_i = \frac{R^2\,(P_i - P_{12}) - \rho_w h}{r^2\,(\rho_a - \rho_w)} \qquad \text{------} \quad (4)$$

where P_i is pressure reading of Channel i,

P_{12} is pressure reading of Channel 12

ρ_w is density of water

ρ_a is density of air

h is the distance between Channel i and Channel 12

R is radius of the riser tube

r is radius of the Taylor bubble

The difference between the radius of the tube and the slug's radius is the liquid film thickness. The liquid film thickness, δ , is assumed to be constant during the rise of the bubble in the tube. R.A.S. Brown (1965) derived an equation to calculate the equilibrium film thickness and is given as

$$\delta = \frac{-1+\sqrt{1+2NR}}{N} \text{ where } N = \sqrt[3]{14.5\frac{\rho_l^2}{\mu_l^2}g} \qquad \text{------} \qquad (5)$$

where R = Radius of the riser tube, ρ_l = density of the liquid and μ_l = viscosity of the liquid.

As the liquid viscosity increases, liquid film thickness increases. For our water-air experiment, the film thickness is 0.069 inch.

The bubble length has been calculated as a function of time for different set of experiments and the time at which the nose of the bubble hit different channels has been selected. Using the time interval of the nose of the bubble at different channels, the translational bubble rising velocity has been calculated and presented for different experiments. As the gas slug or Taylor bubble rising along the column, it translates and expands at the same time. Assessment of these two parameters was a major objective and has been achieved through the method established here. The bubble rising velocity obtained was then compared with video camera data and the literature for consistency. They will be discussed later in this chapter. This same methodology was used to calculate the bubble rising velocity and bubble length for viscous gel and slurry experiments where the bubble cannot be seen with the video camera.

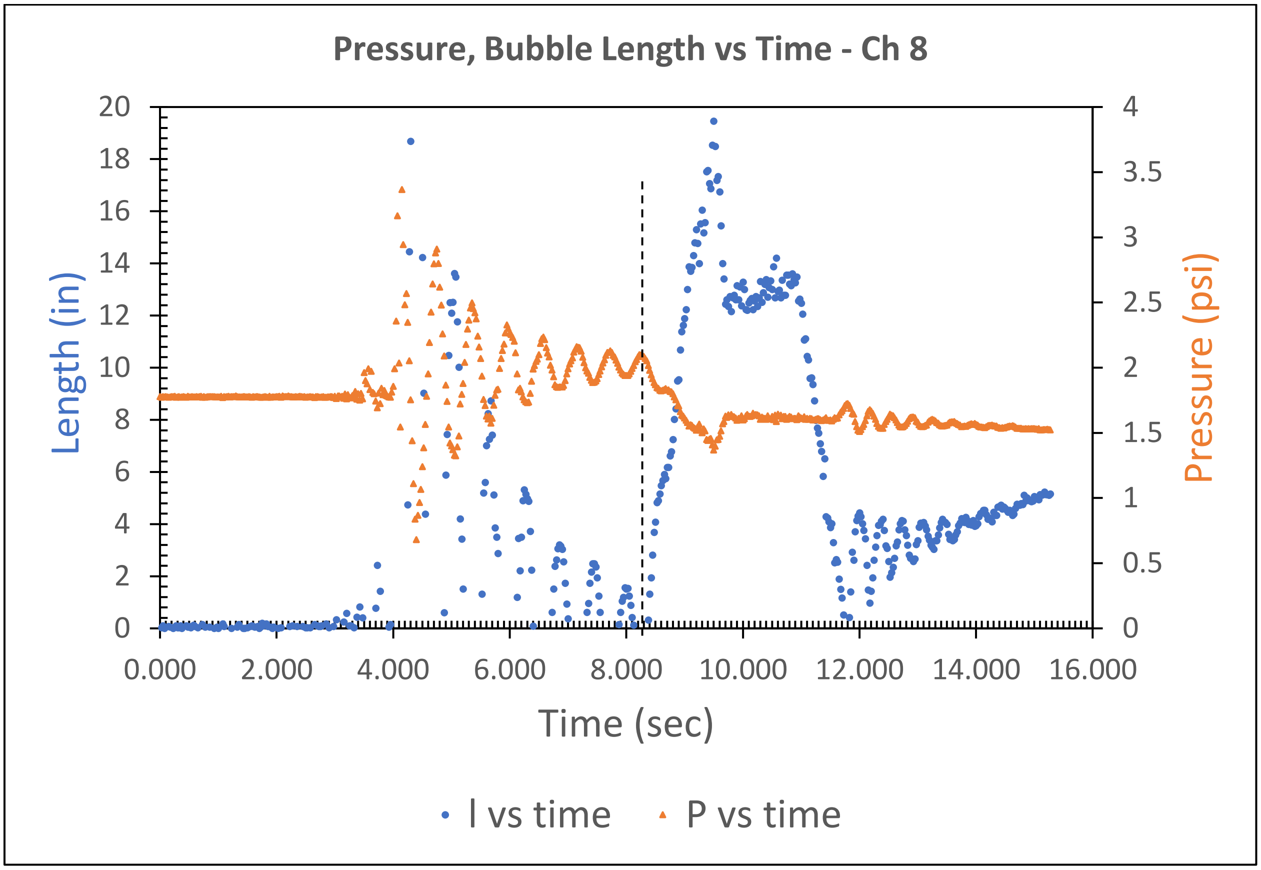

Figure 13: Pressure and bubble length as a function of time for channel 8

Figure 13 shows the recorded pressure of Channel 8 and the calculated bubble length above Channel 8 as a function of time. Instability in the length calculated between 4 and 8 sec intervals, is due to the pressure oscillations from the opening of the main valve. Once the bubble length becomes greater than zero, the bubble starts entering the channel and the length can be seen as a function of time. This bubble length increase corresponds to the pressure drop region in Channel 8. The dashed line highlights the time when the bubble nose enters Channel 8 and the start of the pressure drop. As the bubble moves up its length passing through the gauge increases and there is corresponding continuous pressure drop. The dynamic effects of the wake region passing through a gauge includes a cloud of small bubbles. This gives us a higher volume of air density which results in a longer air slug length. The region away from the dynamic effects, gives us real length of the bubble. The tail of the bubble leaving the channel is reflected with lowest pressure drop point. Figure 14 includes individual plot of pressure and bubble length for Channel 9, 10 and 11.

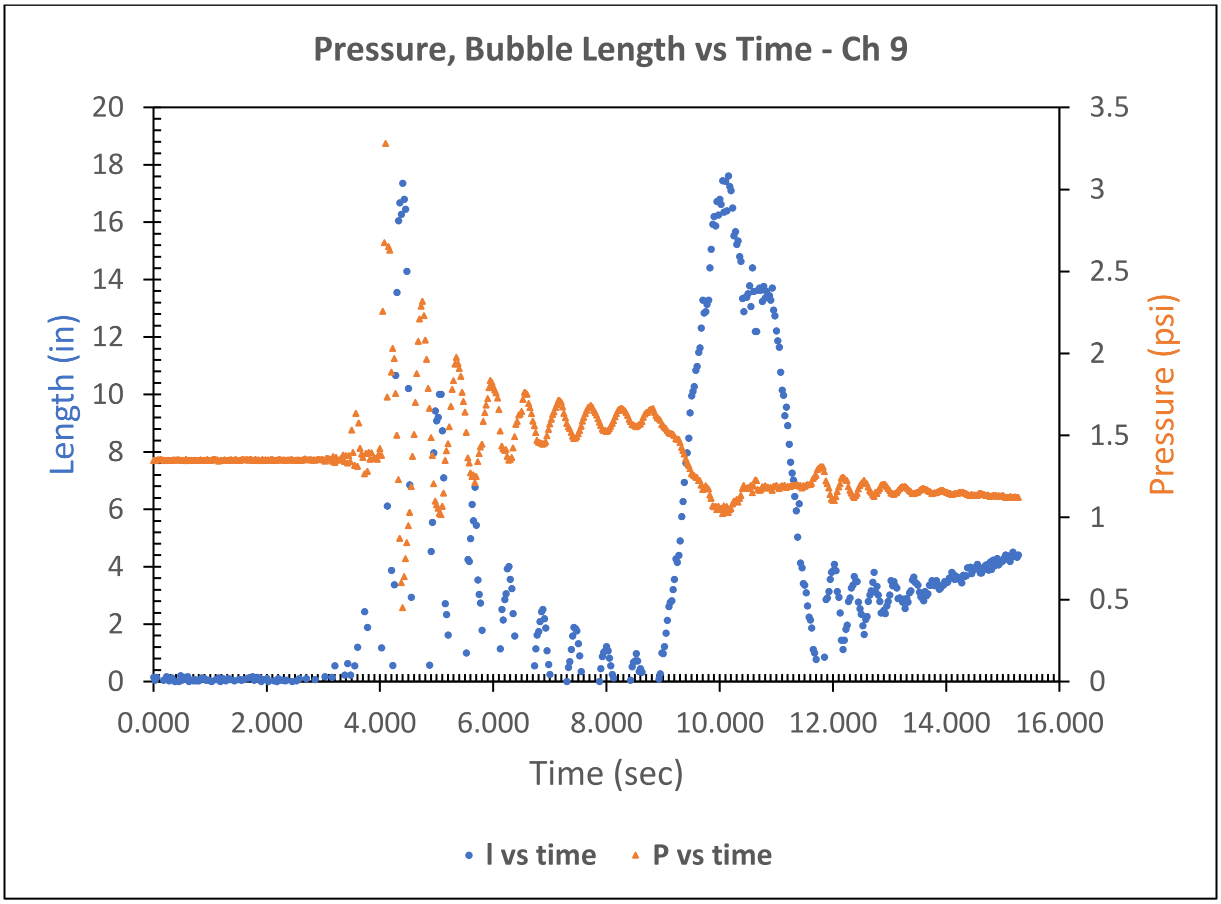

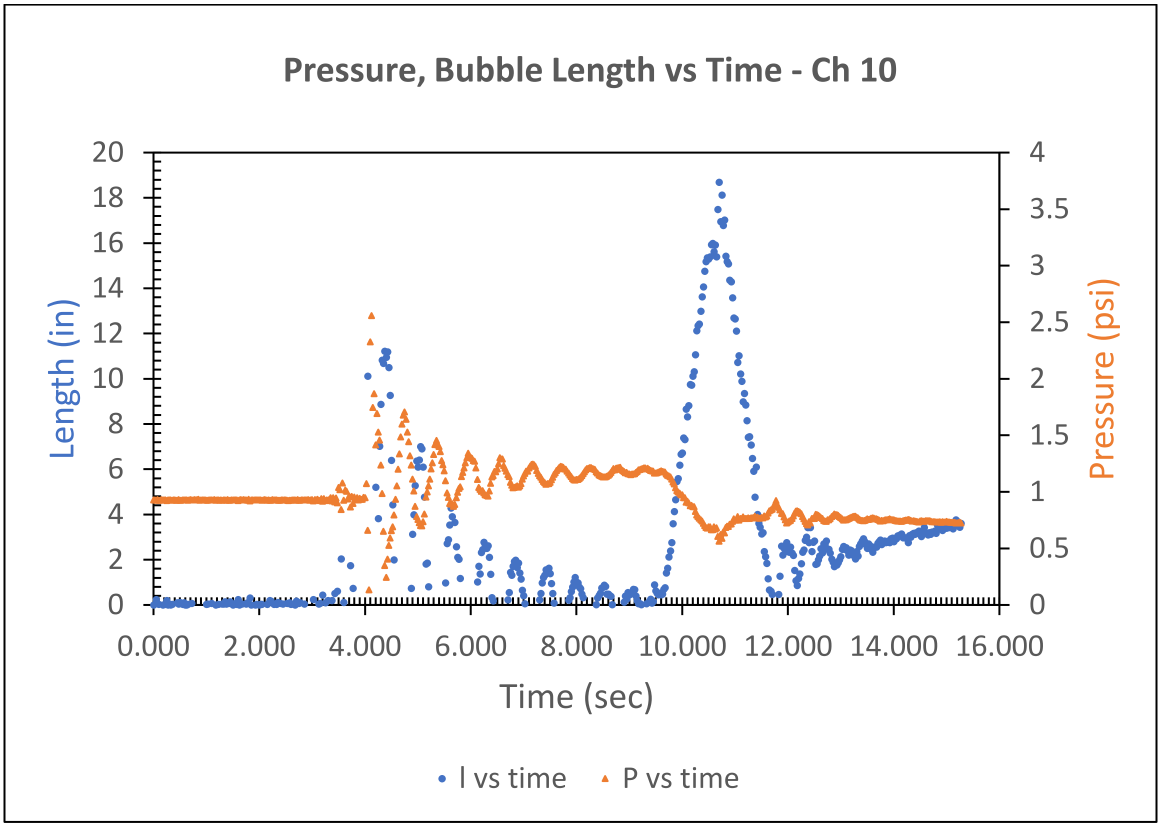

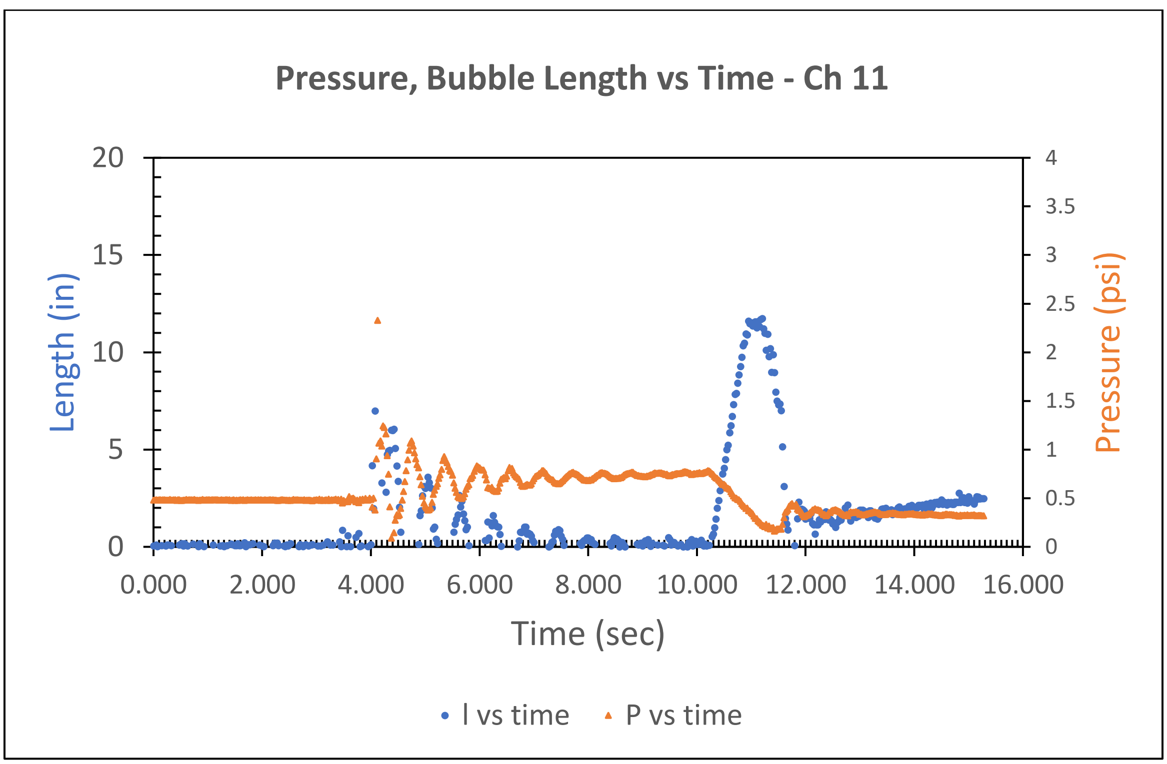

Figure 14: Pressure and bubble length as a function of time for channels 9 -11

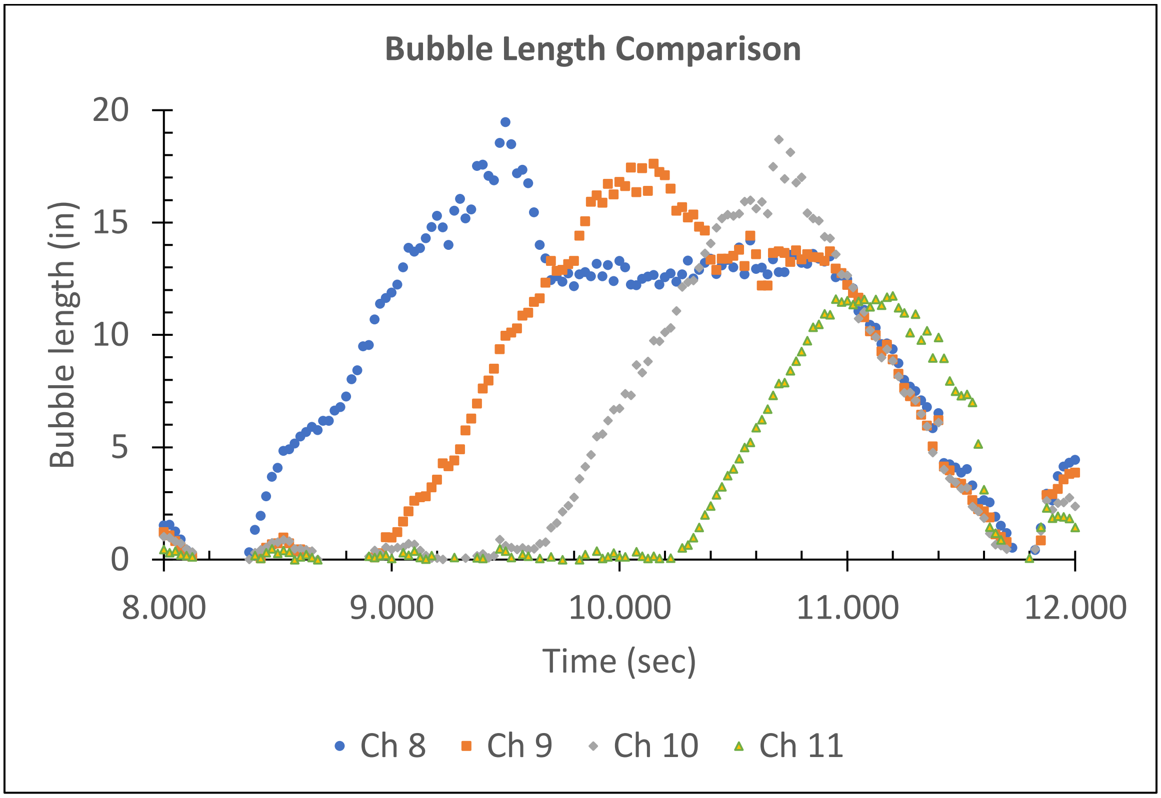

. *Figure 15: Comparison of bubble length as a function of time for channels 8 - 11*

Figure 15 shows a comparison of the bubble lengths calculated for Channels 8 to 11. The consistency of wake turbulence leading to longer length for every channel is observed. The bubble nose entering time for respective channels is noted down to calculate bubble rising velocity.

The consistency of the bubble lengths using the pressure method can be established by comparing the calculated lengths of 2 consecutive channels, i.e., Channel (i-1) and Channel (i). For example, at the time when the bubble's nose enters Channel 9 or Channel (i), the bubble length calculated for Channel 8 or Channel (i-1) should be less than 12 in. The reason is the distance between 2 consecutive channels is 12 in. Figure 16 shows the calculated length for Channel 8 is 11.5 in when the bubble enters Channel 9. Length calculations are consistent with video camera data.

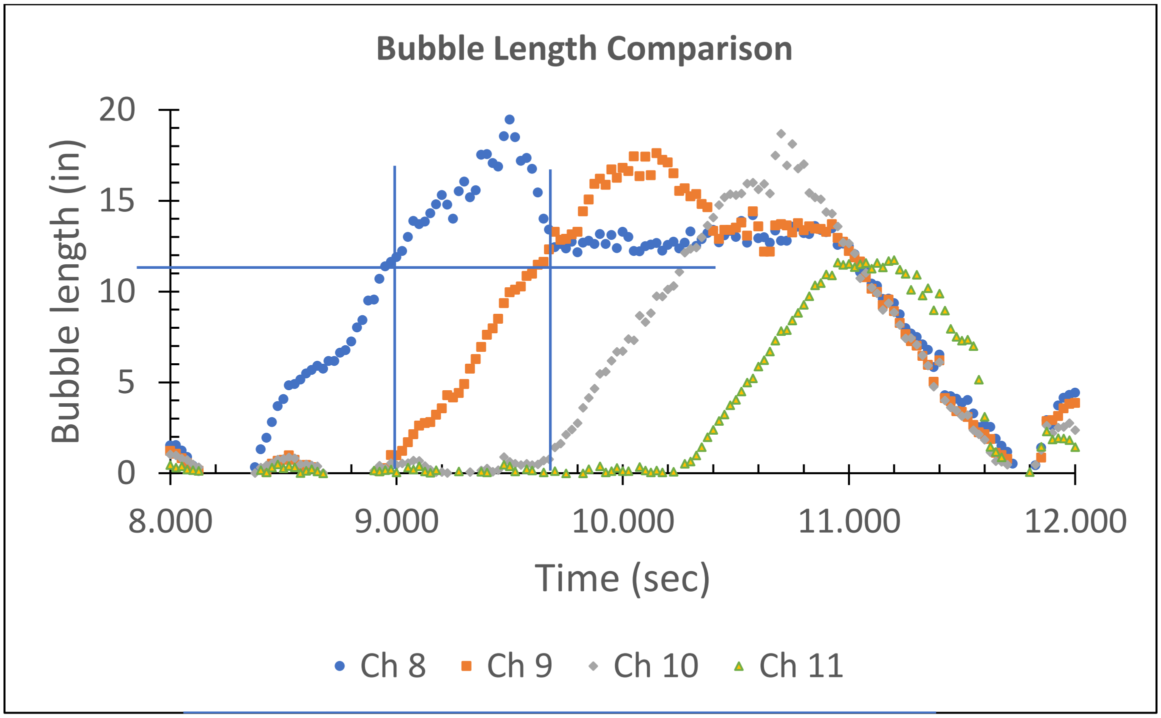

Figure 16: Bubble length consistency check for Channels 8 – 11

Method to Calculate Bubble Rising Velocity

The method to calculate bubble length can also be used to calculate bubble rising velocity. For a given channel, the time when the bubble length starts increasing continuously from zero represents a bubble entering the channel. Given the distance between 2 consecutive channels is 1 ft, the bubble rising velocity is simply 1 over the time differences of the bubble entering in 2 consecutive channels.

Table 2: Bubble rising velocity for water experiment 1

Channel No	Time (sec)	Δ Time (sec)	Bubble rising velocity (ft/sec)
8	8.375	-	-
9	8.950	0.575	1.739
10	9.675	0.725	1.379
11	10.250	0.575	1.739

Bubble rising velocity in the tube at different channels has been calculated and shown in Table 2. The velocity increases as the bubble moves up to Channel 9 and then decreases at Channel 10, before the bubble regains its speed and explodes near the surface. This observation is consistent with experimental results by Santos (2008). Figure 17 shows the calculated bubble velocity for Channels 9 to 11.

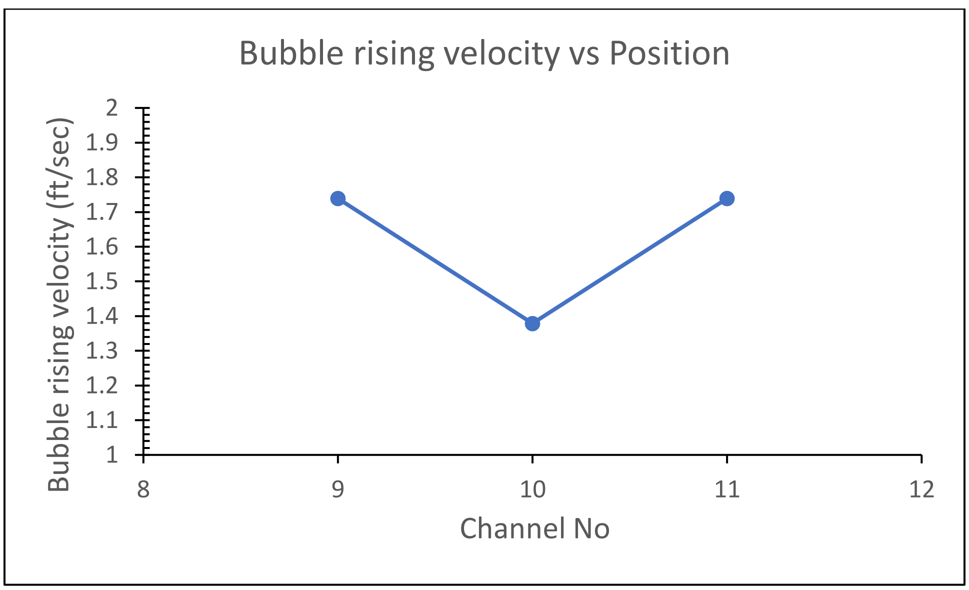

Figure 17: Bubble rising velocity as a function of position

The bubble rising velocities, bubble length as a function of time calculated using the pressure method were compared with the video camera data. The bubble rising velocity is based on nose to nose between two successive channels. Error is introduced into the observations due to the refraction index of the acrylic tube. Table 3 summarizes the results from the video camera. Table 4 compares the bubble velocities from video cameras and pressure method. These results are comparable. Similarly, the absolute velocity calculated using the pressure vs time data and the literature (Chapter 2.2) were 1.425 ft/sec and 1.439 ft/sec, respectively.

Table 3: Bubble rising velocity from video camera

Height	Channel	Video Time (sec)		Bubble rising velocity (ft/sec)
Position (in)		Nose	Δ t (sec)	
131	12	10.575	-	-
119	11	9.875	0.700	1.428
107	10	9.125	0.750	1.333
95	9	8.425	0.700	1.428
83	8	7.750	0.675	-

Table 4: Bubble rising velocity comparison

Channel No	Bubble rising velocity (ft/sec) from pressure methodology	Bubble rising velocity (ft/sec) from video camera
9	1.739	1.428
10	1.379	1.333
11	1.739	1.428

4.3 Experiment 2

The test conditions used for experiment are tabulated below in Table 5. The pressure plot is shown in Figure 18.

Table 5 : Test conditions for water experiment 2

S. No	Parameters	
1	Water level in the riser	132.875 inches
2	Pressure applied to the air pocket	10 psig
3	Length of the air pocket	9.5 inches

The bubble rising velocity is shown in Table 6. As the air pressure supplied decreases, there is increase in bubble rising velocity and decrease in bubble length respectively.

Table 6: Bubble rising velocity for water experiment 2

Channel No	Time (sec)	Δ Time (sec)	Bubble rising velocity (ft/sec)
8	9.050	-	
9	9.575	0.525	1.904
10	10.475	0.900	1.111
11	11.000	0.525	1.904

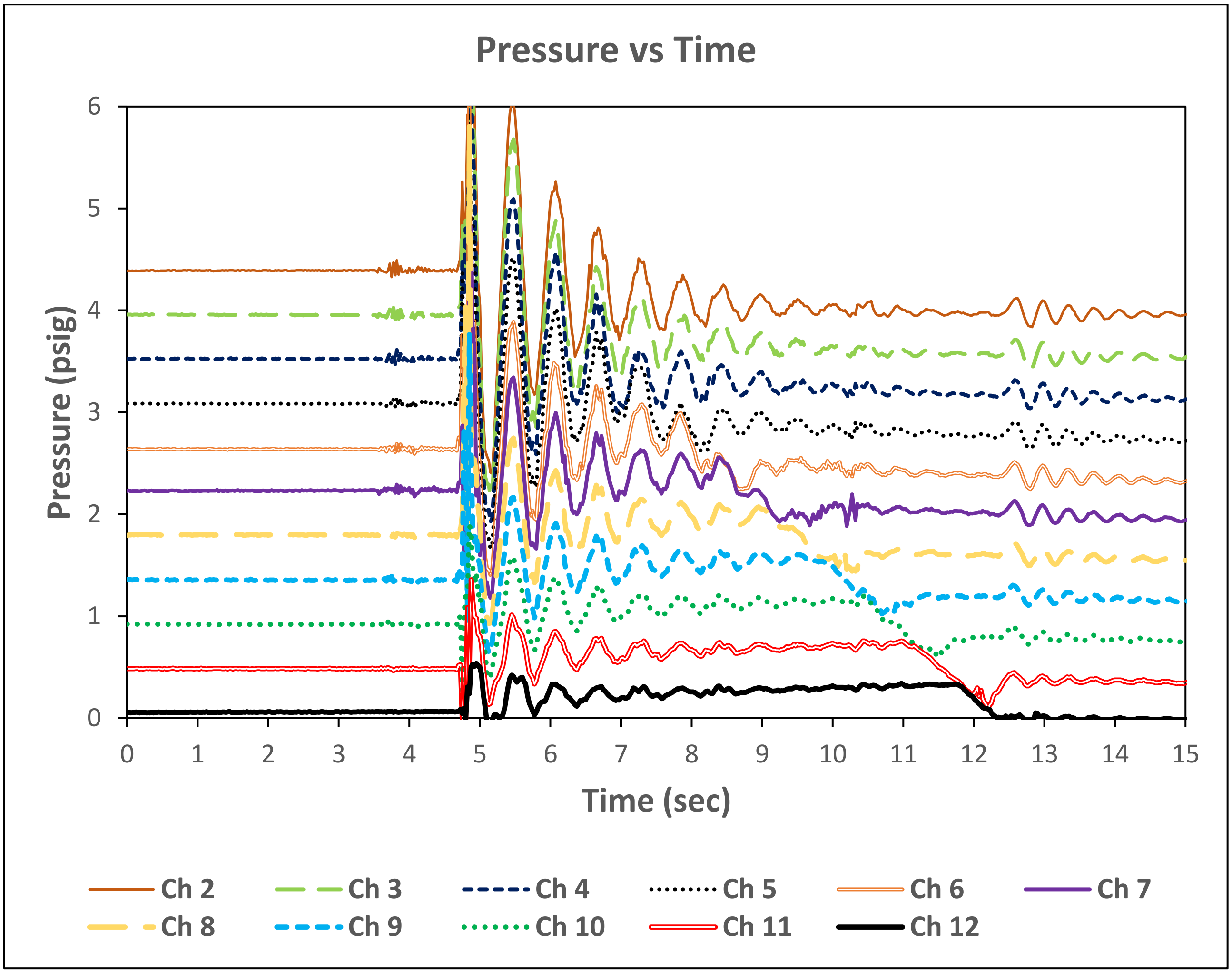

Figure 18: Pressure as a function of time for water experiment 2

Plots of bubble length as a function of time for different channels, comparison of pressure and bubble length as a function of time are shown in Appendix B.

4.4 Experiment 3

The test conditions used for experiment are tabulated below in Table 7. The pressure plot is shown in Figure 19.

Table 7: Test conditions for water experiment 3

S. No	Parameters	
1	Water level in the riser	133 inches
2	Pressure applied to the air pocket	7.5 psig
3	Length of the air pocket	8.125 inches

Table 8: Bubble rising velocity for water experiment 3

Channel No	Time (sec)	Δ Time (sec)	Bubble rising velocity (ft/sec)
8	9.050	-	
9	9.675	0.625	1.600
10	10.325	0.650	1.538
11	10.950	0.625	1.600

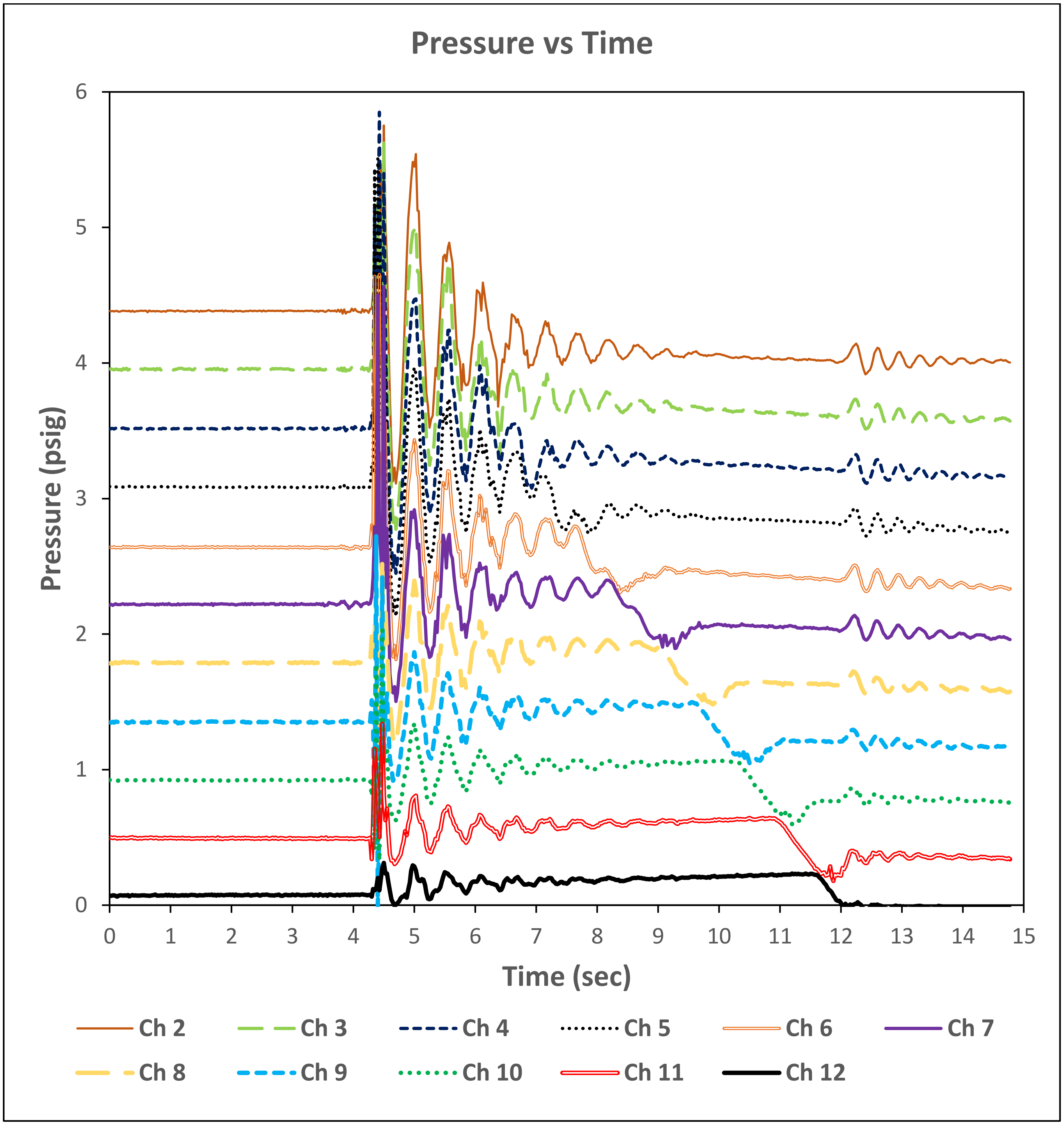

Figure 19: Pressure as a function of time for water experiment 3

Plots of bubble length as a function of time for different channels, comparison of pressure and bubble length as a function of time are shown in Appendix B.

4.5 Experiment 4

The test conditions used for experiment are tabulated below in Table 9. The pressure plot is shown in Figure 20.

Table 9: Test conditions for water experiment 4

S. No	Parameters	
1	Water level in the riser	132.8 inches
2	Pressure applied to the air pocket	15 psig
3	Length of the air pocket	8.25 inches

Table 10: Bubble rising velocity for water experiment 4

Channel No	Time (sec)	Δ Time (sec)	Bubble rising velocity (ft/sec)
8	8.550	-	-
9	9.125	0.575	1.739
10	9.700	0.575	1.739
11	10.150	0.450	2.222

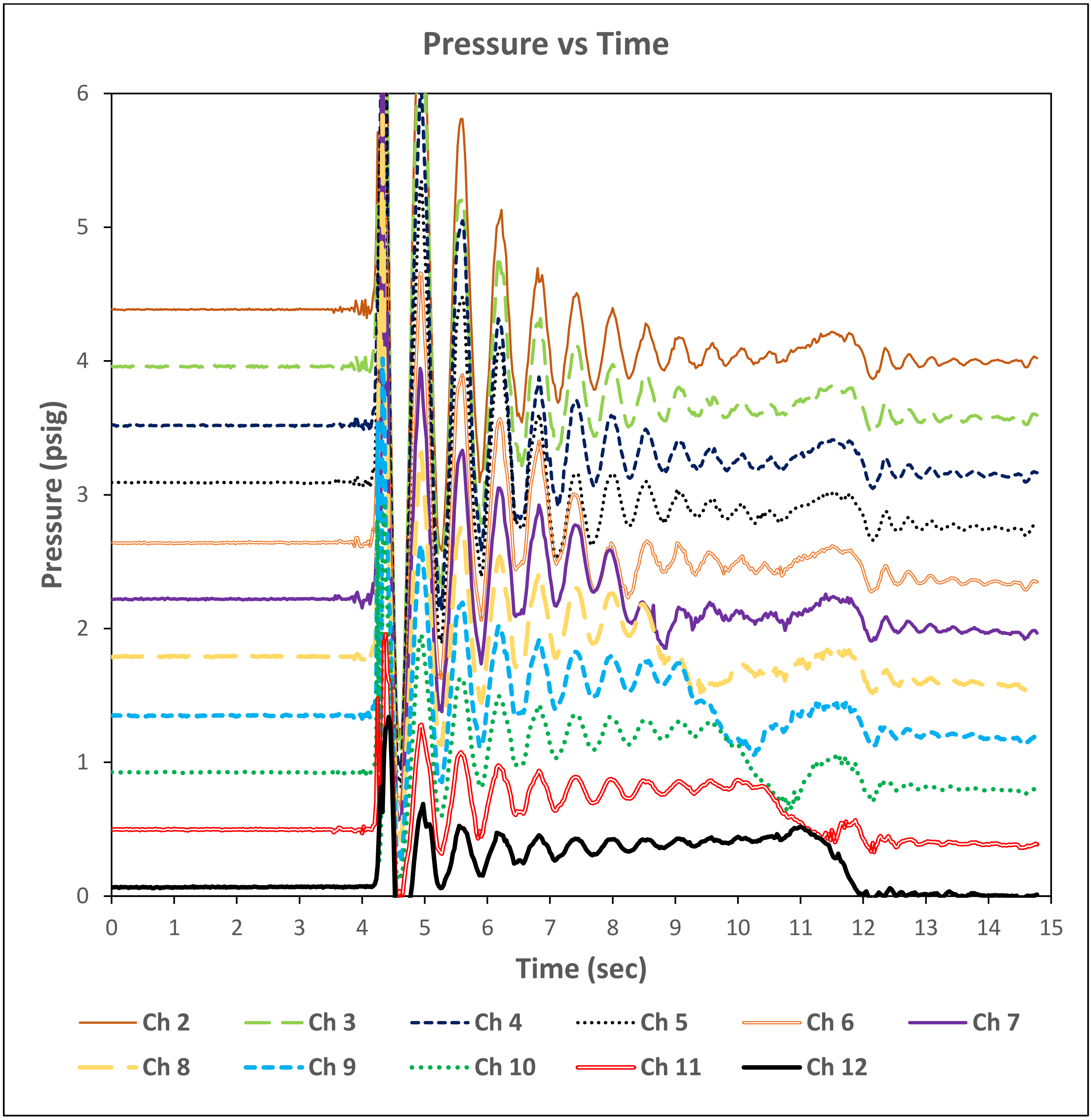

Figure 20: Pressure as a function of time for water experiment 4

Plots of bubble length as a function of time for different channels, comparison of pressure and bubble length as a function of time are shown in Appendix B.

5. Viscous gel – Air Slug Experiments

5.1 Overview

Results from the water – air slug experiments showed the viability of using pressure data to calculate bubble rising velocity and bubble length. This method would enable us to evaluate experiments where air slug is not visible.

This chapter focuses on air slug in a viscous gel medium. The viscous gel is made of 0.75% (by weight) of Xanthan gum. This is used to imitate shear thinning properties of drilling mud. The concentration of Xanthan gum is selected to suspend proppant for the slurry experiments in the next phase.

Concentrations of 0.125, 0.25, 0.5 and 0.75% by weight of Xanthan gum were made and mixed with 2 pound per gallon added (ppga) of 16/20 Carbolite proppant. The slurry was observed for proppant settling for 3 days at room temperature. Figure 21 shows the proppant suspensions of the 0.75% by weight of Xanthan gum gel after 1, 2 , and 3 days (from left to right), respectively. The 0.75% gel concentration slurry was chosen for its ability to suspend proppant.

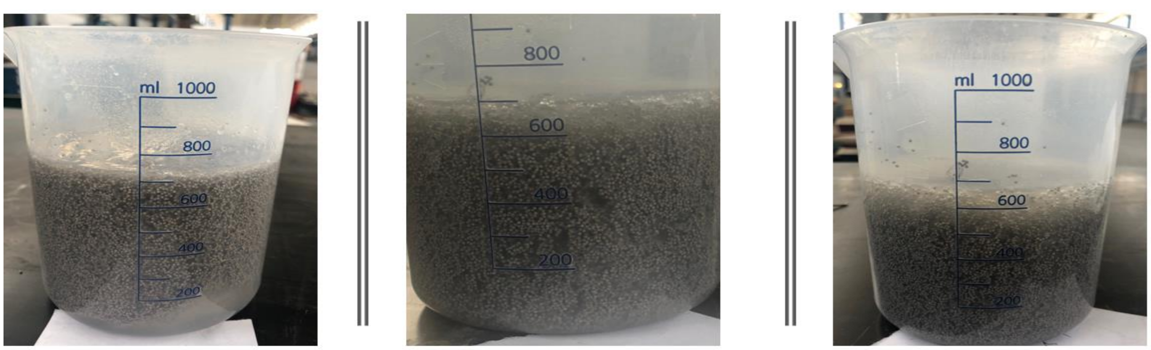

Figure 21: Suspension of proppant in viscous gel over a period of three days

Fann 35 viscometer was used to determine the rheology of the gel. The dial readings were noted down at different shear rate and shown in Table 11.

Table 11: Rheological dial readings

Shear Rate (RPM)	Dial Reading
600	60
300	50
200	44
100	38
60	35
30	31
6	26

The shear rate vs shear stress data and shear rate as function of viscosity were shown in Tables 12 and 13, respectively. Shear stress vs shear rate curve is shown in Figure 22. The regular plot and log - log plot of viscosity versus shear rate are shown in Figures 23 and 24, respectively. These showed the shear thinning effect of the Xanthan gum gel.

Table 12: Shear rate vs Shear stress

Shear Rate (1/s)	Shear Stress (Dyne/cm^2)
1022.1	511.046
511	255.523
340.7	170.349
170.3	85.1743
102.2	51.1046
51.1	25.5523
10.2	5.11046

Table 13: Shear rate as a function of viscosity

Shear Rate (1/s)	Viscosity (Pas)
1022.1	0.0299
511	0.0499
340.7	0.0659
170.3	0.1139
102.2	0.17488
51.1	0.3097
10.2	1.2991

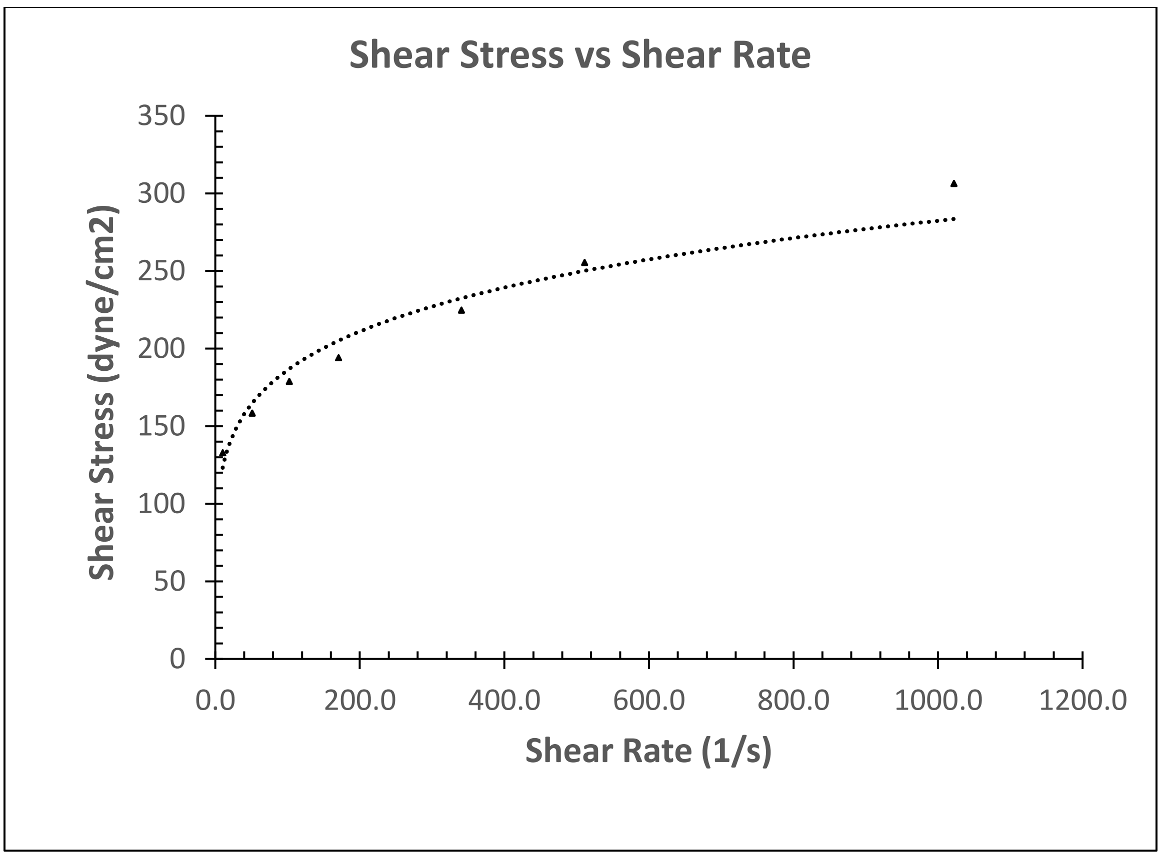

Figure 22: Shear stress as a function of shear rate

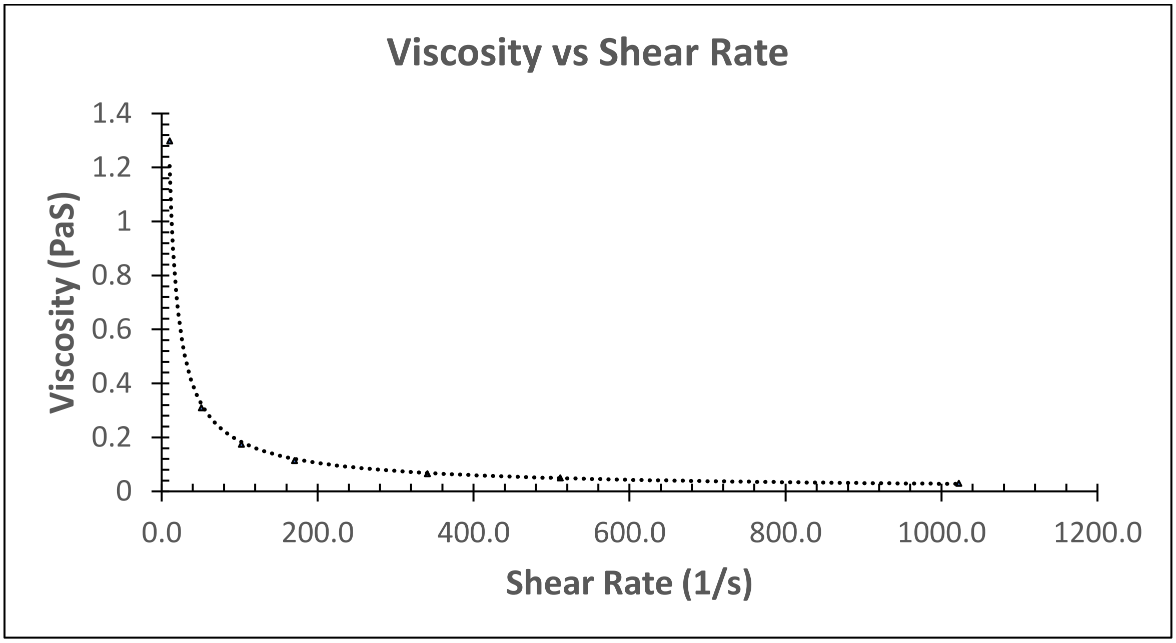

Figure 23: Viscosity as a function of shear rate

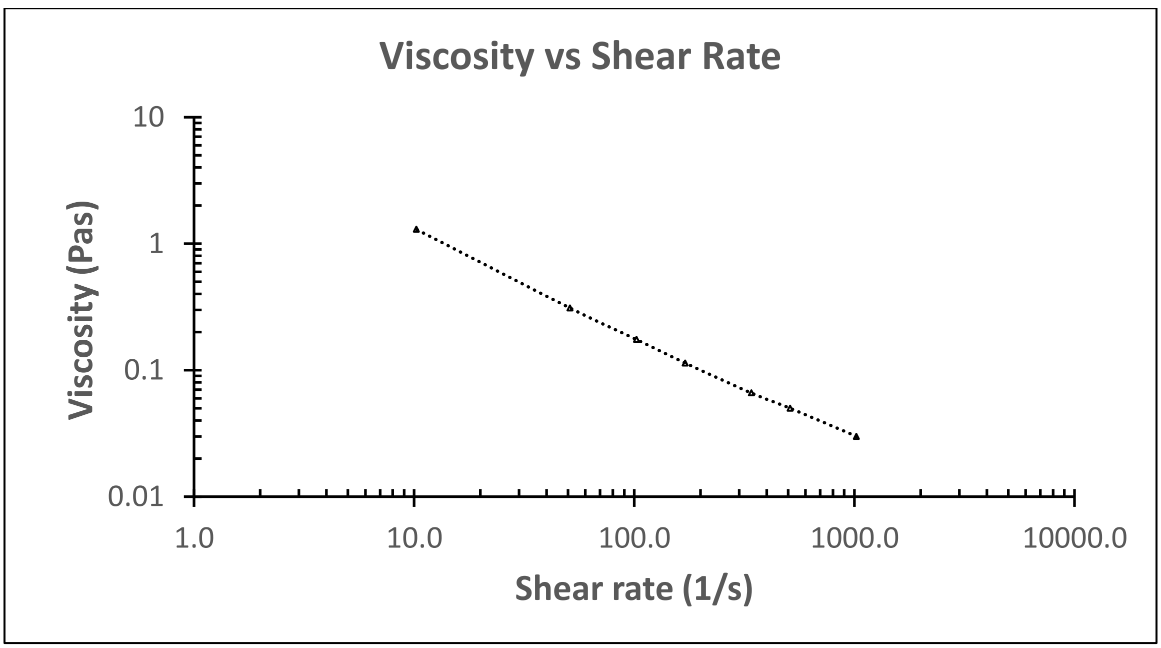

Figure 24: log - log plot of viscosity as a function of shear rate

5.2 Experiment 1 and Data Analysis

The Xanthan gum gel of 40 gallons was prepared by mixing 2.503 pounds of Xanthan gum in water, based on 0.75% by weight. The gel has been loaded into the drilling riser tube as shown in Figure 25 by using double diaphragm pump, which was shown in Figure 8. The gel density is 8.273 lb/gal or 991.359 kg/m^3.

Pressure gauge calibration has been performed before the experimental runs. The voltage data for 12 channels were collected at corresponding pressure and the calibration plots are shown in the Appendix C.

Figure 25: Drilling riser loaded with viscous gel

Table 14 has test conditions for experiment 1.

Table 14 : Test conditions for gel experiment 1

S.No	Parameters	
1	Gel level in the riser	131.5 inches
2	Pressure applied to the air pocket	15 psig
3	Length of the air pocket	10 inches

Figure 26 depicts the pressure data versus time for Channels 2 to 12. The magnitude of pressure oscillation is smaller than in water because of the higher viscosity damping effects. The gel rising level was higher than the water – air slug experiments. The pressure response for Channels 10, 11 and 12 showed a different signature than that of water. There is a sudden rise in liquid's level when the bubble's nose enters Channel 9 at about 8 sec. This is also reflected in increase of pressure versus time slope in Channels 10 to 12. The cause of this pressure behavior is not understood. It could be a combination of large viscosity changes (~100 to 1000 cp) in the low shear rate range of 2 to 4 1/s for this shear thinning gel in our experiments. However, this phenomenon of sudden rise of liquid level is repeatable and observed in Experiments 2 and 4.

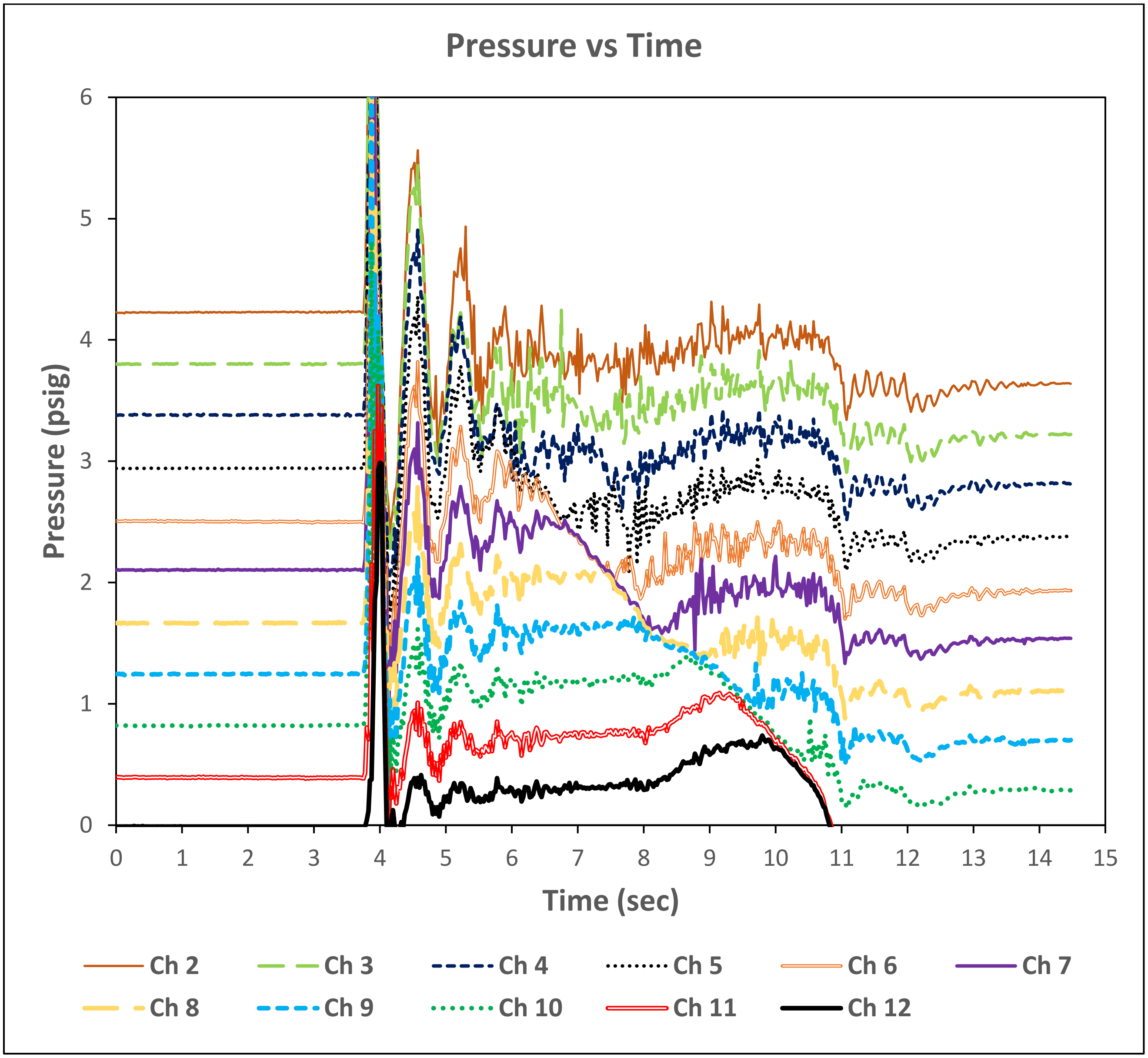

Figure 26: Pressure as a function of time for gel experiment 1

To calculate the bubble length using pressure data we need the input of the liquid film thickness using Equation 5. However, the liquid film thickness depends on fluid viscosity and for our shear thinning fluid the viscosity is shear rate dependent. Sousa (2005) has published experimental data of Taylor bubble rising in stagnant column of shear thinning fluids. The fluids were CMC (Carboxymethylcellulose) polymer gel solutions from 0.1 to

1.0% by weight. The apparent viscosity versus shear rate curve of our 7.5% Xanthan gum gel falls between 0.3% and 0.8% CMC curves in Sousa (2005). Using their measured bubble rising velocities and associated Reynolds numbers we estimated an average viscosity of 380 cp or 0.38 Pa-s for our gel. With this viscosity, Equation 5 calculated a liquid film thickness of 0.401 in which is significantly larger than the 0.069 in for water.

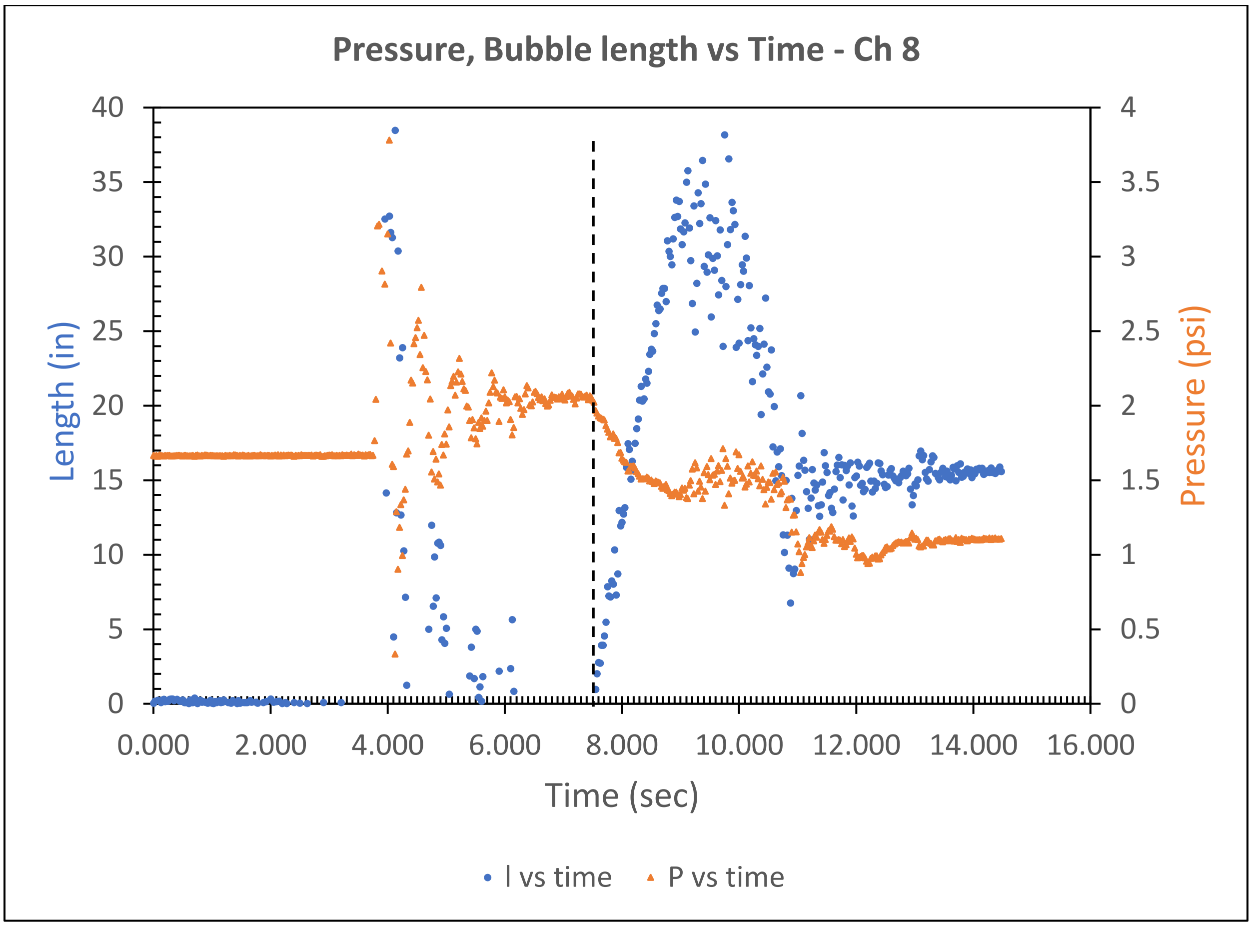

Figure 27: Pressure and bubble length as a function of time for channel 8

Figure 27 shows the recorded pressure of Channel 8 and the calculated bubble length above Channel 8 as a function of time. Similar to experiments with water, we see instability in the length calculations between the 4 and 7 sec interval caused by the pressure oscillations from the opening of the main valve. Once the bubble length becomes greater than zero, the bubble starts entering the channel and the length can be seen as a function of time. This bubble length increase corresponds to the pressure drop region shown in the pressure curve. The dashed line highlights the time when the bubble nose enters Channel 8 and the start of the pressure drop. As the bubble moves up, its length passing through the gauge increases and there is corresponding continuous pressure drop. The dynamic effects of the wake region leads to less erratic calculated lengths than water because of the increased gel viscosity. The thicker liquid film thickness leads to a longer bubble length for a given hydrostatic pressure change. The tail of the bubble leaving the channel is reflected with the lowest pressure drop point. Figure 28 shows individual plot of pressure and bubble length for Channel 9, 10 and 11.

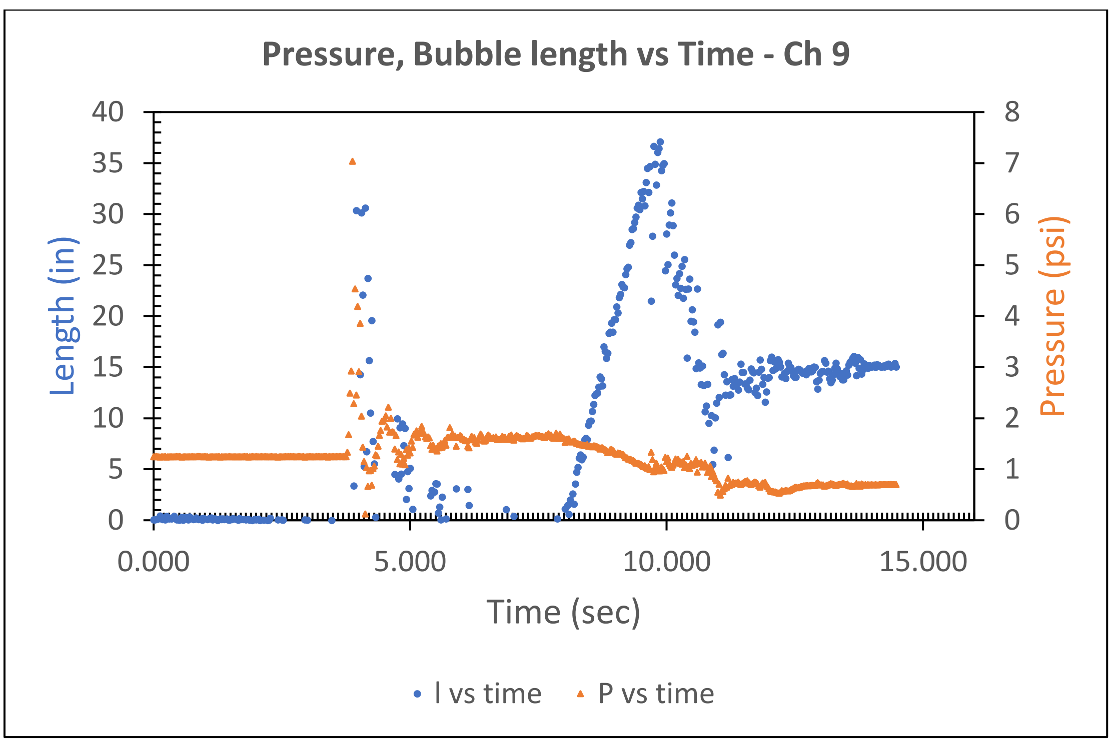

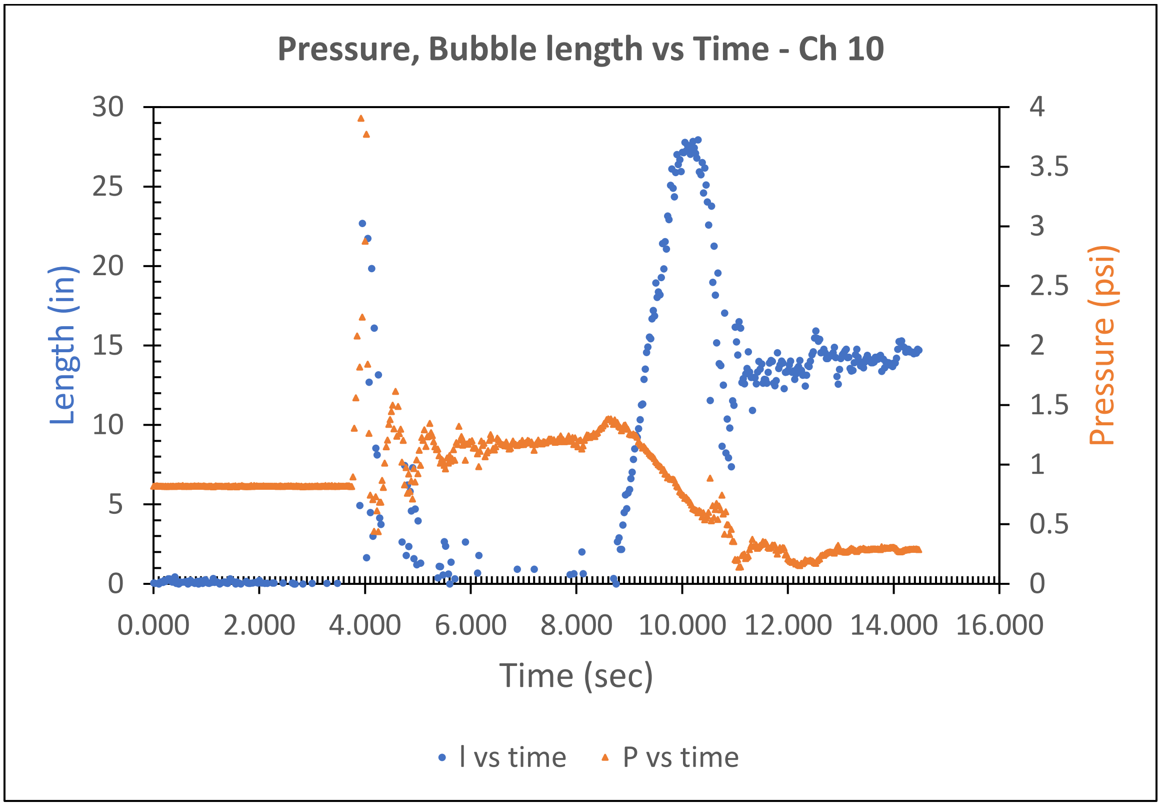

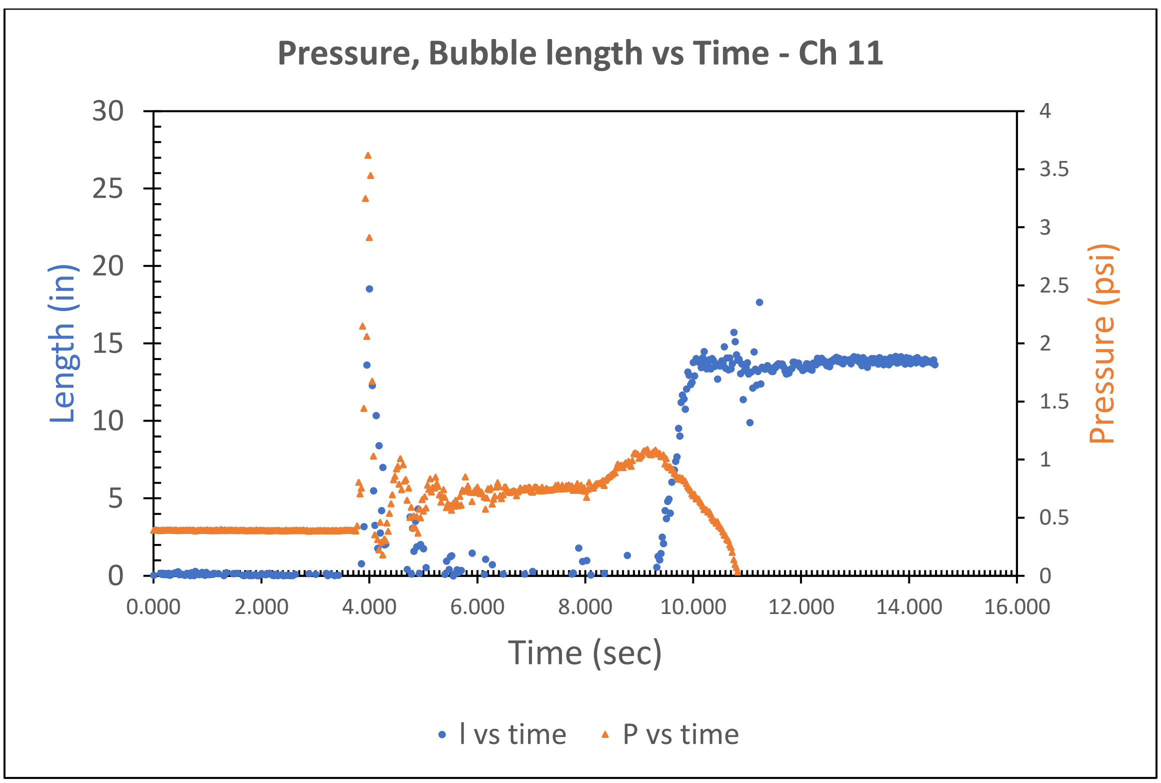

Figure 28: Pressure and bubble length as a function of time for channels 9 - 11

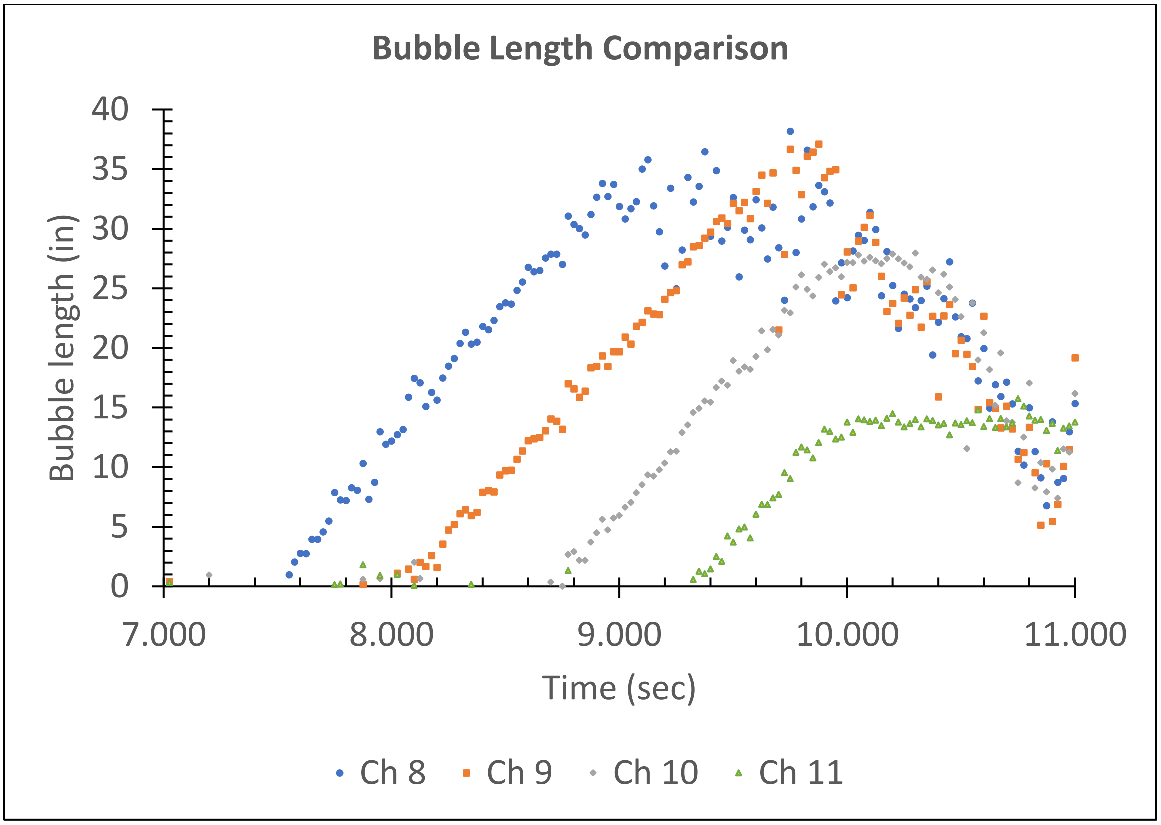

Figure 29: Comparison of bubble length as a function of time for channels 8 – 11

Figure 29 shows a comparison of the bubble lengths calculated for Channels 8 to 11. With viscous gel, there are lesser dynamic effects due to viscosity. The bubble nose entering time for respective channels is noted down to calculate bubble rising velocity. Figure 30 shows the consistency of calculated bubble lengths for different channels as discussed in Chapter 4.2. For the viscous gel, the liquid film thickness is shear rate sensitive. The assumption and use of a constant film thickness led to a small error in bubble length calculation. For example, a bubble length calculated for Channel 8 was 13 in when the bubble enters Channel 9. This should not have been larger than 12 inches.

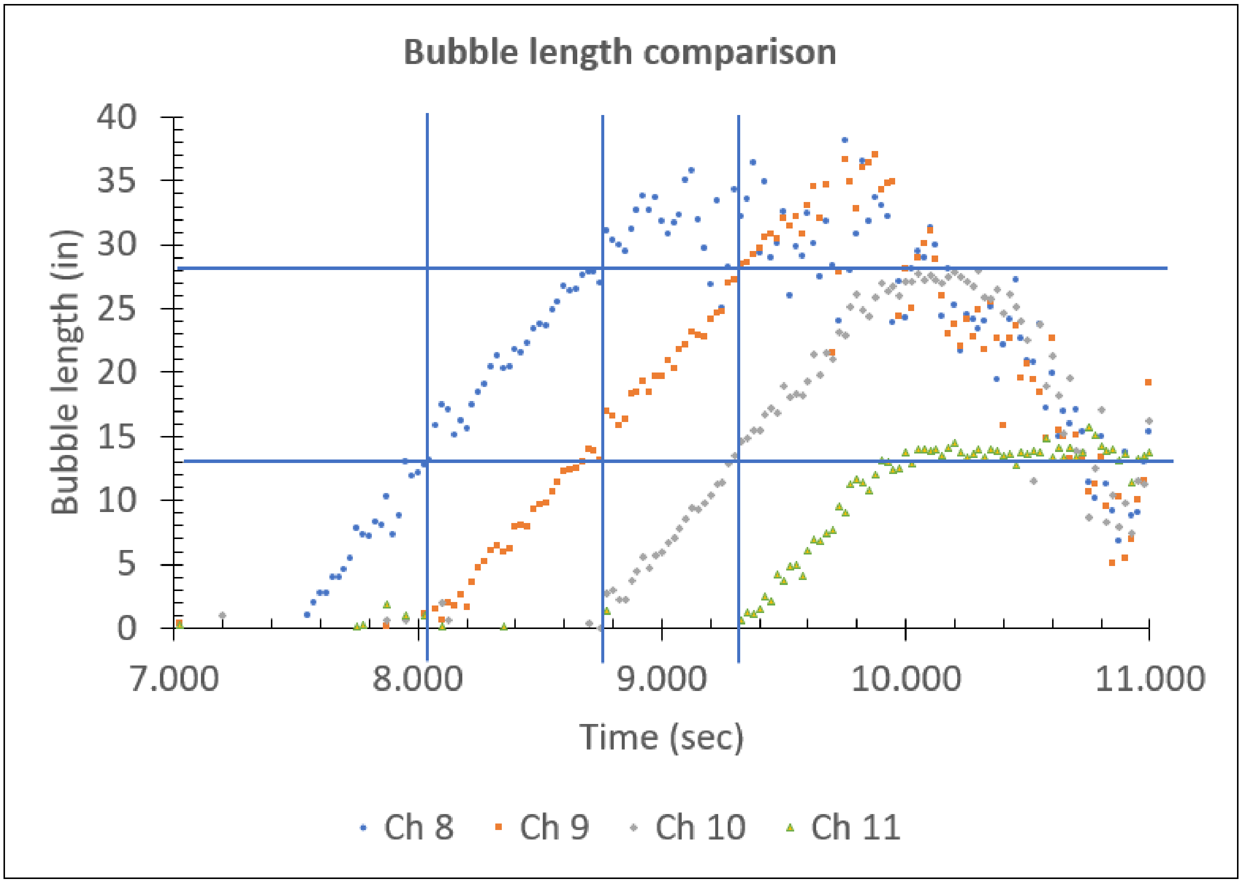

Figure 30: Bubble length consistency check for channels 8 – 11

Bubble rising velocity:

For a given channel, the time when the bubble length starts increasing continuously from zero represents a bubble entering the channel. Given the distance between 2 consecutive channels is 1 ft, the bubble rising velocity is simply 1 over the time differences of the bubble entering in 2 consecutive channels.

Table 15: Bubble rising velocity for gel experiment 1

Channel No	Time (sec)	Δ Time (sec)	Bubble rising velocity (ft/sec)
8	7.550	-	-
9	8.075	0.525	1.904
10	8.700	0.625	1.600
11	9.275	0.575	1.730

Bubble rising velocity in the riser at different channels has been calculated and shown in Table 15 and Figure 31 respectively. The bubble velocity increases as the bubble moves up the riser up to 9 feet and then decreases at channel 10, before the bubble regains its speed to exit to the surface.

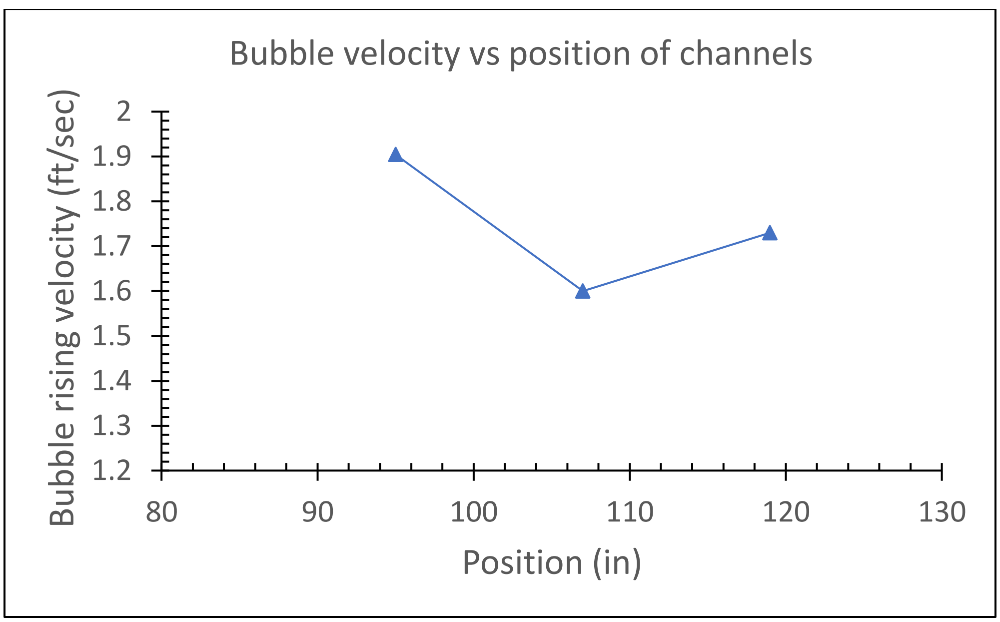

Figure 31: Bubble rising velocity as a function of position

N_f (Inverse viscosity number) for this experiment was found to be 148.40 using the assumed viscosity of 380 cp. The "absolute bubble rising velocity" calculated from Chapter 2.2 was about 0.9 to 1.0 ft/sec for the 6.5 inch tube with a closed end. For Experiment 1 and Figure 26, the absolute velocity is 1.6 - 0.08 = 1.52 ft/sec.

5.3 Experiment 2

The test conditions used for experiment are tabulated below in Table 16. The pressure plot is shown in Figure 32.

Table 16 : Test conditions for gel experiment 2

S. No	Parameters	
1	Gel level in the riser	131.5 inches
2	Pressure applied to the air pocket	15 psig
3	Length of the air pocket	10.75 inches

Table 17: Bubble rising velocity for gel experiment 2

Channel No	Time (sec)	Δ Time (sec)	Bubble rising velocity (ft/sec)
8	4.450	-	-
9	5.100	0.650	1.538
10	5.725	0.625	1.600
11	6.250	0.525	1.904

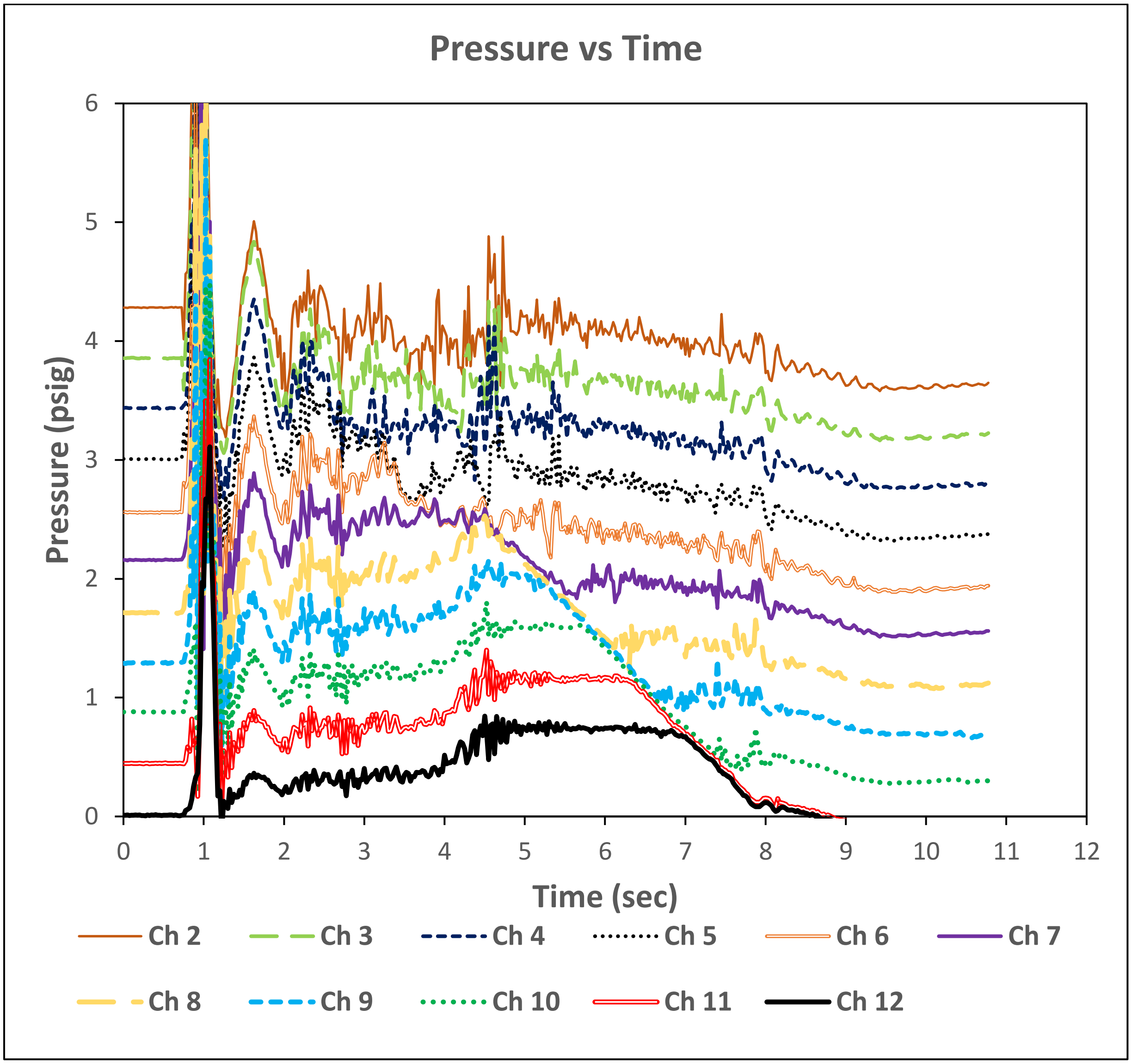

Figure 32: Pressure as a function of time for gel experiment 2

Plots of bubble length as a function of time for different channels, comparison of pressure and bubble length as a function of time are shown in Appendix C.

5.4 Experiment 3

The test conditions used for experiment are tabulated below in Table 18. The pressure plot is shown in Figure 33.

Table 18 : Test conditions for gel experiment 3

S. No	Parameters	
1	Gel level in the riser	132.5 inches
2	Pressure applied to the air pocket	10 psig
3	Length of the air pocket	10.875 inches

Table 19: Bubble rising velocity for gel experiment 3

Channel No	Time (sec)	Δ Time (sec)	Bubble rising velocity (ft/sec)
8	7.825	-	-
9	8.425	0.600	1.666
10	9.100	0.675	1.481
11	9.625	0.525	1.904

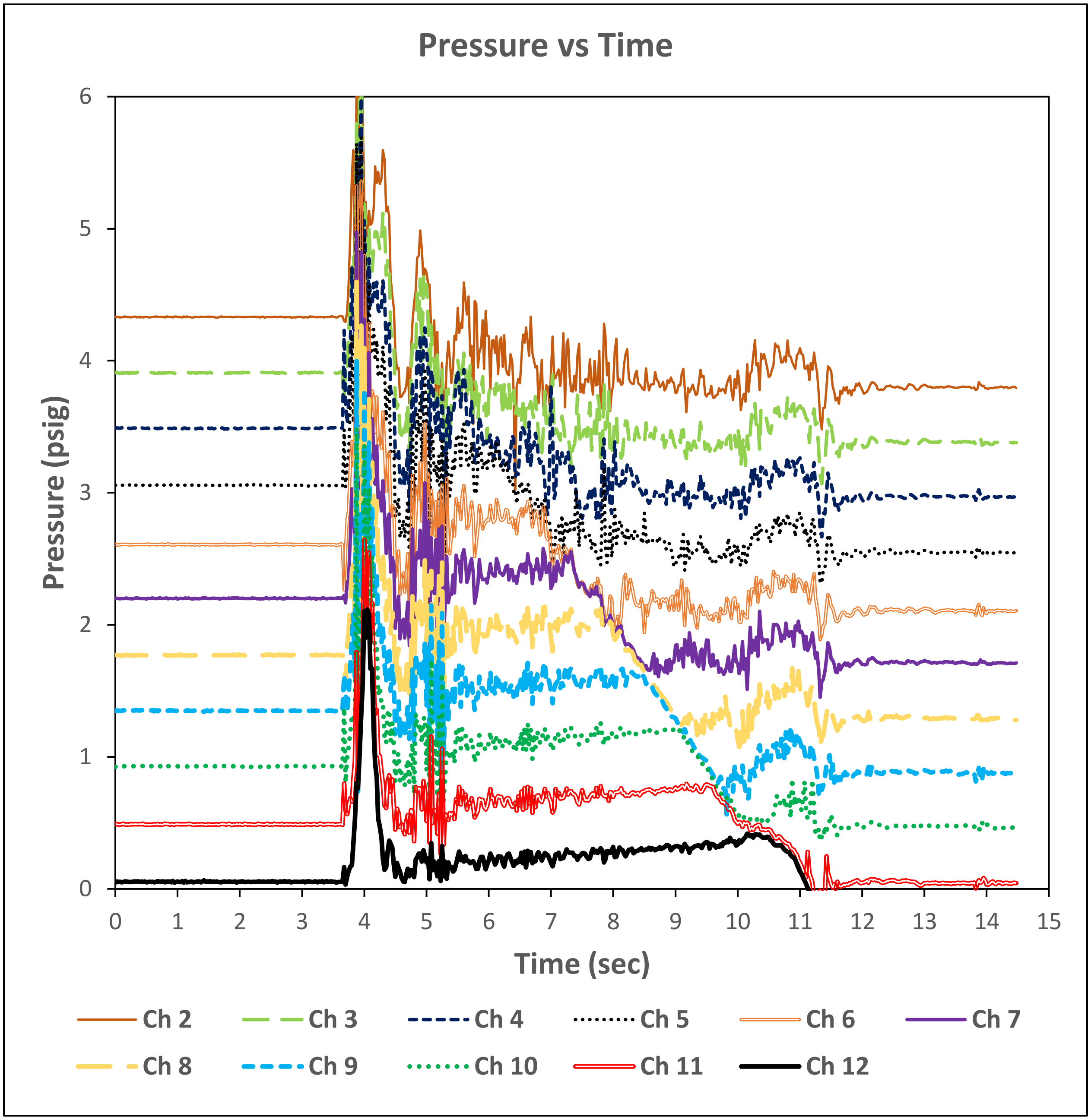

Figure 33: Pressure as a function of time for gel experiment 3

Plots of bubble length as a function of time for different channels, comparison of pressure and bubble length as a function of time are shown in Appendix C.

5.5 Experiment 4

The test conditions used for experiment are tabulated below in Table 20. The pressure plot is shown in Figure 34.

Table 20 : Test conditions for gel experiment 4

S. No	Parameters	
1	Gel level in the riser	133 inches
2	Pressure applied to the air pocket	10 psig
3	Length of the air pocket	11.8125 inches

Table 21: Bubble rising velocity for gel experiment 4

Channel No	Time (sec)	Δ Time (sec)	Bubble rising velocity (ft/sec)
8	6.375	-	-
9	7.200	0.825	1.212
10	7.850	0.650	1.538
11	8.425	0.575	1.739

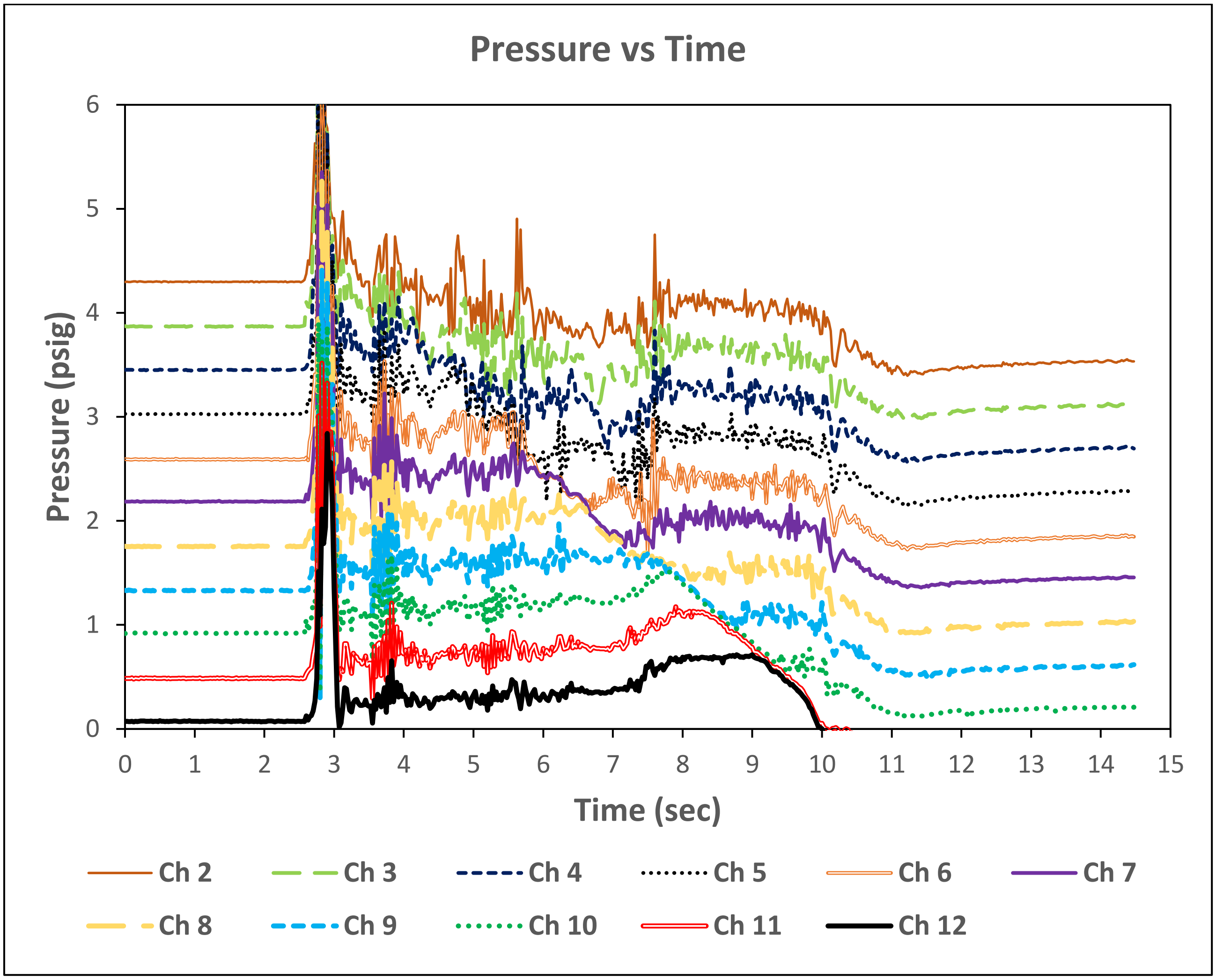

Figure 34: Pressure as a function of time for gel experiment 4

Plots of bubble length as a function of time for different channels, comparison of pressure and bubble length as a function of time are shown in Appendix C.

6. Slurry – Air Slug Experiments

6.1 Overview

Slurry – Air experiments have been performed in the third and final phase of the research. The proppant slurry has been selected to emulate the effect of solid particles in drilling mud. Slurry of proppant with Xanthan gum gel was prepared by adding 2 ppg of 16-20 Mesh Carbolite proppant with a median diameter of 1000 micron. The proppant concentration and the slurry density is 1086.34 kg/m^3 or 9.066 lb/gal.

6.2 Experiment 1 and Data Analysis

The Xanthan gum viscous gel of 40 gallons was prepared by mixing 2.503 pounds of Xanthan gum in water, based on 0.75% by weight and 79.99 pounds of 16/20 proppant was added to the gel. The slurry loaded into the drilling riser is shown in Figure 35. Pressure – voltage calibrations for pressure gauges done for gel were used for slurry experiments. The density of the slurry was 1090 kg/m3 or 9.1 lb/gal. The slurry viscosity with the presence of proppant is calculated using Thomas (1965) equation given by:

$$\mu_s = \mu_f \cdot [1 + 2.5 \cdot C_v + 10.05 \cdot C_v^2 + 0.00273 \cdot Exp(16.6 \cdot C_v)]$$

where μ_f is the gel viscosity and C_v is the volume fraction of proppant in slurry.

For the 2 ppg of 16-20 Mesh Carbolite proppant used in the experiment, the slurry viscosity was estimated to be 0.5285 Pa-s. Using the viscosity and Equation 5, the computed liquid film thickness is 0.492 inches.

Figure 35: Portion of the riser filled with proppant slurry

The test conditions are shown in Table 22.

Table 22 : Test conditions for slurry experiment 1

S. No	Parameters	
1	Slurry level in the riser	97.125 inches
2	Pressure applied to the air pocket	4 psig
3	Length of the air pocket	7.125 inches

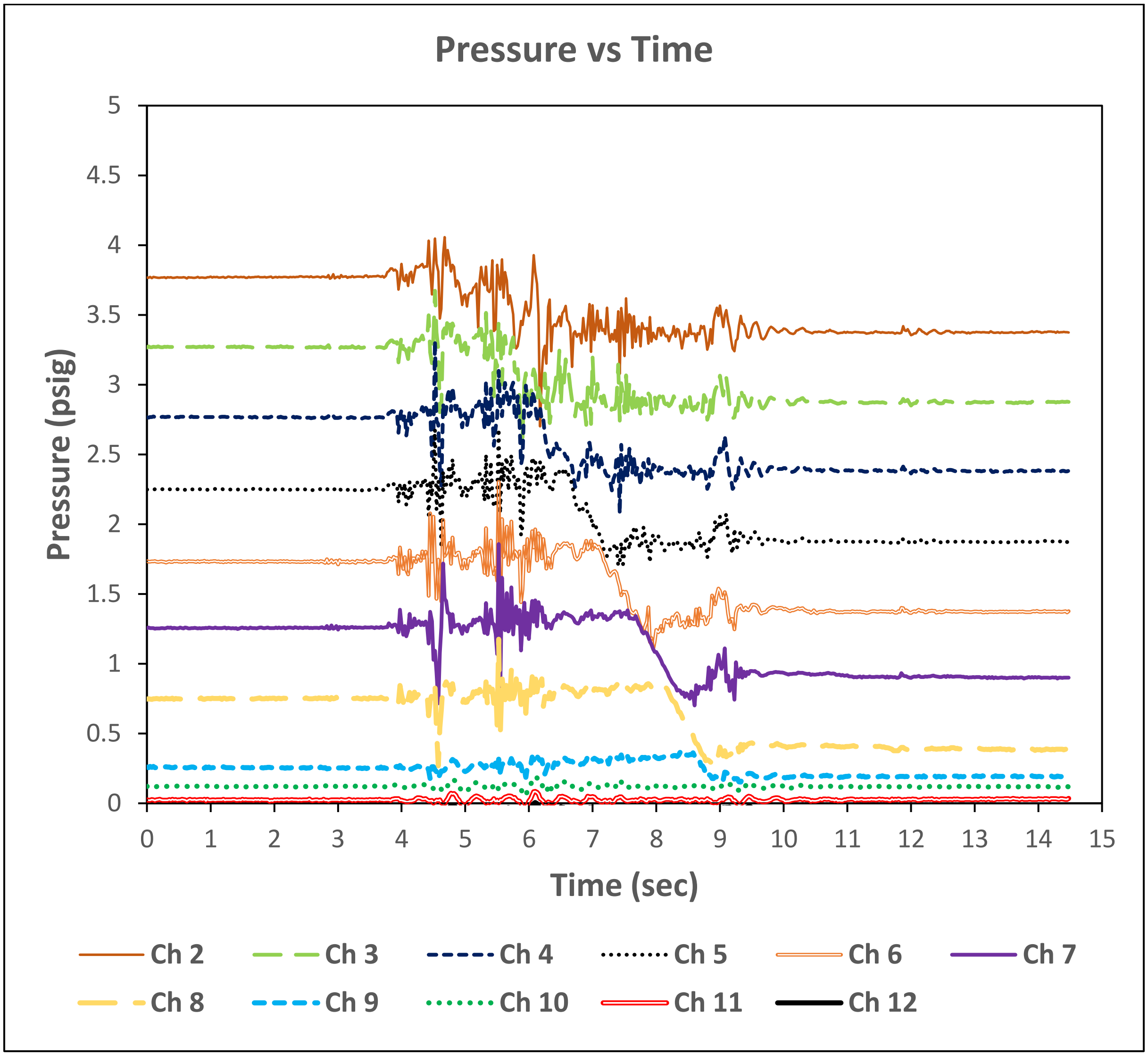

Figure 36: Pressure as a function of time for slurry experiment 1

Slurry obscures the movements of the air slug in the tube. The pressures as a function of time for Channels 2 to 9 are shown in Figure 36. The air pressure supplied to create a Taylor bubble in slurry was very low compared to both water and viscous gel experiments. This is because the proppant in slurry plugged up the injection fluid conduit and the ball-valve. We were only able to fill up the slurry above Channel 9. This explains why the overall pressure magnitude is less than 4 psi. The pressure shown in Channel 10 is due to trapped pressure from proppant plugging the gauge conduit.

Figure 37 shows the pressure and bubble length versus time for Channel 4. Instability in the length calculated from 4 – 6 sec duration, is due to the pressure oscillations from the main valve opening. The dashed line represents the bubble nose entering Channel 4 and the start of pressure drop. As the bubble moves up and increasing its length, there is a continuous drop in the recorded pressure. The lesser wake region gives less erratic calculated lengths, than with water. The pressure and length of the bubble for Channels 5, 6, and 7 are shown in Figure 38.

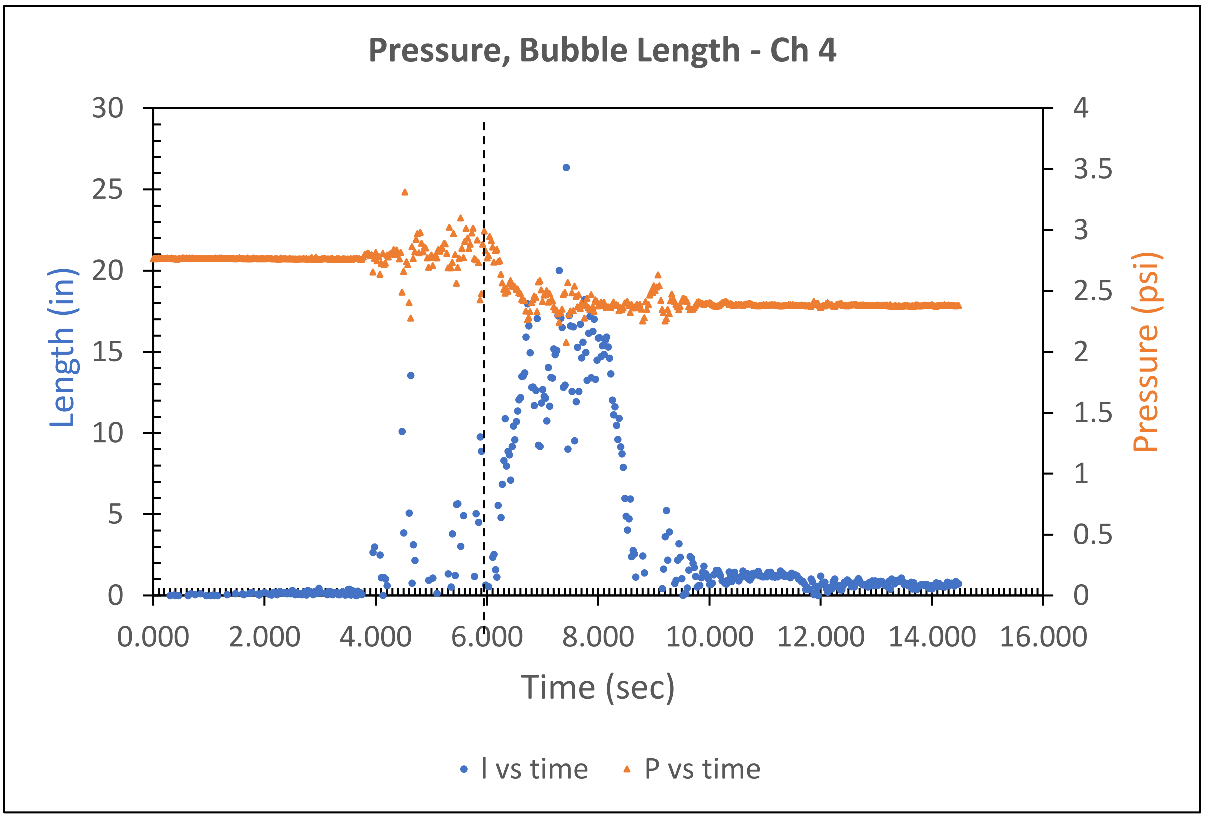

Figure 37: Pressure and bubble length as a function of time for channel 4

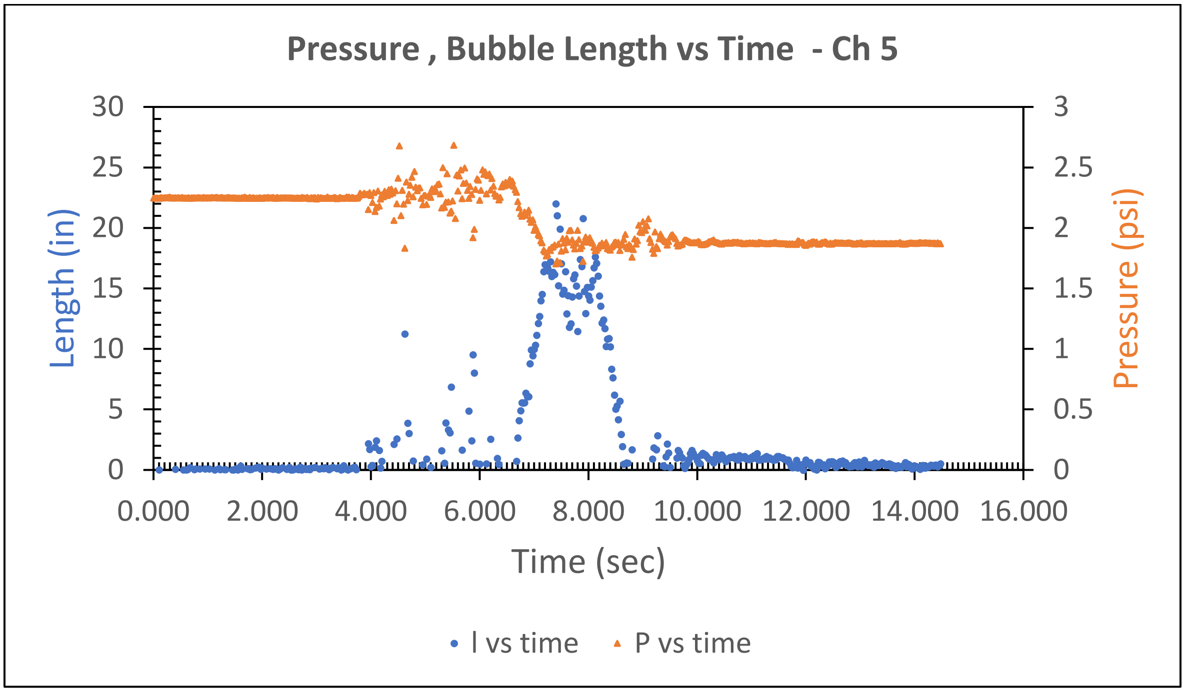

Pressure , Bubble Length vs Time - Ch 5
Length (in)
Pressure (psi)
Time (sec)
0.000
2.000
4.000
6.000
8.000
10.000
12.000
14.000
16.000
30
25
20
15
10
5
0
3
2.5
2
1.5
1
0.5
0
l vs time
P vs time

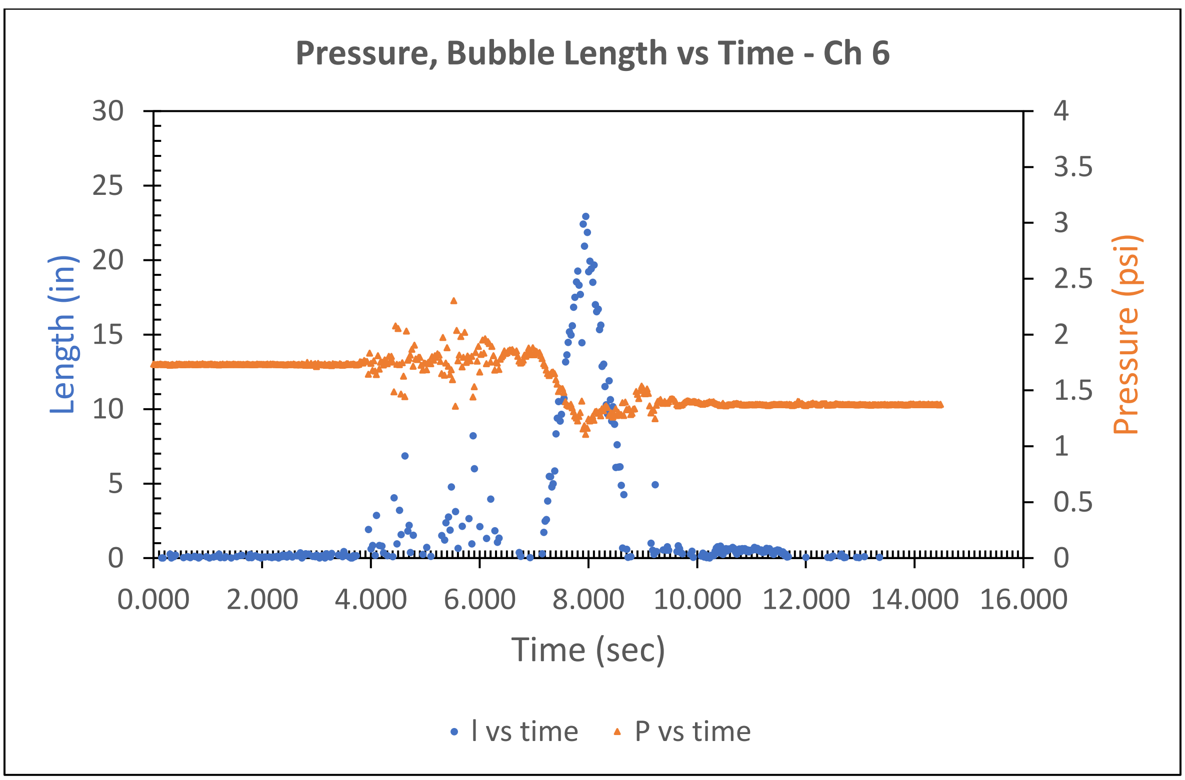

Pressure, Bubble Length vs Time - Ch 6
Length (in)
Pressure (psi)
Time (sec)
0.000
2.000
4.000
6.000
8.000
10.000
12.000
14.000
16.000
30
25
20
15
10
5
0
4
3.5
3
2.5
2
1.5
1
0.5
0
l vs time
P vs time

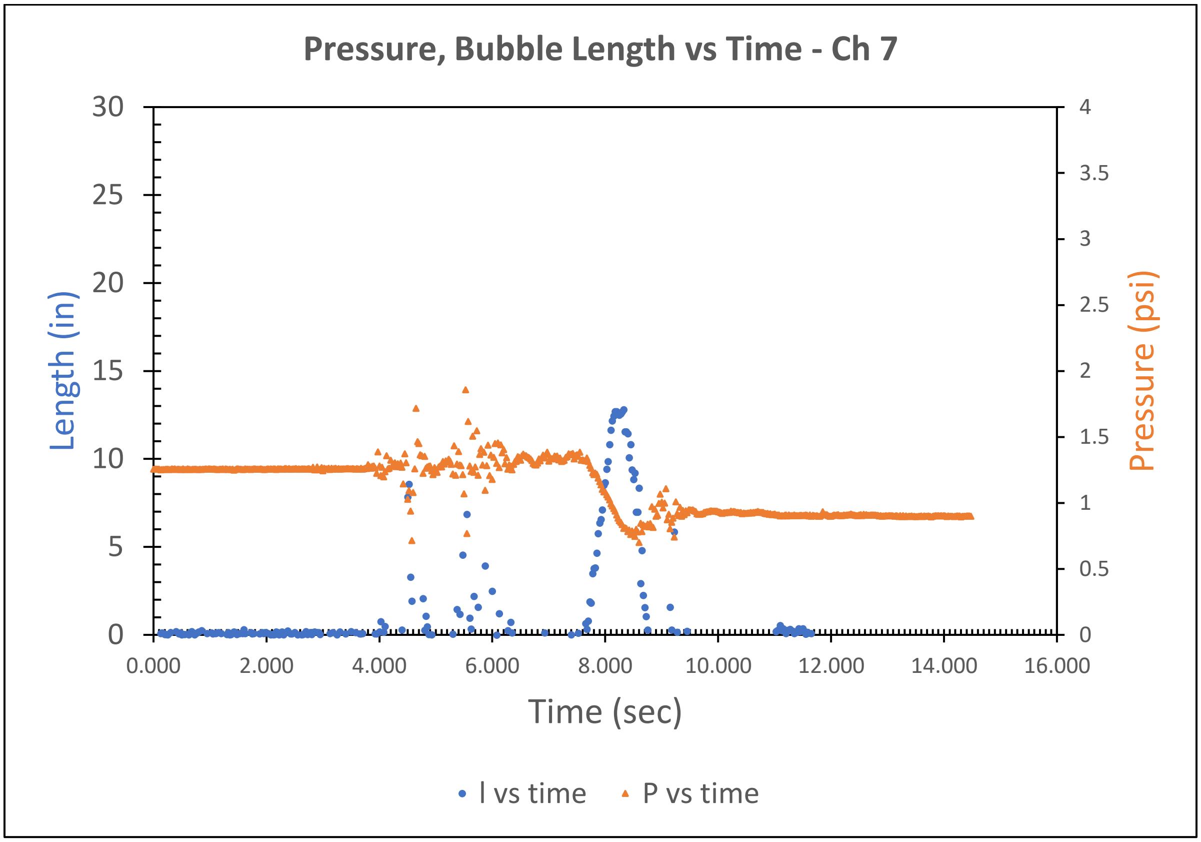

Figure 38: Pressure and bubble length as a function of time for channels 5 - 7

Figure 39 compares the bubble length calculated for Channels 4 to 7. With slurry, there are lesser dynamic effects due to viscosity. The bubble nose entering time for respective channels is noted down to calculate bubble rising velocity.

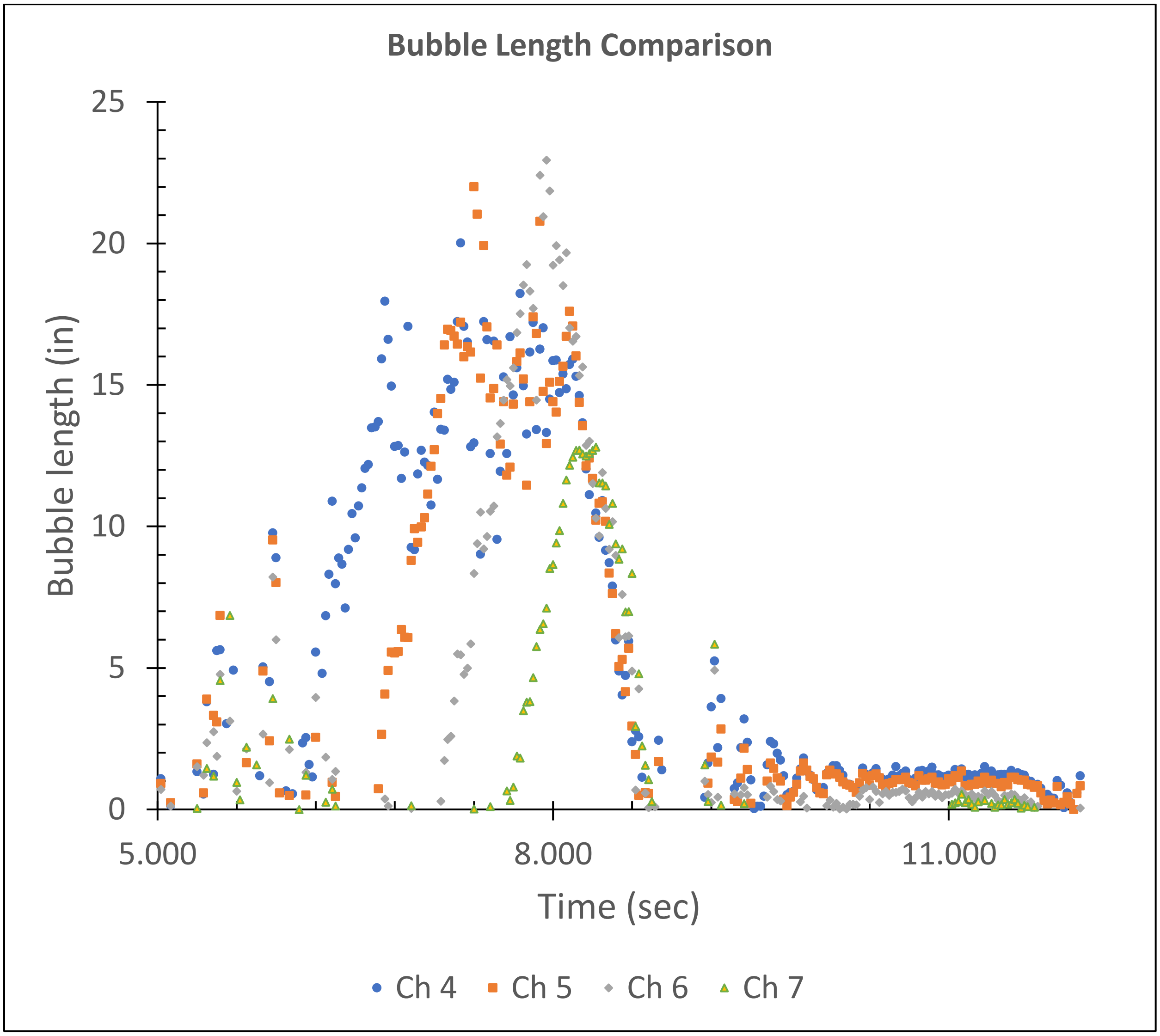

Figure 39: Comparison of bubble length as a function of time for channels 4 – 7

Bubble rising velocity:

Just like the previous 2 experiments in Chapters 4 and 5, for a given channel, the time when the bubble length starts increasing continuously from zero represents a bubble entering the channel. Given the distance between 2 consecutive channels is 1 ft, the bubble rising velocity is simply 1 over the time differences of the bubble entering in 2 consecutive channels. Table 23 summarizes the calculated bubble rising velocity for Channels 5 to 7.

Table 23: Bubble rising velocity for slurry experiment 1

Channel No	Time (sec)	Δ Time (sec)	Bubble rising velocity (ft/sec)
4	6.025	-	-
5	6.675	0.650	1.530
6	7.150	0.475	2.105
7	7.625	0.475	2.105

The comparison of the pressure plots for water – air, viscous gel – air and slurry – air experiments can be seen in the Figure 40.

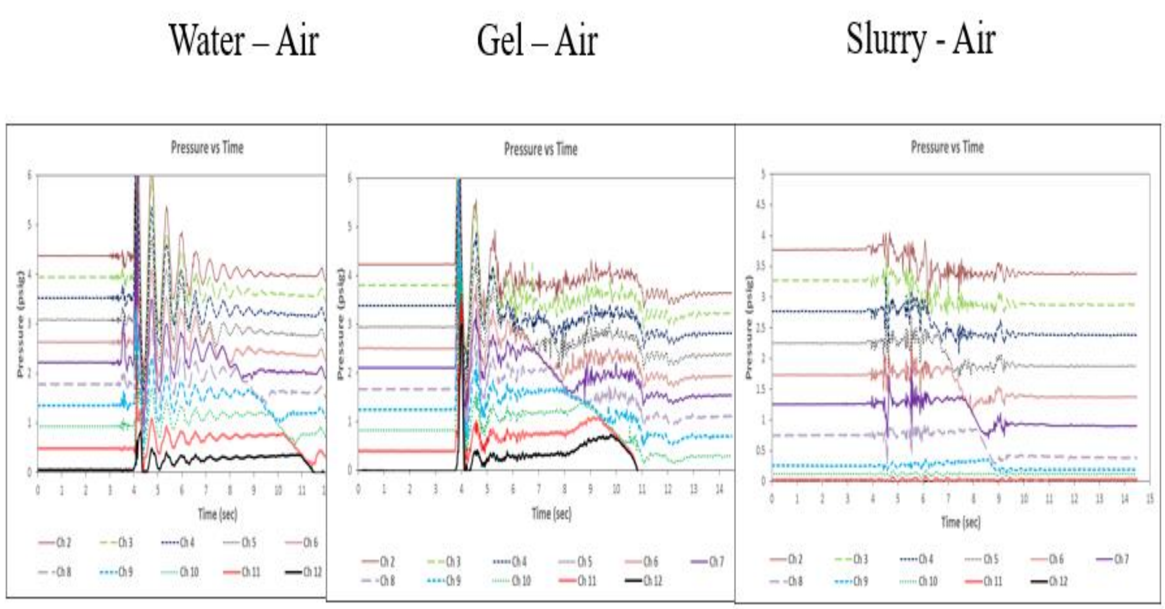

Figure 40: Comparison of pressure responses from water, viscous gel, slurry - air tests

The pressure versus time plots for air slug in water, viscous gel, and slurry tested showed some common and different patterns that reveal some insights of air slug in riser:

- We see a general trend of pressure increase versus time following the entrance of air slug into the riser tube and as the slug travels toward the open ended top. The mechanism is as the bubble rises, it displaces some liquid ahead of the bubble's nose and raises the liquid level. At the same time a partial amount of liquid is travelling down through the film region around the bubble. The relative proportion of liquid displaced ahead of the bubble's nose and flowing around the liquid films would depend on the fluid viscosity and the liquid film thickness.
- Comparing responses from the 3 liquids, we can see the viscous gel data show a sudden increase of pressure for 3 closest channels near the open top end.

6.3 Experiment 2:

The test conditions used for experiment are tabulated below in Table 24. The pressure plot is shown in Figure 41.

Table 24 : Test conditions for slurry experiment 2

S. No	Parameters	
1	Slurry level in the riser	101 inches
2	Pressure applied to the air pocket	4.5 psig
3	Length of the air pocket	11.5625 inches

Table 25: Bubble rising velocity for slurry experiment 2

Channel No	Time (sec)	Δ Time (sec)	Bubble rising velocity (ft/sec)
4	6.625	-	-
5	7.325	0.700	1.428
6	7.825	0.500	2.000
7	8.300	0.475	2.105

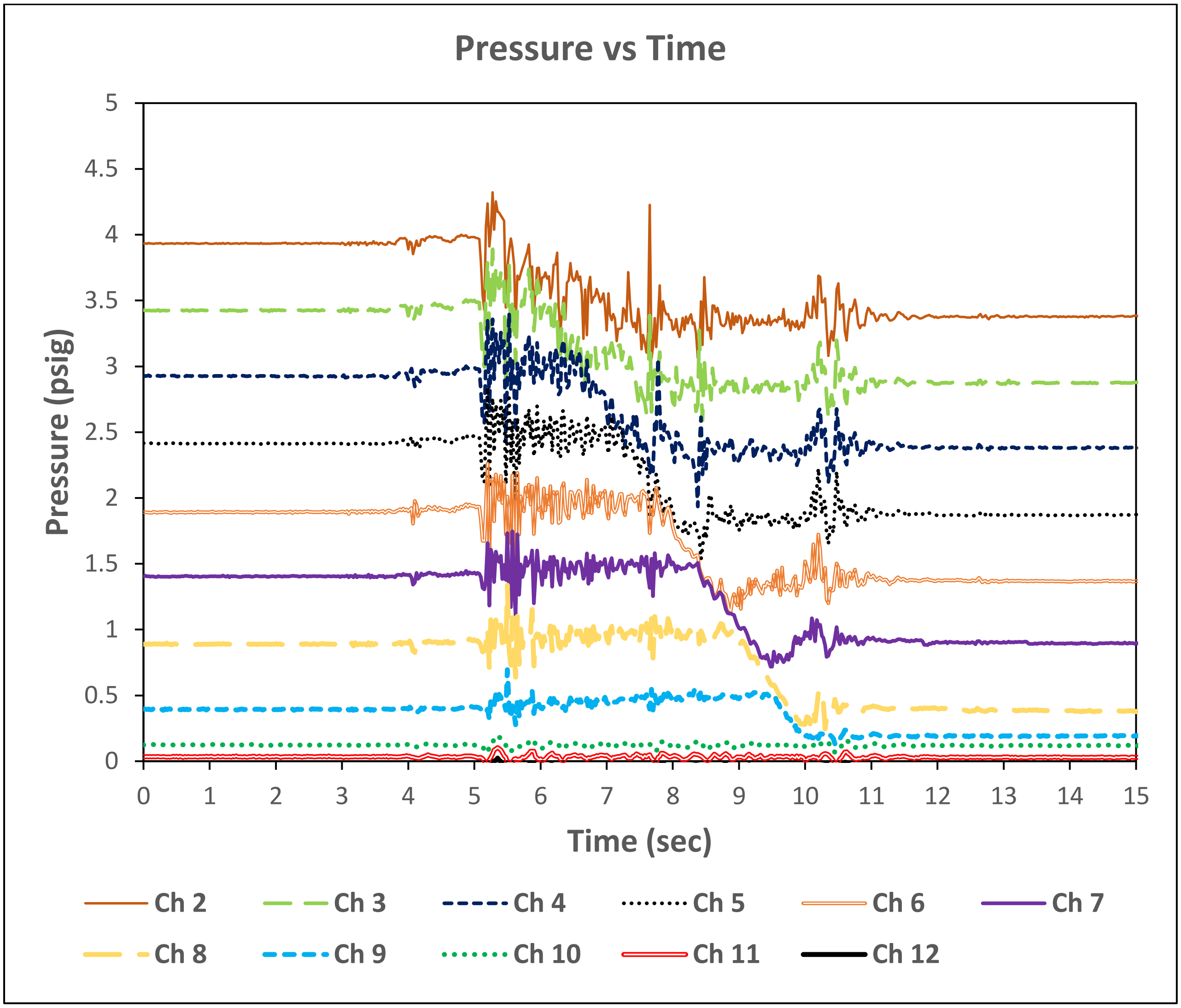

Figure 41: Pressure as a function of time for slurry experiment 2

Plots of bubble length as a function of time for different channels, comparison of pressure and bubble length as a function of time are shown in Appendix D.

6.4 Experiment 3:

The test conditions used for experiment are tabulated below in Table 26. The pressure plot is shown in Figure 42.

Table 26 : Test conditions for slurry experiment 3

S. No	Parameters	
1	Slurry level in the riser	108 inches
2	Pressure applied to the air pocket	5 psig
3	Length of the air pocket	18.5 inches

Table 27: Bubble rising velocity for slurry experiment 3

Channel No	Time (sec)	Δ Time (sec)	Bubble rising velocity (ft/sec)
4	5.725	-	
5	6.225	0.500	2.000
6	6.775	0.550	1.818
7	7.425	0.650	1.538

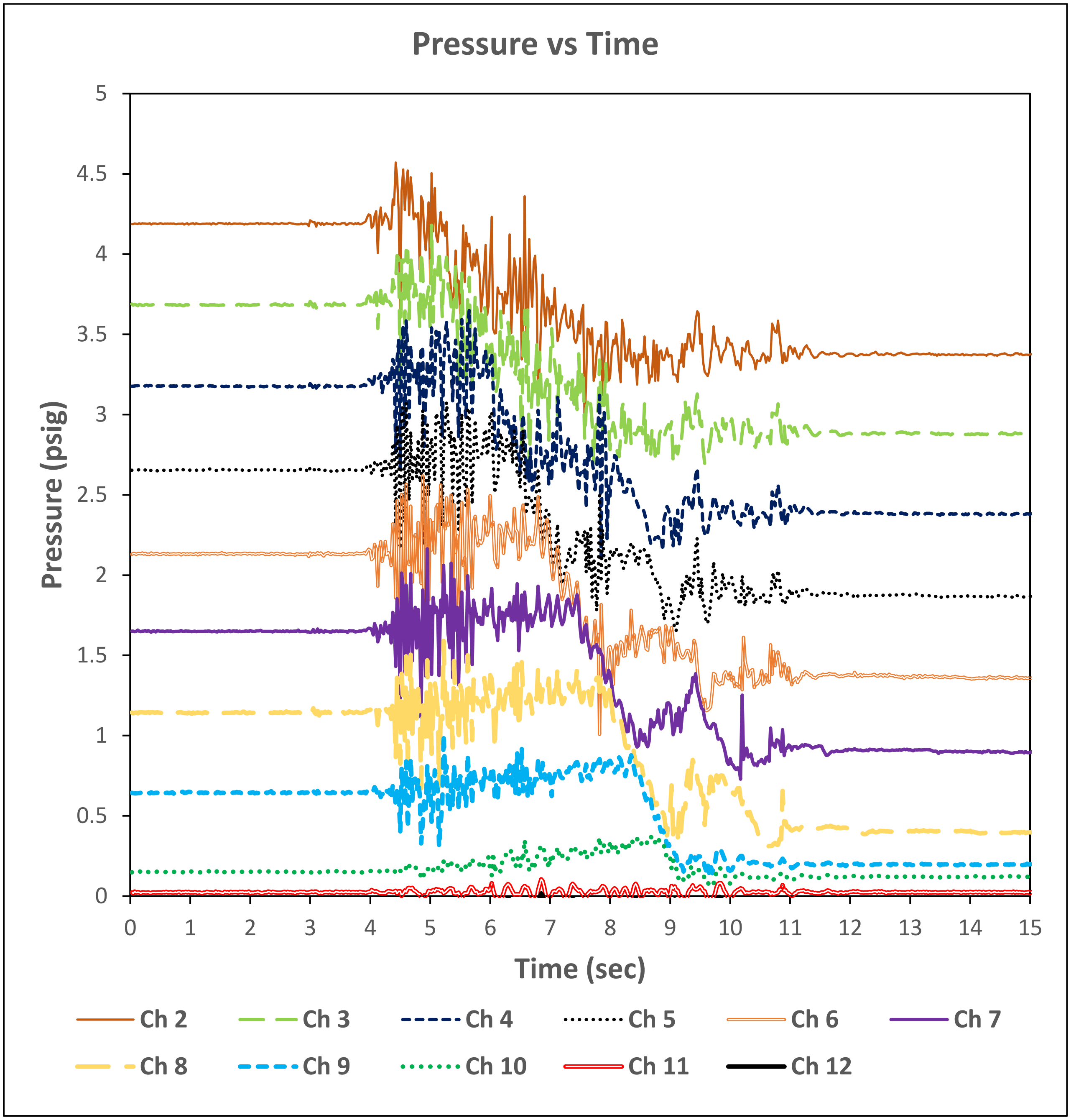

Figure 42: Pressure as a function of time for slurry experiment 3

Plots of bubble length as a function of time for different channels, comparison of pressure and bubble length as a function of time are shown in Appendix D.

6.5 Experiment 4:

The test conditions used for experiment are tabulated below in Table 28. The pressure plot is shown in Figure 43.

Table 28 : Test conditions for slurry experiment 4

S. No	Parameters	
1	Slurry level in the riser	126.5 inches
2	Pressure applied to the air pocket	5.5 psig
3	Length of the air pocket	42.5 inches

Table 29: Bubble rising velocity for slurry experiment 4

Channel No	Time (sec)	Δ Time (sec)	Bubble rising velocity (ft/sec)
6	7.125	-	-
7	8.050	0.925	1.081
8	8.750	0.700	1.428
9	9.375	0.625	1.600

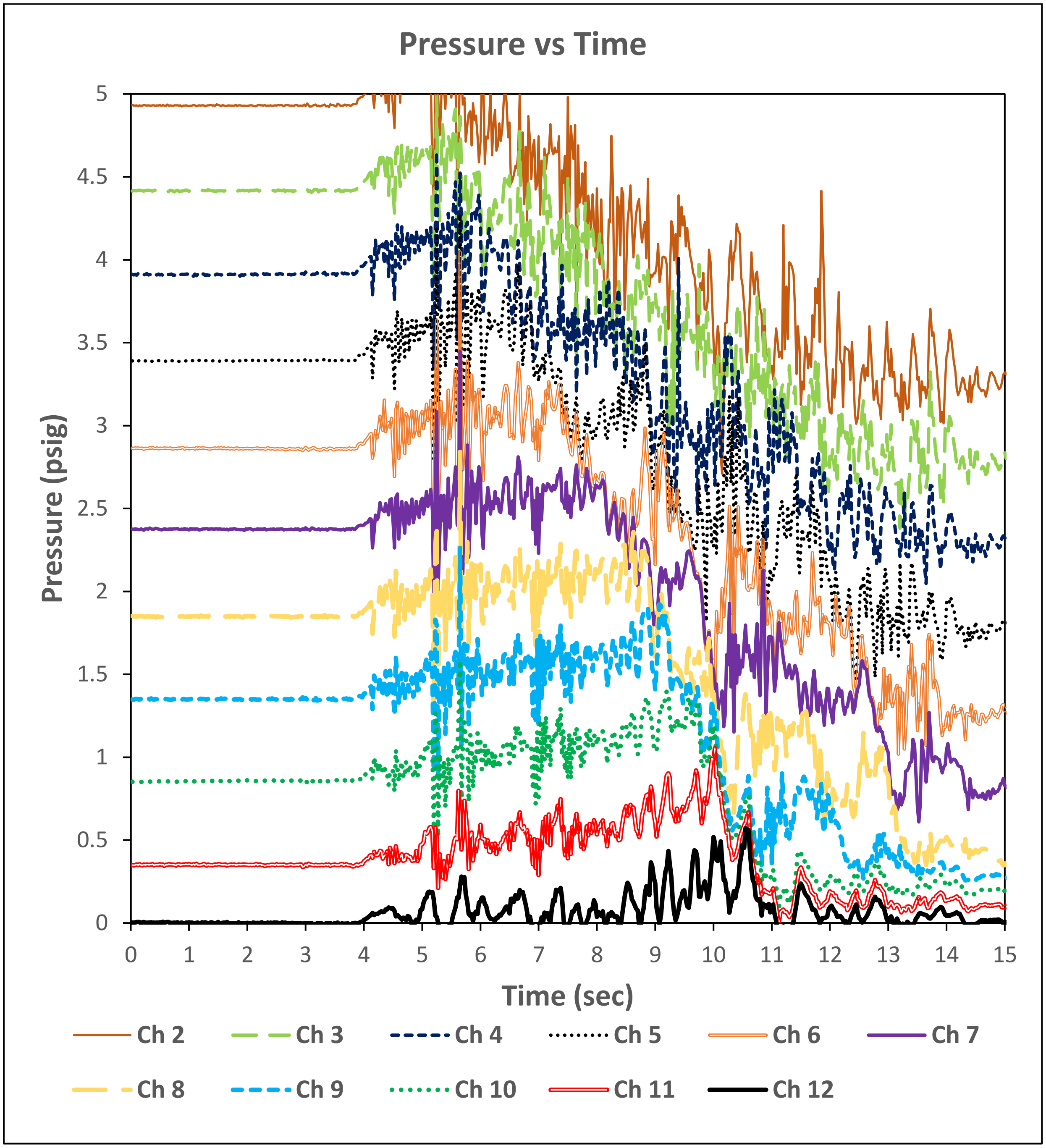

Figure 43: Pressure as a function of time for slurry experiment 4

Plots of bubble length as a function of time for different channels, comparison of pressure and bubble length as a function of time are shown in Appendix D.

7. Conclusions

This study designed and conducted a series of experiments with air slug or Taylor bubble rising in a vertical tube and in a stagnant column of 3 different liquids with the top open to atmospheric pressure. We completed tests with air slug in three different fluids: (a) water, (b) viscous shear-thinning gel made with 0.75% (by weight) concentration of Xanthan Gum, and (c) slurry of ceramic proppant with Xanthan Gum gel. We selected Xanthan Gum gel and the proppant slurry to emulate the shear thinning fluid properties and effects of solids in drilling mud, respectively.

Experimental results showed, as the bubble rises in the tube, the bubble expands due to the gradually decreasing hydrostatic pressure in the column. Air slug-water tests showed the bubble rising velocity and bubble length were comparable to results in open literature. The absolute bubble rising velocity (representing a top end that is closed) from our tests was 1.425 ft/sec as compared to 1.439 ft/sec from the open literature. The slug traveling velocities were 1.74, 1.38, and 1.73 ft/s for a distance from the open top end of 3.13, 2.125, and 1.125 ft, respectively. Bubble lengths interpreted from video cameras and pressure data, measured along the height of the riser tube, were consistent and complementary. Based on air bubble-water results, we established and verified a method to calculate bubble rising velocity and bubble length using only pressure data and without video camera data. This method is useful when air slugs in liquid media that are not visible.

Air slug-viscous gel tests showed the gel rising level was higher than the water tests. The pressure response from Channels 10 to 12, (2 ft away from the top) showed a sudden rise in liquid's level or pressure increase when the bubble's nose is 3 ft from the top. The cause of this pressure behavior is not understood. It could be a combination of large viscosity changes (~100 to 1000 cp) in the low shear rate range of 2 to 4 sec^{-1} for this shear thinning gel. Two other experiments showed similar pressure behaviors. The application of pressure method calculated longer bubble lengths because of the higher gel viscosity resulting to a thicker liquid film.

Air bubble-slurry tests calculated slower bubble rising velocity and similar bubble length to that of air bubble-water case. We did not find data of Taylor bubble in slurry fluids in the literature for comparison. We had difficulties with slurry tests due to proppant plugging the ball-valve and pressure gauges.

8. Recommendations

The pressure method uses a cylinder to model the air slug and to calculate bubble length. Adding a nose cap of curve geometry to the cylinder would improve the model's results. The liquid film thickness is very sensitive to fluid viscosity. For shear thinning fluids the viscosity is shear rate sensitive which is affected by the bubble rising velocity. Modifying the pressure method with a variable liquid film thickness as a function of shear rate can improve the bubble length calculations for shear thinning fluids. Consider and evaluate the potential of extending the pressure method to calculate the rate of bubble expansion. To better understand the bubble rising mechanisms in the annulus region between the drill pipe and riser geometry, run tests with concentric pipe inside the existing riser tube.

The physical action of opening the main valve to introduce the air slug into the riser tube causes a pressure surge that disrupts the formation of a clean air bubble and induces pressure oscillations. These complications affect the pressure analyses of the bubble velocity and bubble length. Possible modifications are to place the main valve in a horizontal section upstream and away from the vertical tube to reduce the pressure surge. Strengthening the riser–tube supporting frame with braces will increase structural rigidity; thereby decreasing the structural vibration during the experiments.

The opaque gel, slurry and mud obscure the movements of the air bubble. Applications of non-optical sensors such as acoustic and thermal can be used to complement pressure sensors. The Fann 35 viscometer used in this study doesn't provide low shear rate viscosities in the range of less than 10 reciprocal second needed in our experiments. Recommendation is to use Capillary Rheometer.

References

Abdulkadir, M., Hernandez-Perez, V., Lowndes, I. S., Azzopardi, B. J., & Dzomeku, S. (2014). Experimental study of the hydrodynamic behaviour of slug flow in a vertical riser. *Chemical Engineering Science*, *106*, 60–75. https://doi.org/10.1016/j.ces.2013.11.021

Ambrose, S. (2015). *Rise of Taylor Bubbles in Vertical Pipes*. (July)

Amirnia, S., de Bruyn, J. R., Bergougnou, M. A., & Margaritis, A. (2013). Continuous rise velocity of air bubbles in non-Newtonian biopolymer solutions. *Chemical Engineering Science*, *94*, 60–68. https://doi.org/10.1016/j.ces.2013.02.032

Anfinsen, B. T., & Rommetveit, R. (1992). Sensitivity of early kick detection parameters in full-scale gas kick experiments with oil- and water-based drilling muds. *Drilling Conference - Proceedings*, 775–782. https://doi.org/10.2523/23934-ms

Araújo, J. D. P., Miranda, J. M., Pinto, A. M. F. R., & Campos, J. B. L. M. (2012). Wide-ranging survey on the laminar flow of individual Taylor bubbles rising through stagnant Newtonian liquids. *International Journal of Multiphase Flow*, *43*, 131–148. https://doi.org/10.1016/j.ijmultiphaseflow.2012.03.007

Azevedo, Marcos B De, & Su, J. (2015). *Experimental Study of Single Taylor Bubbles Rising in Stagnant Liquid Mixtures Inside of*.

Azevedo, Marcos Bertrand De, Andrade, P., & Vinhas, M. (2012). *Characterization of Velocity and Shape of Rising Bubbles in a Stagnant Liquid Vertical Column by Ultrasonic and Visualization Techniques*. (1943), 0–7.

Brown, R.A.S., (1965). The Mechanism of Large Bubbles in Tubes. I. Bubble Velocities in Stagnant

Liquids. Canadian Jornal of Chemical Engineering, 43, 217-223

Bureau, N., De Hemptinne, J. C., Audibert, A., & Herzhaft, B. (2002). Interactions between Drilling Fluid and Reservoir Fluid. *Proceedings - SPE Annual Technical Conference and Exhibition*, 1251–1262. https://doi.org/10.2523/77475-ms

Chen, H. Y., Weigert, E., Fedeyko, J., Cox, J., & Andersen, P. (2010). Advanced catalysts for combined (NAC + SCR) emission control systems. *SAE Technical Papers*, *1*(4), 220–224. https://doi.org/10.4271/2010-01-0302

Chhabra, R. P. (2010). Non-Newtonian fluids: An introduction. *Rheology of Complex Fluids*, 3–34. https://doi.org/10.1007/978-1-4419-6494-6_1

Davies, R. M. & Taylor, G. I. 1950 The mechanics of large bubbles rising through liquids in tubes. Proc. R. Soc. Lond. A 200, 375–390.

Dumitrescu, D. T. 1943 Stromung and Einer Luftbluse in Senkrechten rohr. Z. Angew. Math. Mech. 23(3), 139–149

De Oliveira Mendes, C. L., & Qassim, R. Y. (1984). Application of the Davies-Taylor equation to a large bubble rise in liquid-fluidized beds. *The Chemical Engineering Journal*, *28*(1), 21–23. https://doi.org/10.1016/0300-9467(84)85003-0

Falcone, G., & Teodoriu, C. (2008). Multiphase-Flow Modeling Based on Experimental Testing: An Overview of Research Facilities Worldwide and the Need for Future Developments. *SPE Projects, Facilities* (September), 11–14.

Ghobadi, M., & Muzychka, Y. S. (2015). Two-phase flow measurements under static and dynamic conditions for modeling the top kill process. *Journal of Petroleum Exploration and Production Technology*, *5*(3), 285–294. https://doi.org/10.1007/s13202-014-0133-y

Griffith, P. & Wallis, G. B. 1961 Two-phase slug flow. J. Heat Transfer 83, 307–320

Hassan, N. M. S., Khan, M. M. K., & Rasul, M. G. (2007). Bubble Rise Velocity and Drag Co-efficient at High Reynolds Number in Power-Law Fluids. *5th IASME / WSEAS International Conference on Fluid Mechanics and Aerodynamics, Athens, Greece*, 123–128.

Hassan, N. M. S., Khan, M. M. K., Rasul, M. G., & Rackemann, D. W. (2010). Bubble rise velocity and trajectory in xanthan gum crystal suspension. *Applied Rheology*, *20*(6), 65102. https://doi.org/10.3933/ApplRheol-20-65102

Hatta, N., Omodaka, M., Nakajima, F., Takatsu, T., Fujimoto, H., & Takuda, H. (1999). Predictable model for characteristics of onedimensional solid-gas-liquid three-phase mixtures flow along a vertical pipeline with an abrupt enlargement in diameter. *Journal of Fluids Engineering, Transactions of the ASME*, *121*(2), 330–342. https://doi.org/10.1115/1.2822211

James, M. R., Lane, S. J., & Corder, S. B. (2008). Modelling the rapid near-surface expansion of gas slugs in low-viscosity magmas. *Geological Society Special Publication*, *307*, 147–167. https://doi.org/10.1144/SP307.9

Johnson, A. B., & White, D. B. (1991). Gas-rise velocities during kicks. *SPE Drilling Engineering*, *6*(4), 257–263. https://doi.org/10.2118/20431-PA

Lao, L., Xing, L., & Yeung, H. (2012). Behaviours of elongated bubbles in a large diameter riser. *BHR Group - 8th North American Conference on Multiphase Technology*, (1998), 381–391.

Li, H., & Prakash, A. (2000). Influence of slurry concentrations on bubble population and their rise velocities in a three-phase slurry bubble column. *Powder Technology*, *113*(1–2), 158–167. https://doi.org/10.1016/S0032-5910(00)00228-X

Li, Hao, Sun, B., Gao, Y., Guo, Y., Zhao, X., Wang, J., & Wang, J. B. (2017). Study on rising velocity of methane bubble in deepwater wellbore during the shut-in period. *Society of Petroleum Engineers - SPE Abu Dhabi International Petroleum Exhibition and Conference 2017*, *2017-January*. https://doi.org/10.2118/188866-ms

Liao, Q., & Zhao, T. S. (2003). Modeling of Taylor bubble rising in a vertical mini noncircular channel filled with a stagnant liquid. *International Journal of Multiphase Flow*, *29*(3), 411–434. https://doi.org/10.1016/S0301-9322(03)00004-1

Lim, E., & Yao, J. (2009). Modeling and simulation of the polymeric nanocapsule formation process. *IFAC Proceedings Volumes (IFAC-PapersOnline)*, *7*(4), 405–410. https://doi.org/10.1002/aic

Lizarraga-Garcia, E., Buongiorno, J., Al-Safran, E., & Lakehal, D. (2017). A broadly-applicable unified closure relation for Taylor bubble rise velocity in pipes with stagnant liquid. *International Journal of Multiphase Flow*, *89*, 345–358. https://doi.org/10.1016/j.ijmultiphaseflow.2016.11.001

Llewellin, E. W., Del Bello, E., Taddeucci, J., Scarlato, P., & Lane, S. J. (2012). The thickness of the falling film of liquid around a Taylor bubble. *Proceedings of the Royal Society A: Mathematical, Physical and Engineering Sciences*, *468*(2140), 1041–1064. https://doi.org/10.1098/rspa.2011.0476

Lu, X., & Prosperetti, A. (2006). Axial stability of Taylor bubbles. *Journal of Fluid Mechanics*, *568*, 173–192. https://doi.org/10.1017/S0022112006002205

Luo, X., Zhang, J., Tsuchiya, K., & Fan, L. S. (1997). On the rise velocity of bubbles in liquid-solid suspensions at elevated pressure and temperature. *Chemical Engineering Science*, *52*(21–

22), 3693–3699. https://doi.org/10.1016/S0009-2509(97)00215-7

Massoud, E. Z., Xiao, Q., El-Gamal, H. A., & Teamah, M. A. (2018). Numerical study of an individual Taylor bubble rising through stagnant liquids under laminar flow regime. *Ocean Engineering*, *162*(April), 117–137. https://doi.org/10.1016/j.oceaneng.2018.04.096

Mulhem, B., Schulte, G., & Fritsching, U. (2006). Solid–liquid separation in suspension atomization. *Chemical Engineering Science*, *61*(8), 2582–2589. https://doi.org/10.1016/j.ces.2005.11.035

Neal Adams and Larry Kuhlman. (1994). Kicks and Blowout Control. Pennwell Corporation, 92 - 98

Nicklin, D. J., Wilkes, J. O. & Davidson, J. F. 1962 Two-phase flow in vertical tubes. Trans. Inst. Chem. Engrs 40, 61–68

Nogueira, S. (2005). *Flow around a single Taylor bubble rising through stagnant and co-current flowing newtonian liquids*.

R. M. Davies and G. I. Taylor, (1950) The mechanics of large bubbles rising through extended liquids and through liquids in tubes, Proc. R. Soc. London 200, 375 .

Rommetveit, R., & Olsen, T. L. (1989). Gas kick experiments in oil-based drilling muds in a full-scale, inclined research well. *Society of Petroleum Engineers of AIME, (Paper) SPE*, *DELTA*. https://doi.org/10.2523/19561-ms

Rommetveit, Rolv, & Blyberg, A. (1989). Simulation of gas kicks during oil well drilling. *Modeling, Identification and Control*, Vol. 10, pp. 213–225. https://doi.org/10.4173/mic.1989.4.3

Rulison, C., & Scientific, A. (n.d.). *The DuNouy Ring Method, Wilhelmy Plate Method, Pendant Drop Method, and Bubble Pressure Method for Surface Tension Measurement-a Comparison of Methods and Capabilities*.

Sabah, M., Ameri, M. J., & Sedigh, M. (2018). Natural bridging as a tertiary well control method in deep-water wells: A case study from Caspian Sea. *Journal of Petroleum Science and Engineering*, *169*(December 2017), 725–738. https://doi.org/10.1016/j.petrol.2018.06.018

Santos, L. M. T., & Coelho Pinheiro, M. N. (2014). Flow around individual Taylor bubbles rising in a vertical column with water: Effect of gas expansion. *International Journal of Multiphase Flow*, *63*, 39–51. https://doi.org/10.1016/j.ijmultiphaseflow.2014.03.003

Santos, L. M. T., Sena Esteves, M. T. M., & Coelho Pinheiro, M. N. (2008). Effect of gas expansion on the velocity of individual Taylor bubbles rising in vertical columns with water: Experimental studies at atmospheric pressure and under vacuum. *Chemical Engineering Science*, *63*(18), 4464–4474. https://doi.org/10.1016/j.ces.2008.06.018

Sharaf, S., van der Meulen, G. P., Agunlejika, E. O., & Azzopardi, B. J. (2016). Structures in gas-liquid churn flow in a large diameter vertical pipe. *International Journal of Multiphase Flow*, *78*, 88–103. https://doi.org/10.1016/j.ijmultiphaseflow.2015.09.005

Silva, C. T., Mariolani, J. R. L., Bonet, E. J., Lomba, R. F. T., Santos, O. L. A., & Ribeiro, P. R. (2004). Gas solubility in synthetic fluids: A well control issue. *Proceedings - SPE Annual Technical Conference and Exhibition*, (C), 4631–4636. https://doi.org/10.2523/91009-ms

Sobieszuk, P., Cygański, P., & Pohorecki, R. (2010). Bubble lengths in the gas-liquid Taylor flow in microchannels. *Chemical Engineering Research and Design*, *88*(3), 263–269. https://doi.org/10.1016/j.cherd.2009.07.007

Sousa, R.G., Riethmuller, M.L., Pinto, A.M.F.R., Campos, J.B.L.M. (2005). Flow around individual Taylor bubbles rising in stagnant CMC solutions: PIV measurements. Chem. Eng. Sci. 60, 1859–1873.

Sousa, R. G., Pinto, A. M. F. R., & Campos, J. B. L. M. (2006). Effect of gas expansion on the velocity of a Taylor bubble: PIV measurements. *International Journal of Multiphase Flow*, *32*(10–11), 1182–1190. https://doi.org/10.1016/j.ijmultiphaseflow.2006.06.002

Sousa, R. G., Pinto, A. M. F. R., & Campos, J. B. L. M. (2007). Interaction between Taylor bubbles rising in stagnant non-Newtonian fluids. *International Journal of Multiphase Flow*, *33*(9), 970–986. https://doi.org/10.1016/j.ijmultiphaseflow.2007.03.009

Strauß, M., McNamara, S., Herrmann, H. J., Niederreiter, G., & Sommer, K. (2006). Plug conveying in a vertical tube. *Powder Technology*, *162*(1), 16–26. https://doi.org/10.1016/j.powtec.2005.10.006

Tarvin, J. A., Hamilton, A. P., Gaynord, P. J., & Lindsay, G. D. (1994). Gas Rises Rapidly Through Drilling Mud. *Drilling Conference - Proceedings*, 637–649. https://doi.org/10.2523/27499-ms

Thomas D. G. (1965). Transport characteristics of suspension: Viii. a note on the viscosity of Newtonian suspensions of uniform spherical particles, J. Colloid Sci., 20, 267–277

Toskey, E. D. (2015). Kick detection at the subsea mudline. *Proceedings of the Annual Offshore Technology Conference*, *3*(May), 2297–2306. https://doi.org/10.4043/25847-ms

Tsuchiya, K., Furumoto, A., Fan, L. S., & Zhang, J. (1997). Suspension viscosity and bubble rise velocity in liquid-solid fluidized beds. *Chemical Engineering Science*, *52*(18), 3053–3066. https://doi.org/10.1016/S0009-2509(97)00127-9

Tudose, E. T., & Kawaji, M. (1999). Experimental investigation of Taylor bubble acceleration mechanism in slug flow. *Chemical Engineering Science*, *54*(23), 5761–5775. https://doi.org/10.1016/S0009-2509(99)00149-9

Vandu, C. O., Koop, K., & Krishna, R. (2004). Large bubble sizes and rise velocities in a bubble column slurry reactor. *Chemical Engineering and Technology*, *27*(11), 1195–1199. https://doi.org/10.1002/ceat.200402126

Velmurugan, N., Godhavn, J. M., & Hauge, E. (2016). Dynamic simulation of gas migration in marine risers. *Society of Petroleum Engineers - SPE Bergen One Day Seminar*, (June). https://doi.org/10.2118/180022-ms

Viana, F., Pardo, R., Yánez, R., Trallero, J. L., & Joseph, D. D. (2003). Universal correlation for the rise velocity of long gas bubbles in round pipes. *Journal of Fluid Mechanics*, *494*(494), 379–398. https://doi.org/10.1017/S0022112003006165

Wallis, G. B. 1969 One Dimensional Two-phase Flow, Chaps. 9 and 10. McGraw-Hill

White, E. T. &Beardmore, R. H. 1962 The velocity of rise of single cylindrical air bubbles through liquids contained in vertical tubes. Chem. Engng Sci. 17, 351–361

Yong Bai and Qiang Bai. (2018). Subsea Engineering Handbook, Second Edition, Gulf Professional Publishing

Yuan, Z., Morrell, D., Sonnemann, P., & Leach, C. (2016). Mitigating gas in riser rapid unloading for deepwater dual gradient well control. *Proceedings of the Annual Offshore Technology Conference*, *5*(November 2016), 4026–4038. https://doi.org/10.2118/185179-pa

Zhou, G., & Prosperetti, A. (2019). Violent expansion of a rising Taylor bubble. *Physical Review Fluids*, *4*(7), 1–20. https://doi.org/10.1103/physrevfluids.4.073903

Zhou, Y., Wojtanowicz, A. K., Li, X., Miao, Y., & Chen, Y. (2018). Improved model for gas migration velocity of stagnant non-Newtonian fluids in annulus. *Journal of Petroleum Science and Engineering*, *168*(May), 190–200. https://doi.org/10.1016/j.petrol.2018.05.025

Drilling rig explosion and fire at the Macondo well. Investigation Report 2010-10-I-OS. U.S. Chemical Safety and Hazard Investigation Board (2016).

Appendix

Appendix A

Calibration:

Instacal software by Omega Engineering Inc. was used to calibrate the data acquisition hardware system before the actual equipment calibration. InstaCal is a comprehensive software utility for installing, configuring, and testing Omega Engineering DAQ devices and discussed in the coming section.

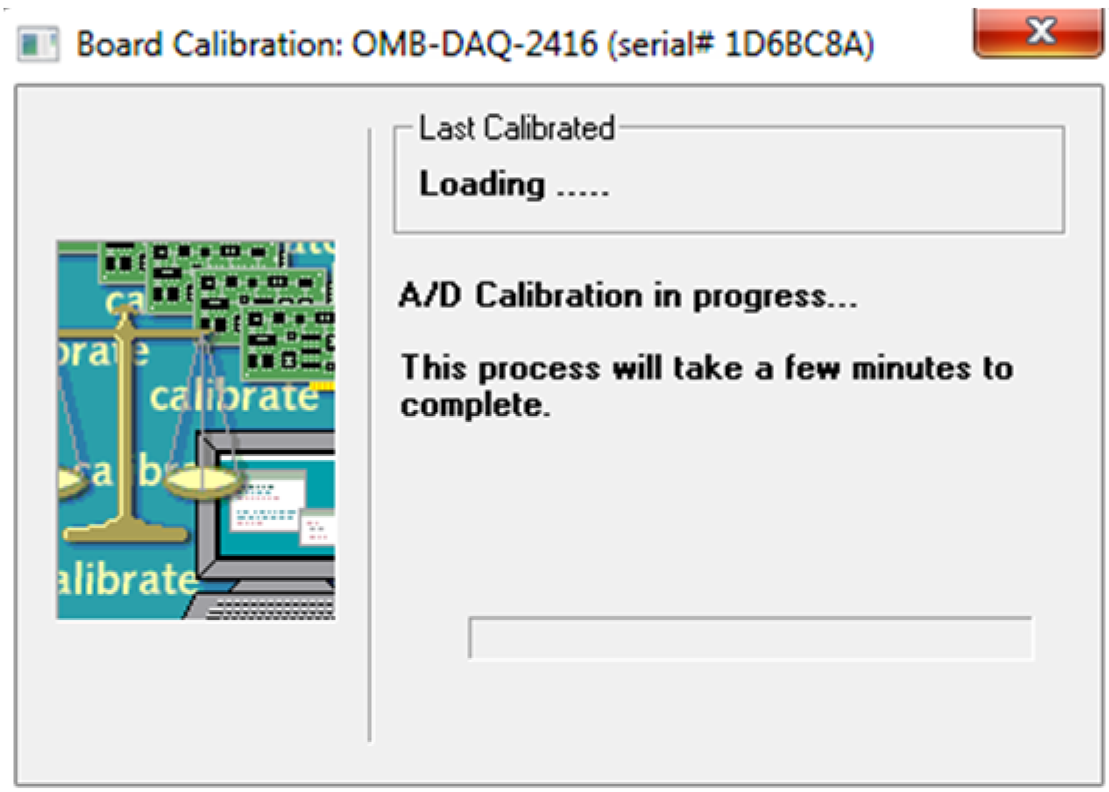

The operational calibration procedure has been followed to establish a relationship between the output voltage reading and its corresponding pressure value before every experimental run.

The main valve should be in open position so that the pressure induced through the air compressor pressurizes the column all the way through its top. Five set of steps were followed throughout the calibration procedure. In the first step, the vent valve is open to atmosphere and the pressure gauge reading was noted. The data collection system DAQ PRO was used to capture voltage and time data. In the next steps, the vent valve is closed to atmosphere and 1 psi gauge pressure was supplied each time in subsequent steps to capture the voltage data. Once the data was captured, pressure vs voltage graphs were plotted to establish a relation between voltage and pressure for every channel, which were used further in the experimental data analysis.

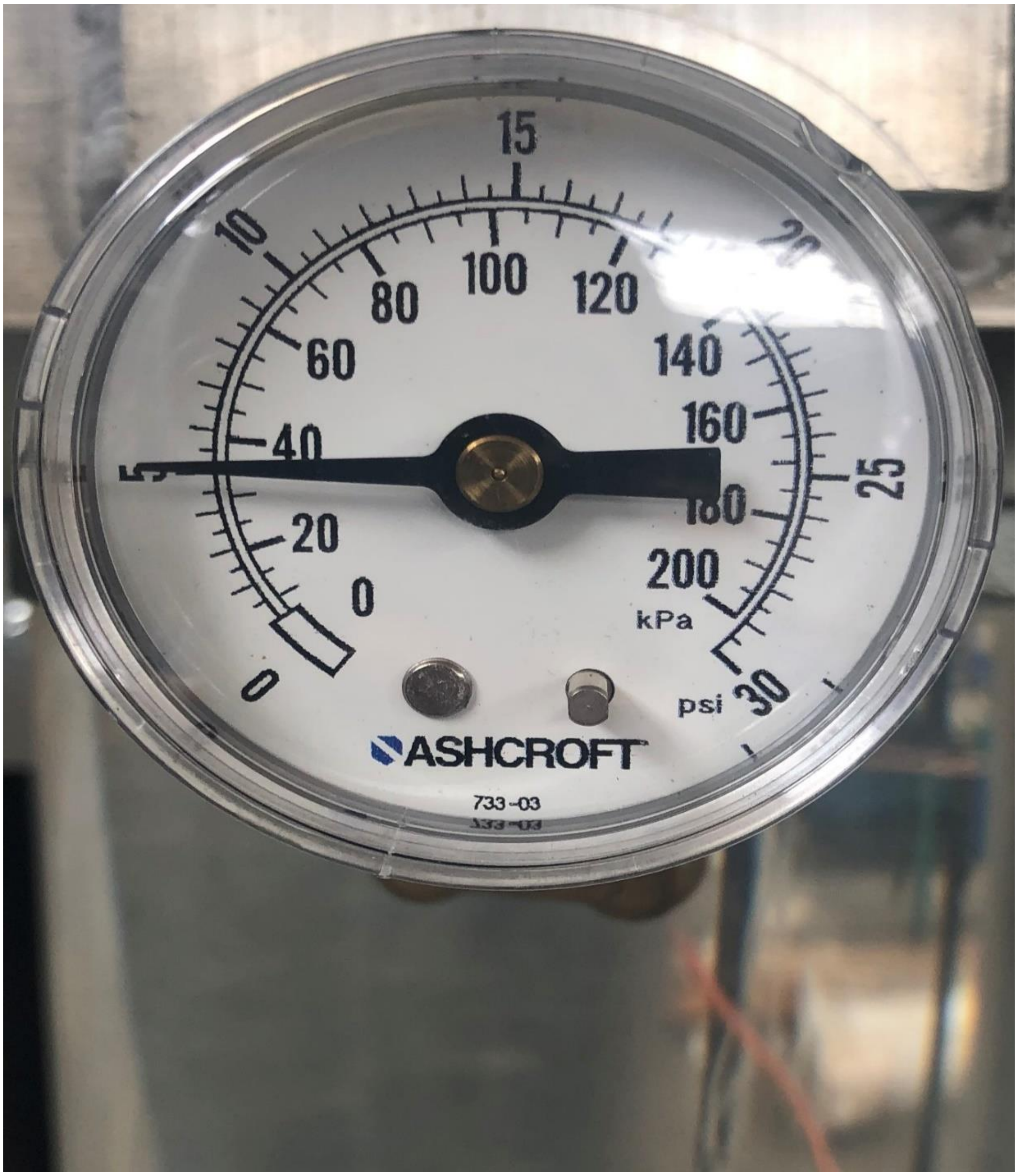

Pressure gauge used for calibration and experiment

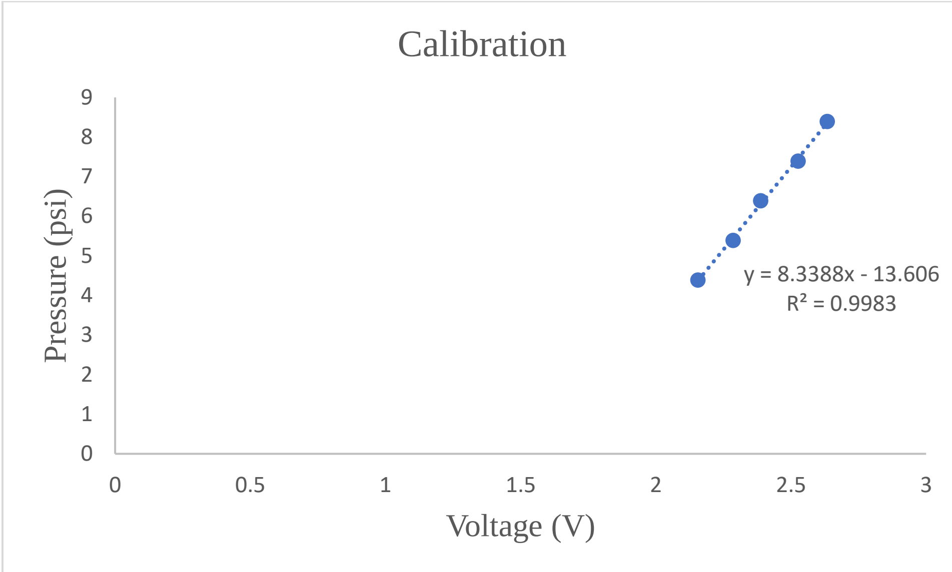

Sample calibration plot

For instance, pressure and voltage for the above channel shown in the above figure are related by, Pressure = (8.3388 * Voltage) – 13.606 and this relation established will be used in the further experimental calculations.

InstaCal can also calibrate Omega Engineering devices that support field calibration. . InstaCal is an easy to use installation, calibration and test utility for our data acquisition hardware. When measurement computing hardware is plugged in, InstaCal detects the hardware and assigns resources automatically. We may set special features of the hardware so that software programs run as we wish. All the settings are stored in a configuration file. InstaCal can calibrate the analog input or output channels for devices that support field calibration. Select the device in the InstaCal main screen and select Calibrate»A/D (to calibrate analog inputs) or Calibrate»D/A (to calibrate analog outputs) to open . InstaCal provides analog and digital tests to determine if the analog inputs and digital bits are working properly.

Analog Loopback Test tab was used to verify the analog connections and that the basic analog measurement operation is working properly as shown below. Loop back one of the onboard signals or use an external signal to test one channel at a time in a slow (non-clocked) sampling mode.

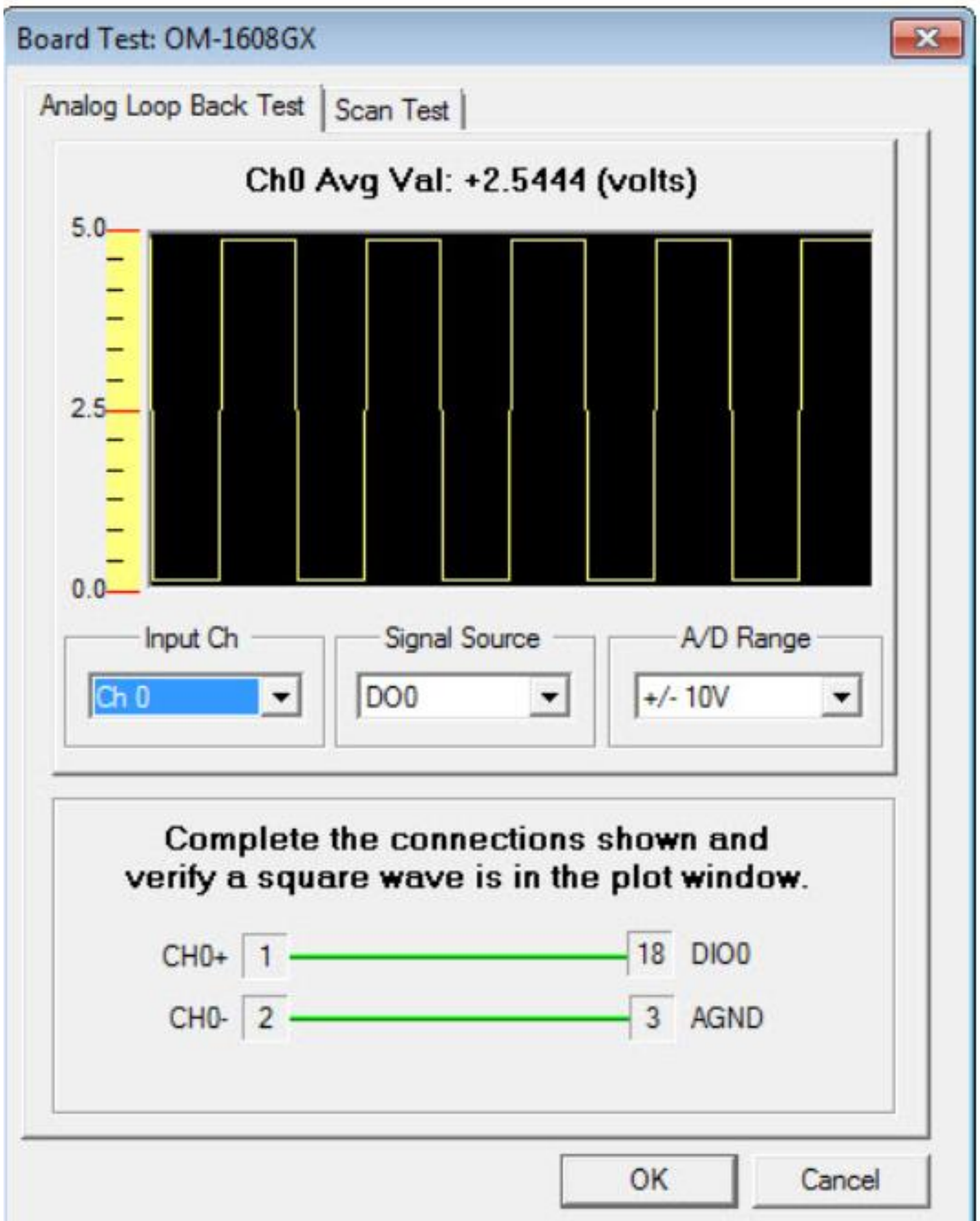

Analog loop back test

Scan Test tab was used to sample multiple channels simultaneously at a specified clock rate, and to test the DMA and IRQ resources assigned to the device which is shown below. Acquired data can be displayed graphically or numerically.

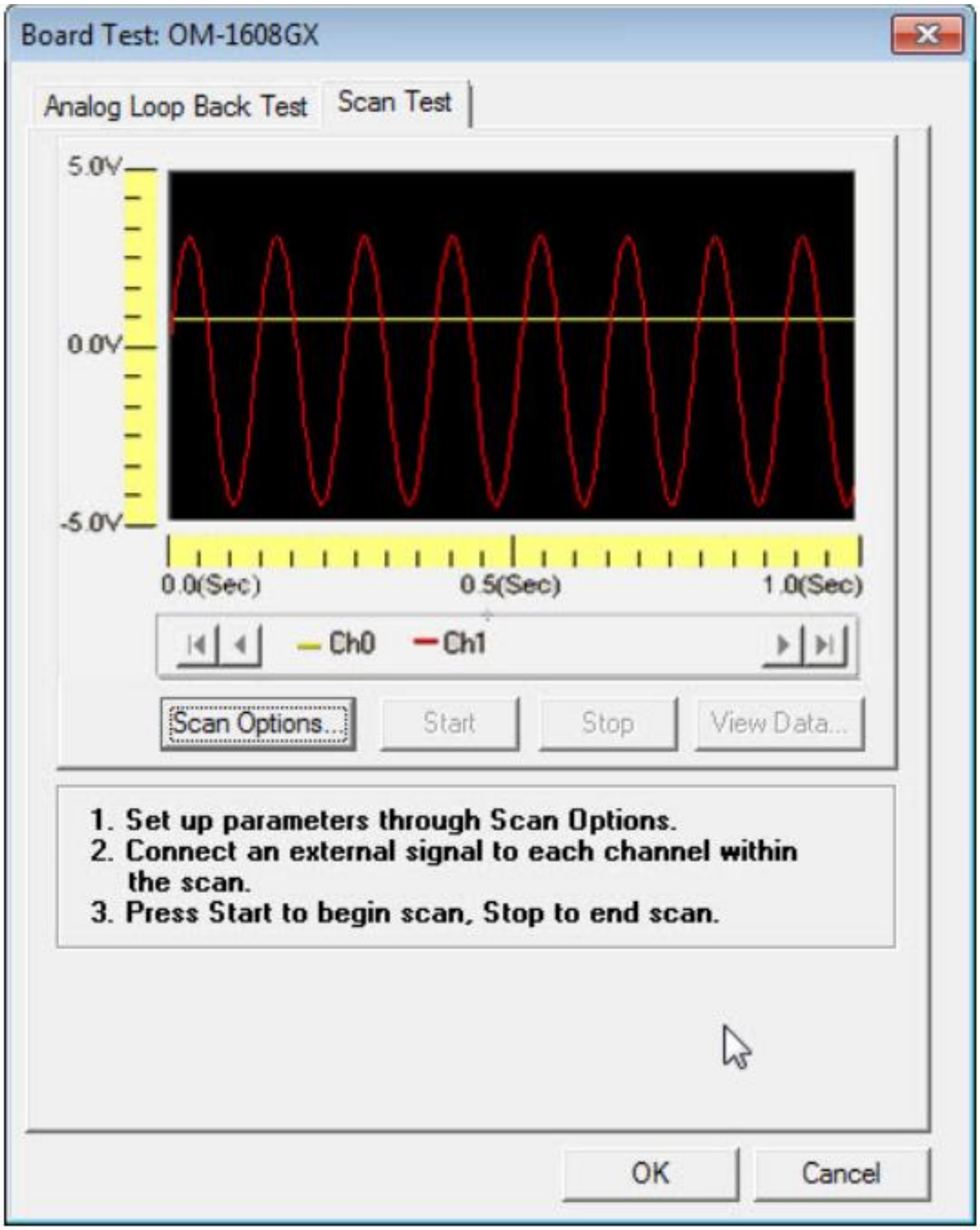

Figure: Scan test

InstaCal stores hardware configuration settings in a configuration file. This file may be shared and read by other Omega Engineering DAQ software. InstaCal uses the same device driver as other Omega Engineering software packages – such as the Universal Library and TracerDAQ, a data collection software which are discussed below.

TracerDAQ was used for data collection of voltage and time for an experimental run. It is an instrument application used to graphically display and store input data and generate output signals using Omega Engineering data acquisition hardware.

Strip Chart - log and graph values acquired from analog inputs, digital inputs, temperature inputs, and counter inputs.

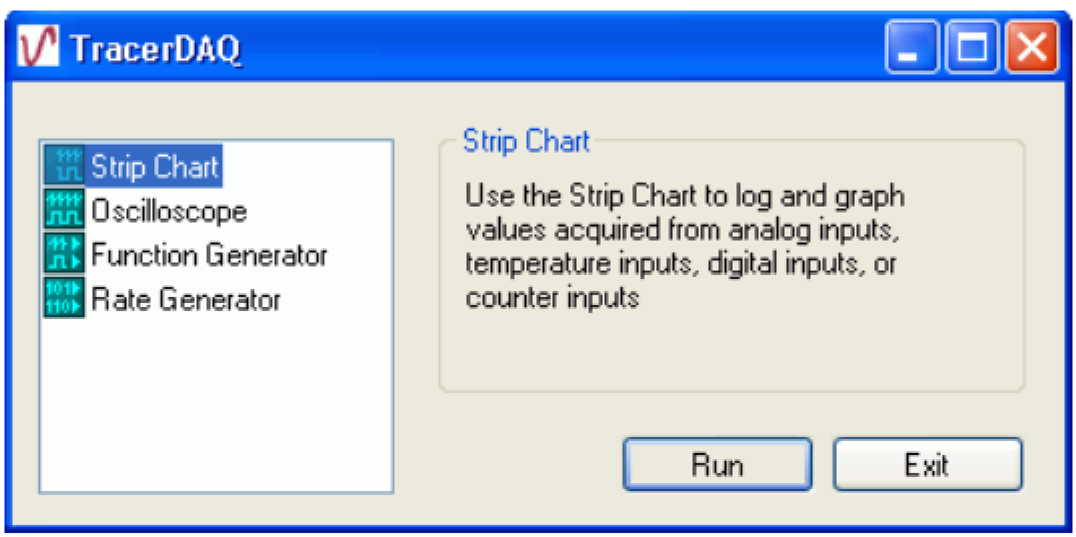

Tracer DAQ

We can scale channel data, change the time base to view data on the plot, save data as a history file (.sch) or text file (.txt or .csv). We can also import and plot binary (.bin) and text data (.csv and .txt), isolate specific data for analysis, play back an acquisition and store hardware configurations for future use.

The strip chart supports the maximum speed of DAQ hardware. When acquiring data from hardware channels that support paced I/O, the strip chart uses a scan function to acquire the data.

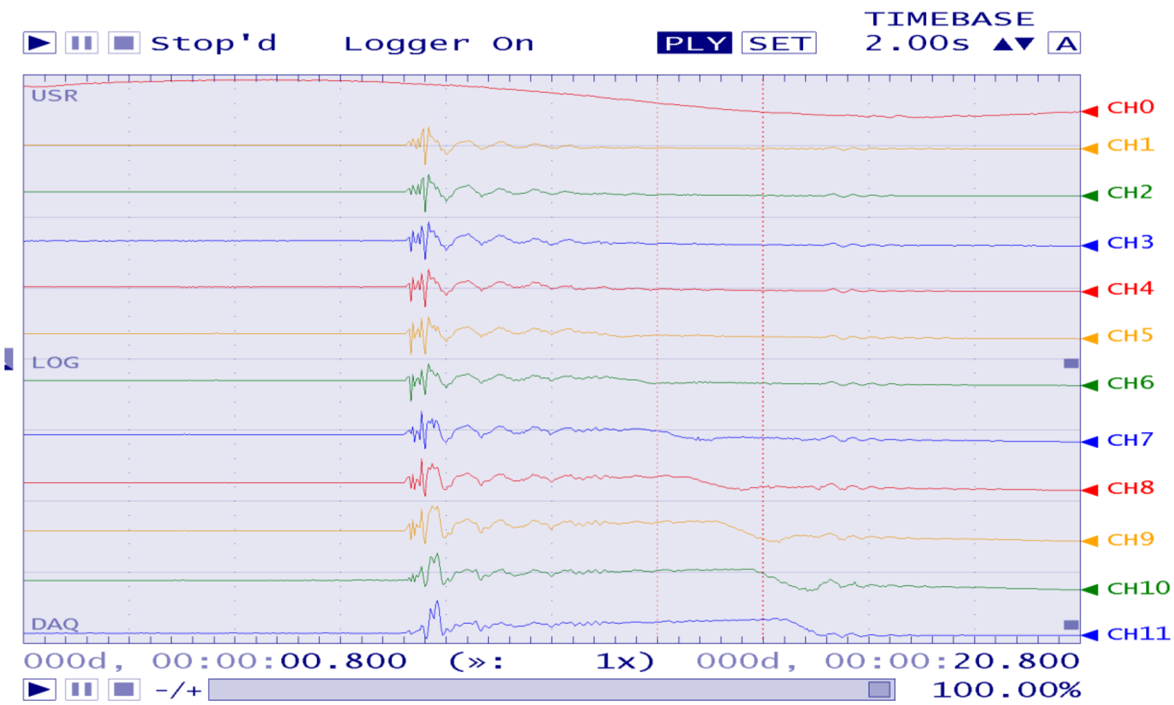

Strip chart during experimental run displaying voltage and time on y-axis and x-axis respectively

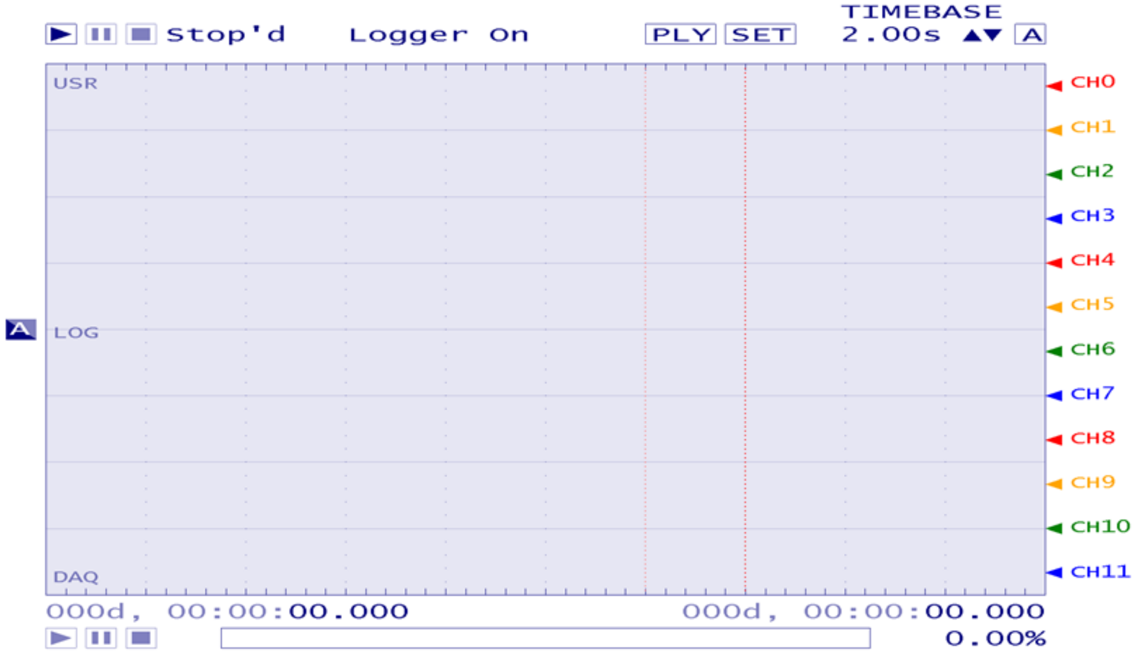

Default Configuration of Strip Chart with different channels before starting experiment

Appendix B

Calibration plots for Water – Air experiment

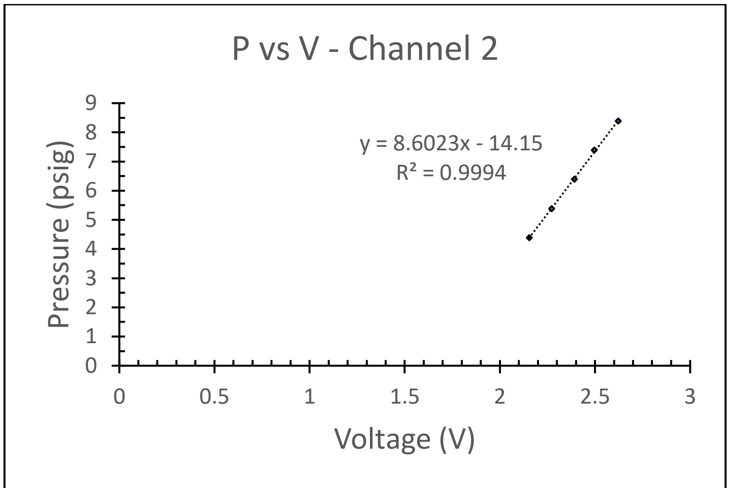

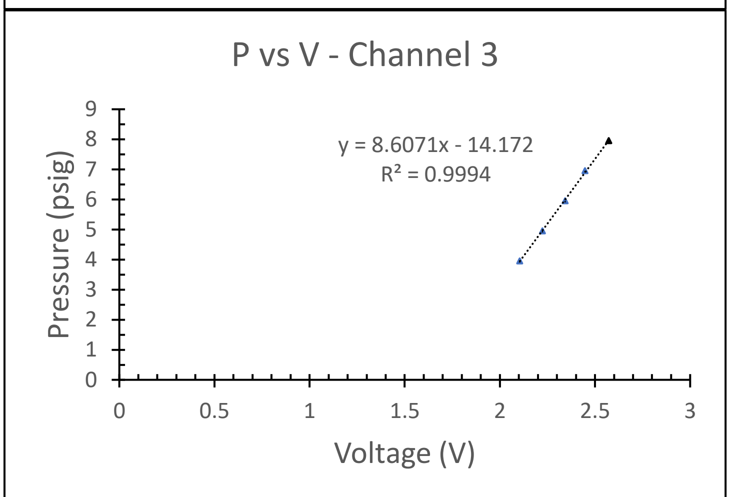

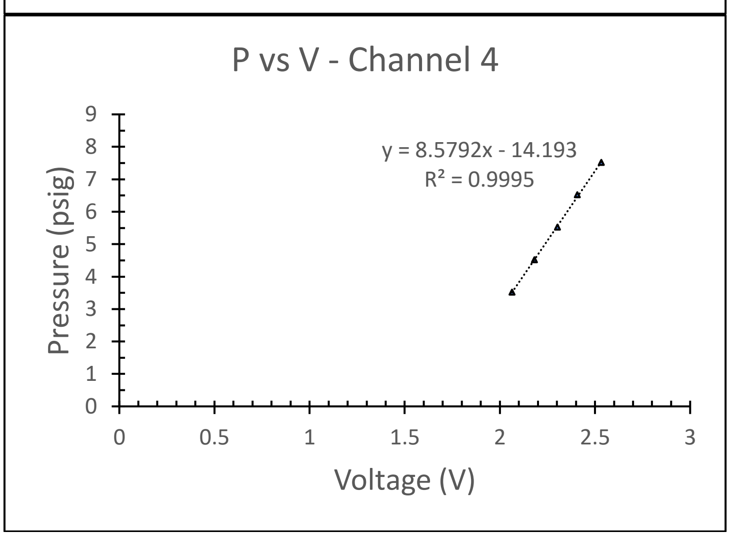

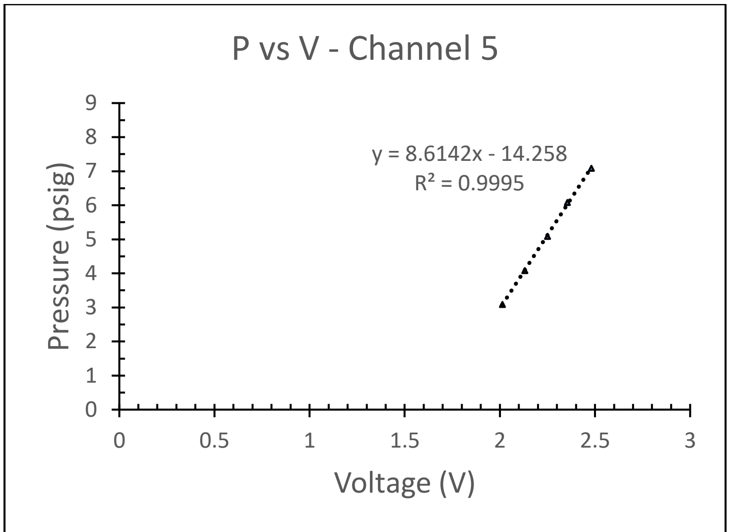
P vs V - Channel 5
y = 8.6142x - 14.258
R² = 0.9995
Pressure (psig)
Voltage (V)
0
1
2
3
4
5
6
7
8
9
0
0.5
1
1.5
2
2.5
3

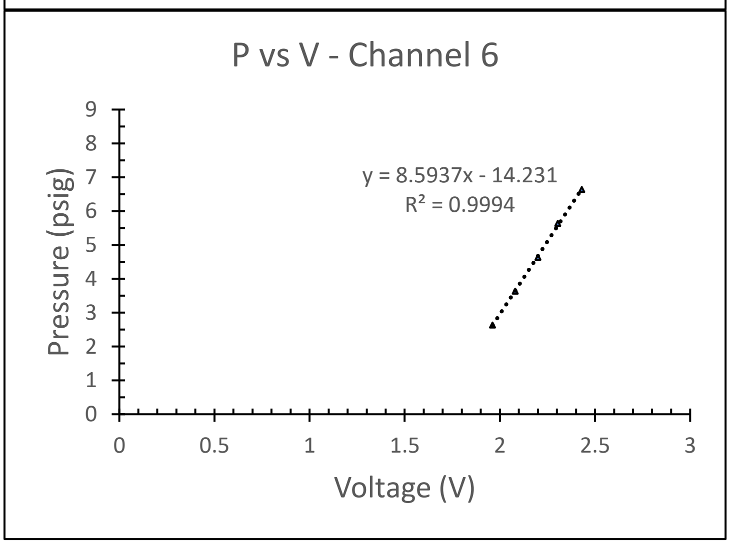
P vs V - Channel 6
y = 8.5937x - 14.231
R² = 0.9994
Pressure (psig)
Voltage (V)
0
1
2
3
4
5
6
7
8
9
0
0.5
1
1.5
2
2.5
3

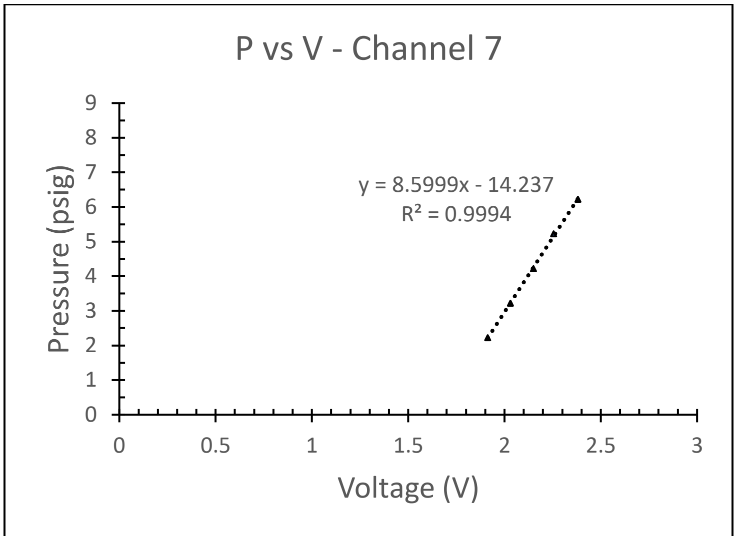
P vs V - Channel 7
y = 8.5999x - 14.237
R² = 0.9994
Pressure (psig)
Voltage (V)
0
1
2
3
4
5
6
7
8
9
0.5
1.5
2.5

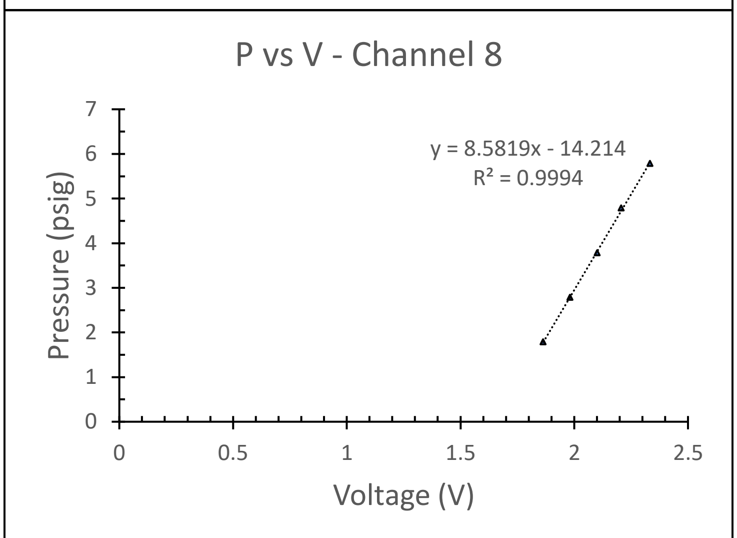
P vs V - Channel 8
y = 8.5819x - 14.214
R² = 0.9994
Pressure (psig)
Voltage (V)
0
1
2
3
4
5
6
7
0.5
1.5
2.5

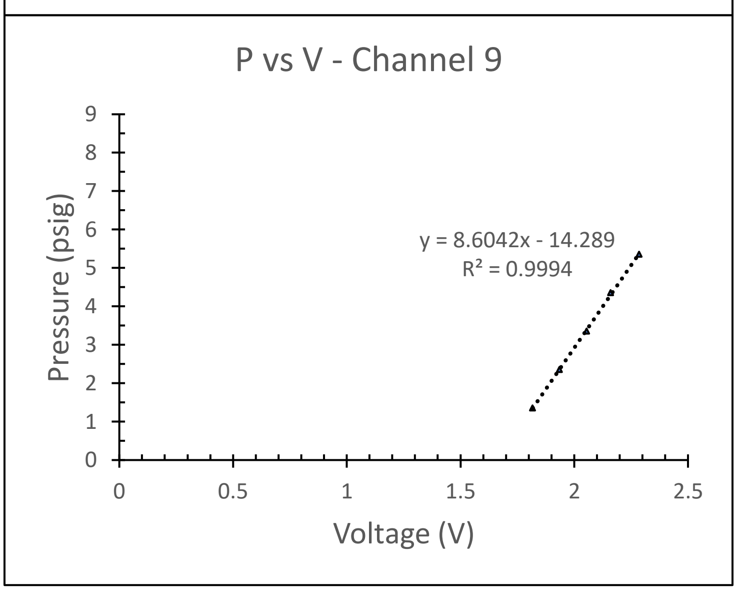
P vs V - Channel 9
y = 8.6042x - 14.289
R² = 0.9994
Pressure (psig)
Voltage (V)
0
1
2
3
4
5
6
7
8
9
0.5
1.5
2.5

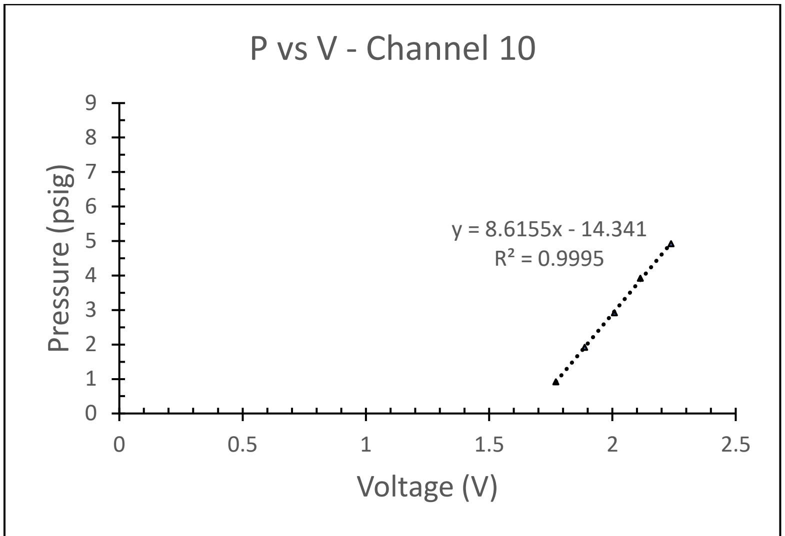
P vs V - Channel 10
y = 8.6155x - 14.341
R² = 0.9995
Pressure (psig)
Voltage (V)
0
1
2
3
4
5
6
7
8
9
0
0.5
1
1.5
2
2.5

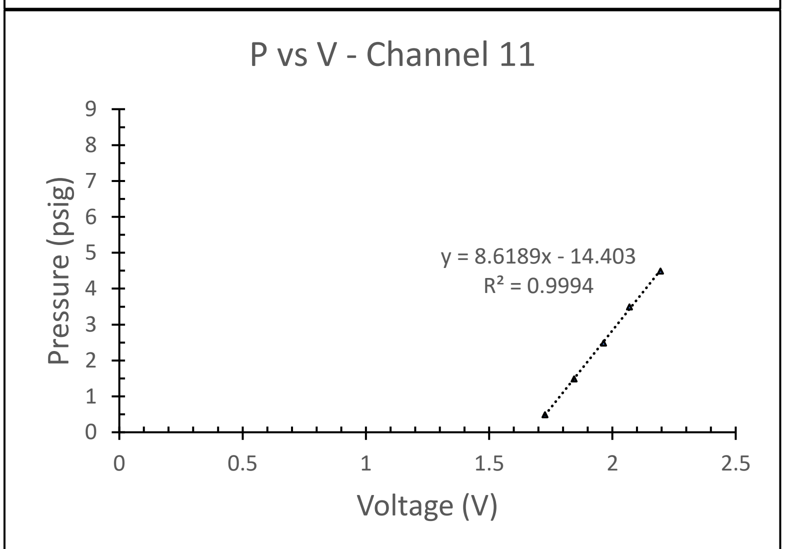
P vs V - Channel 11
y = 8.6189x - 14.403
R² = 0.9994
Pressure (psig)
Voltage (V)
0
1
2
3
4
5
6
7
8
9
0
0.5
1
1.5
2
2.5

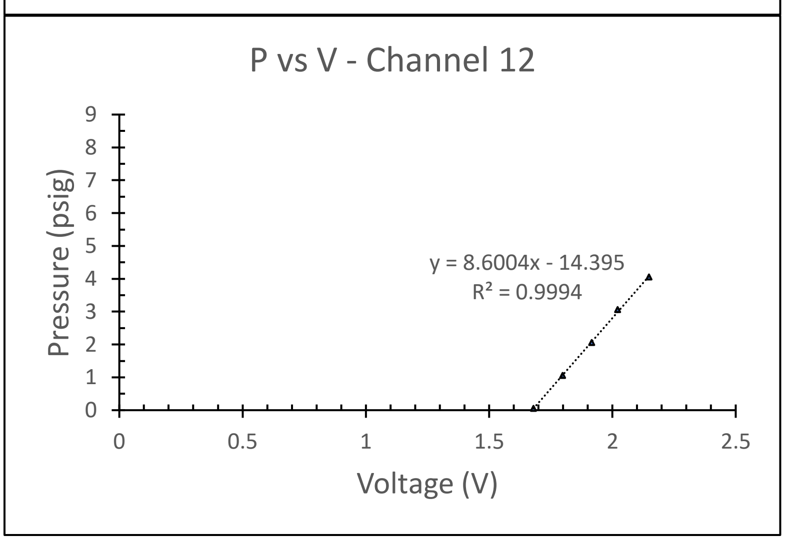
P vs V - Channel 12
y = 8.6004x - 14.395
R² = 0.9994
Pressure (psig)
Voltage (V)
0
1
2
3
4
5
6
7
8
9
0
0.5
1
1.5
2
2.5

Water – Air Experiment 1

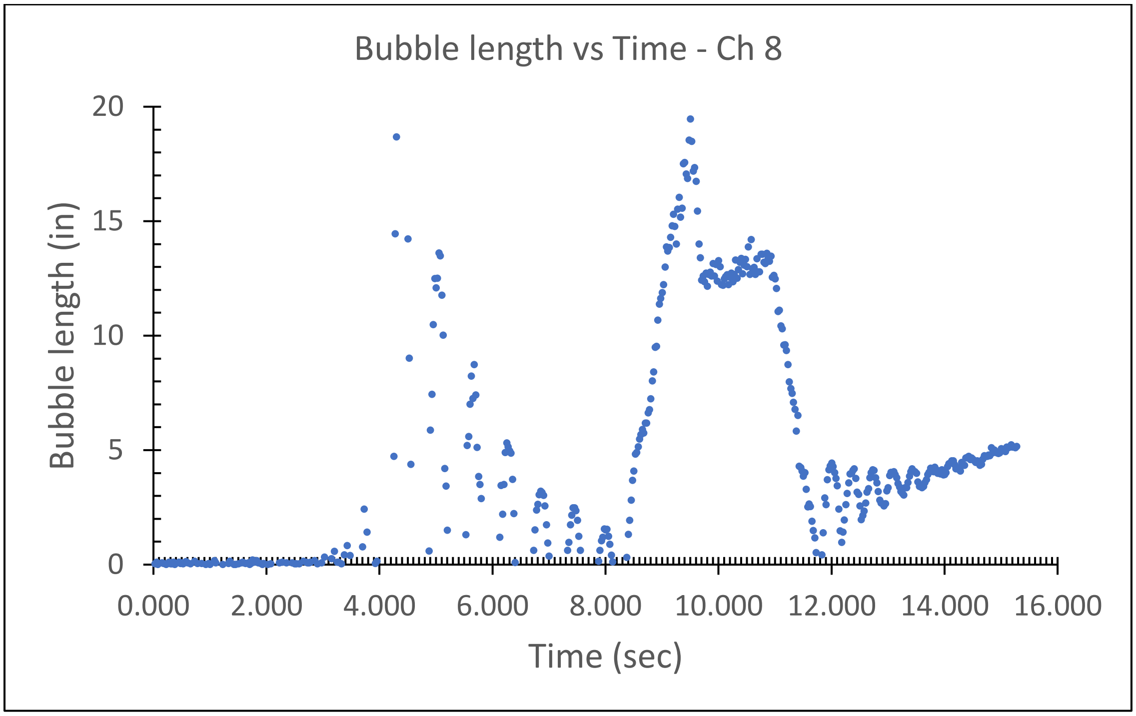

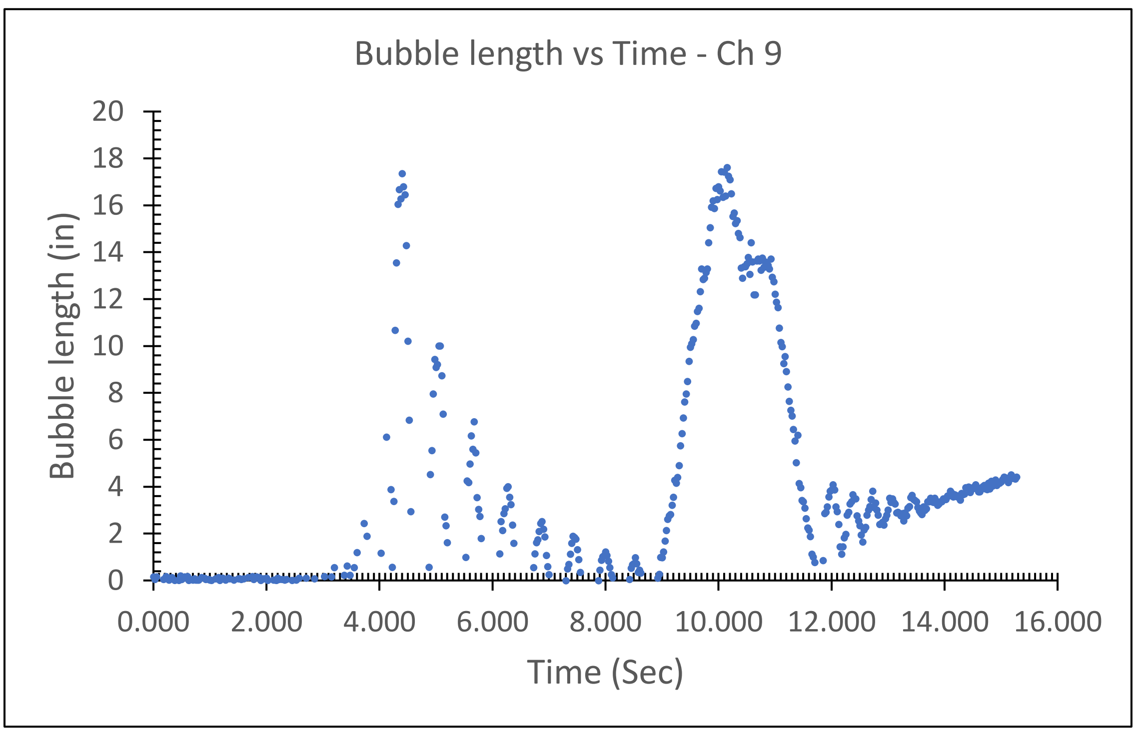

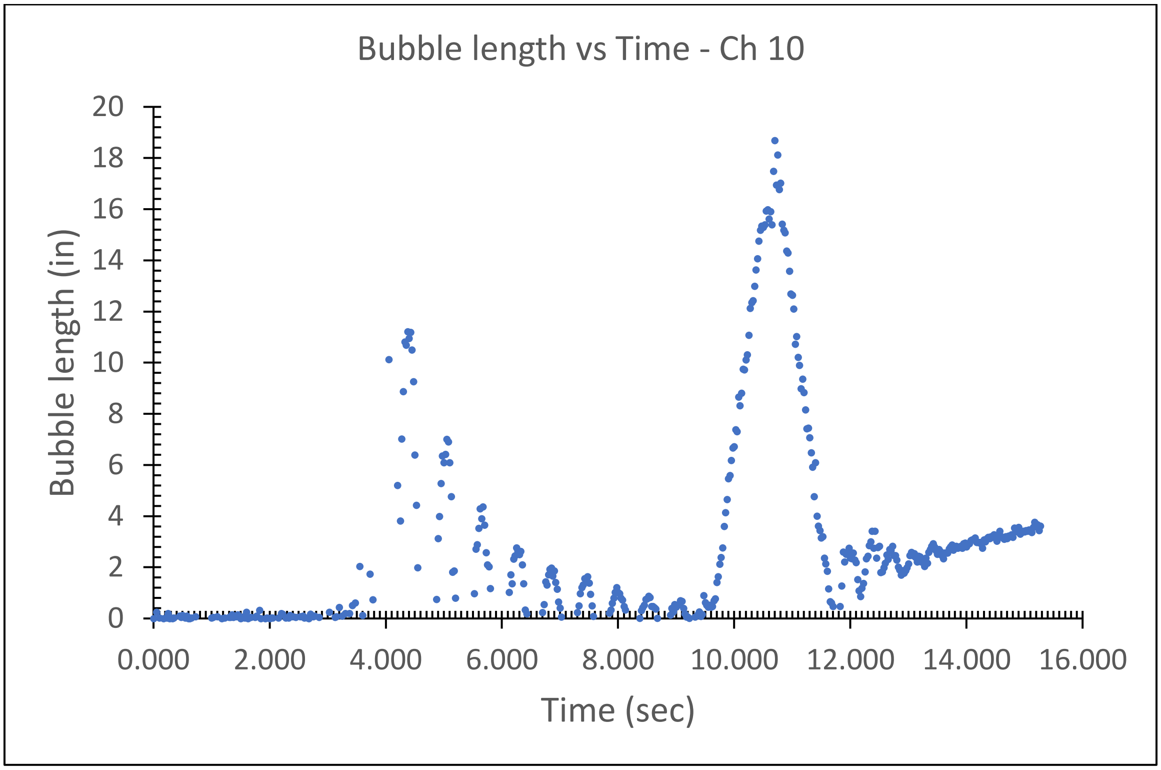
Bubble length vs Time - Ch 10
Bubble length (in)
20
18
16
14
12
10
8
6
4
2
0
0.000
2.000
4.000
6.000
8.000
10.000
12.000
14.000
16.000
Time (sec)

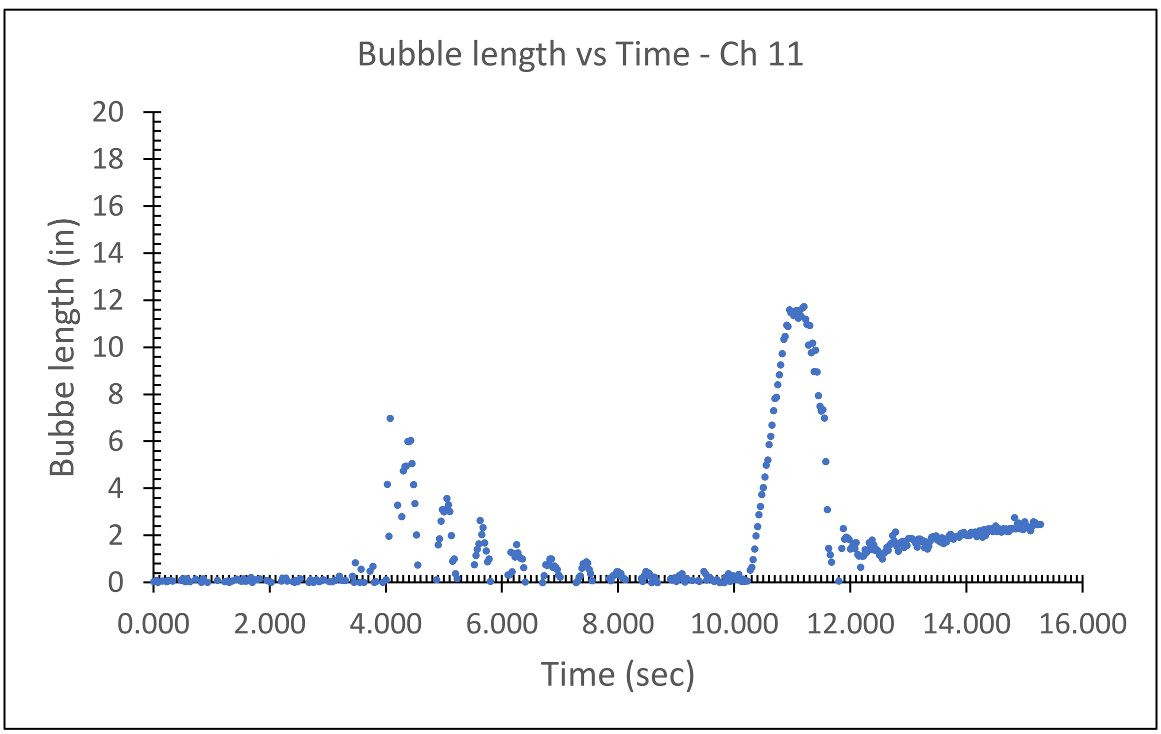
Bubble length vs Time - Ch 11
Bubbe length (in)
20
18
16
14
12
10
8
6
4
2
0
0.000
2.000
4.000
6.000
8.000
10.000
12.000
14.000
16.000
Time (sec)

Water – Air Experiment 2

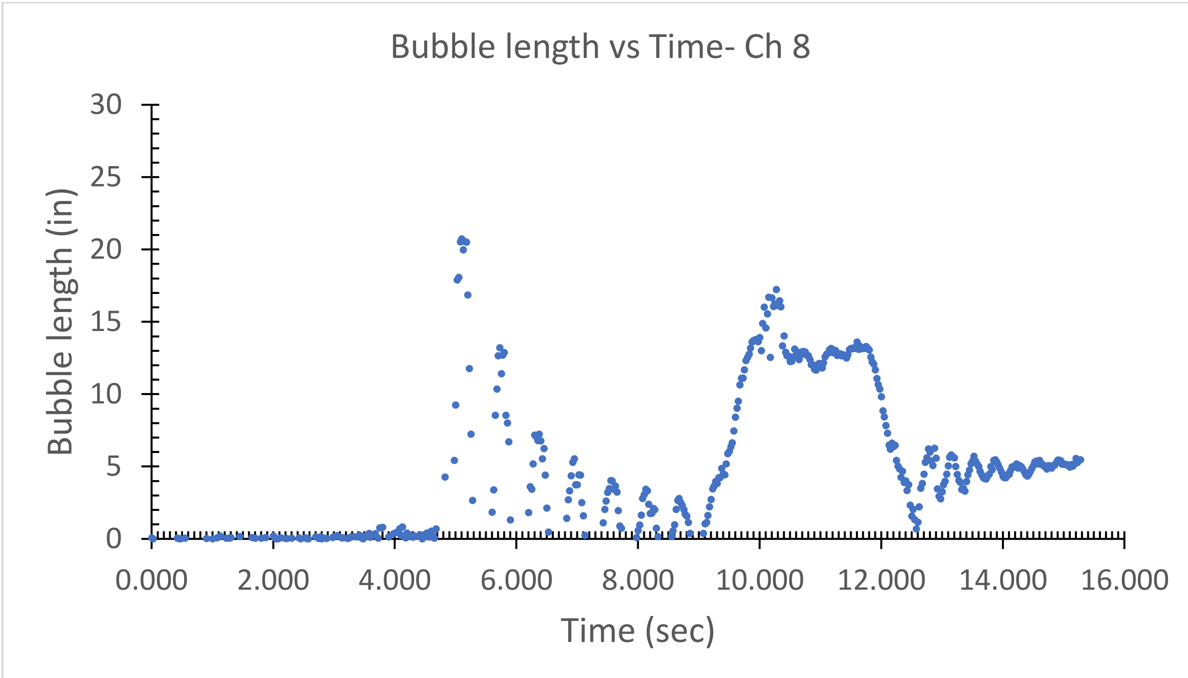

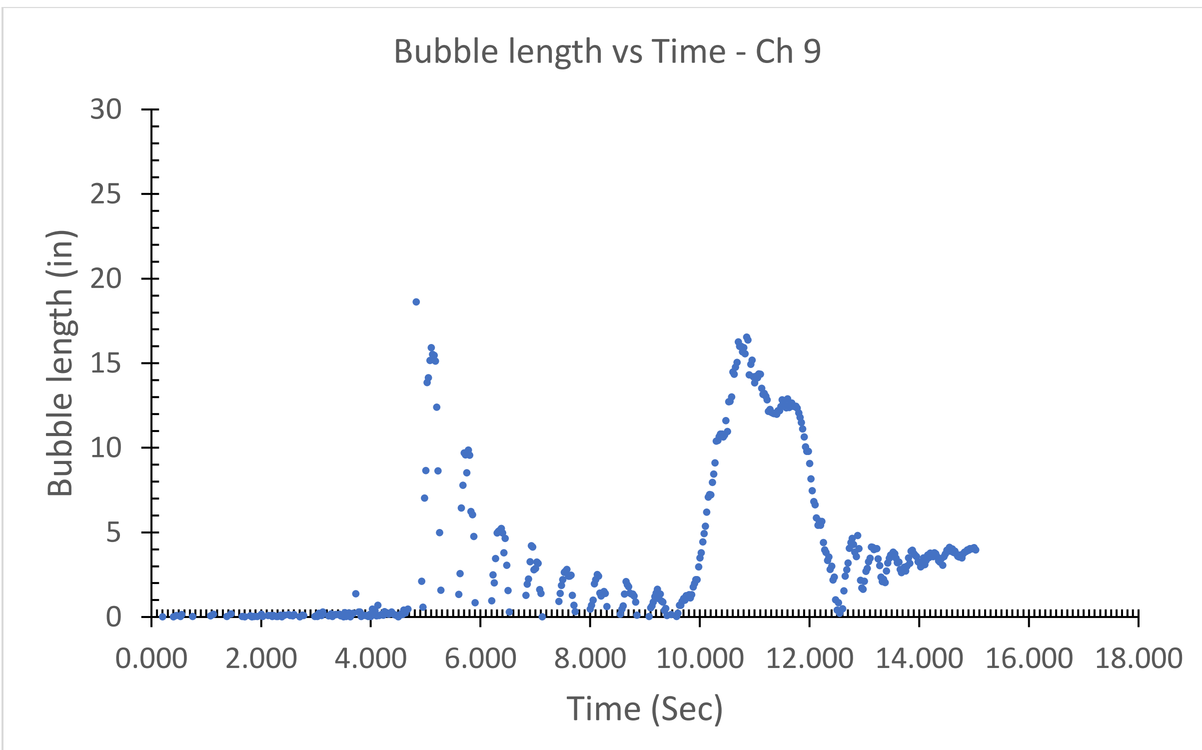

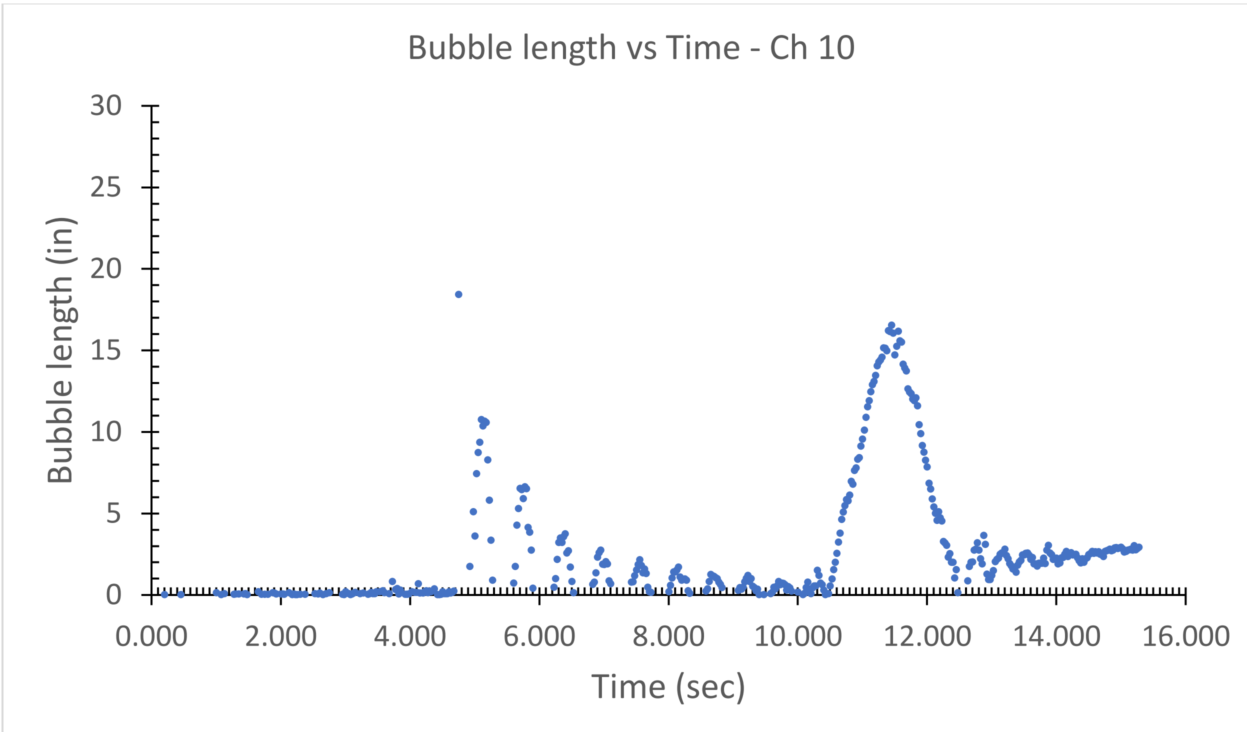
Bubble length vs Time - Ch 10
Bubble length (in)
30
25
20
15
10
5
0
0.000
2.000
4.000
6.000
8.000
10.000
12.000
14.000
16.000
Time (sec)

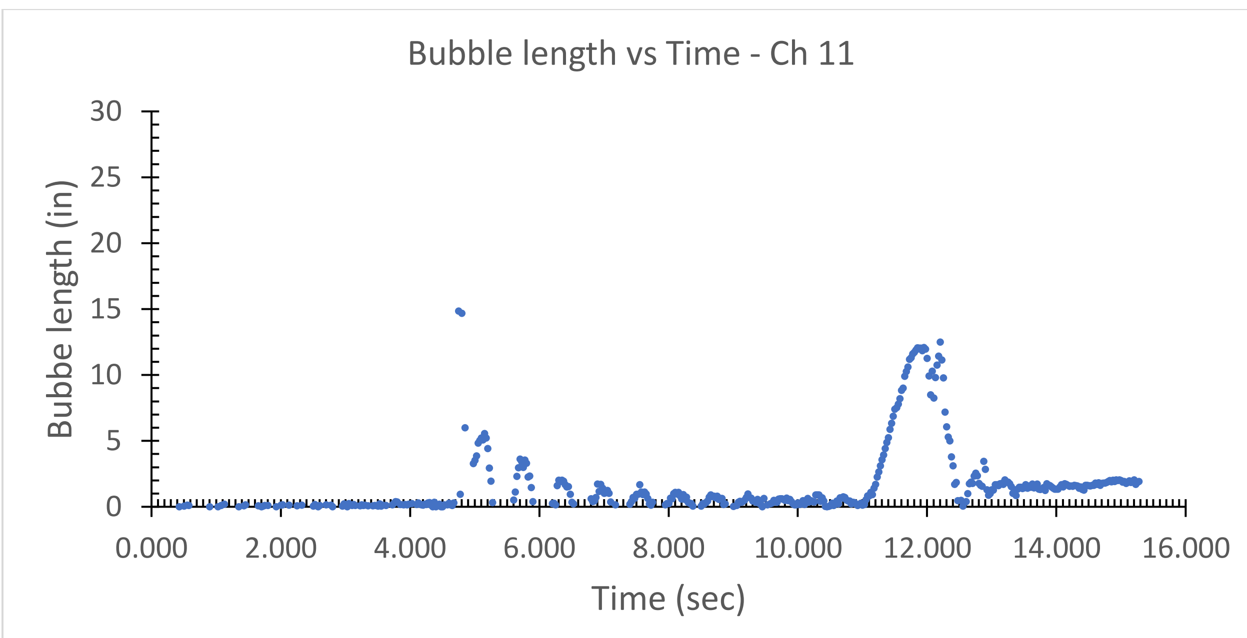
Bubble length vs Time - Ch 11
Bubbe length (in)
30
25
20
15
10
5
0
0.000
2.000
4.000
6.000
8.000
10.000
12.000
14.000
16.000
Time (sec)

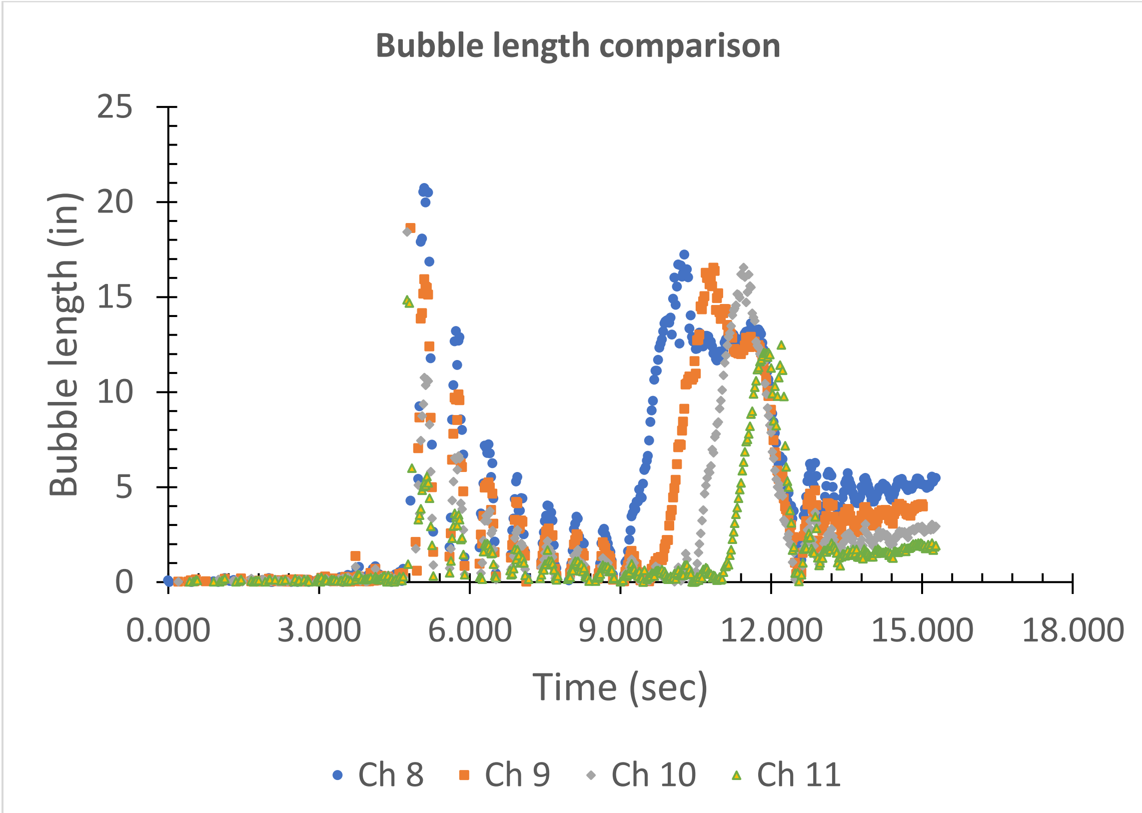
Bubble length comparison
Bubble length (in)
25
20
15
10
5
0
0.000
3.000
6.000
9.000
12.000
15.000
18.000
Time (sec)
Ch 8
Ch 9
Ch 10
Ch 11

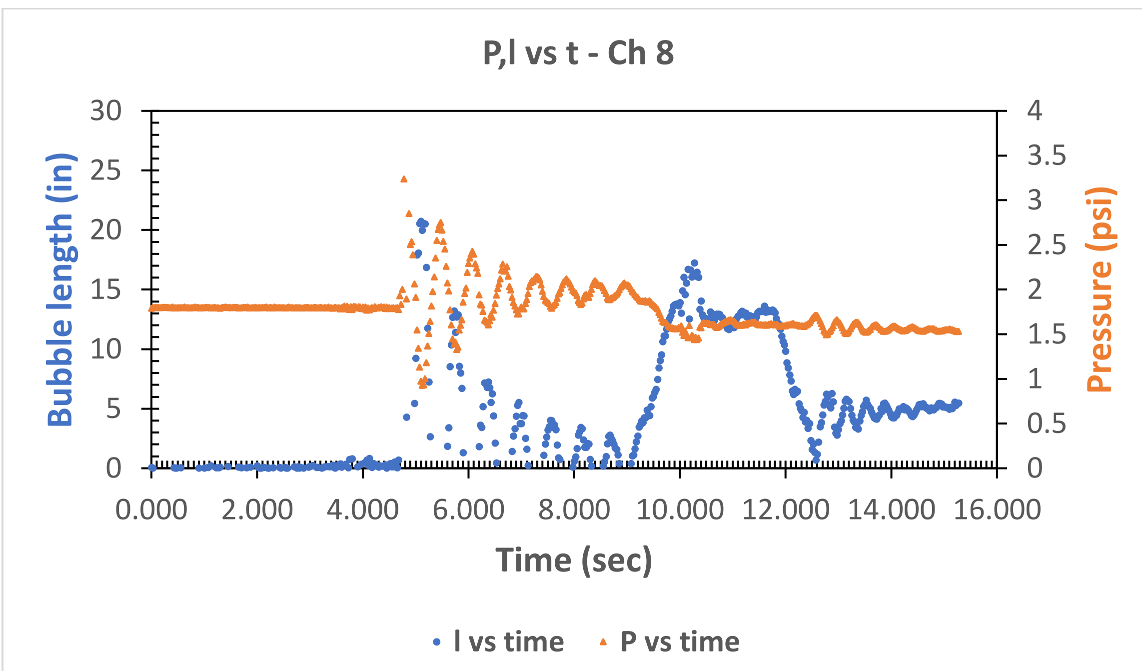
P,l vs t - Ch 8
Bubble length (in)
30
25
20
15
10
5
0
Pressure (psi)
4
3.5
3
2.5
2
1.5
1
0.5
0
0.000
2.000
4.000
6.000
8.000
10.000
12.000
14.000
16.000
Time (sec)
l vs time
P vs time

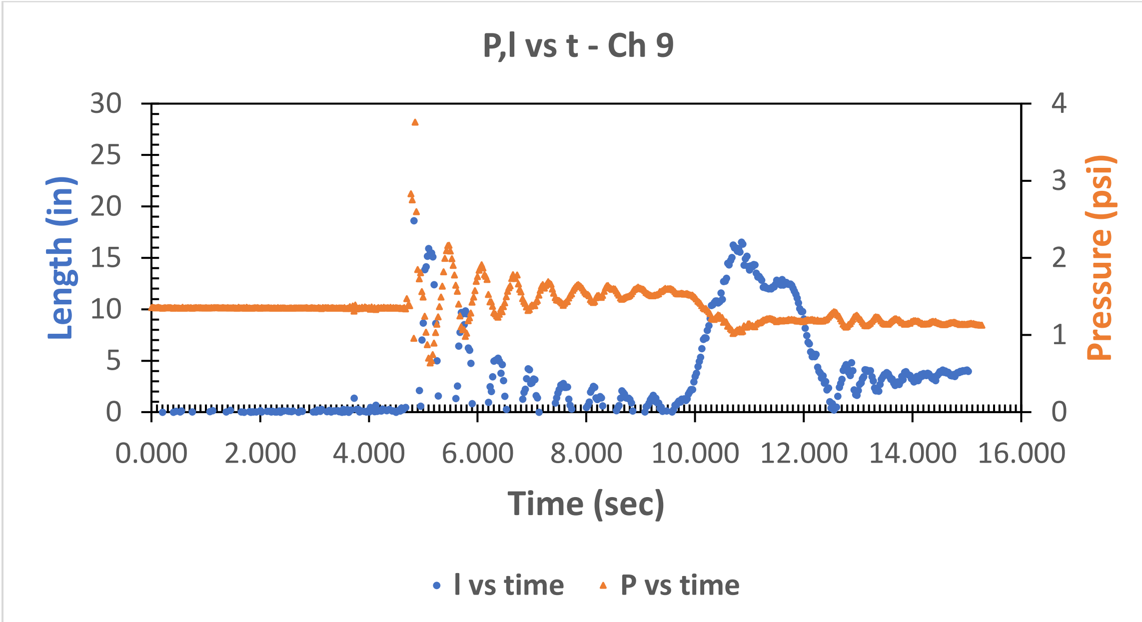
P,l vs t - Ch 9
Length (in)
Pressure (psi)
Time (sec)
0
5
10
15
20
25
30
0
1
2
3
4
0.000
2.000
4.000
6.000
8.000
10.000
12.000
14.000
16.000
l vs time
P vs time

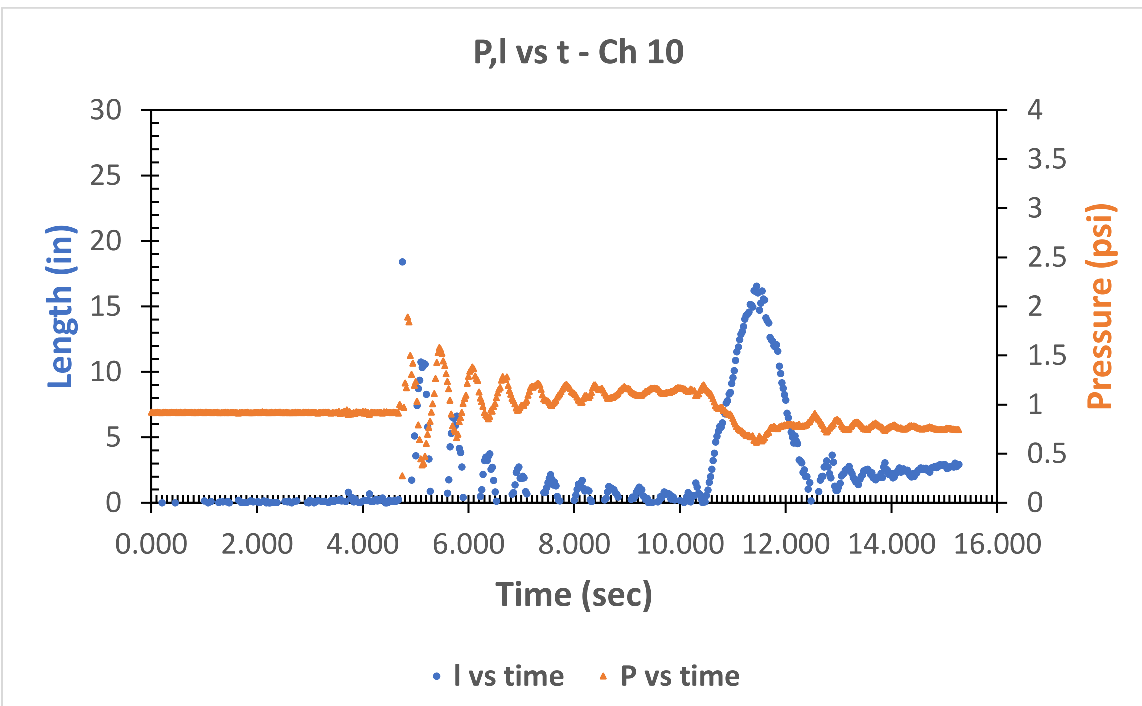
P,l vs t - Ch 10
Length (in)
Pressure (psi)
Time (sec)
0
5
10
15
20
25
30
0
0.5
1
1.5
2
2.5
3
3.5
4
0.000
2.000
4.000
6.000
8.000
10.000
12.000
14.000
16.000
l vs time
P vs time

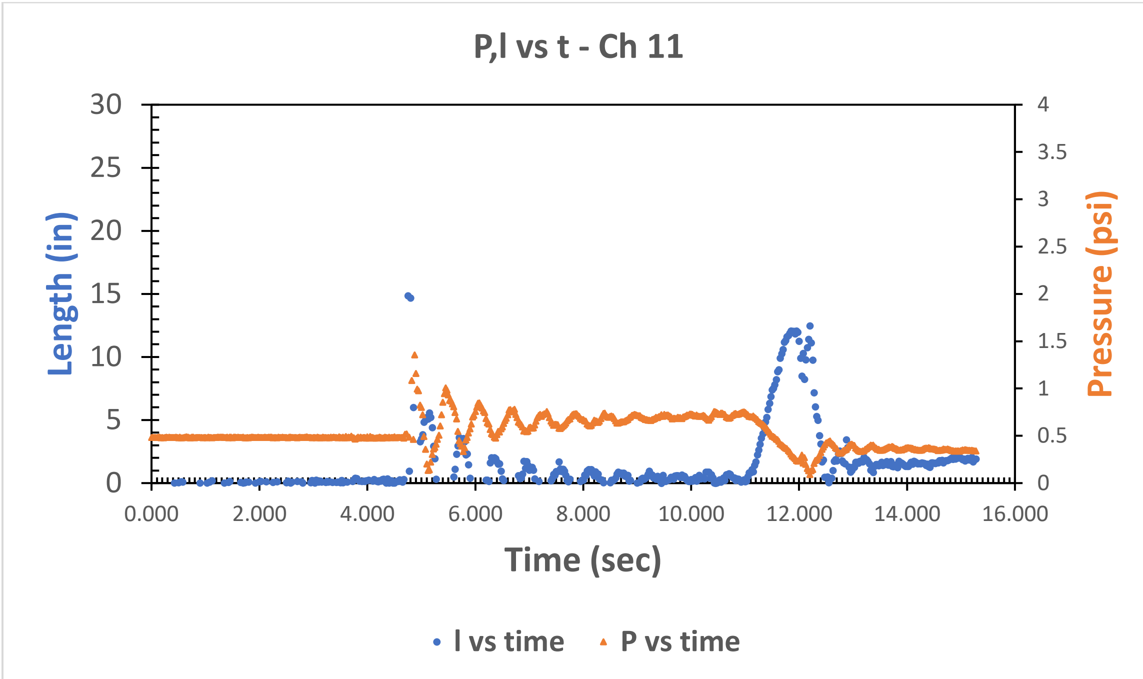

P,l vs t - Ch 11
Length (in)
Pressure (psi)
Time (sec)
0
5
10
15
20
25
30
0
0.5
1
1.5
2
2.5
3
3.5
4
0.000
2.000
4.000
6.000
8.000
10.000
12.000
14.000
16.000
l vs time
P vs time

Water – Air Experiment 3

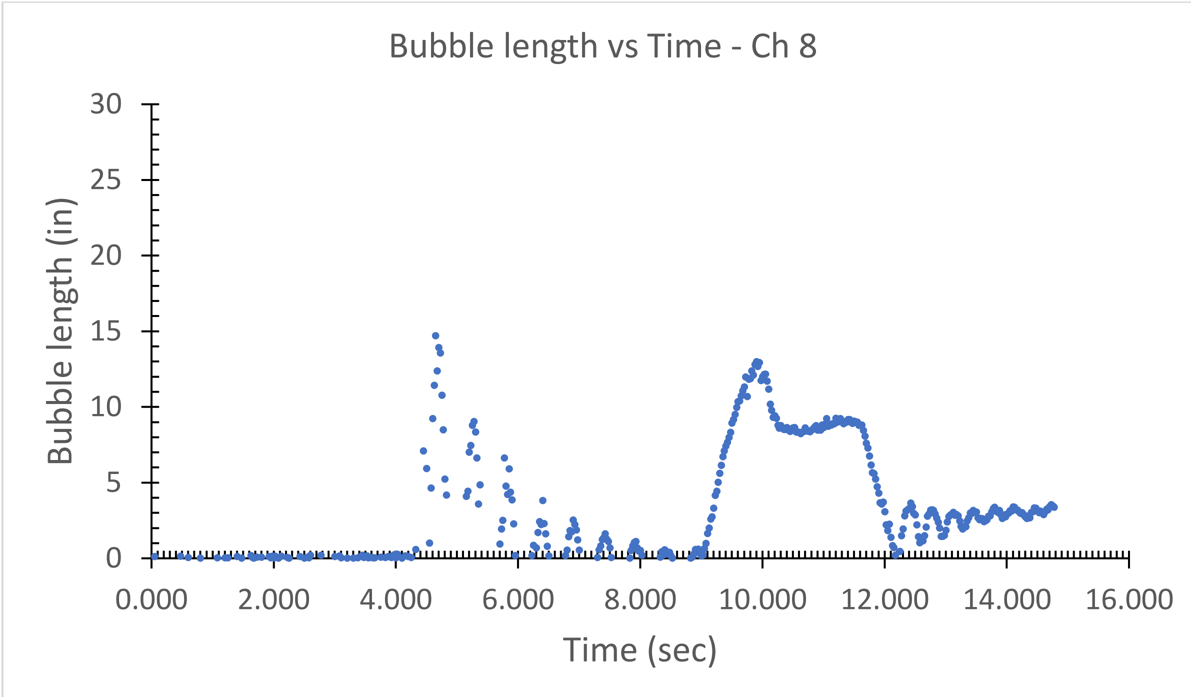

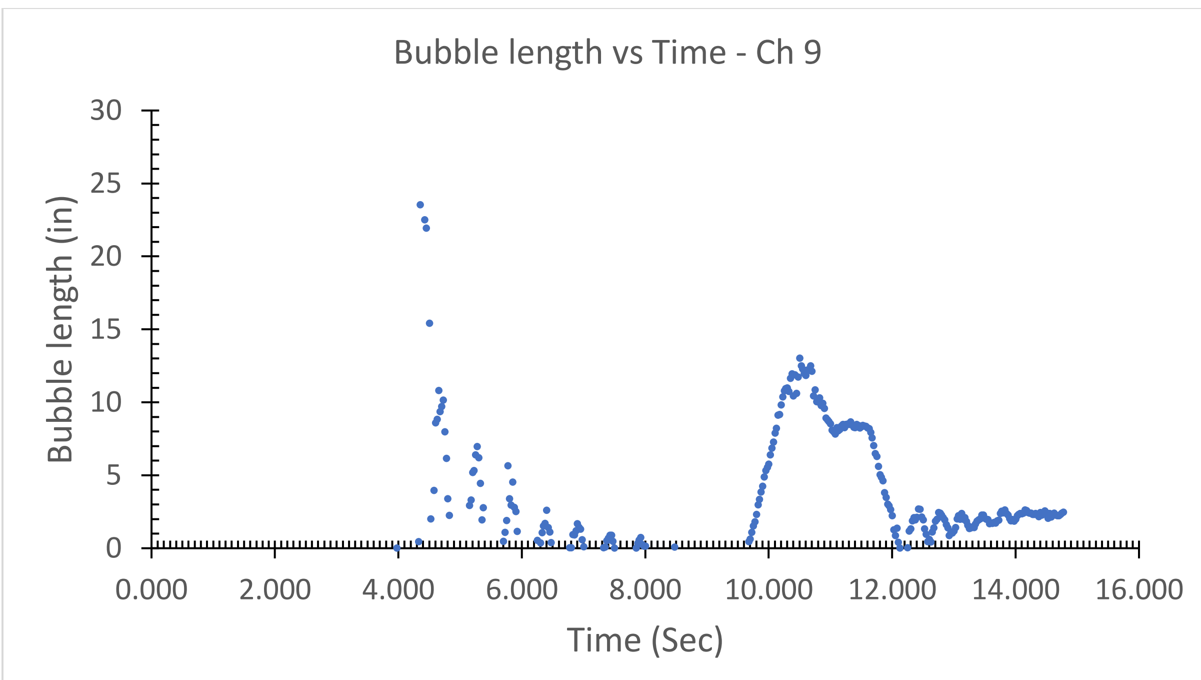

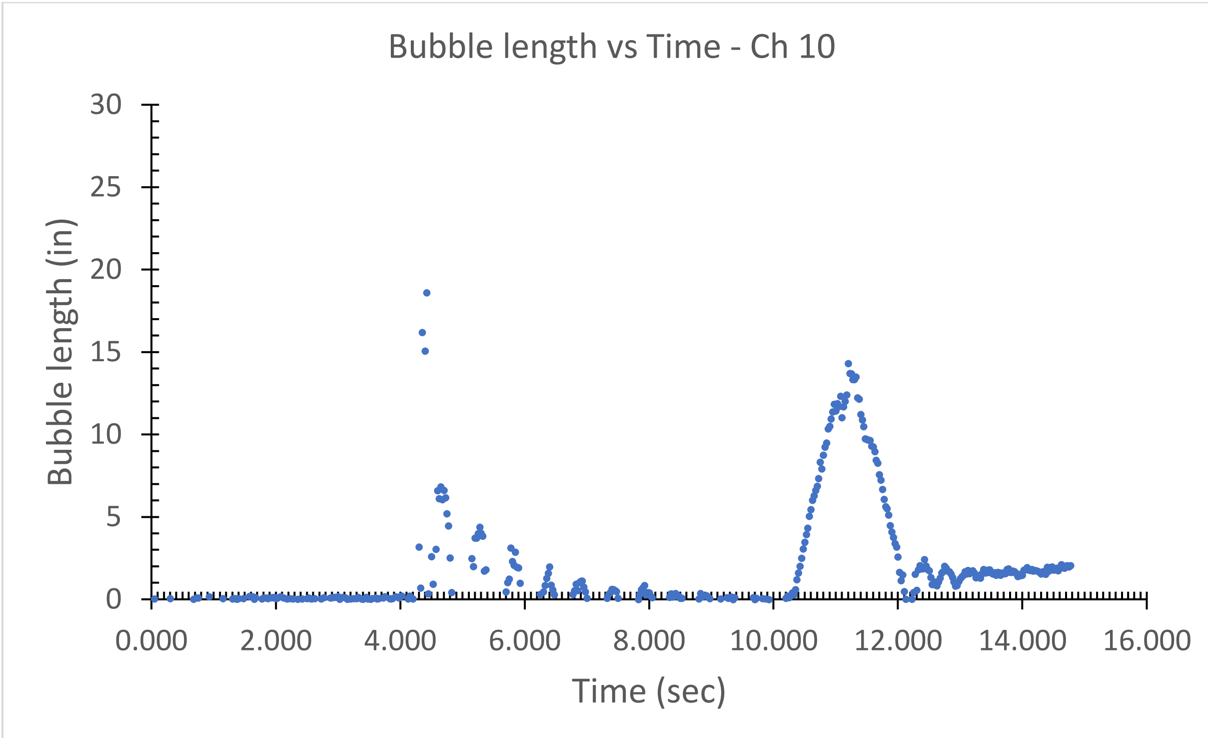
Bubble length vs Time - Ch 10
Bubble length (in)
30
25
20
15
10
5
0
0.000
2.000
4.000
6.000
8.000
10.000
12.000
14.000
16.000
Time (sec)

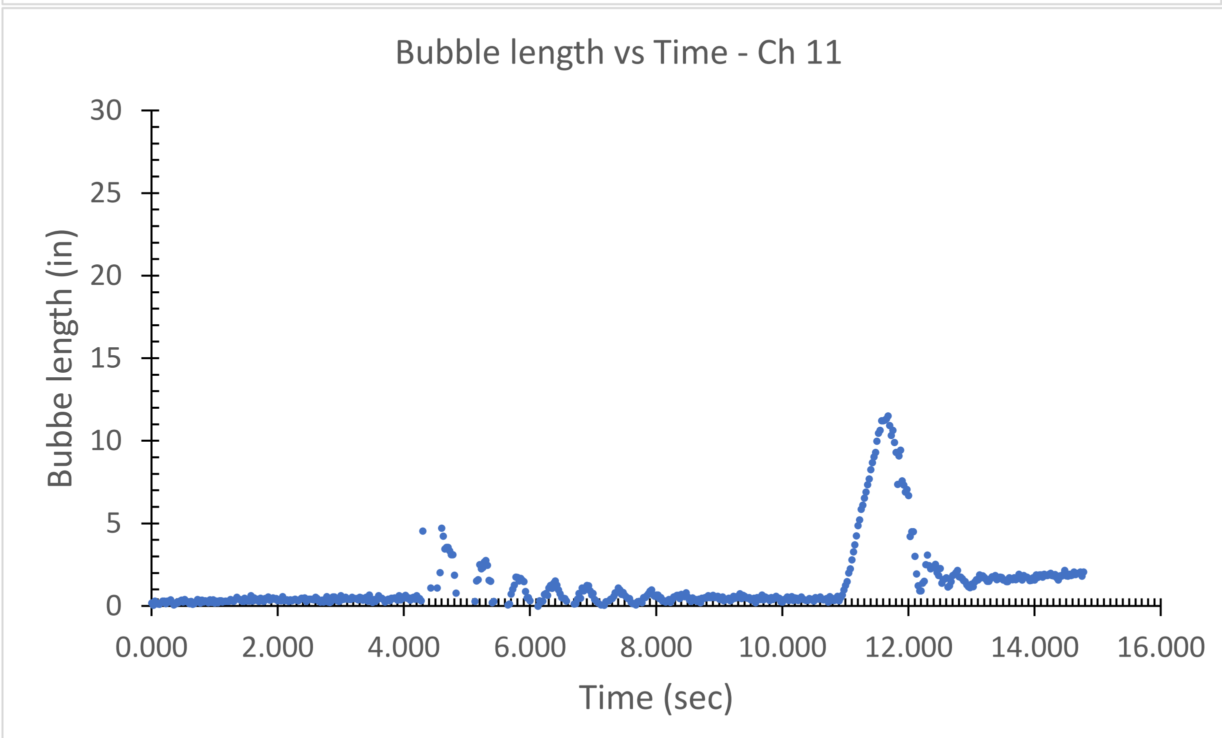
Bubble length vs Time - Ch 11
Bubbe length (in)
30
25
20
15
10
5
0
0.000
2.000
4.000
6.000
8.000
10.000
12.000
14.000
16.000
Time (sec)

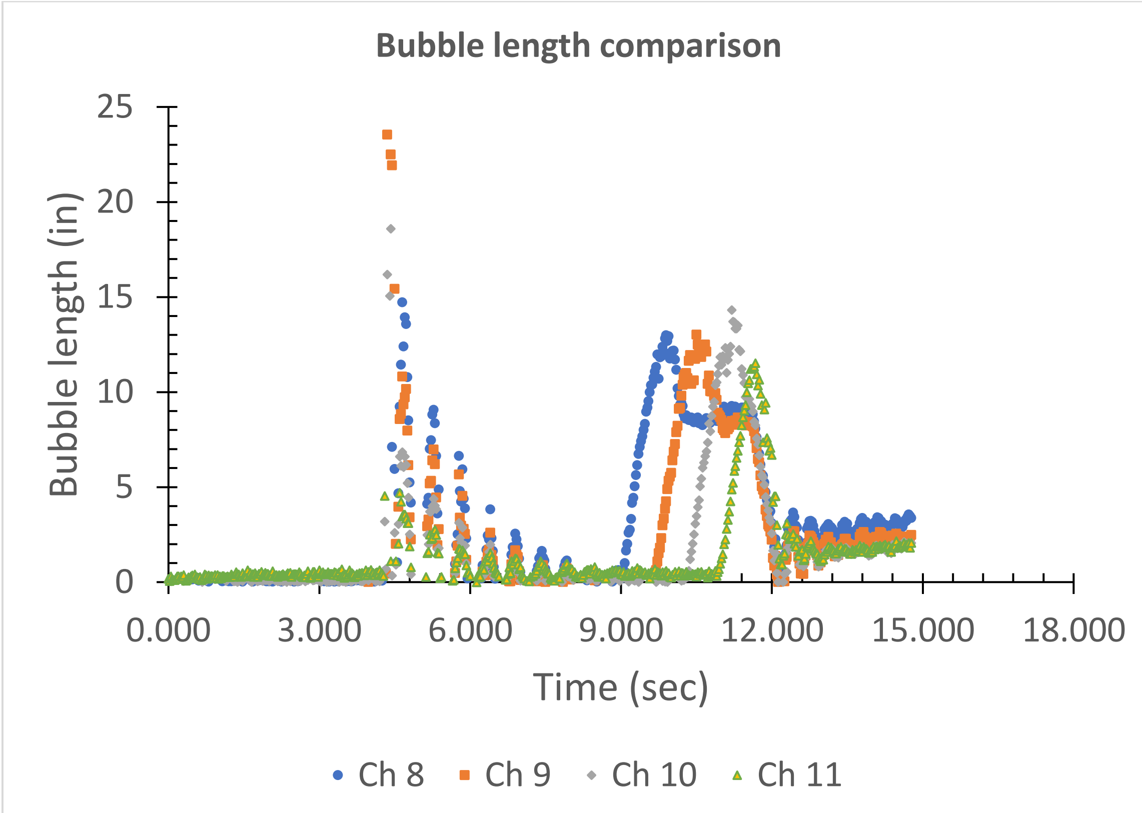
Bubble length comparison
Bubble length (in)
25
20
15
10
5
0
0.000
3.000
6.000
9.000
12.000
15.000
18.000
Time (sec)
Ch 8
Ch 9
Ch 10
Ch 11

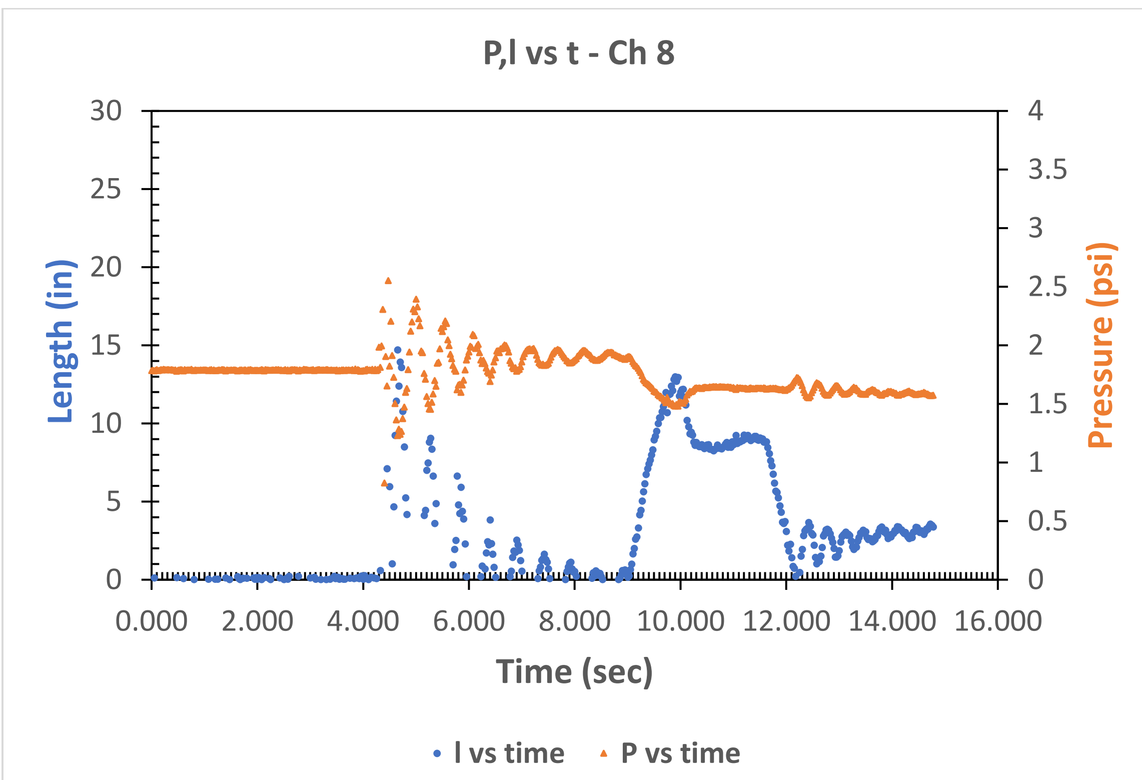
P,l vs t - Ch 8
Length (in)
30
25
20
15
10
5
0
Pressure (psi)
4
3.5
3
2.5
2
1.5
1
0.5
0
0.000
2.000
4.000
6.000
8.000
10.000
12.000
14.000
16.000
Time (sec)
l vs time
P vs time

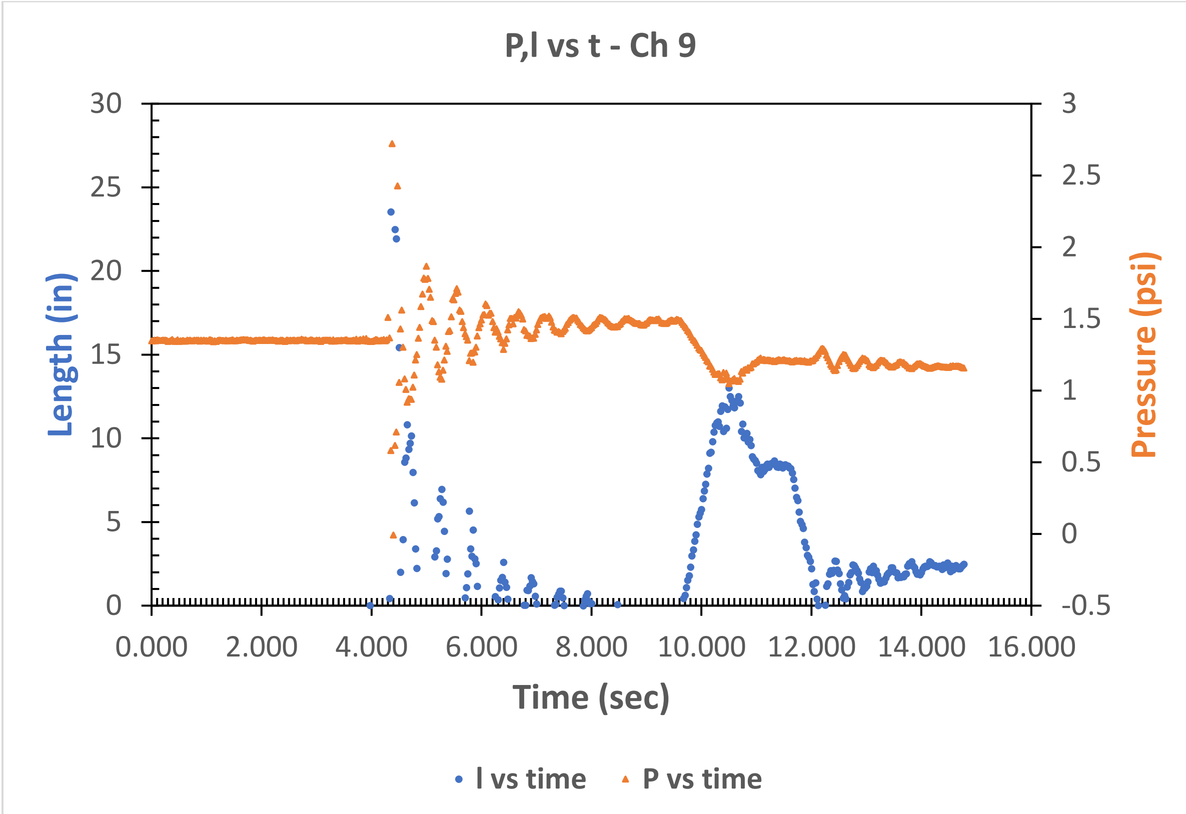
P,l vs t - Ch 9
Length (in)
Pressure (psi)
Time (sec)
30
25
20
15
10
5
0
3
2.5
2
1.5
1
0.5
0
-0.5
0.000
2.000
4.000
6.000
8.000
10.000
12.000
14.000
16.000
l vs time
P vs time

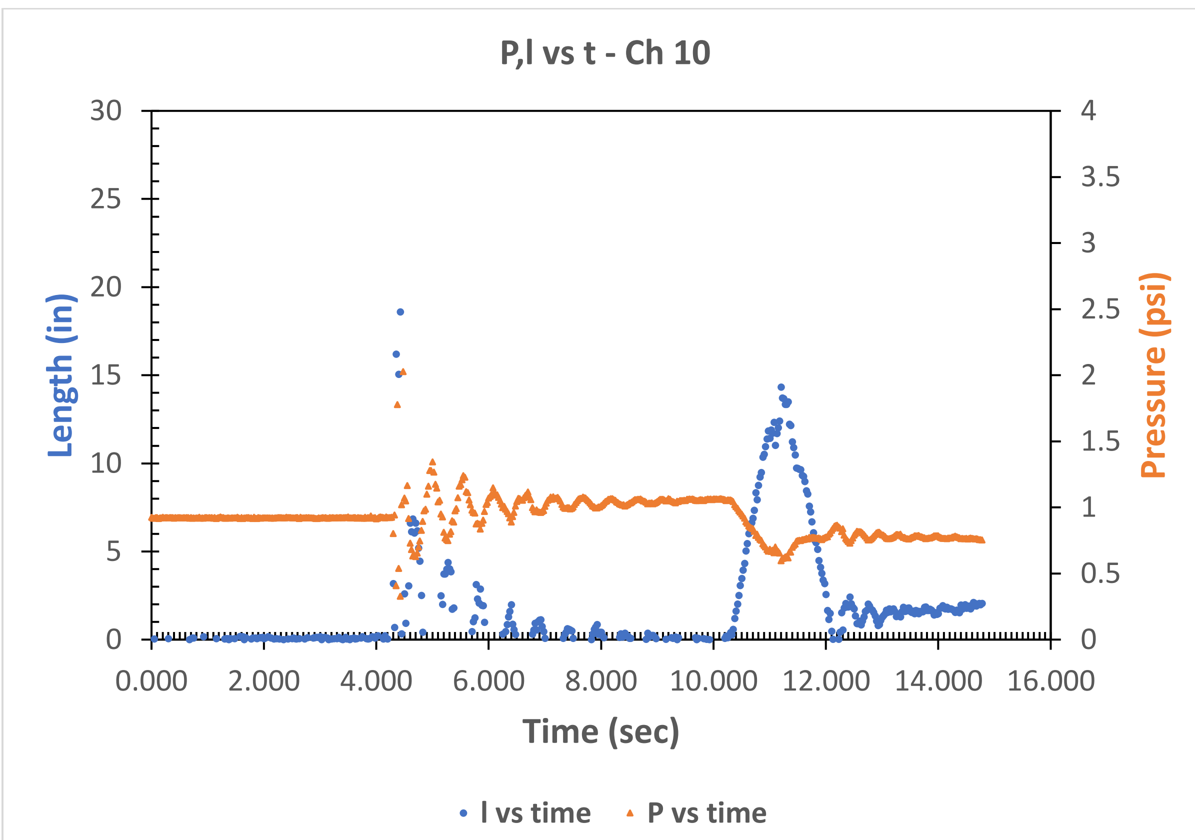
P,l vs t - Ch 10
Length (in)
Pressure (psi)
Time (sec)
30
25
20
15
10
5
0
4
3.5
3
2.5
2
1.5
1
0.5
0
0.000
2.000
4.000
6.000
8.000
10.000
12.000
14.000
16.000
l vs time
P vs time

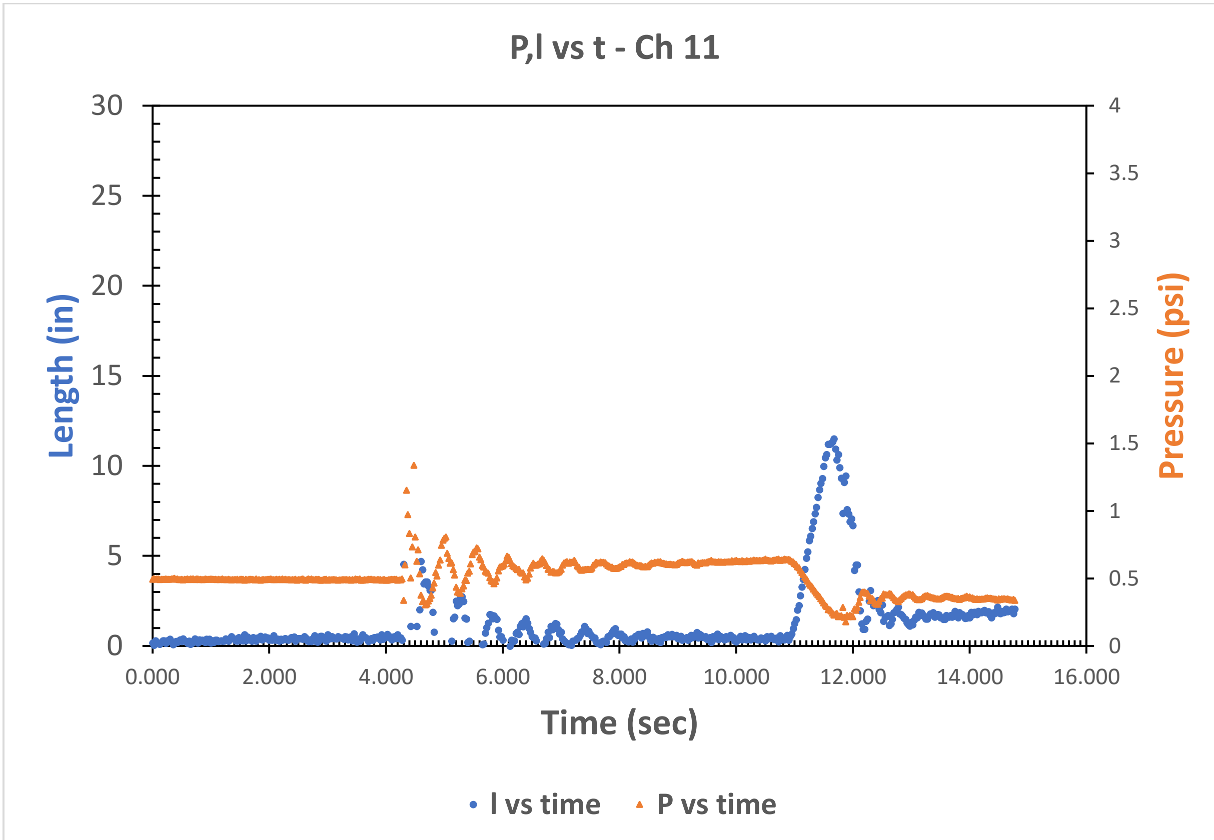
P,l vs t - Ch 11
Length (in)
Pressure (psi)
Time (sec)
0
5
10
15
20
25
30
0
0.5
1
1.5
2
2.5
3
3.5
4
0.000
2.000
4.000
6.000
8.000
10.000
12.000
14.000
16.000
l vs time
P vs time

Water – Air Experiment 4

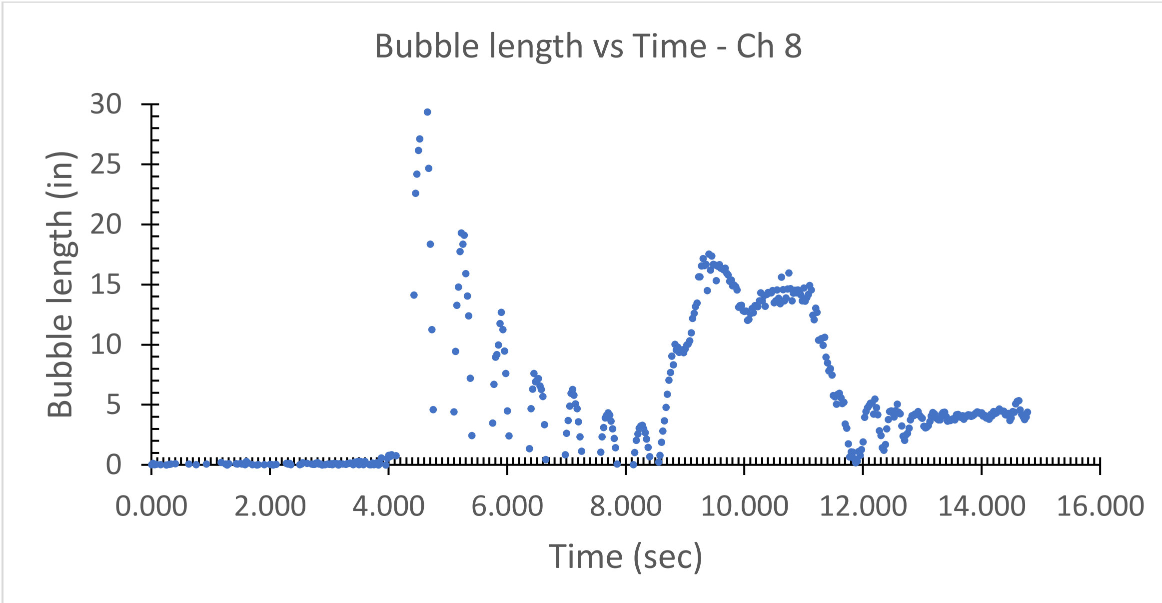

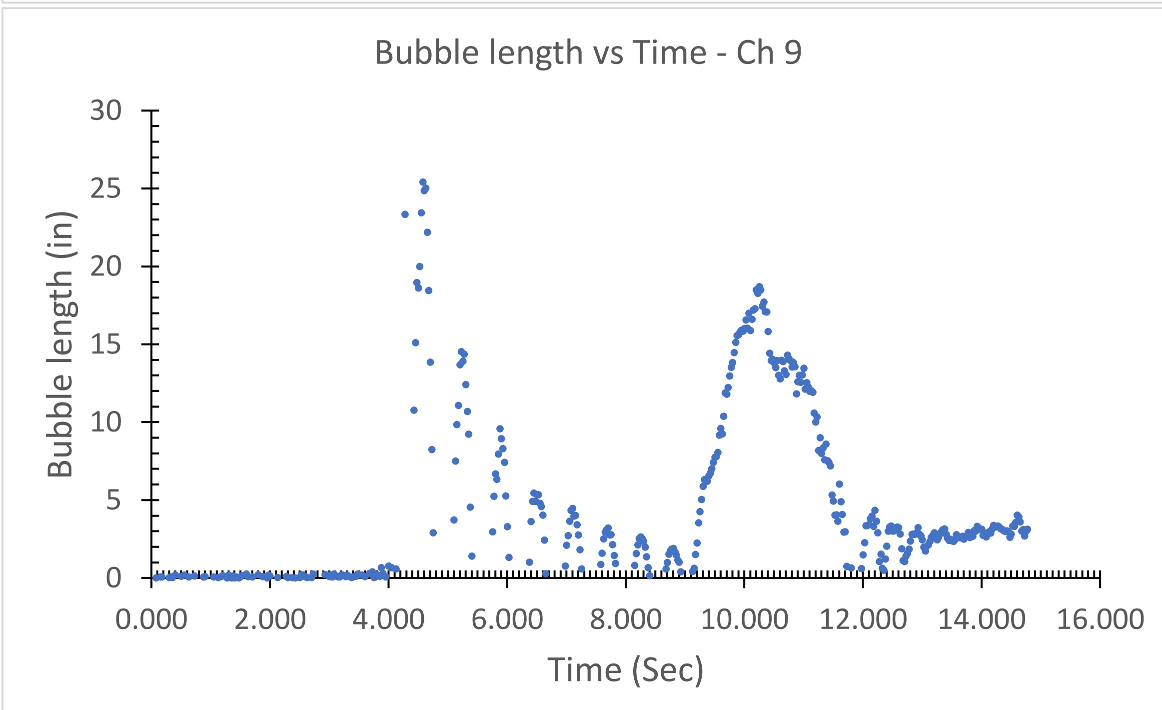

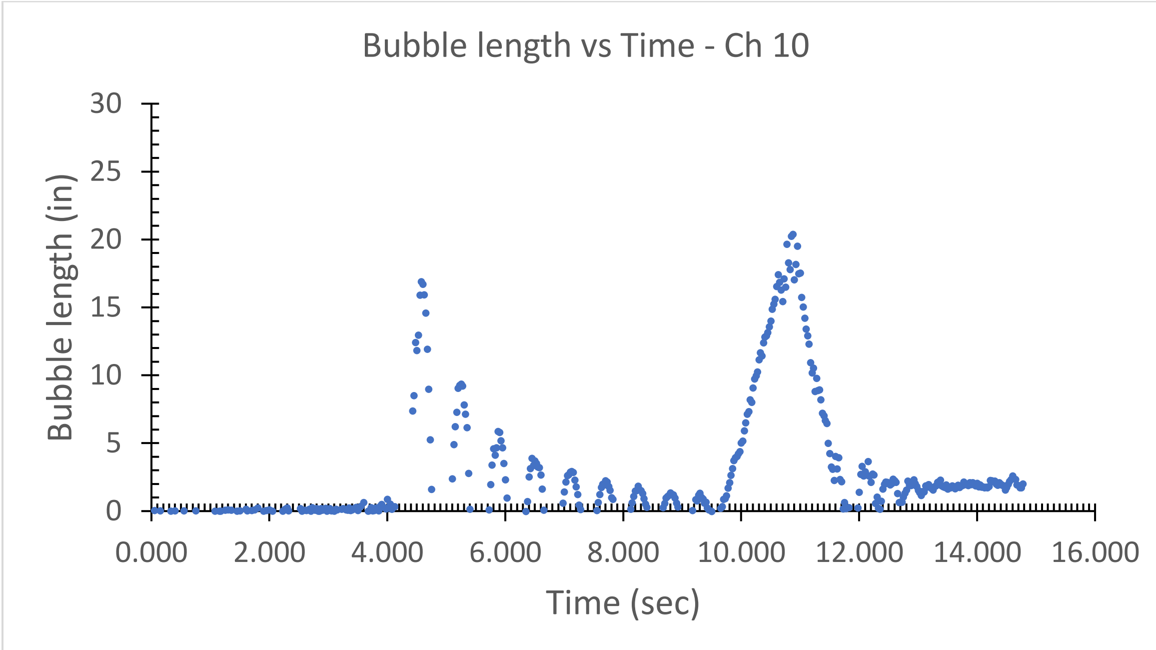
Bubble length vs Time - Ch 10
Bubble length (in)
30
25
20
15
10
5
0
0.000
2.000
4.000
6.000
8.000
10.000
12.000
14.000
16.000
Time (sec)

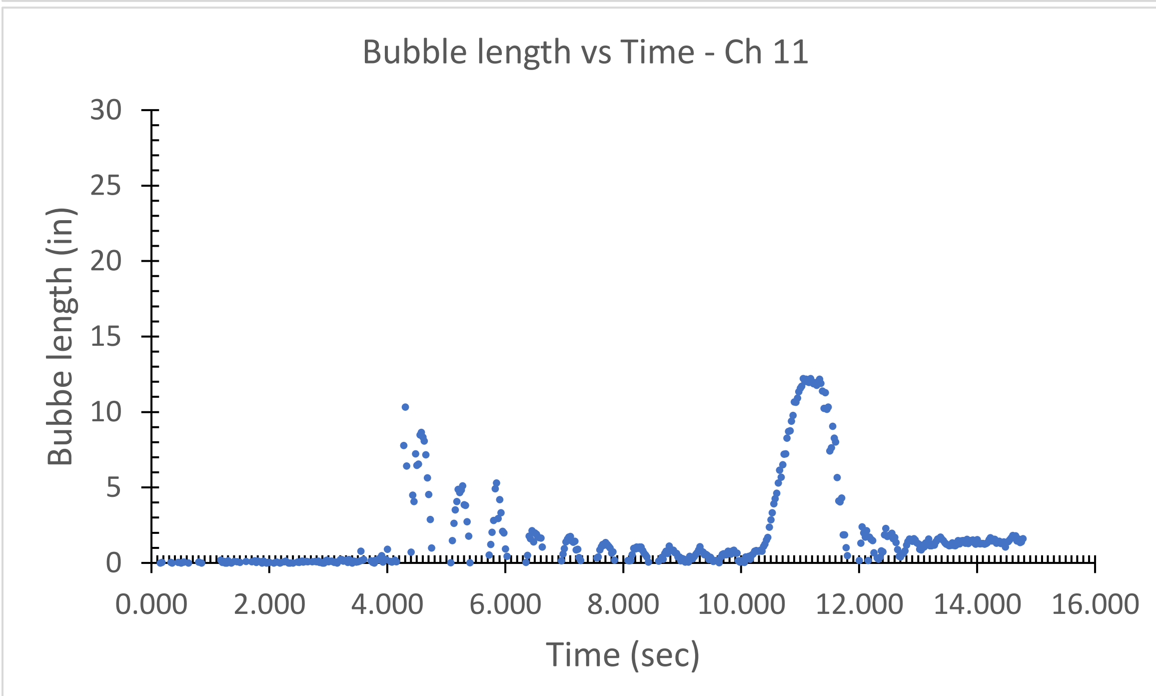
Bubble length vs Time - Ch 11
Bubbe length (in)
30
25
20
15
10
5
0
0.000
2.000
4.000
6.000
8.000
10.000
12.000
14.000
16.000
Time (sec)

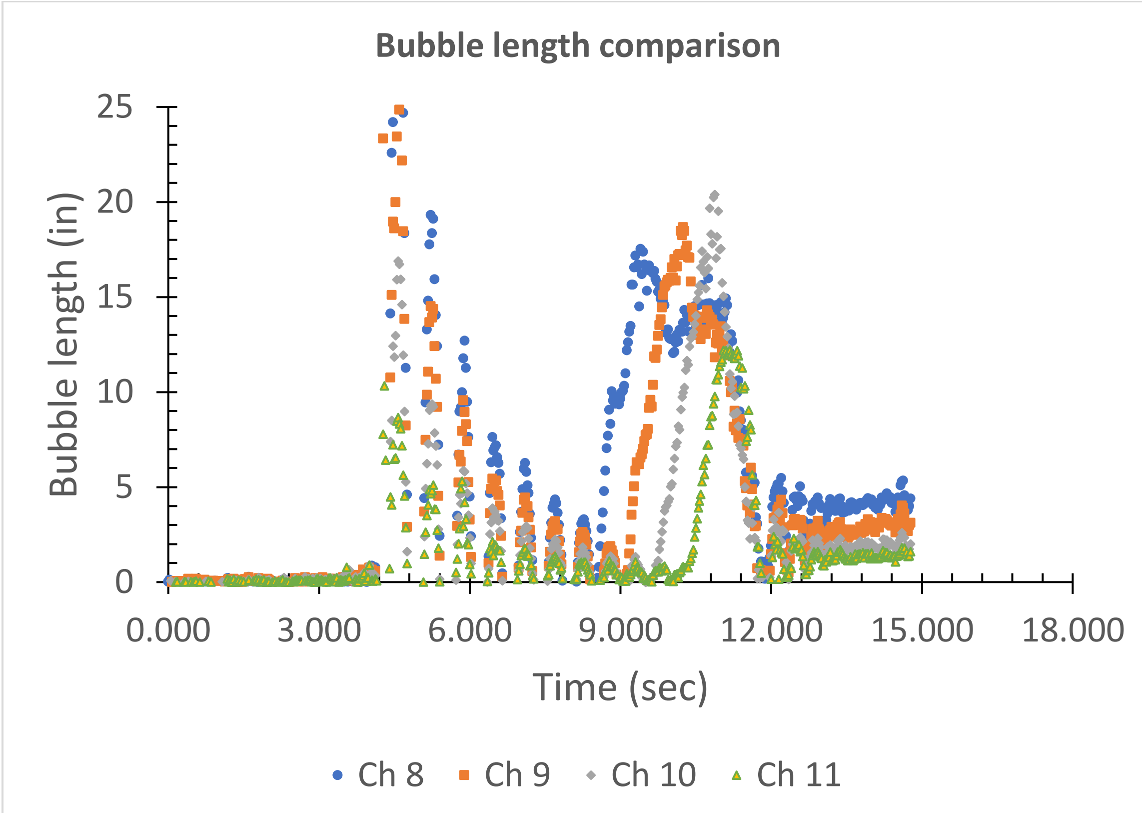
Bubble length comparison
Bubble length (in)
0
5
10
15
20
25
0.000
3.000
6.000
9.000
12.000
15.000
18.000
Time (sec)
Ch 8
Ch 9
Ch 10
Ch 11

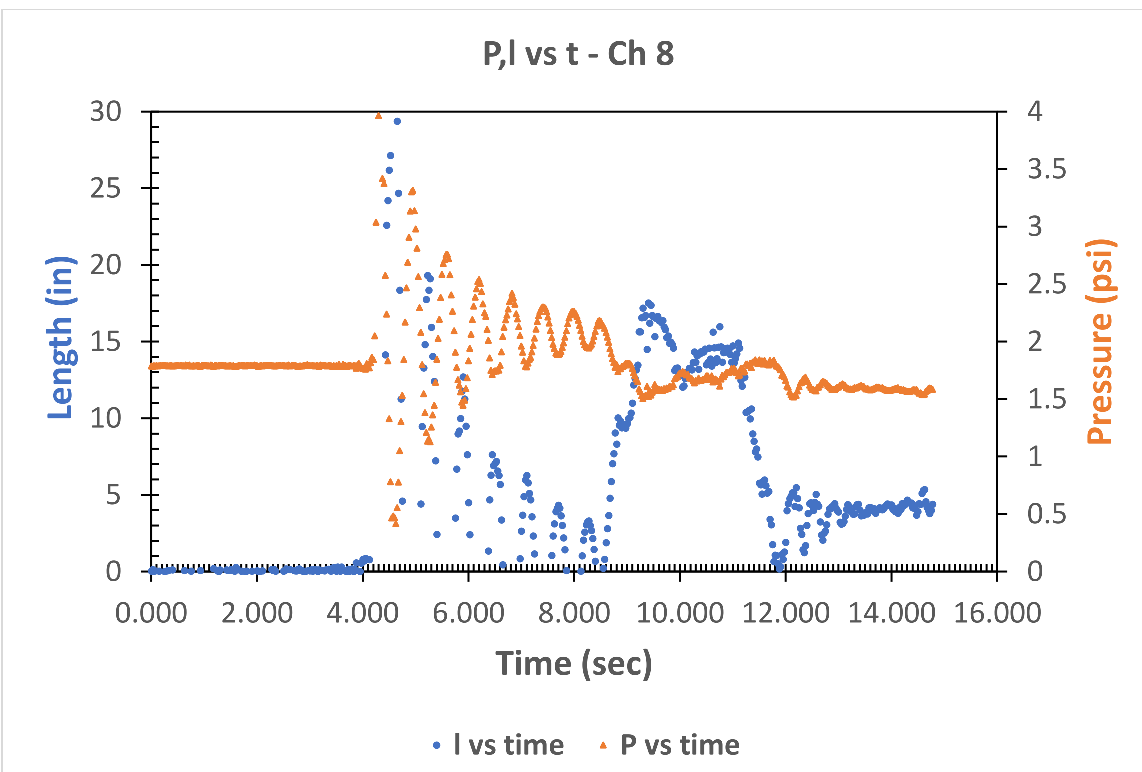
P,l vs t - Ch 8
Length (in)
0
5
10
15
20
25
30
Pressure (psi)
0
0.5
1
1.5
2
2.5
3
3.5
4
0.000
2.000
4.000
6.000
8.000
10.000
12.000
14.000
16.000
Time (sec)
l vs time
P vs time

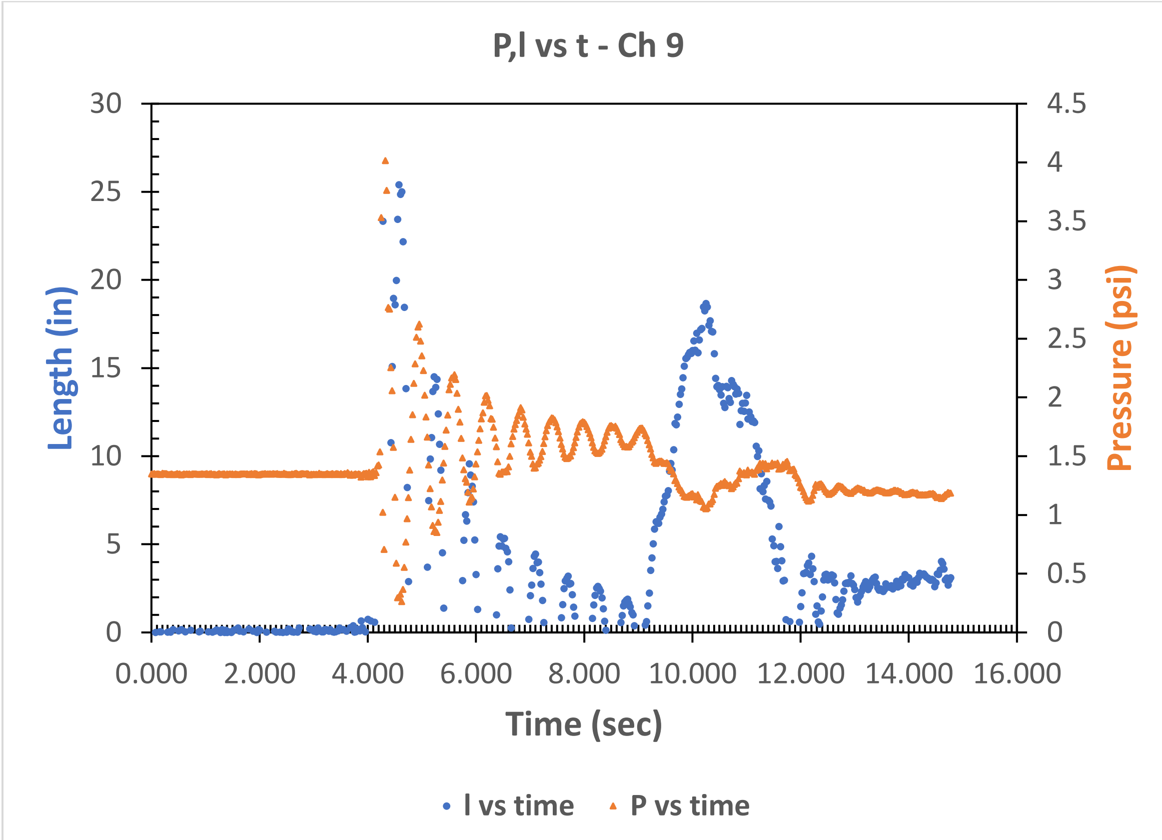
P,l vs t - Ch 9
Length (in)
Pressure (psi)
Time (sec)
0.000
2.000
4.000
6.000
8.000
10.000
12.000
14.000
16.000
0
5
10
15
20
25
30
0
0.5
1
1.5
2
2.5
3
3.5
4
4.5
l vs time
P vs time

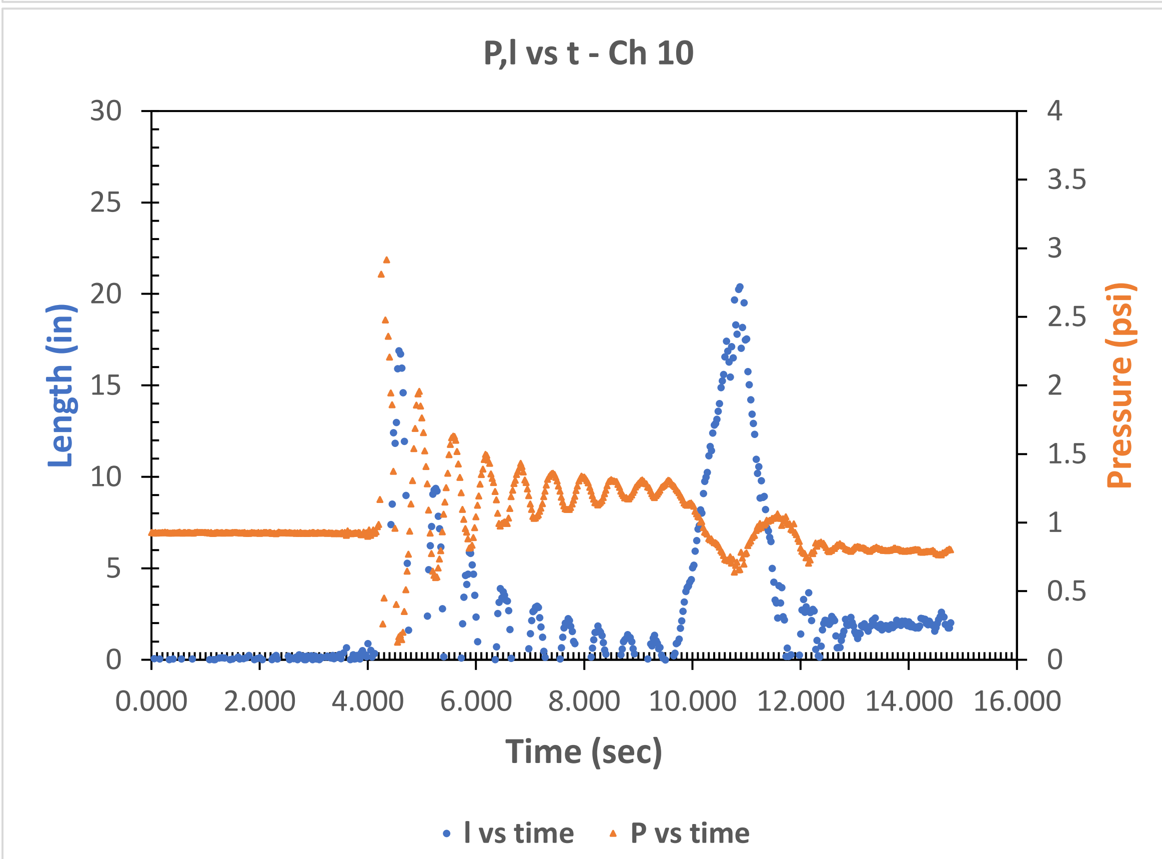
P,l vs t - Ch 10
Length (in)
Pressure (psi)
Time (sec)
0.000
2.000
4.000
6.000
8.000
10.000
12.000
14.000
16.000
0
5
10
15
20
25
30
0
0.5
1
1.5
2
2.5
3
3.5
4
l vs time
P vs time

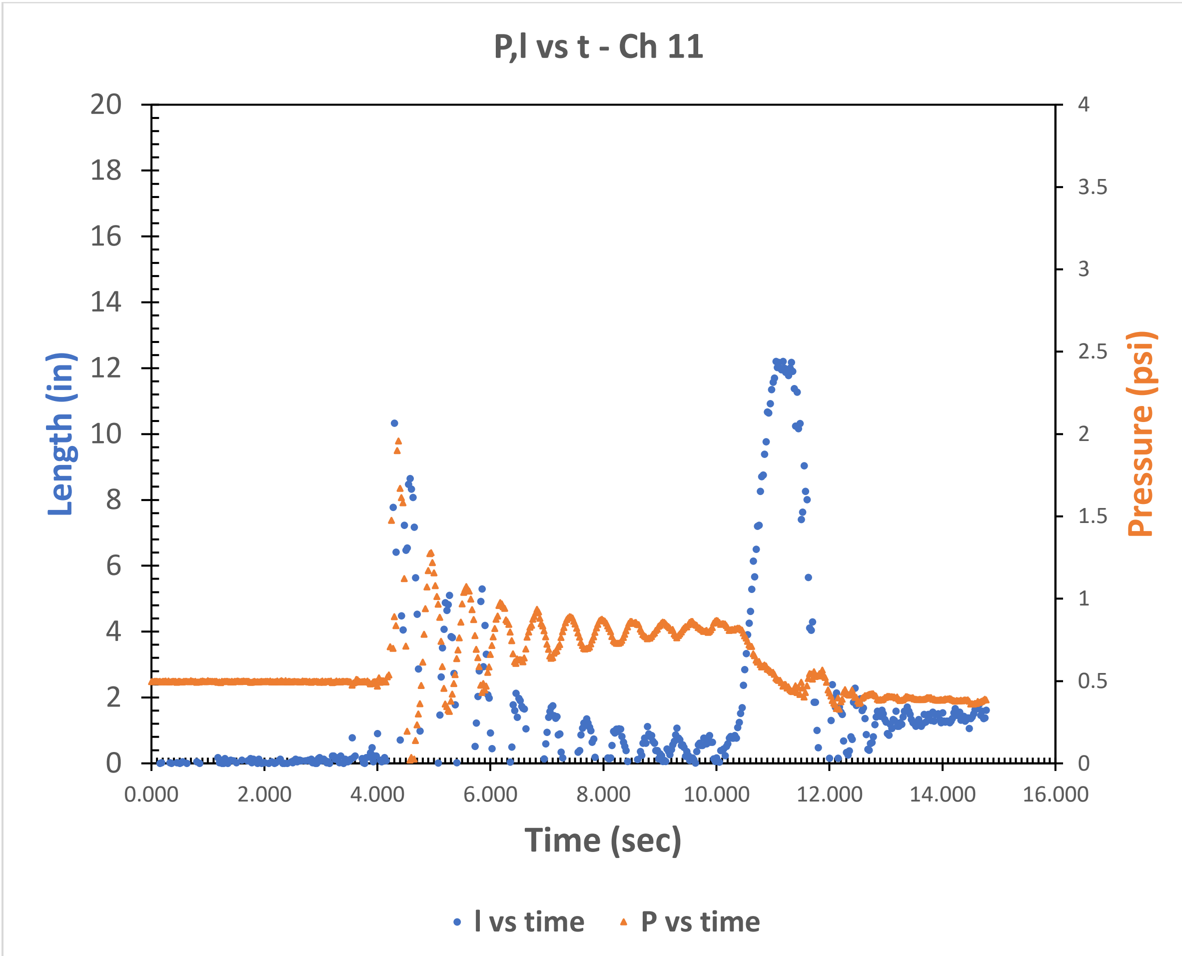
P,l vs t - Ch 11
Length (in)
Pressure (psi)
Time (sec)
0
2
4
6
8
10
12
14
16
18
20
0
0.5
1
1.5
2
2.5
3
3.5
4
0.000
2.000
4.000
6.000
8.000
10.000
12.000
14.000
16.000
l vs time
P vs time

Appendix C

Calibration Plots for Viscous Gel – Air Experiments

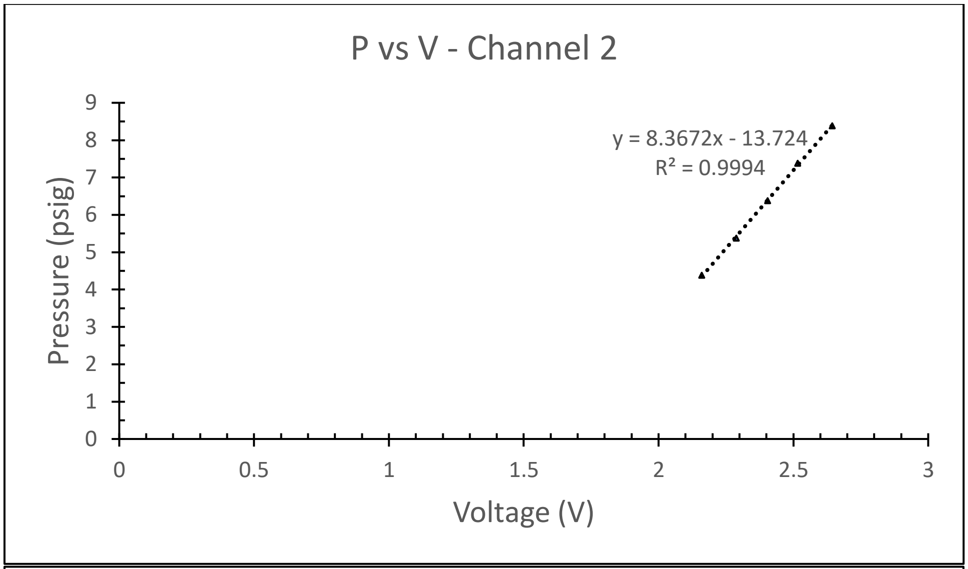

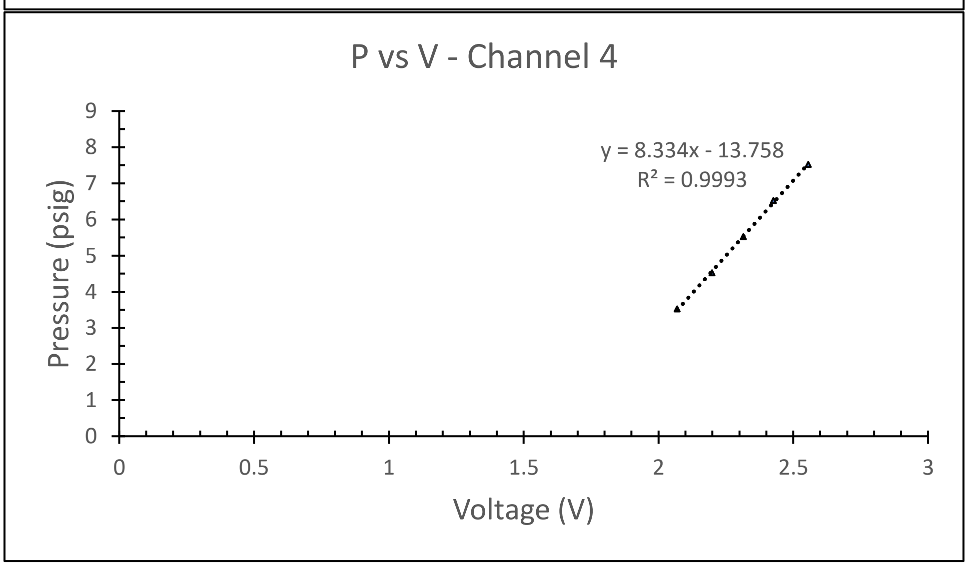

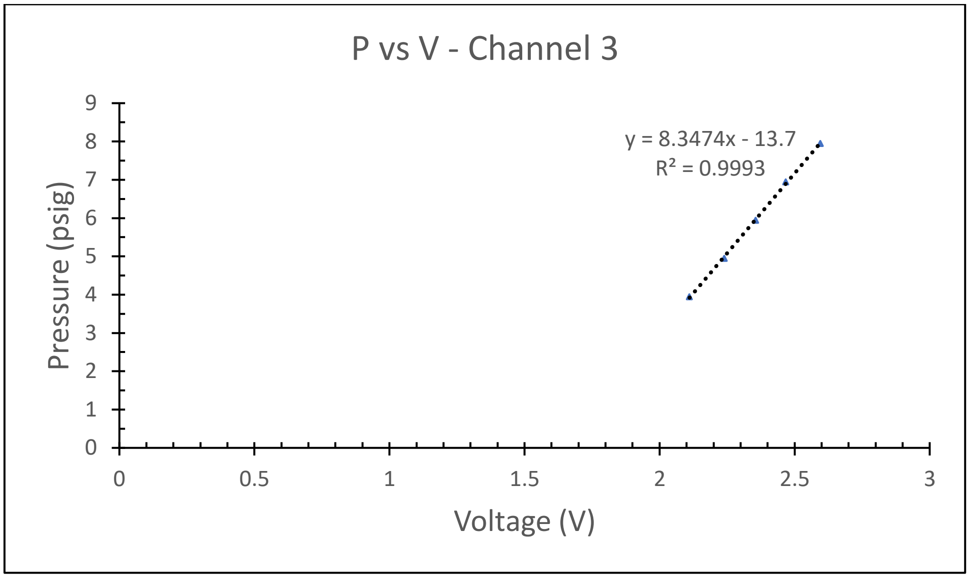
P vs V - Channel 3
y = 8.3474x - 13.7
R² = 0.9993
Pressure (psig)
Voltage (V)
0
0.5
1
1.5
2
2.5
3
9
8
7
6
5
4
3
2
1
0

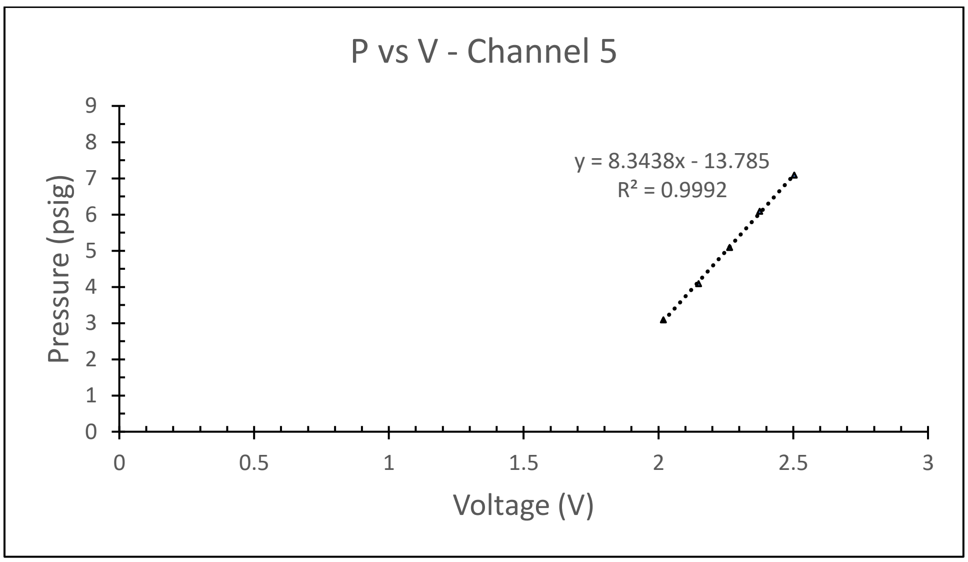
P vs V - Channel 5
y = 8.3438x - 13.785
R² = 0.9992
Pressure (psig)
Voltage (V)
0
0.5
1
1.5
2
2.5
3
9
8
7
6
5
4
3
2
1
0

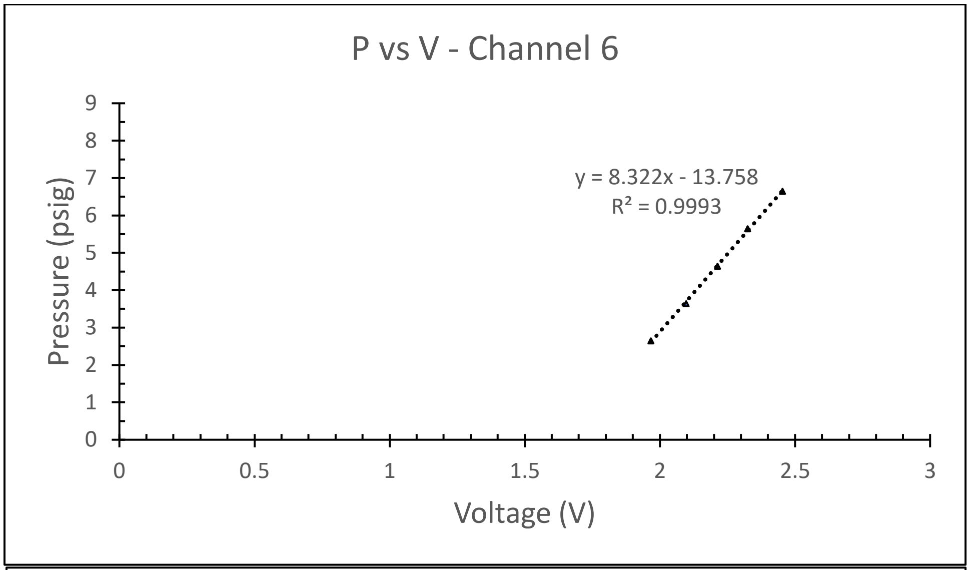
P vs V - Channel 6
y = 8.322x - 13.758
R² = 0.9993
Pressure (psig)
Voltage (V)
0
1
2
3
4
5
6
7
8
9
0
0.5
1
1.5
2
2.5
3

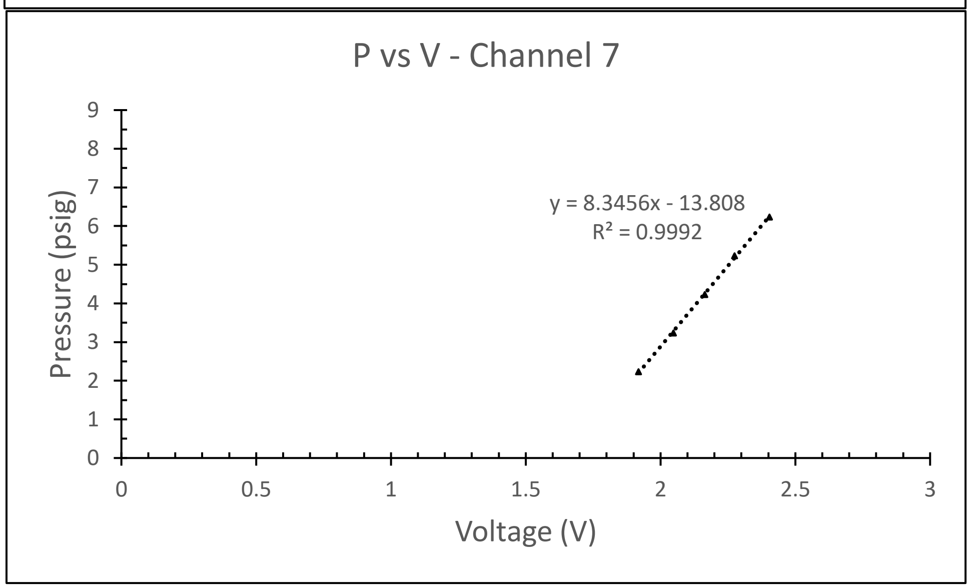
P vs V - Channel 7
y = 8.3456x - 13.808
R² = 0.9992
Pressure (psig)
Voltage (V)
0
1
2
3
4
5
6
7
8
9
0
0.5
1
1.5
2
2.5
3

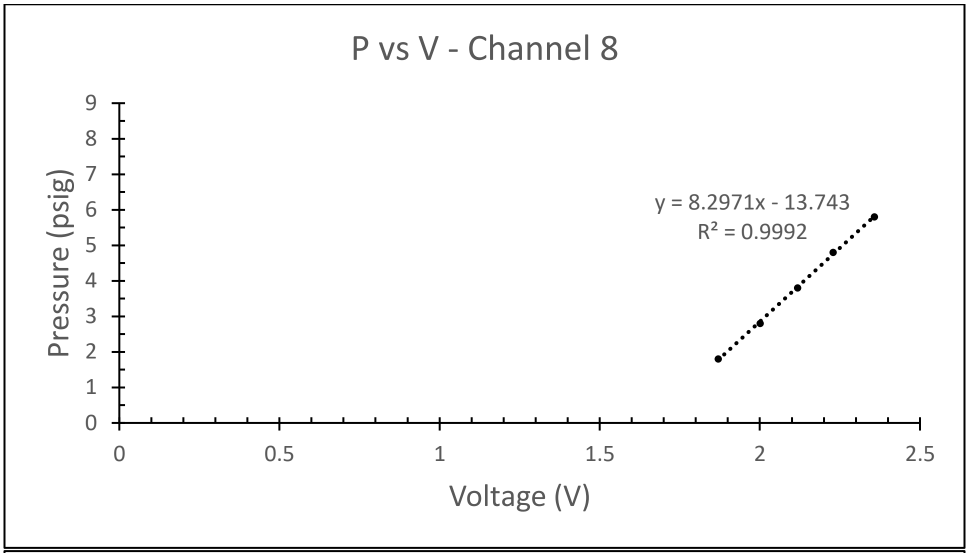
P vs V - Channel 8
y = 8.2971x - 13.743
R² = 0.9992
Pressure (psig)
Voltage (V)
0
1
2
3
4
5
6
7
8
9
0.5
1.5
2.5

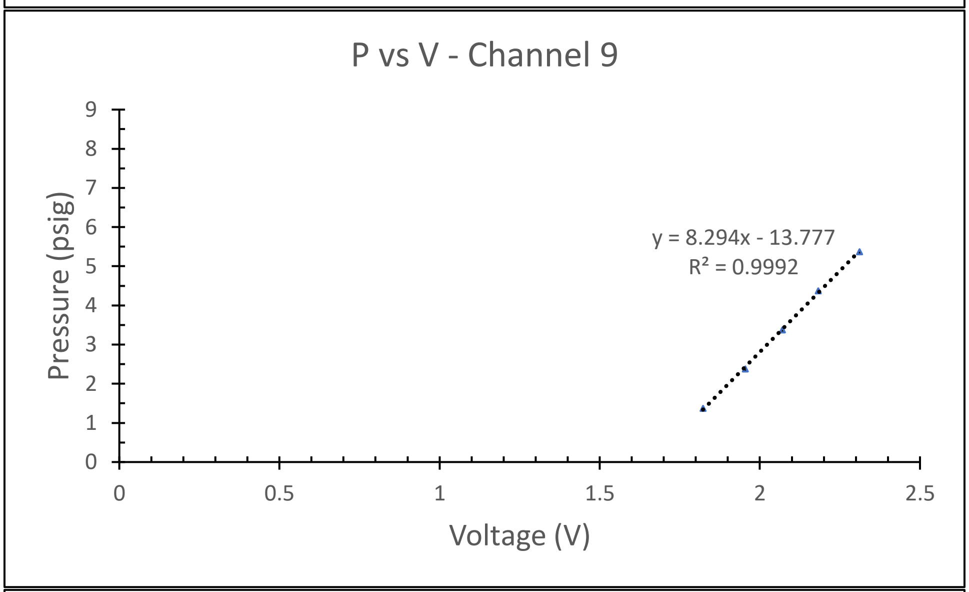
P vs V - Channel 9
y = 8.294x - 13.777
R² = 0.9992
Pressure (psig)
Voltage (V)
0
1
2
3
4
5
6
7
8
9
0.5
1.5
2.5

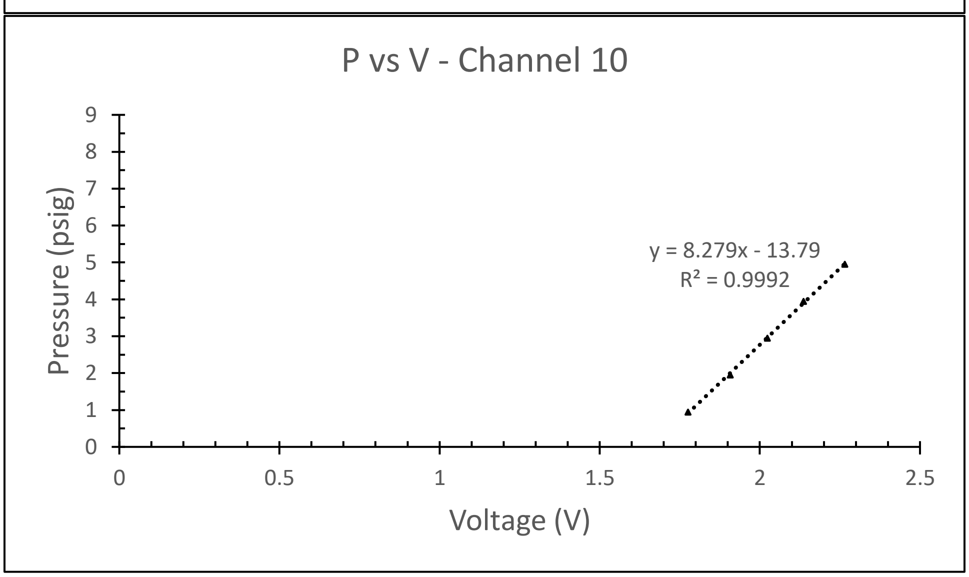
P vs V - Channel 10
y = 8.279x - 13.79
R² = 0.9992
Pressure (psig)
Voltage (V)
0
1
2
3
4
5
6
7
8
9
0.5
1.5
2.5

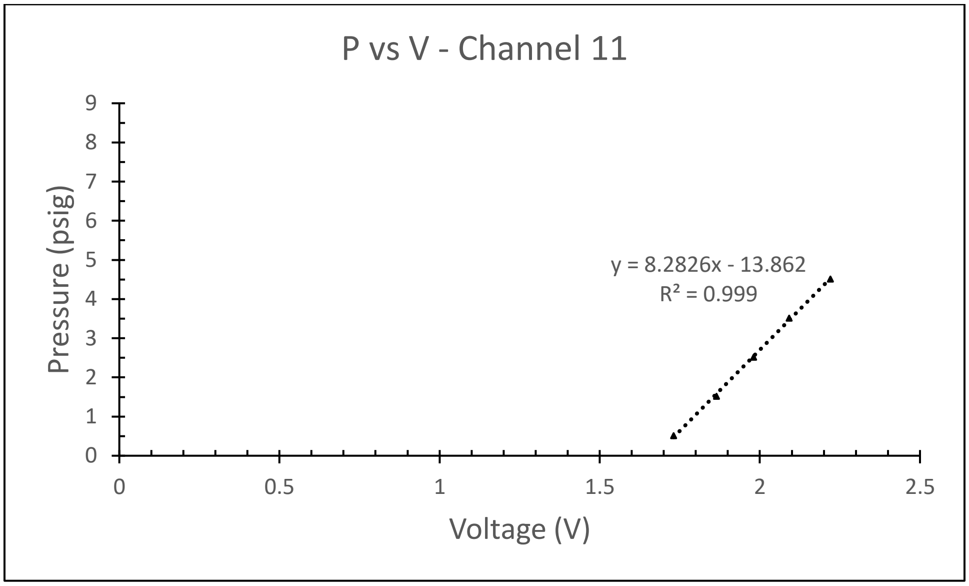
P vs V - Channel 11
y = 8.2826x - 13.862
R² = 0.999
Pressure (psig)
Voltage (V)
0
1
2
3
4
5
6
7
8
9
0
0.5
1
1.5
2
2.5

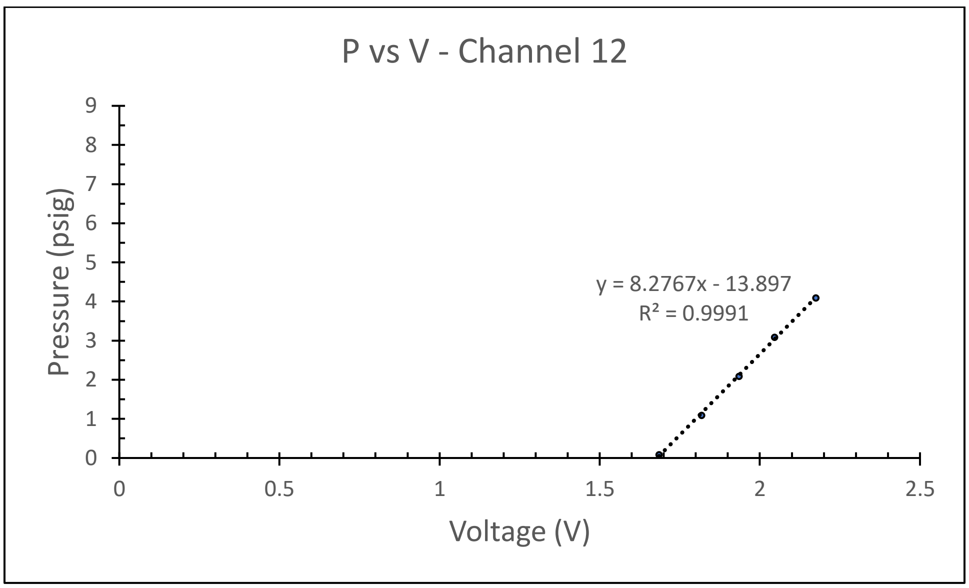
P vs V - Channel 12
y = 8.2767x - 13.897
R² = 0.9991
Pressure (psig)
Voltage (V)
0
1
2
3
4
5
6
7
8
9
0
0.5
1
1.5
2
2.5

Viscous Gel – Air Experiment 1

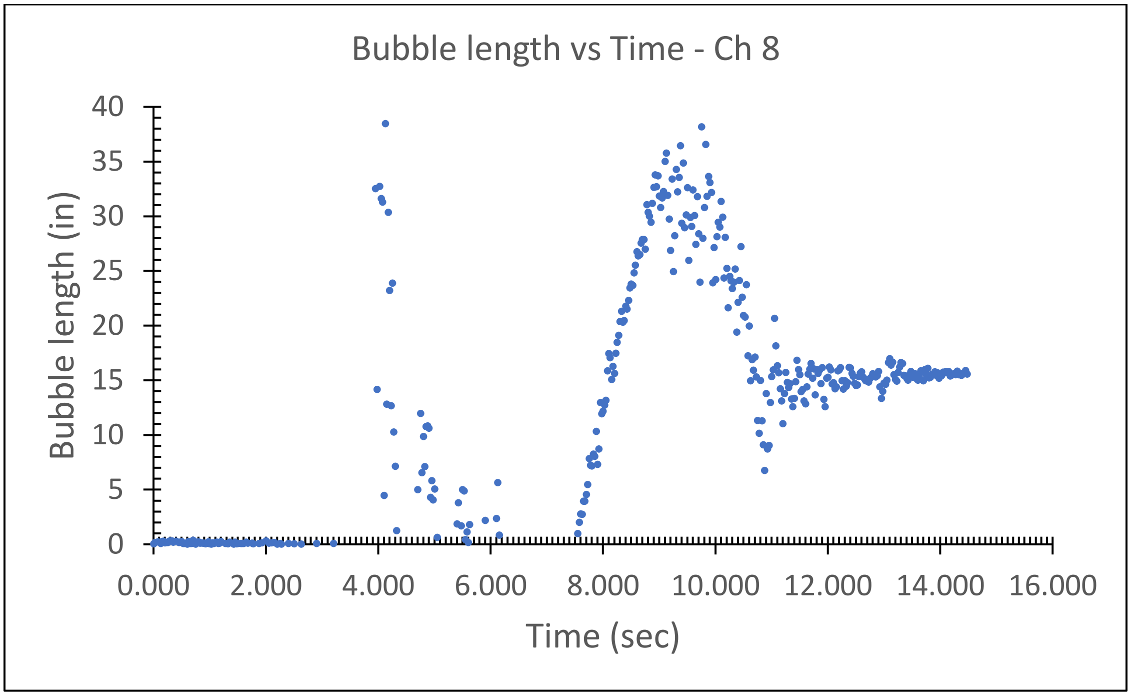

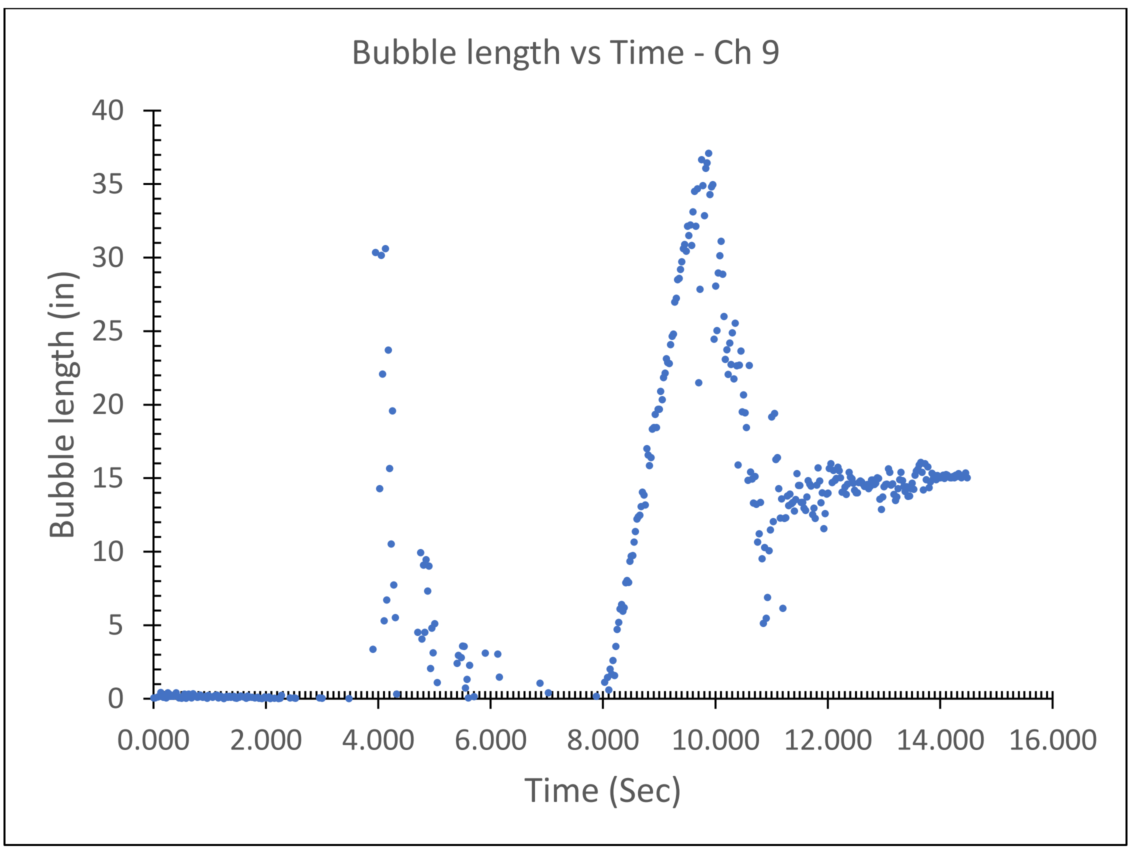

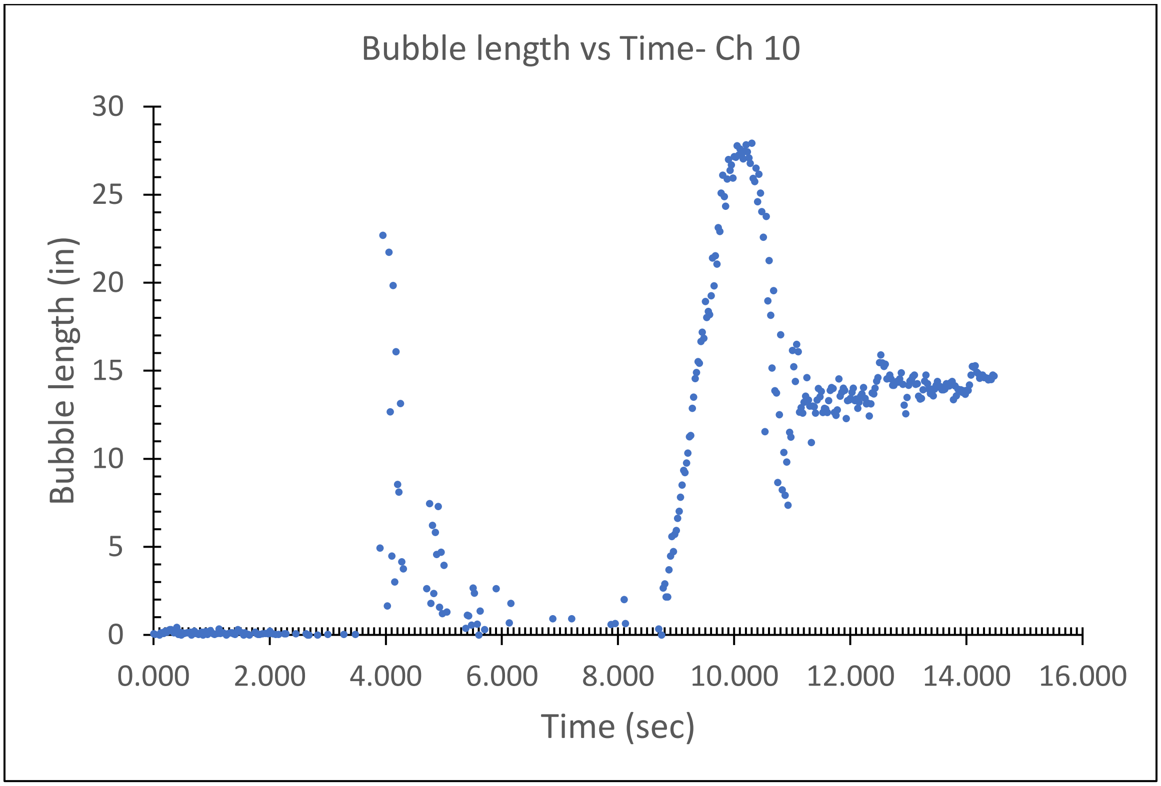
Bubble length vs Time- Ch 10
Bubble length (in)
Time (sec)
0
5
10
15
20
25
30
0.000
2.000
4.000
6.000
8.000
10.000
12.000
14.000
16.000

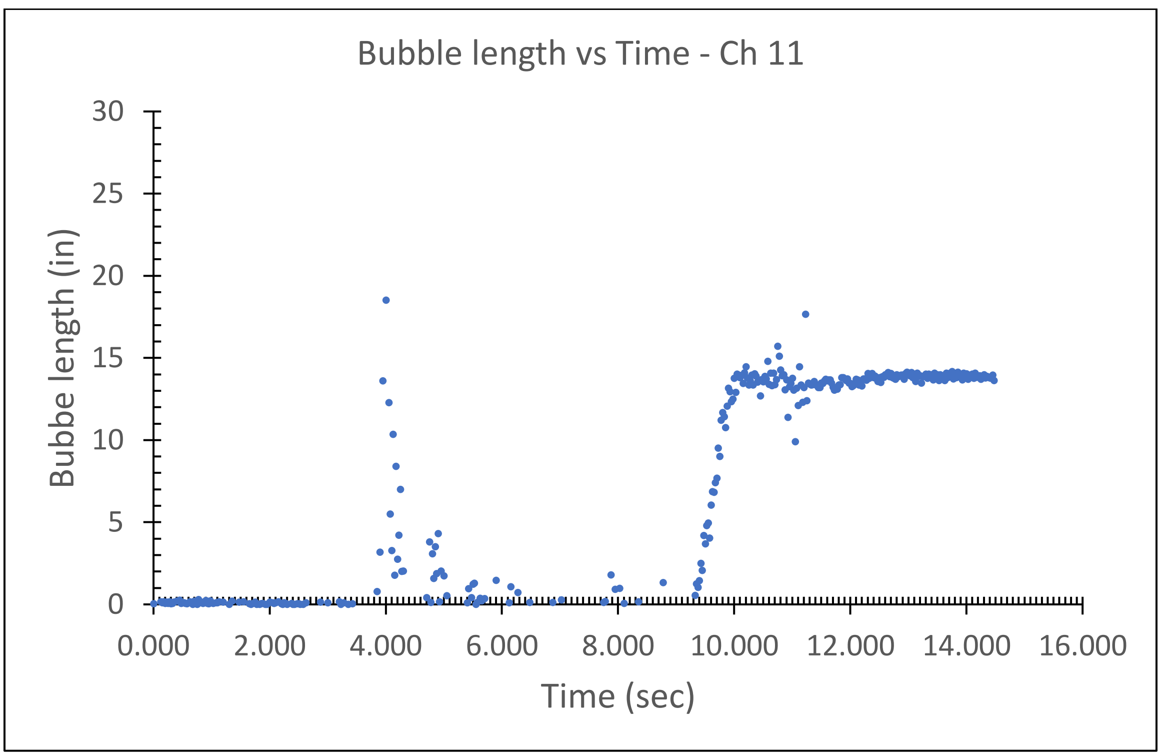
Bubble length vs Time - Ch 11
Bubbe length (in)
Time (sec)
0
5
10
15
20
25
30
0.000
2.000
4.000
6.000
8.000
10.000
12.000
14.000
16.000

Viscous Gel – Air Experiment 2

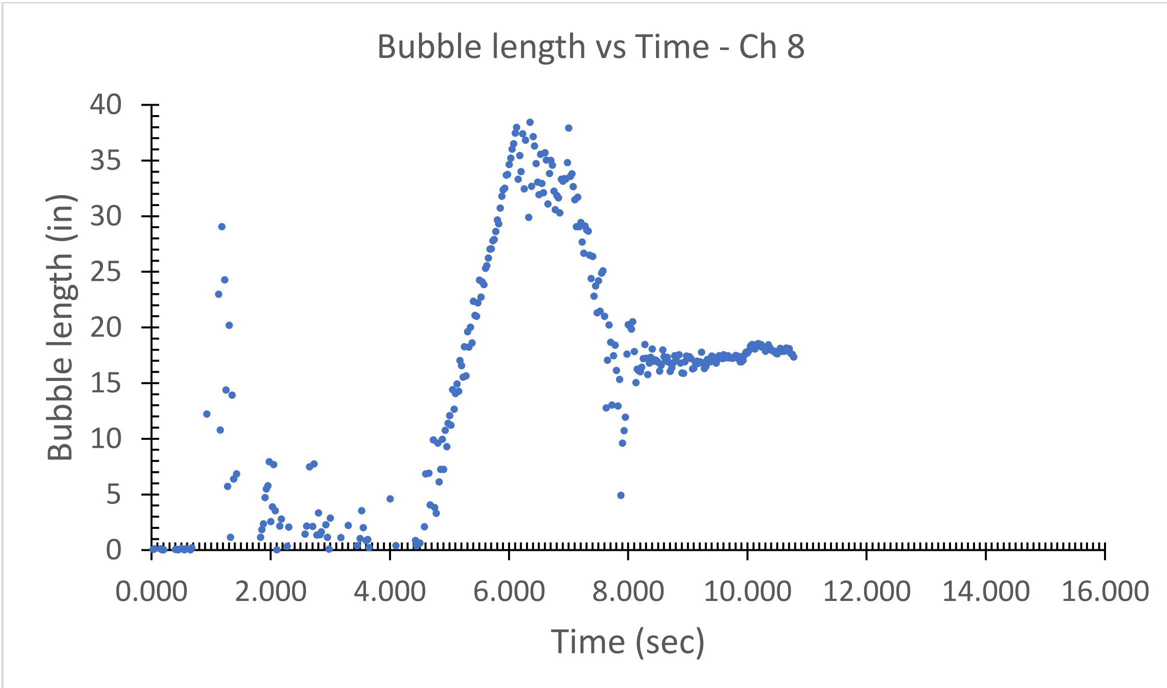

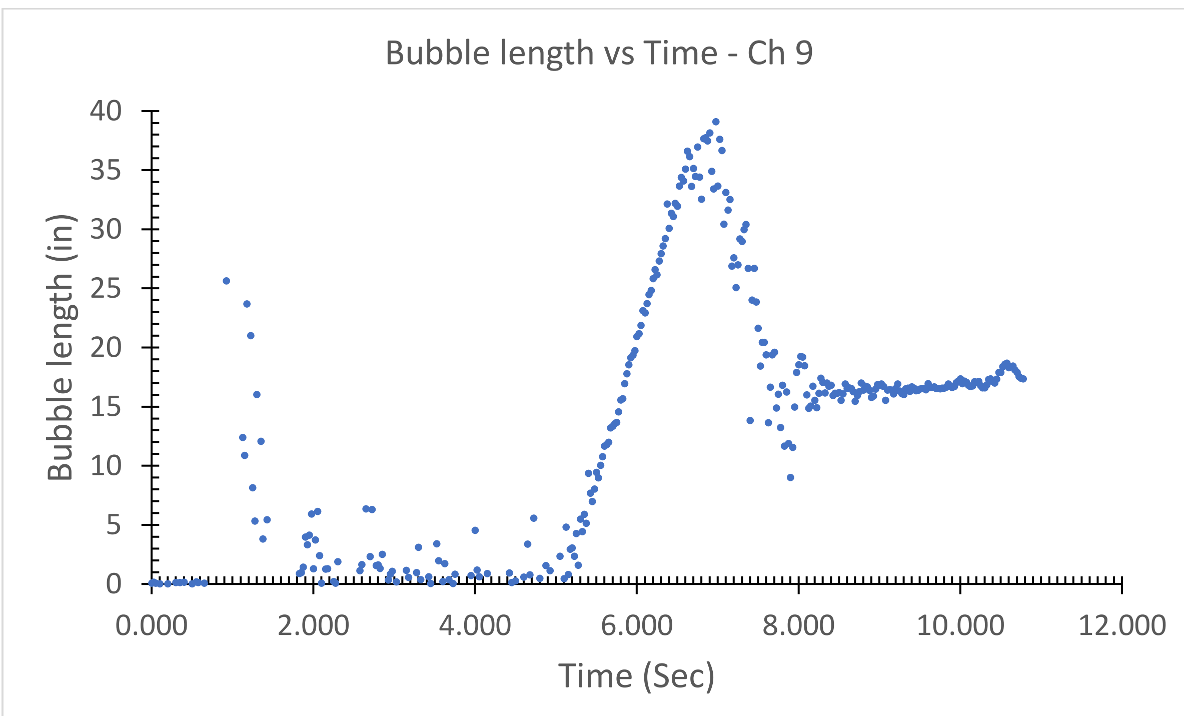

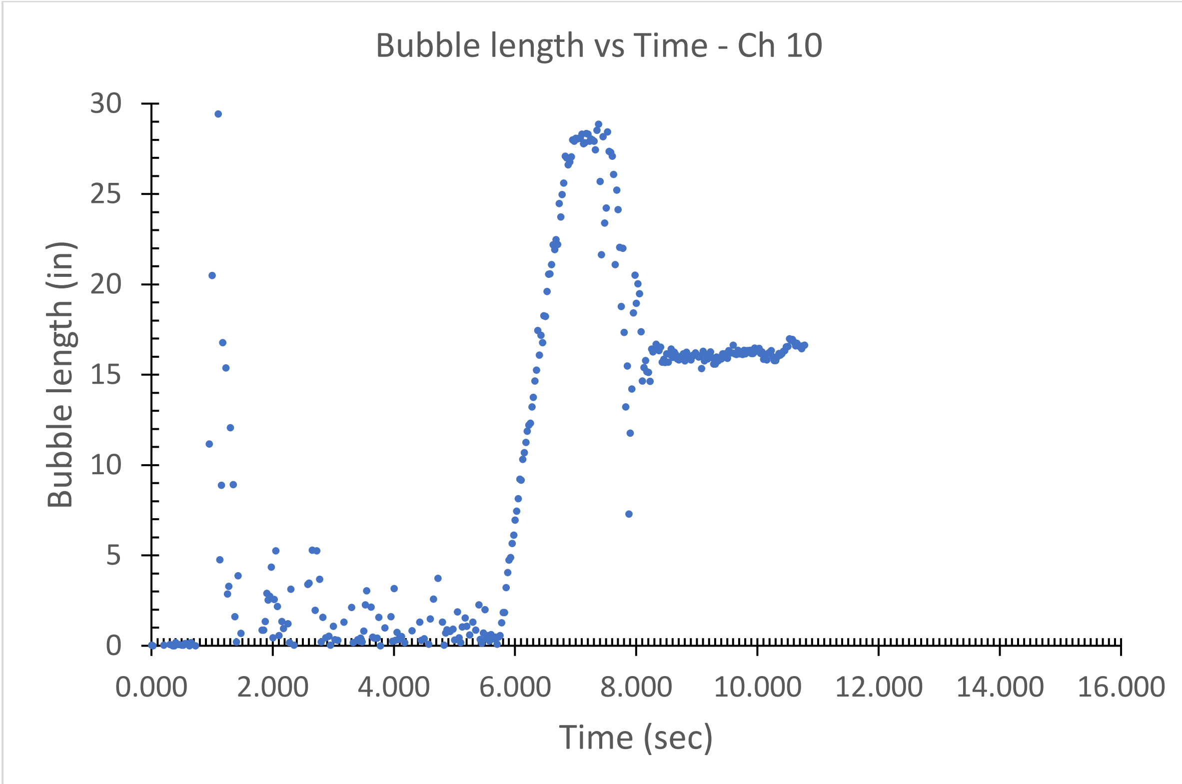
Bubble length vs Time - Ch 10
Bubble length (in)
30
25
20
15
10
5
0
0.000
2.000
4.000
6.000
8.000
10.000
12.000
14.000
16.000
Time (sec)

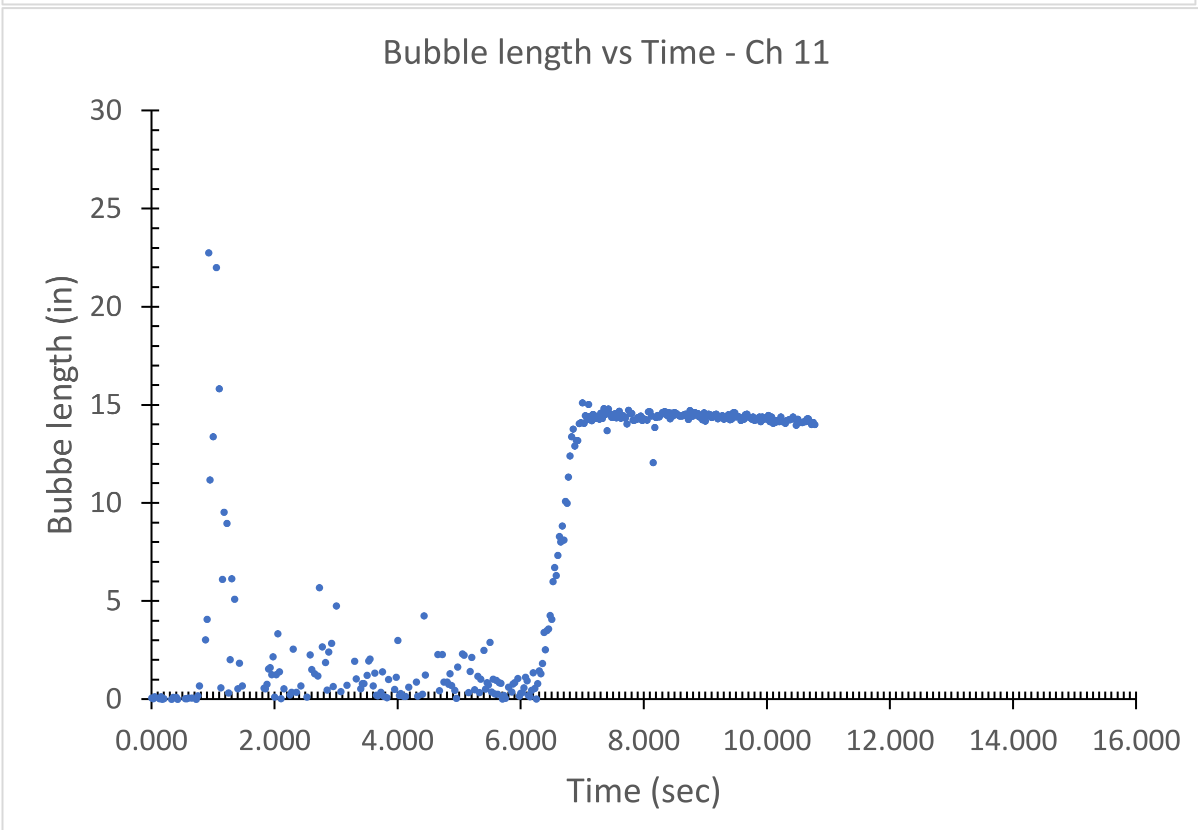
Bubble length vs Time - Ch 11
Bubbe length (in)
30
25
20
15
10
5
0
0.000
2.000
4.000
6.000
8.000
10.000
12.000
14.000
16.000
Time (sec)

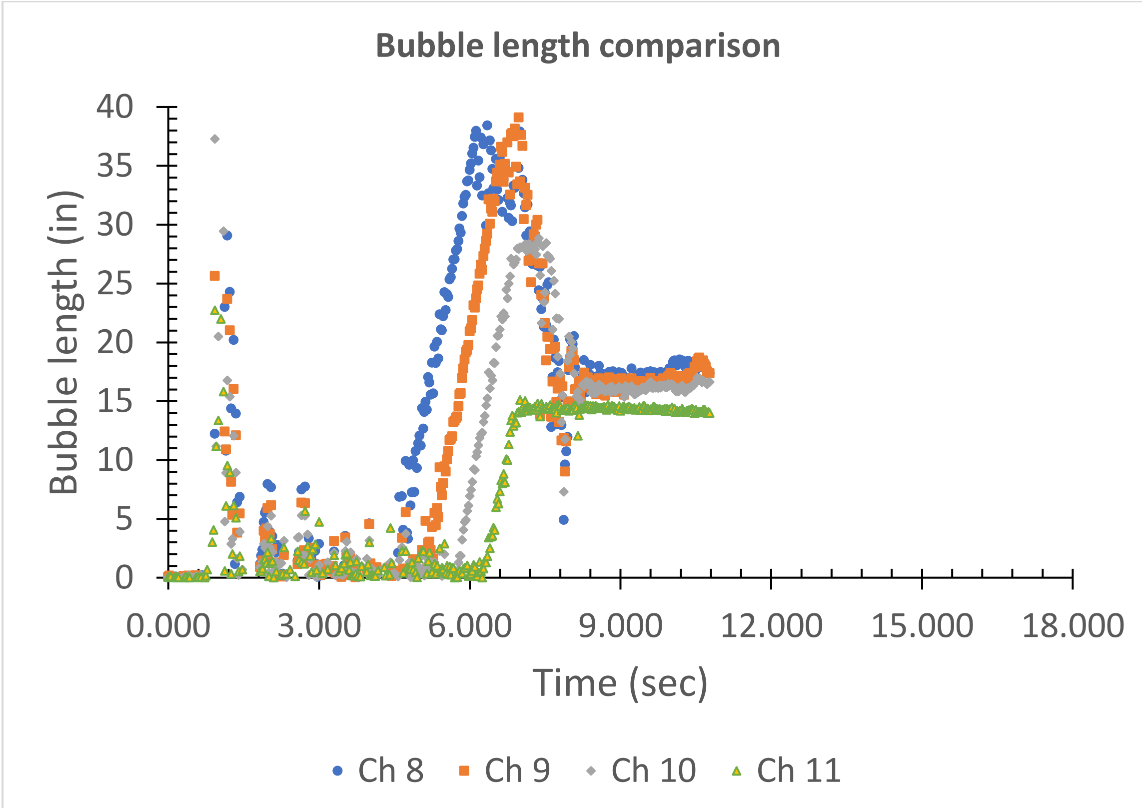
Bubble length comparison
Bubble length (in)
40
35
30
25
20
15
10
5
0
0.000
3.000
6.000
9.000
12.000
15.000
18.000
Time (sec)
Ch 8
Ch 9
Ch 10
Ch 11

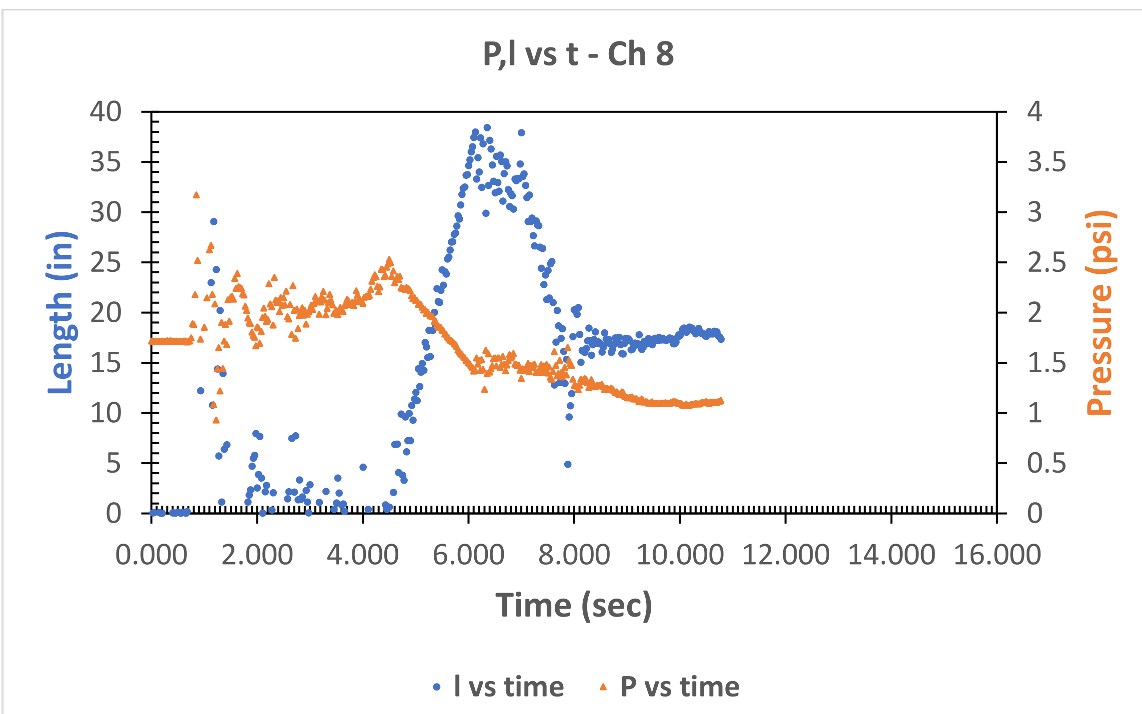
P,l vs t - Ch 8
Length (in)
40
35
30
25
20
15
10
5
0
Pressure (psi)
4
3.5
3
2.5
2
1.5
1
0.5
0
0.000
2.000
4.000
6.000
8.000
10.000
12.000
14.000
16.000
Time (sec)
l vs time
P vs time

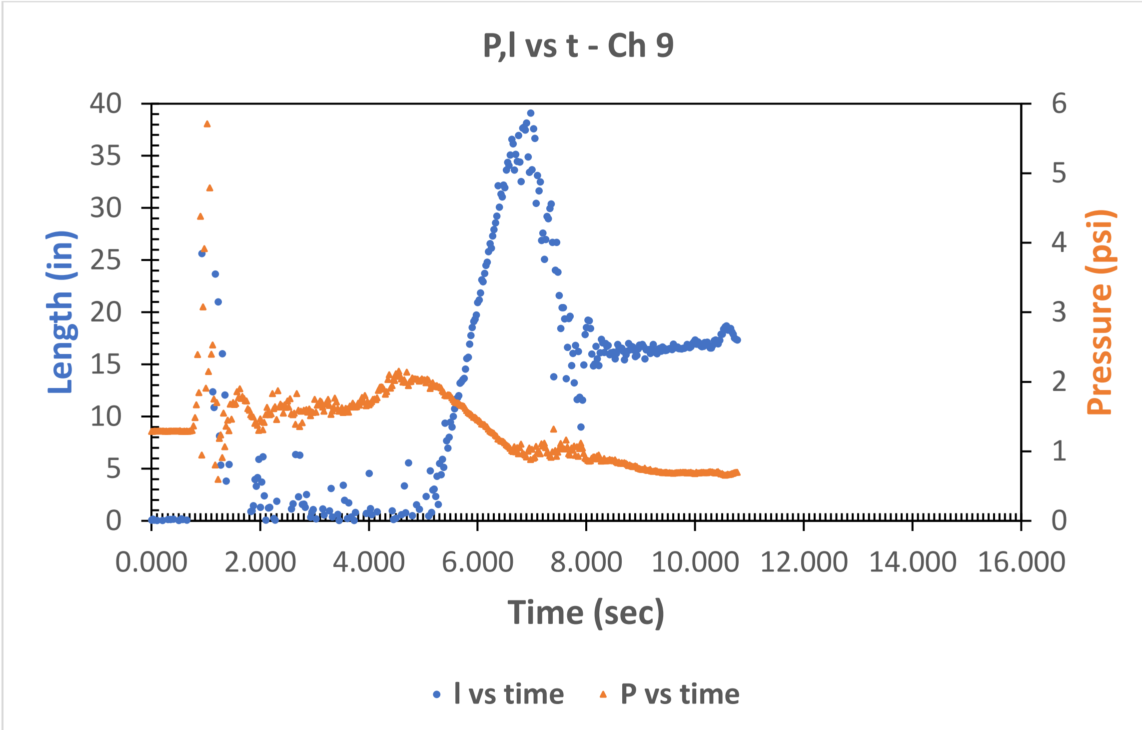
P,l vs t - Ch 9
Length (in)
Pressure (psi)
Time (sec)
0.000
2.000
4.000
6.000
8.000
10.000
12.000
14.000
16.000
0
5
10
15
20
25
30
35
40
0
1
2
3
4
5
6
l vs time
P vs time

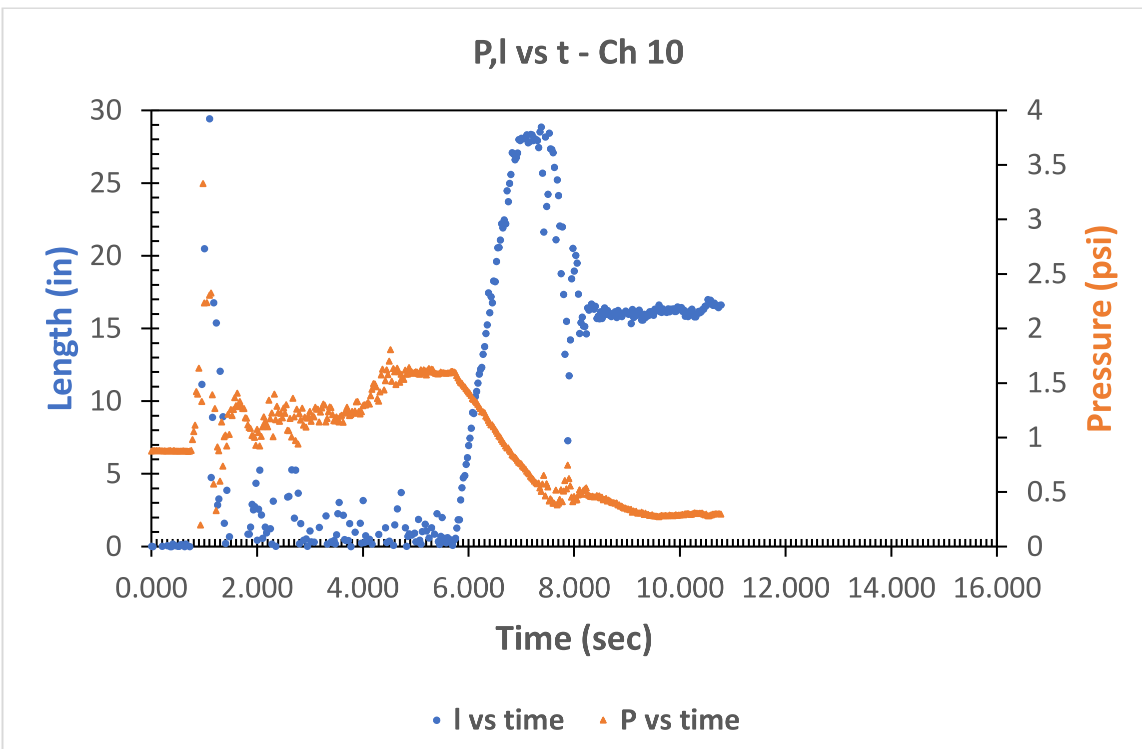
P,l vs t - Ch 10
Length (in)
Pressure (psi)
Time (sec)
0.000
2.000
4.000
6.000
8.000
10.000
12.000
14.000
16.000
0
5
10
15
20
25
30
0
0.5
1
1.5
2
2.5
3
3.5
4
l vs time
P vs time

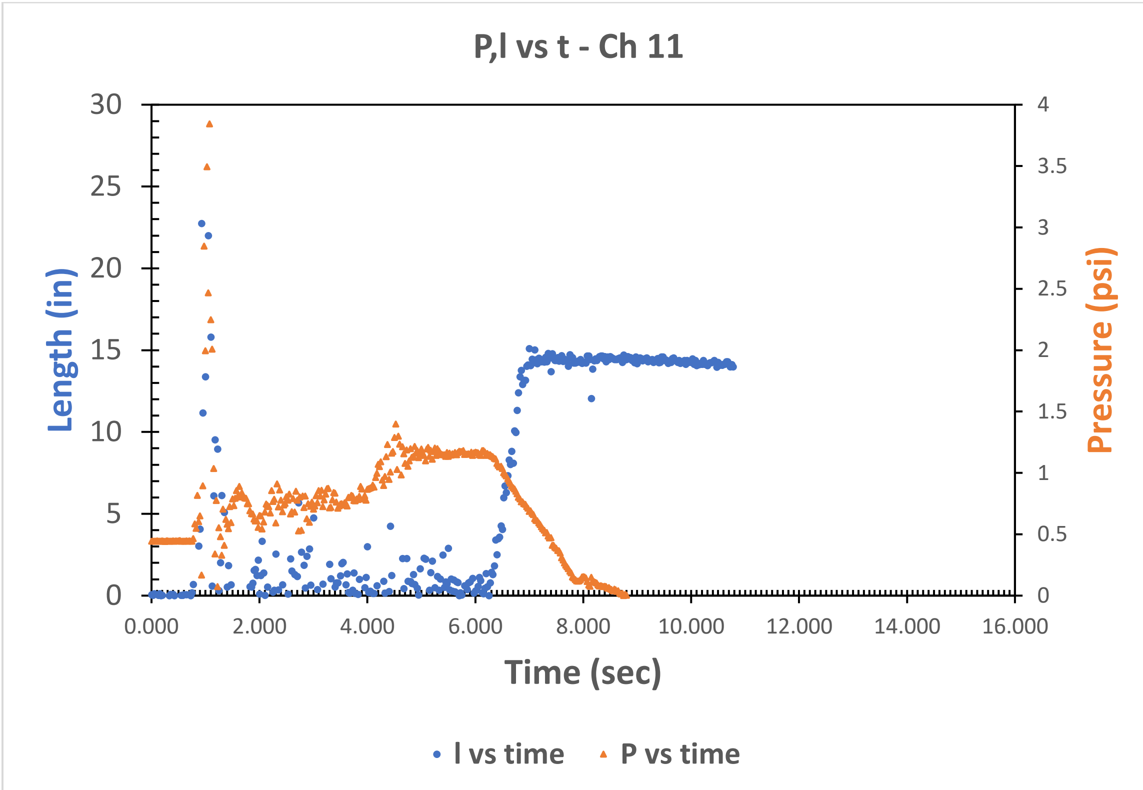

P,l vs t - Ch 11
Length (in)
Pressure (psi)
Time (sec)
30
25
20
15
10
5
0
4
3.5
3
2.5
2
1.5
1
0.5
0
0.000
2.000
4.000
6.000
8.000
10.000
12.000
14.000
16.000
l vs time
P vs time

Viscous Gel – Air Experiment 3

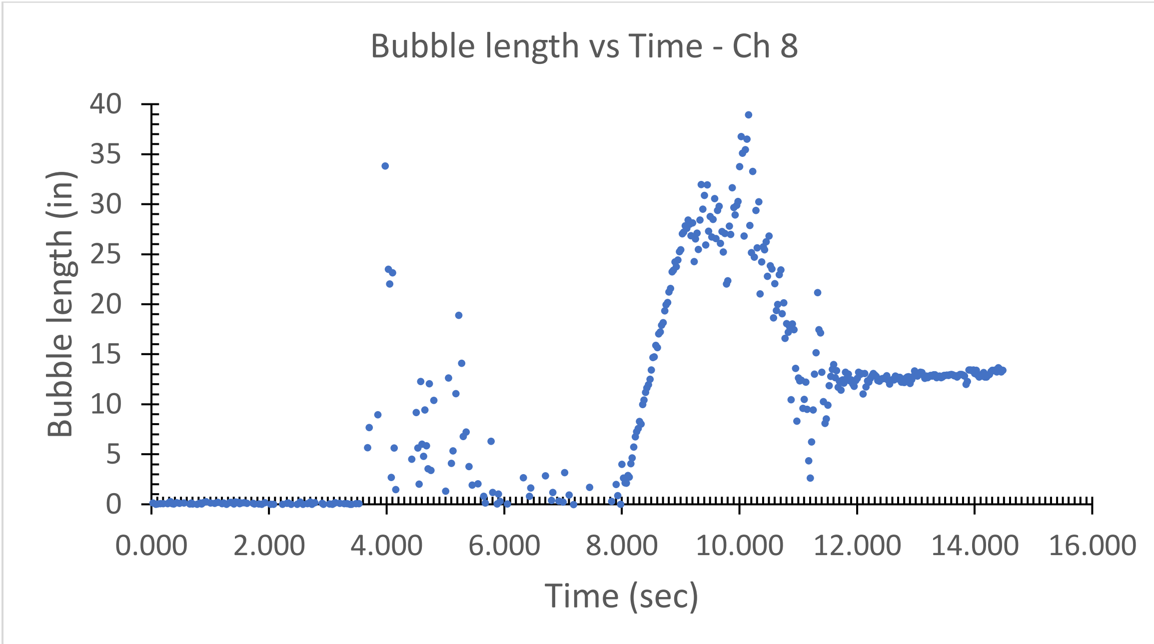

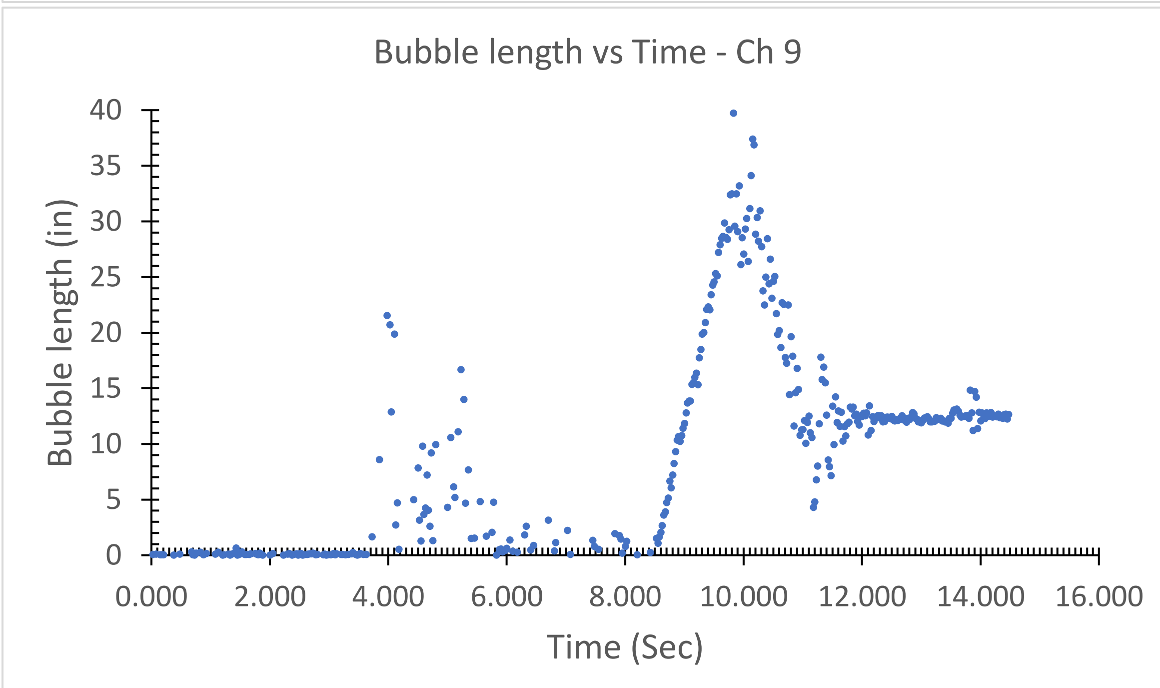

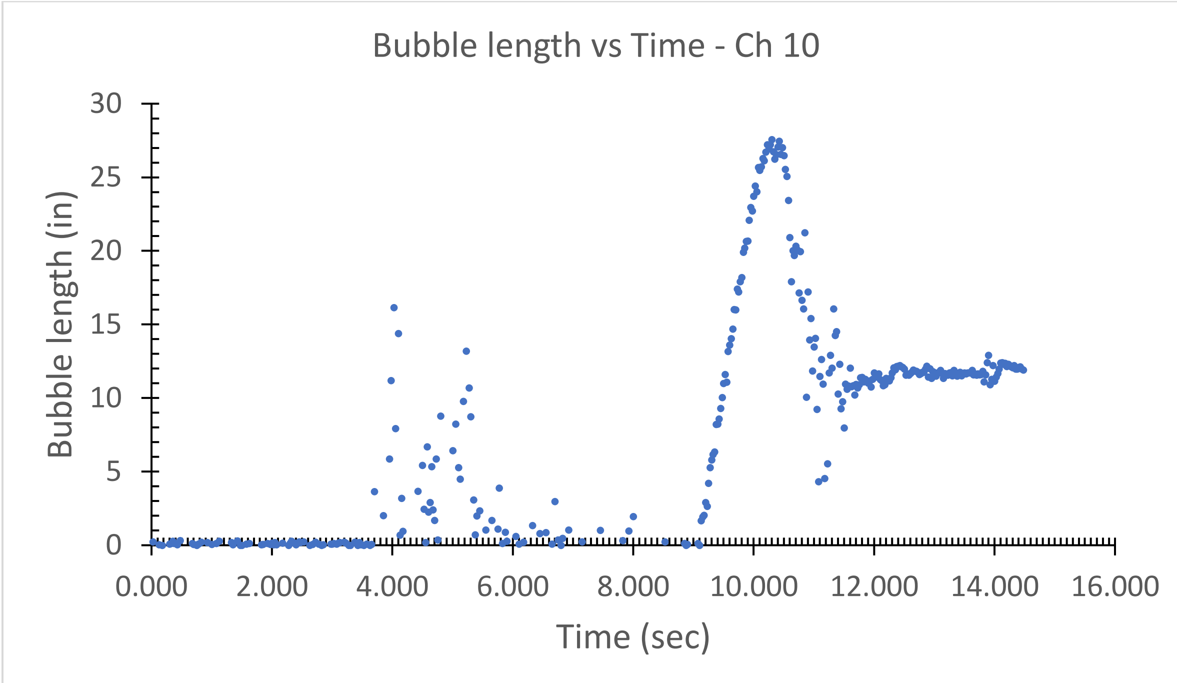

Bubble length vs Time - Ch 10
Bubble length (in)
30
25
20
15
10
5
0
0.000
2.000
4.000
6.000
8.000
10.000
12.000
14.000
16.000
Time (sec)

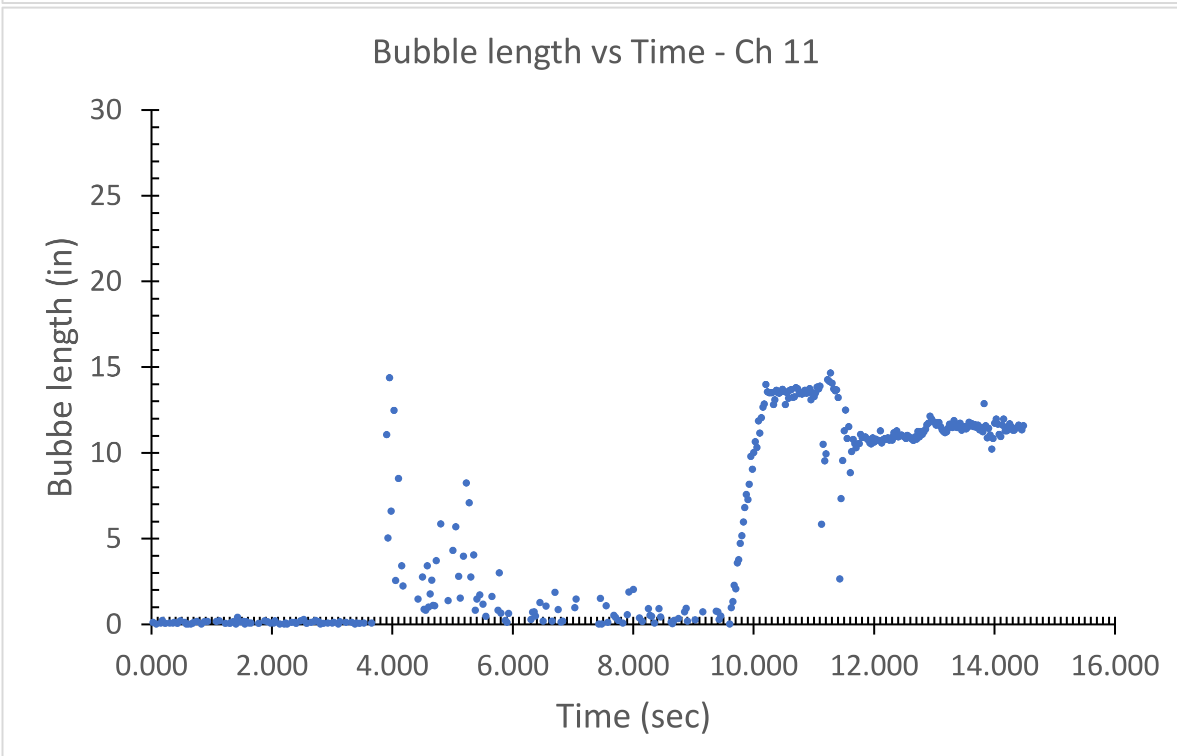

Bubble length vs Time - Ch 11
Bubbe length (in)
30
25
20
15
10
5
0
0.000
2.000
4.000
6.000
8.000
10.000
12.000
14.000
16.000
Time (sec)

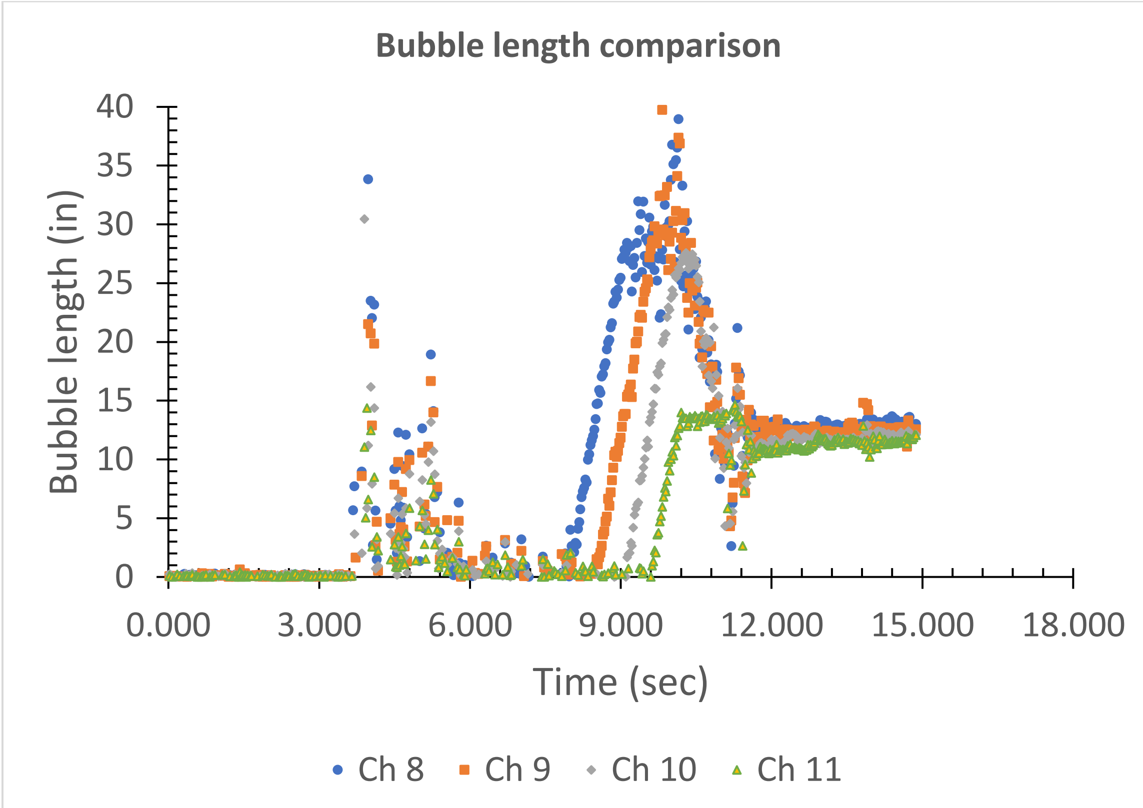

Bubble length comparison
Bubble length (in)
40
35
30
25
20
15
10
5
0
0.000
3.000
6.000
9.000
12.000
15.000
18.000
Time (sec)
Ch 8
Ch 9
Ch 10
Ch 11

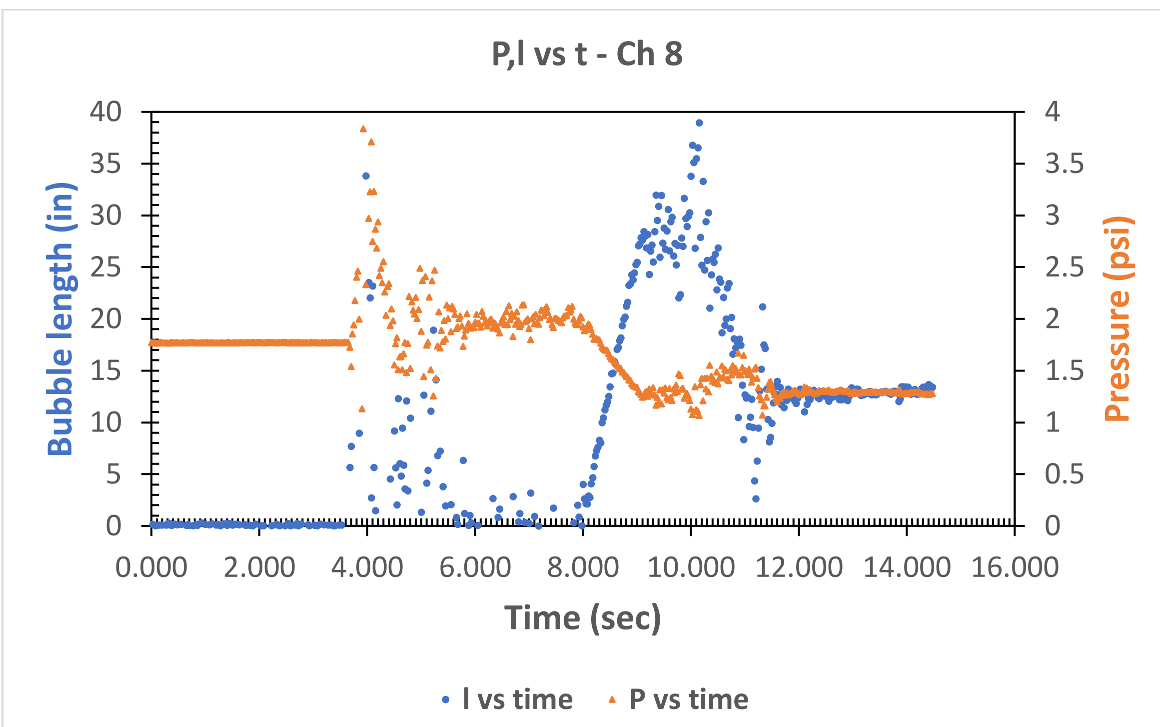

P,l vs t - Ch 8
Bubble length (in)
Pressure (psi)
40
35
30
25
20
15
10
5
0
4
3.5
3
2.5
2
1.5
1
0.5
0
0.000
2.000
4.000
6.000
8.000
10.000
12.000
14.000
16.000
Time (sec)
l vs time
P vs time

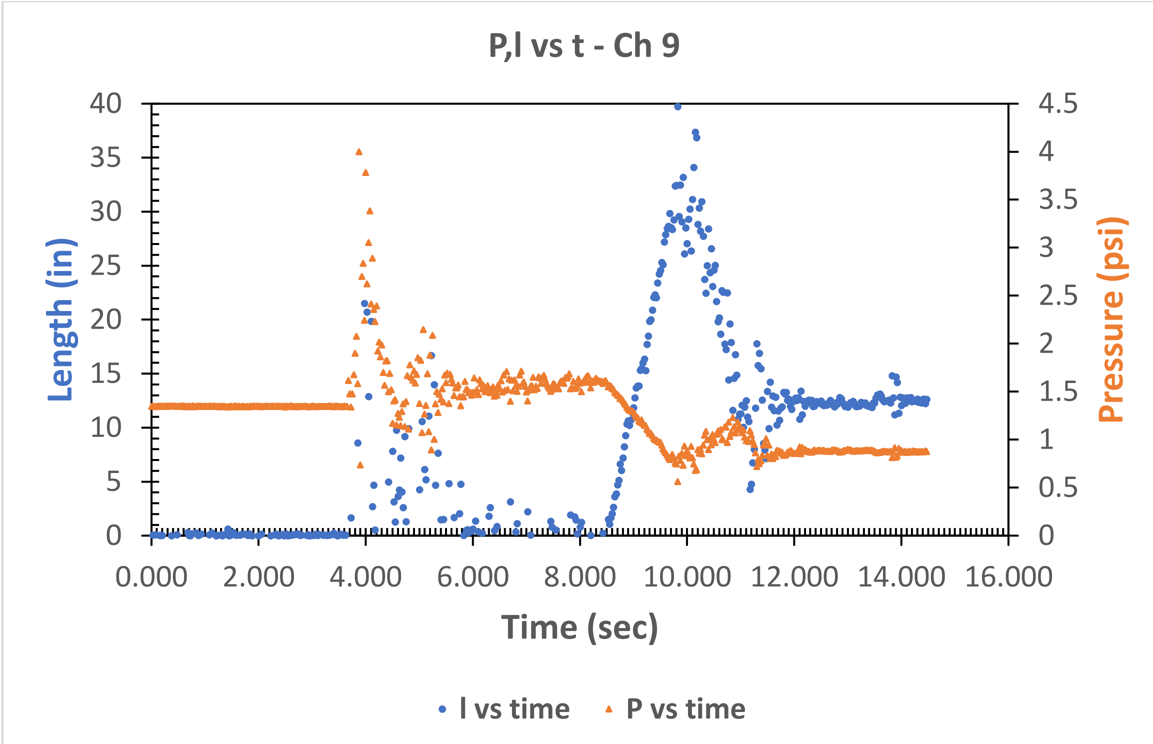
P,l vs t - Ch 9
Length (in)
Pressure (psi)
Time (sec)
l vs time
P vs time
40
35
30
25
20
15
10
5
0
4.5
4
3.5
3
2.5
2
1.5
1
0.5
0
0.000
2.000
4.000
6.000
8.000
10.000
12.000
14.000
16.000

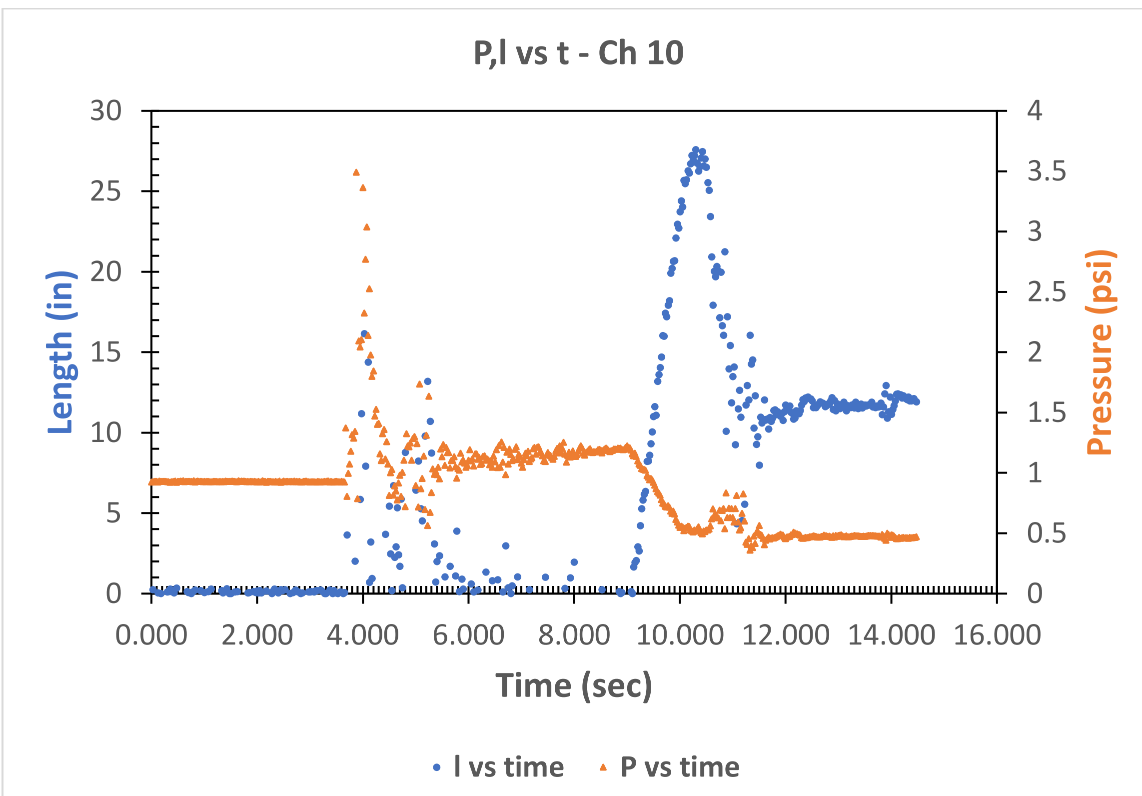
P,l vs t - Ch 10
Length (in)
Pressure (psi)
Time (sec)
l vs time
P vs time
30
25
20
15
10
5
0
4
3.5
3
2.5
2
1.5
1
0.5
0
0.000
2.000
4.000
6.000
8.000
10.000
12.000
14.000
16.000

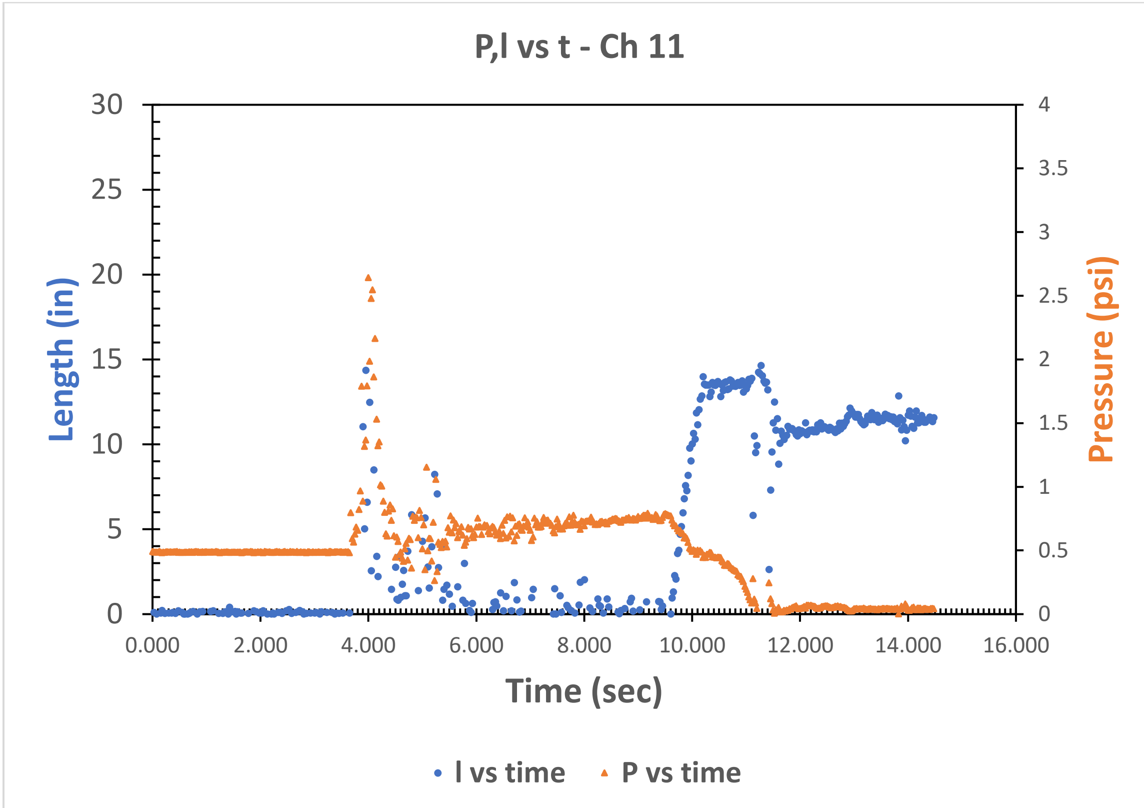
P,l vs t - Ch 11
Length (in)
Pressure (psi)
Time (sec)
0
5
10
15
20
25
30
0
0.5
1
1.5
2
2.5
3
3.5
4
0.000
2.000
4.000
6.000
8.000
10.000
12.000
14.000
16.000
l vs time
P vs time

Viscous Gel – Air Experiment 4

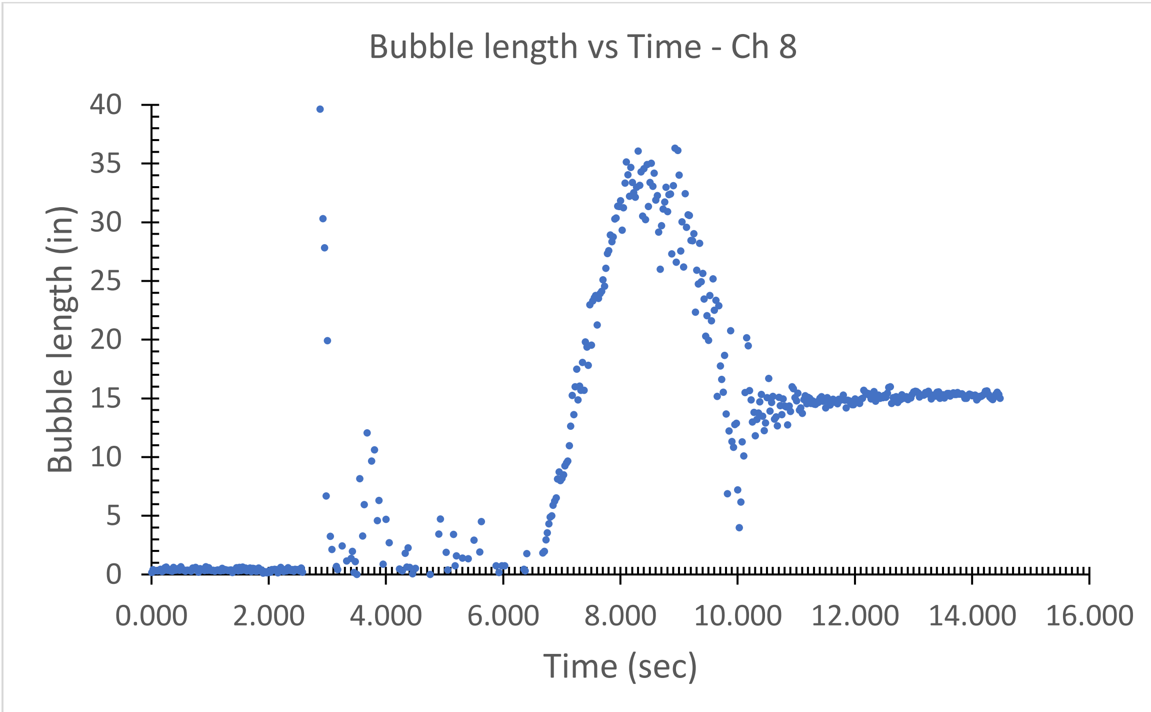

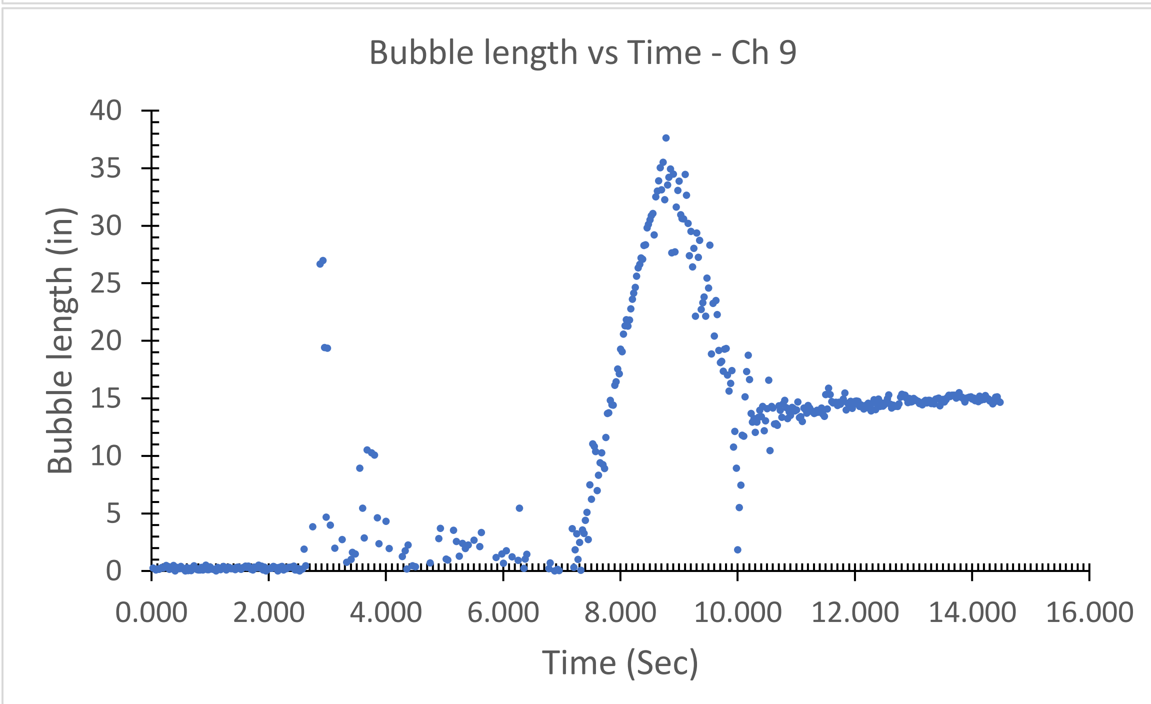

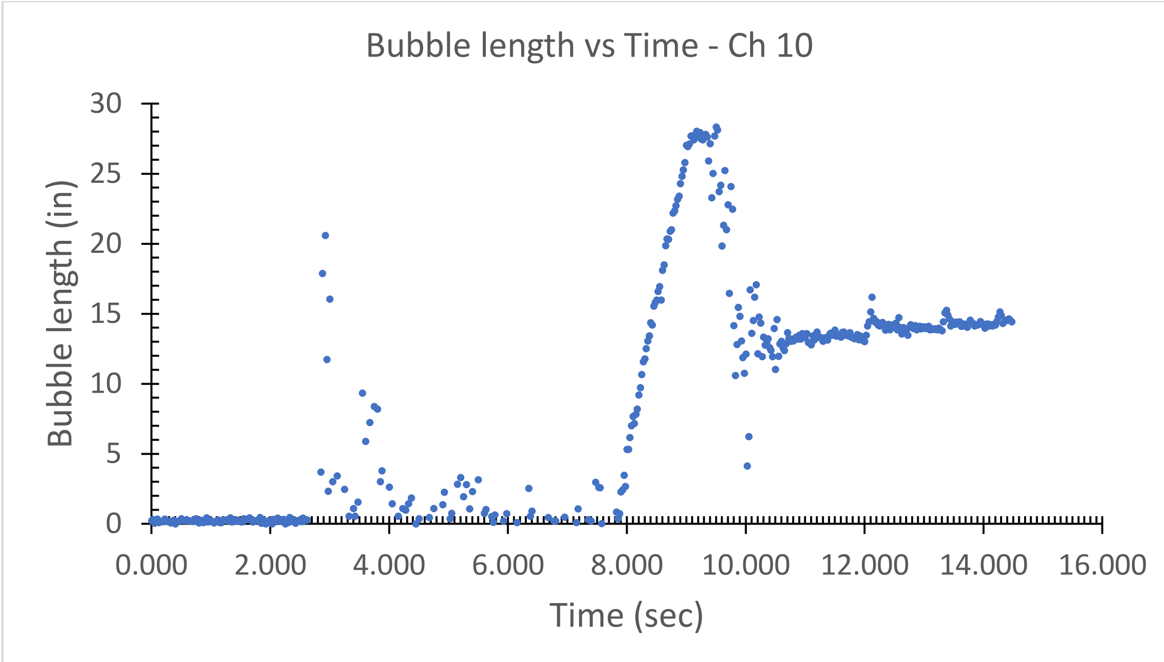
Bubble length vs Time - Ch 10
Bubble length (in)
30
25
20
15
10
5
0
0.000
2.000
4.000
6.000
8.000
10.000
12.000
14.000
16.000
Time (sec)

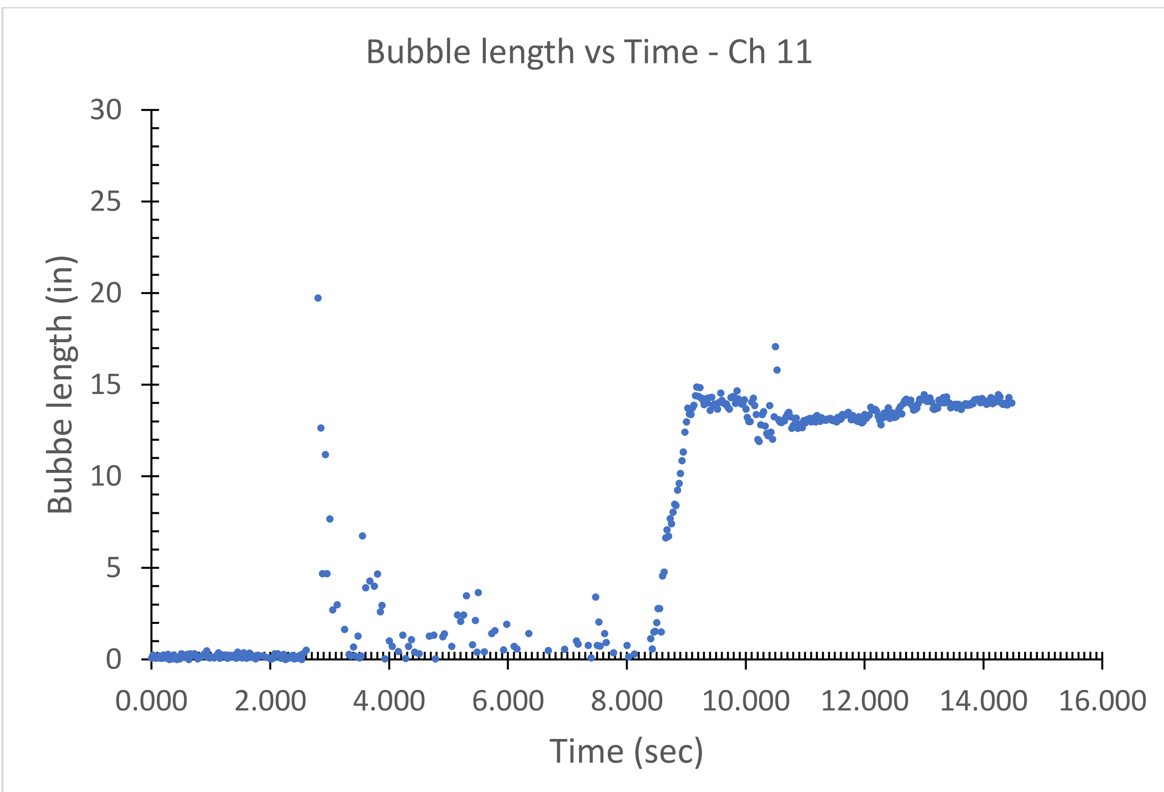
Bubble length vs Time - Ch 11
Bubbe length (in)
30
25
20
15
10
5
0
0.000
2.000
4.000
6.000
8.000
10.000
12.000
14.000
16.000
Time (sec)

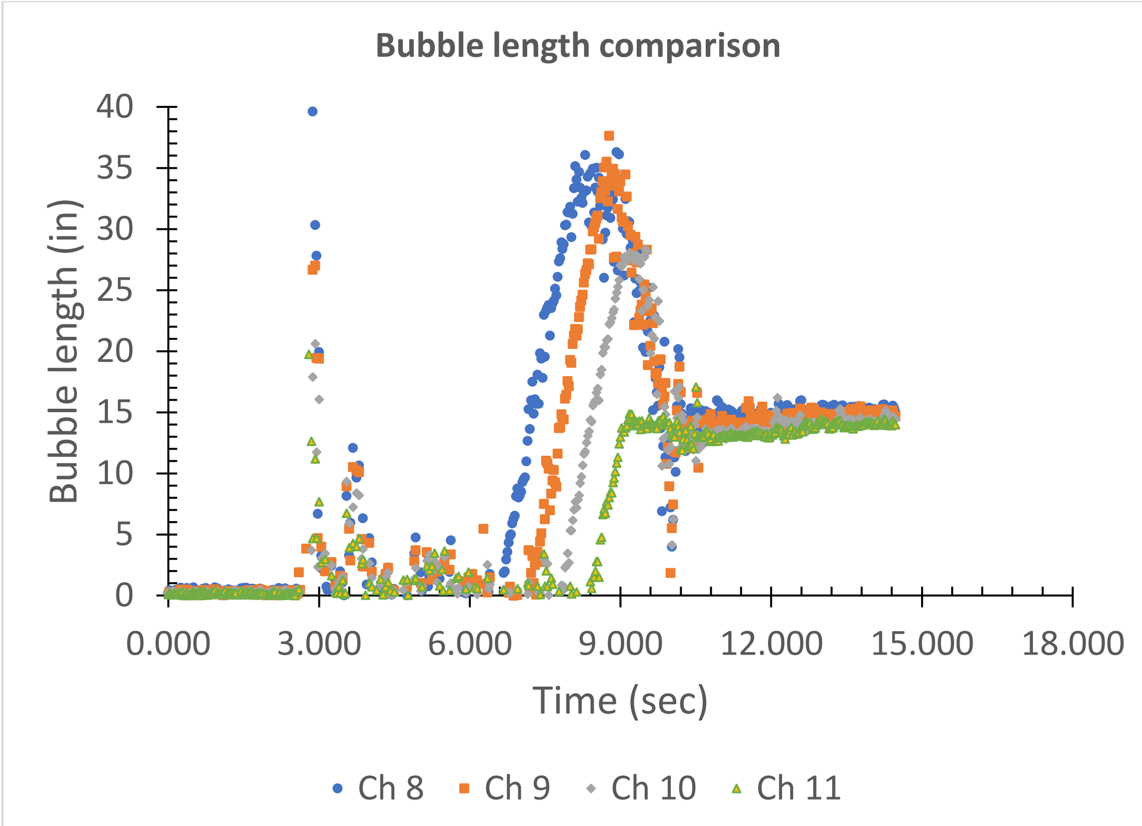

Bubble length comparison
Bubble length (in)
40
35
30
25
20
15
10
5
0
0.000
3.000
6.000
9.000
12.000
15.000
18.000
Time (sec)
Ch 8
Ch 9
Ch 10
Ch 11

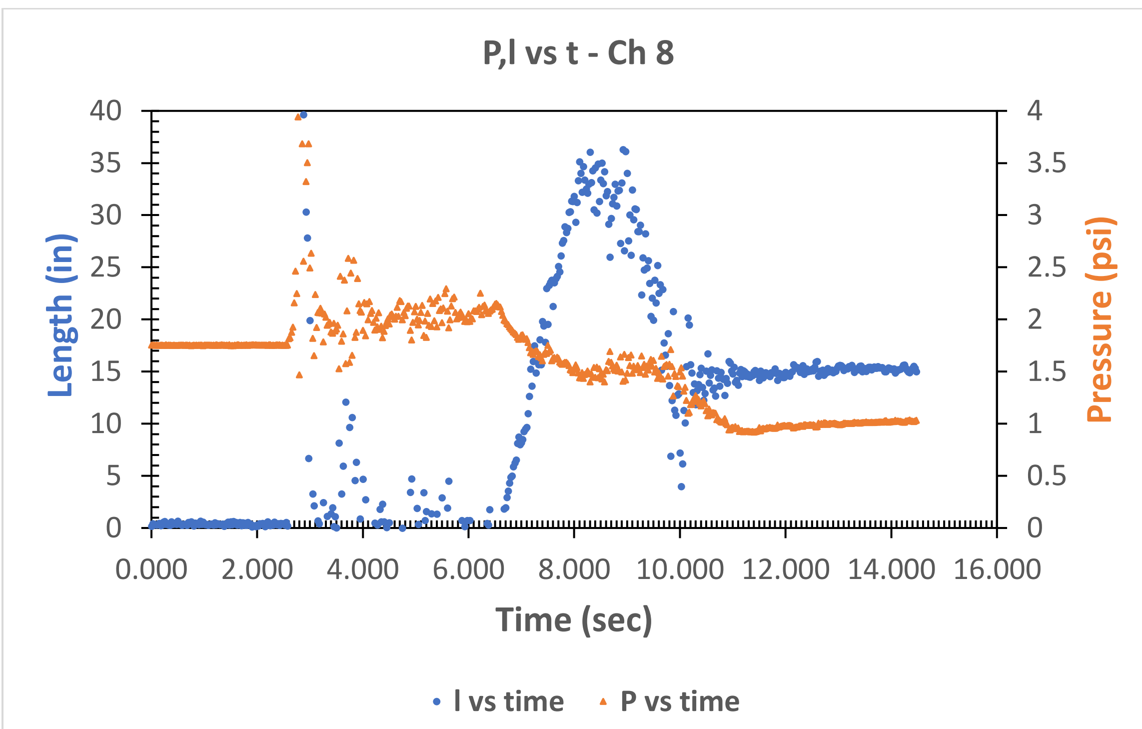

P,l vs t - Ch 8
Length (in)
Pressure (psi)
40
35
30
25
20
15
10
5
0
4
3.5
3
2.5
2
1.5
1
0.5
0
0.000
2.000
4.000
6.000
8.000
10.000
12.000
14.000
16.000
Time (sec)
l vs time
P vs time

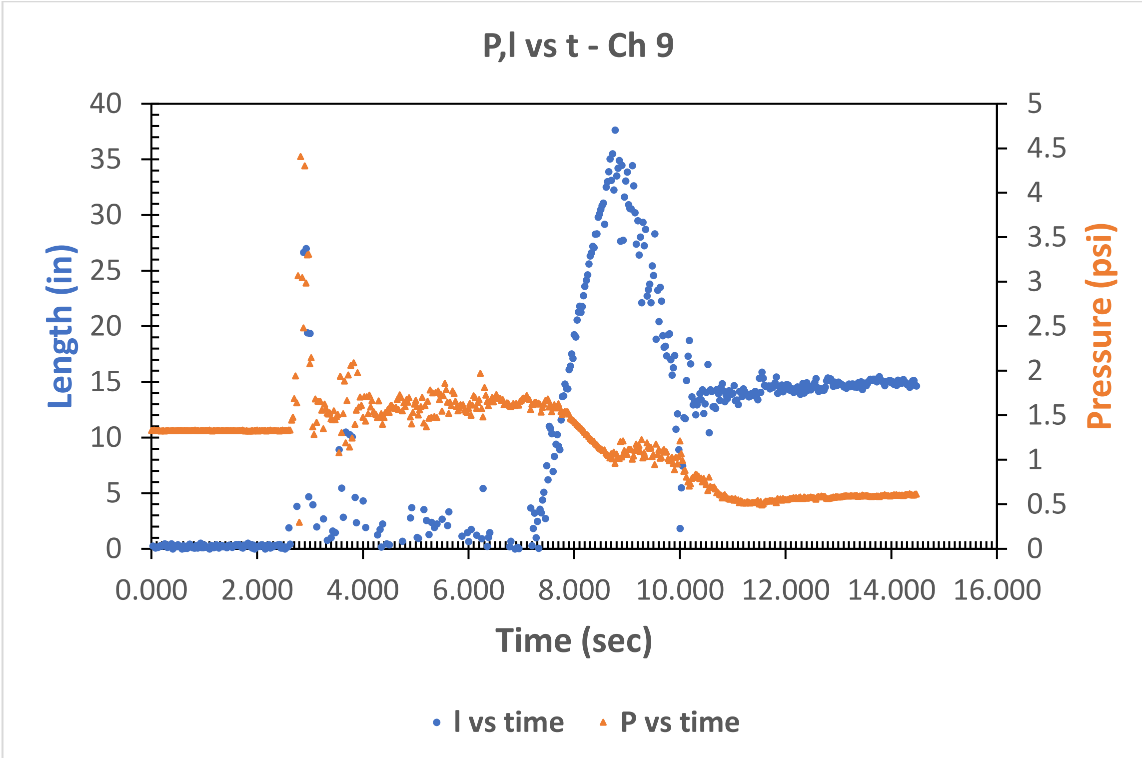
P,l vs t - Ch 9
Length (in)
Pressure (psi)
Time (sec)
0
5
10
15
20
25
30
35
40
0
0.5
1
1.5
2
2.5
3
3.5
4
4.5
5
0.000
2.000
4.000
6.000
8.000
10.000
12.000
14.000
16.000
l vs time
P vs time

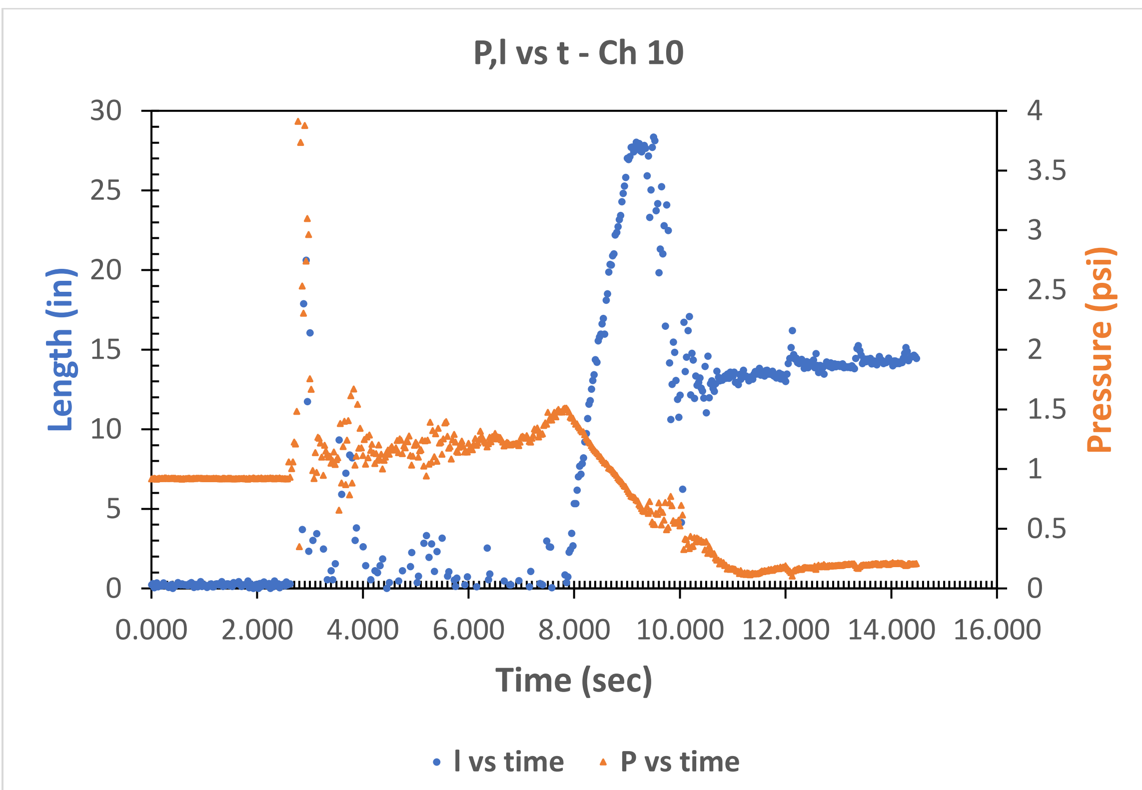
P,l vs t - Ch 10
Length (in)
Pressure (psi)
Time (sec)
0
5
10
15
20
25
30
0
0.5
1
1.5
2
2.5
3
3.5
4
0.000
2.000
4.000
6.000
8.000
10.000
12.000
14.000
16.000
l vs time
P vs time

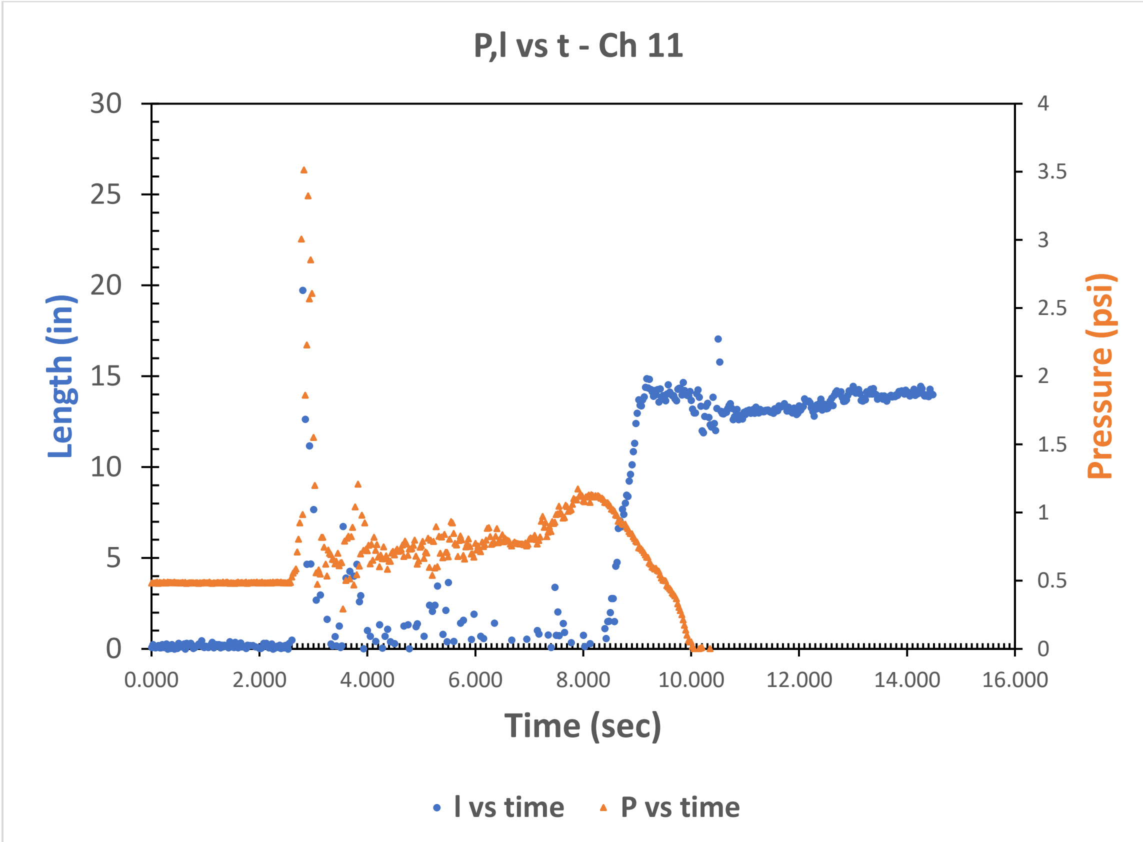

P,l vs t - Ch 11
Length (in)
Pressure (psi)
Time (sec)
30
25
20
15
10
5
0
4
3.5
3
2.5
2
1.5
1
0.5
0
0.000
2.000
4.000
6.000
8.000
10.000
12.000
14.000
16.000
l vs time
P vs time

Appendix D

Slurry – Air Experiment 1

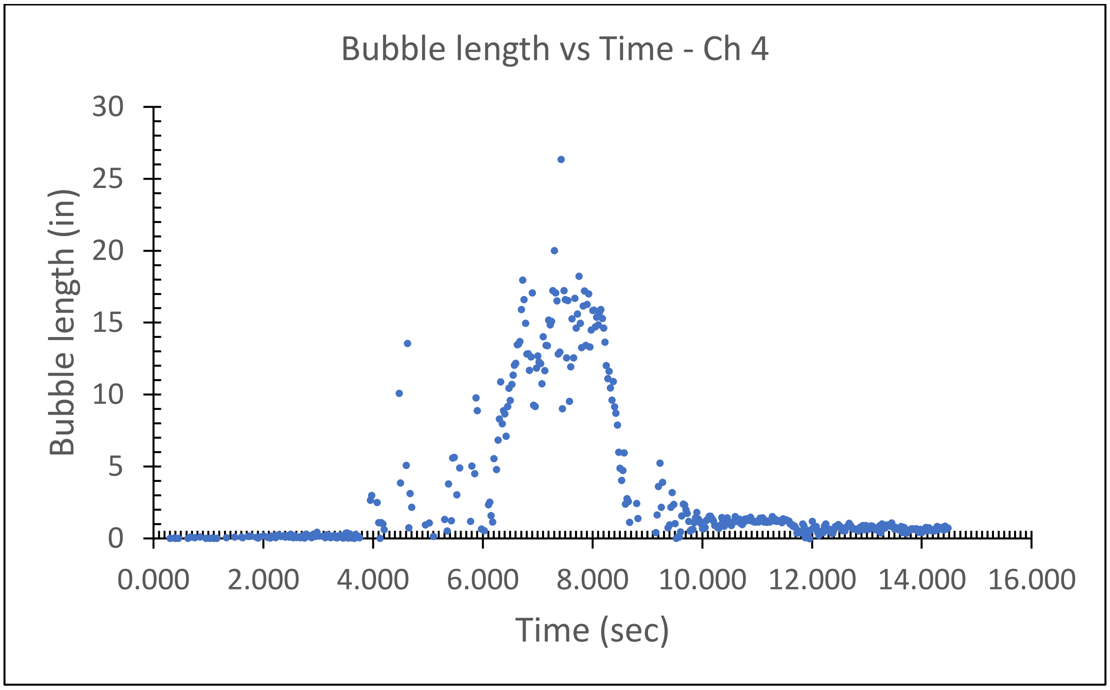

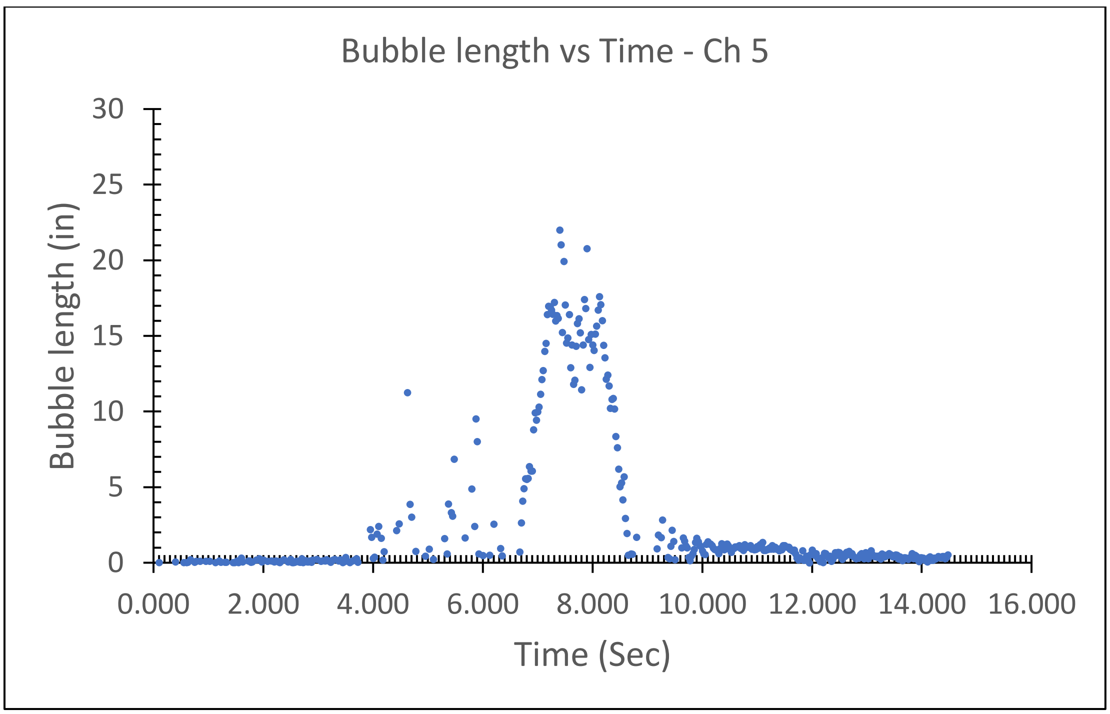

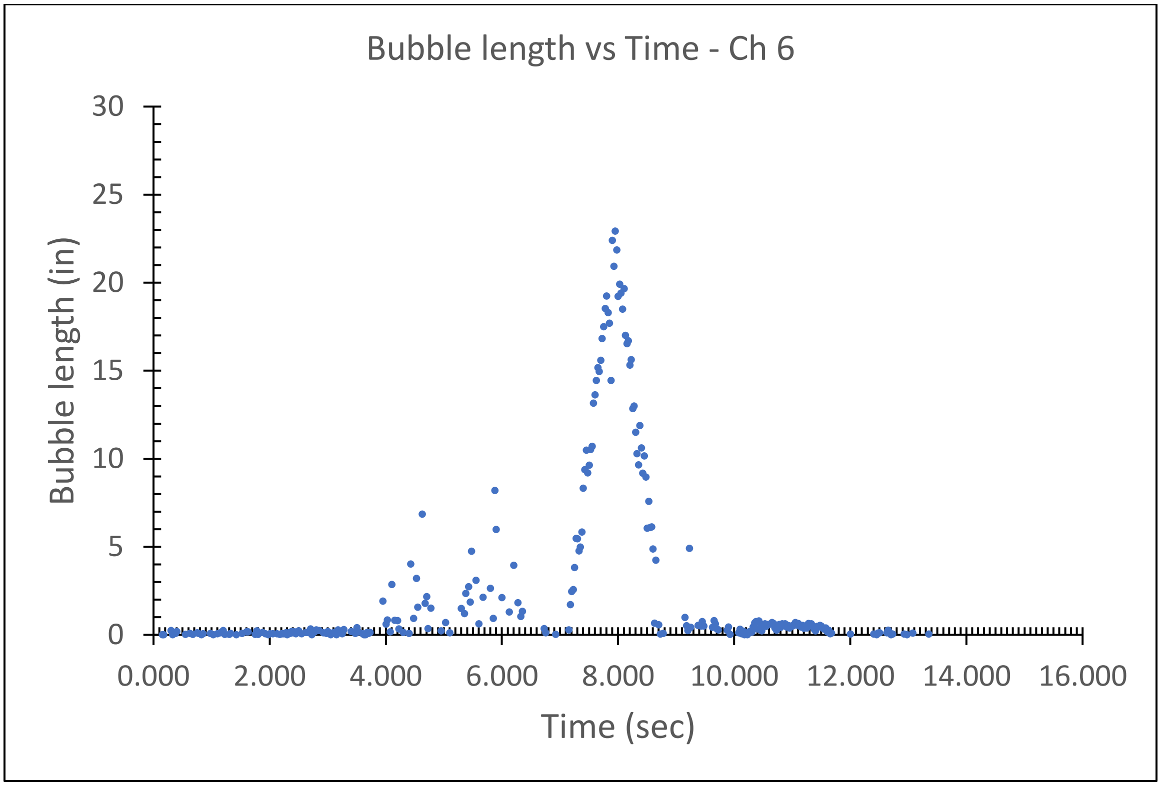
Bubble length vs Time - Ch 6
Bubble length (in)
30
25
20
15
10
5
0
0.000
2.000
4.000
6.000
8.000
10.000
12.000
14.000
16.000
Time (sec)

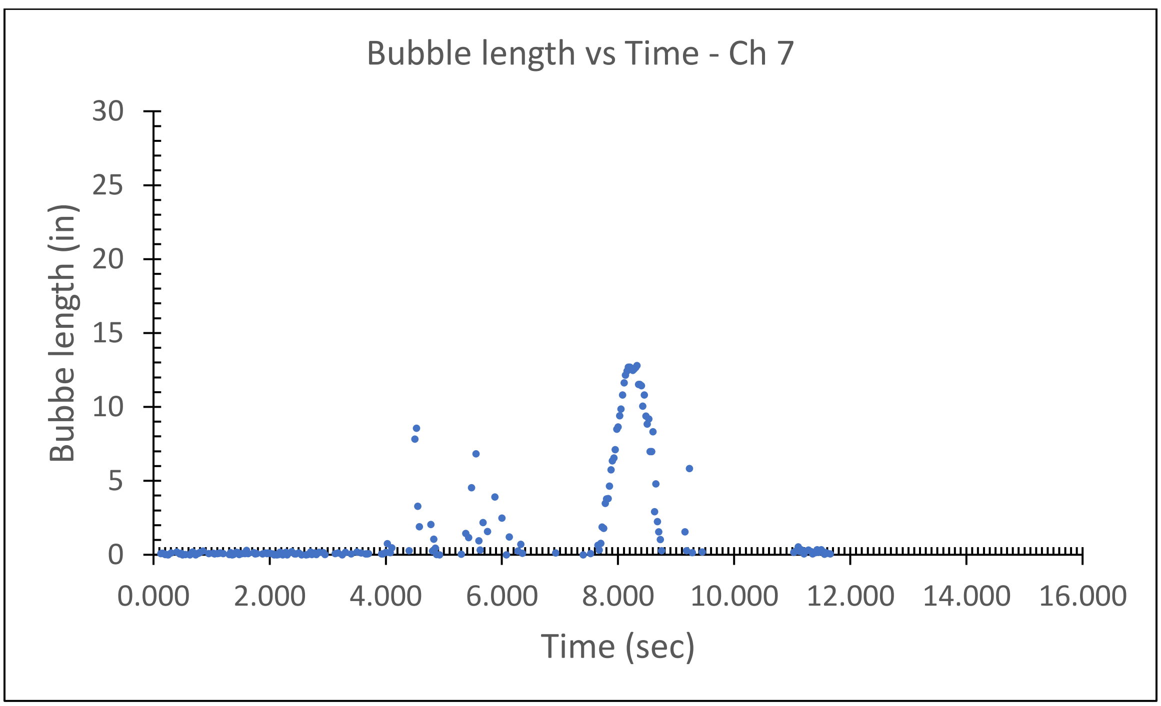
Bubble length vs Time - Ch 7
Bubbe length (in)
30
25
20
15
10
5
0
0.000
2.000
4.000
6.000
8.000
10.000
12.000
14.000
16.000
Time (sec)

Slurry – Air Experiment 2

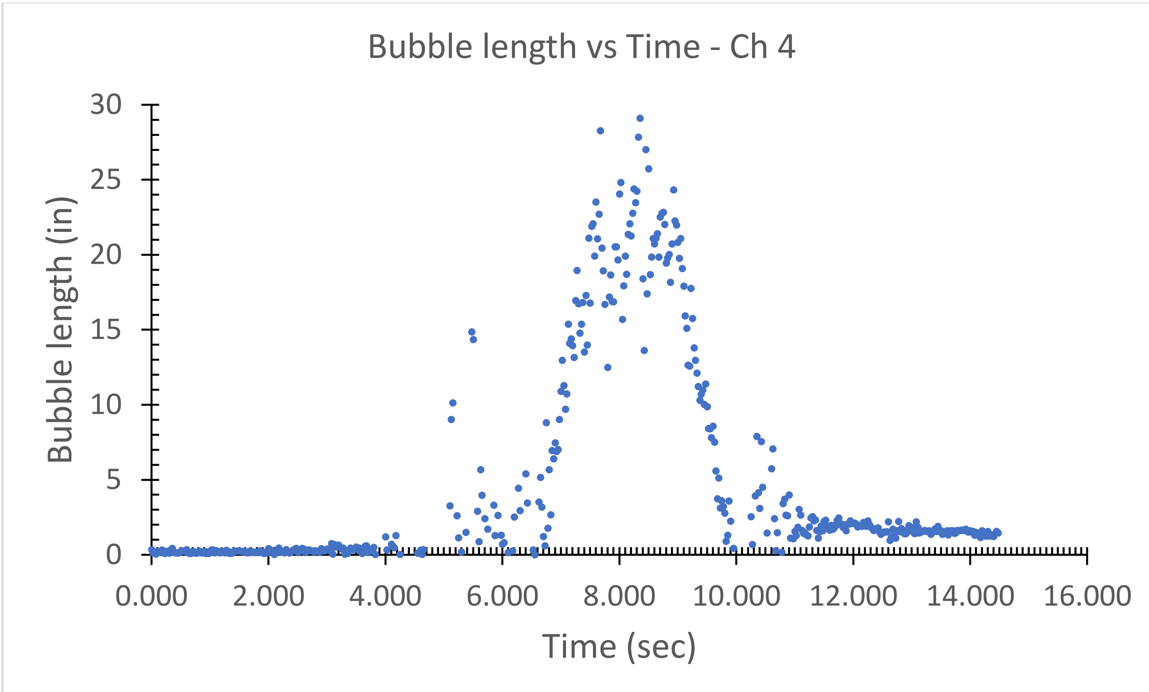

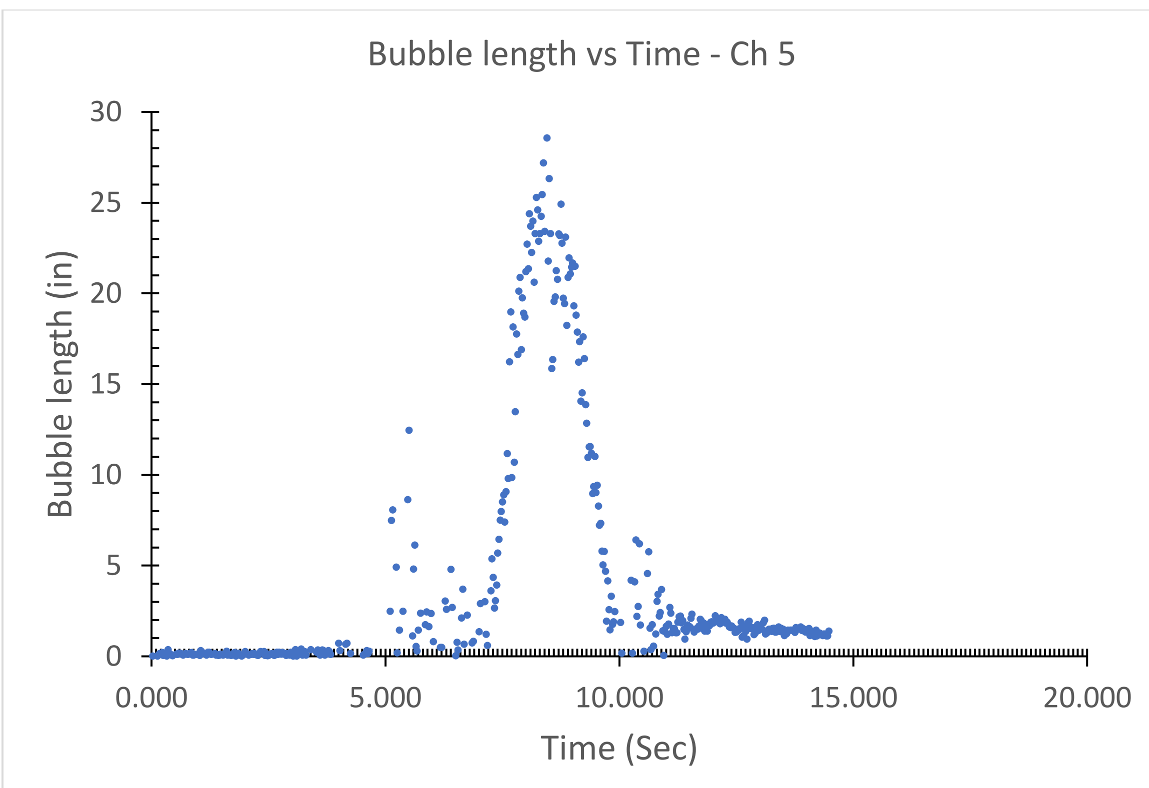

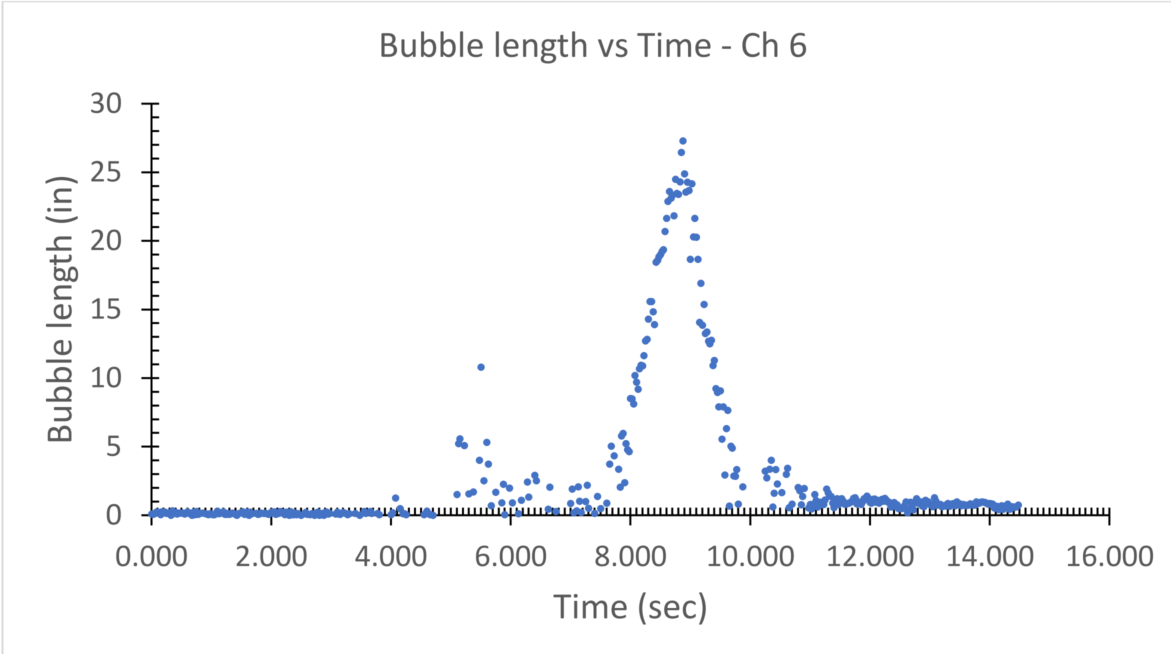
Bubble length vs Time - Ch 6
Bubble length (in)
30
25
20
15
10
5
0
0.000
2.000
4.000
6.000
8.000
10.000
12.000
14.000
16.000
Time (sec)

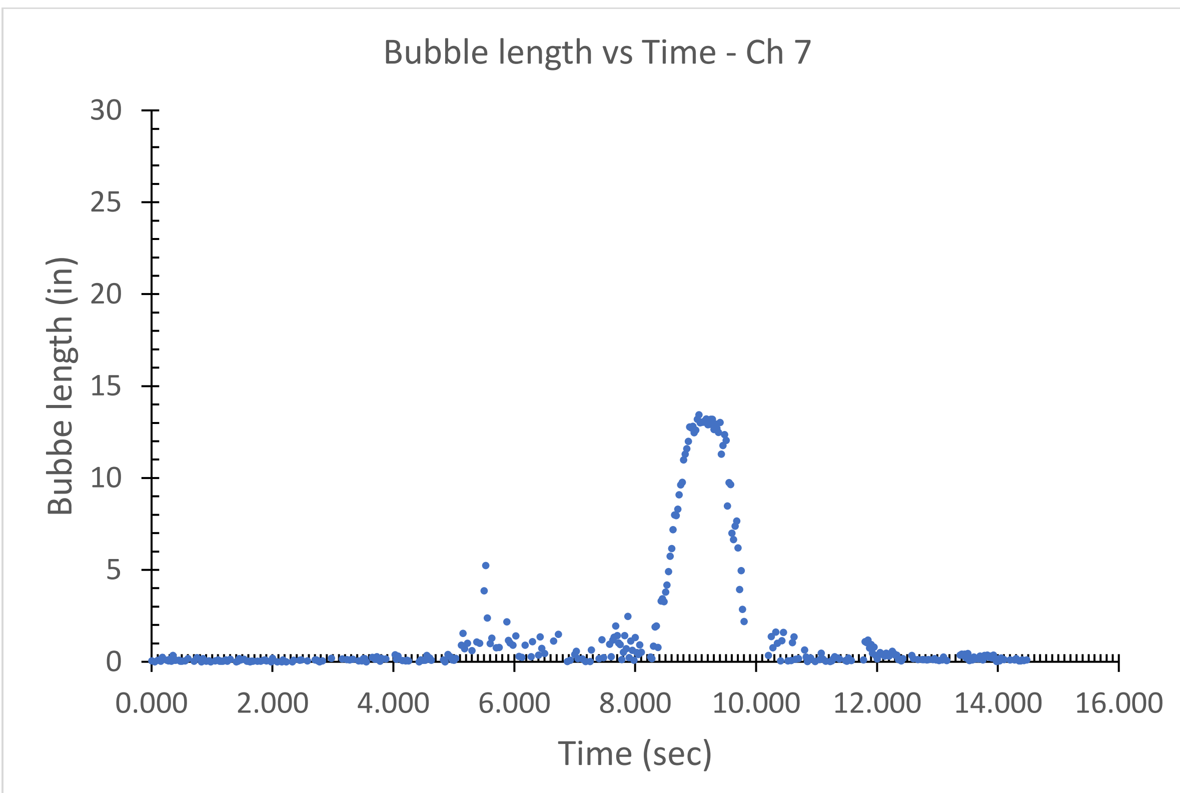
Bubble length vs Time - Ch 7
Bubbe length (in)
30
25
20
15
10
5
0
0.000
2.000
4.000
6.000
8.000
10.000
12.000
14.000
16.000
Time (sec)

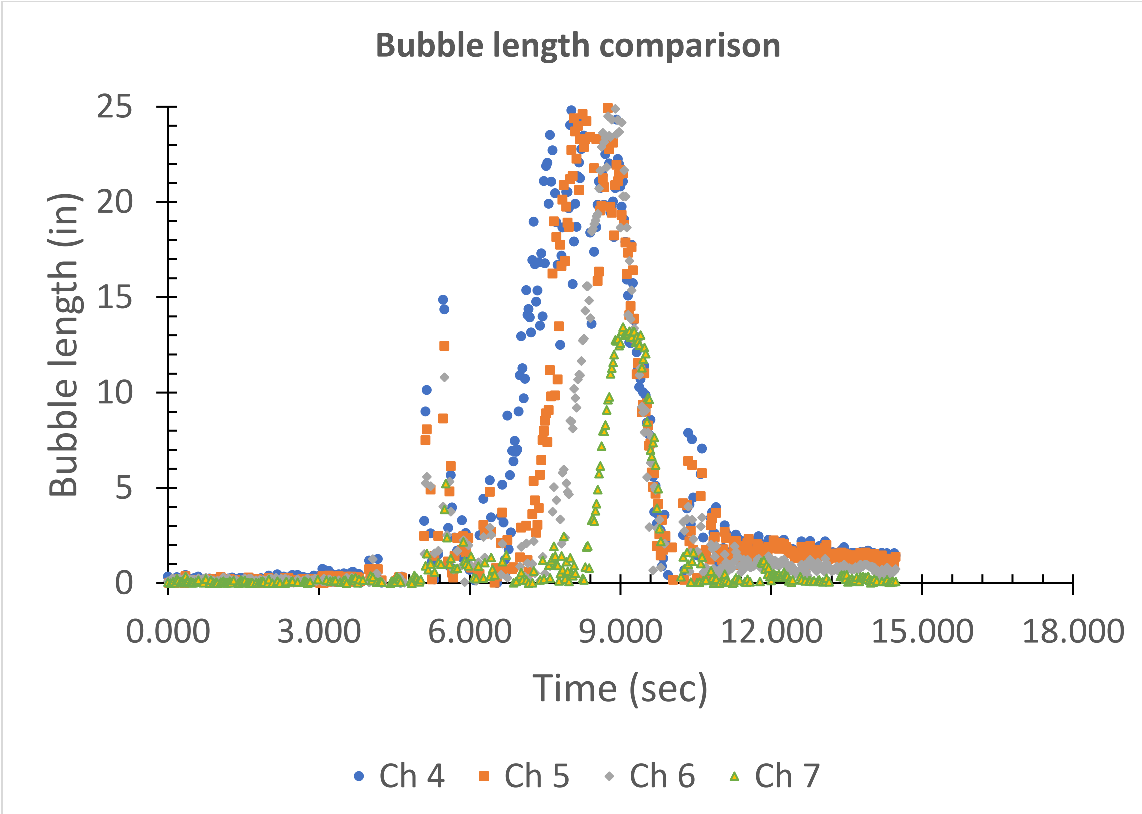

Bubble length comparison
25
20
15
10
5
0
Bubble length (in)
0.000
3.000
6.000
9.000
12.000
15.000
18.000
Time (sec)
Ch 4
Ch 5
Ch 6
Ch 7

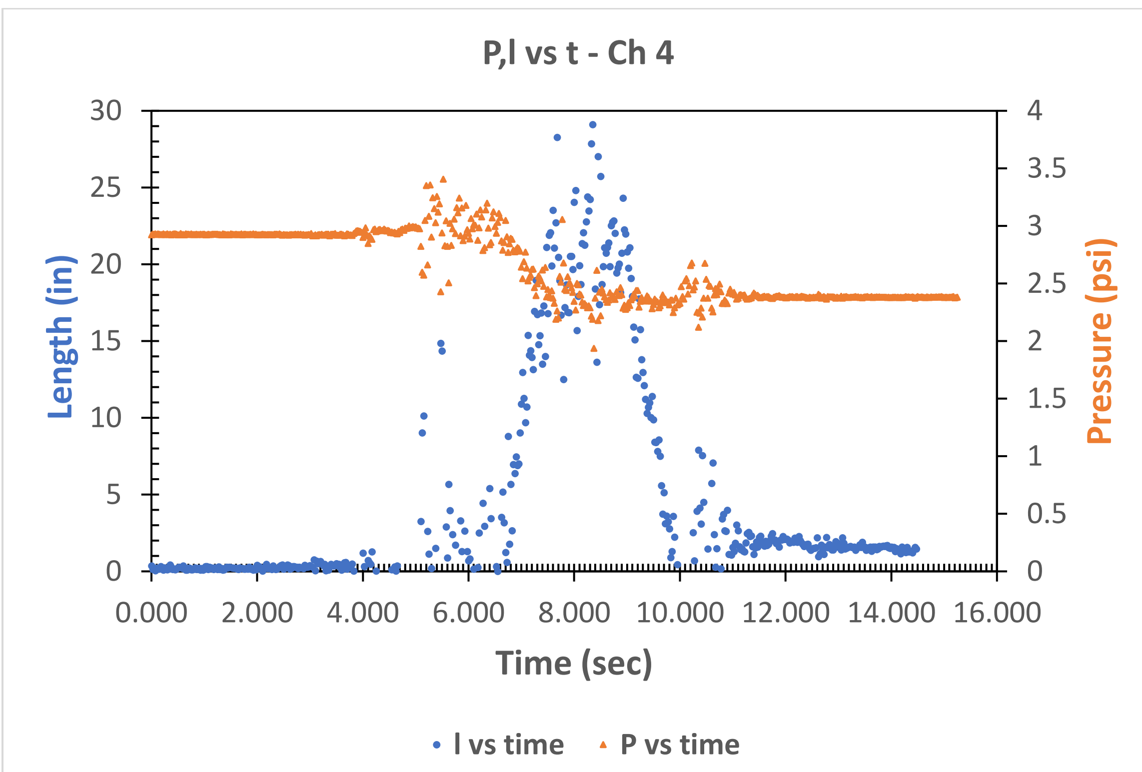

P,l vs t - Ch 4
30
25
20
15
10
5
0
Length (in)
4
3.5
3
2.5
2
1.5
1
0.5
0
Pressure (psi)
0.000
2.000
4.000
6.000
8.000
10.000
12.000
14.000
16.000
Time (sec)
l vs time
P vs time

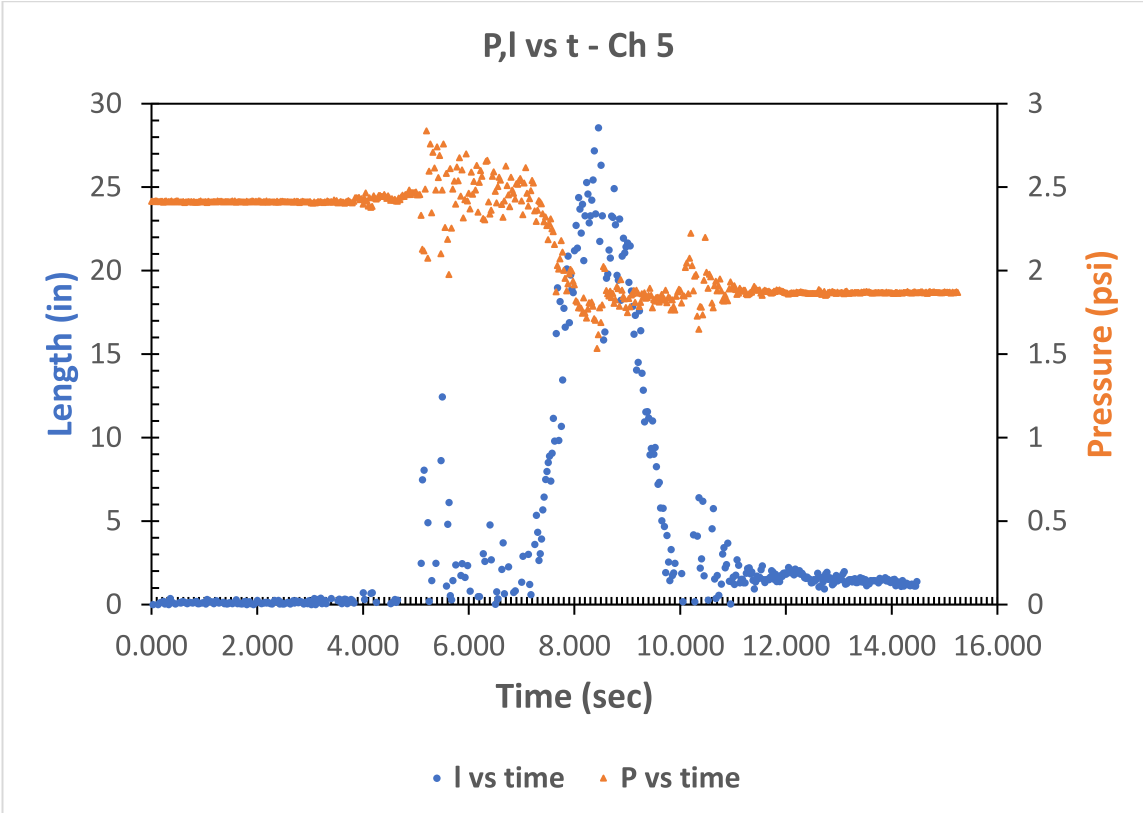
P,l vs t - Ch 5
Length (in)
Pressure (psi)
Time (sec)
0.000 2.000 4.000 6.000 8.000 10.000 12.000 14.000 16.000
0 5 10 15 20 25 30
0 0.5 1 1.5 2 2.5 3
l vs time
P vs time

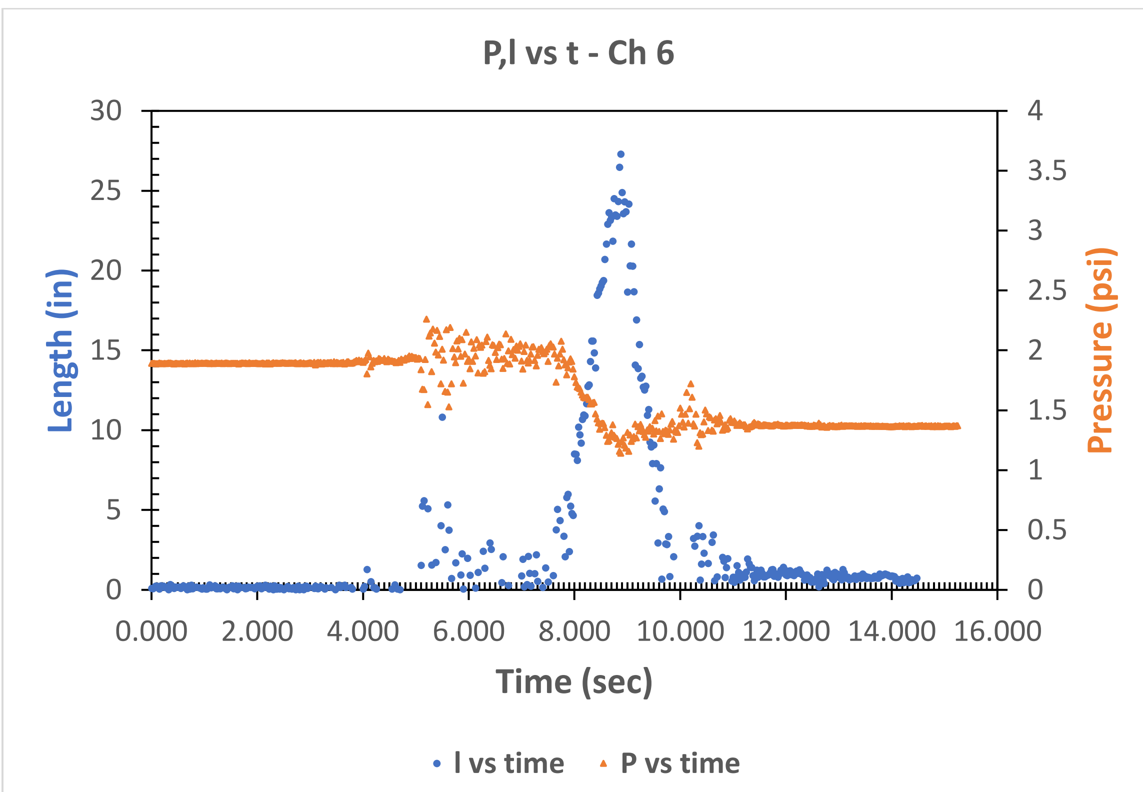
P,l vs t - Ch 6
Length (in)
Pressure (psi)
Time (sec)
0.000 2.000 4.000 6.000 8.000 10.000 12.000 14.000 16.000
0 5 10 15 20 25 30
0 0.5 1 1.5 2 2.5 3 3.5 4
l vs time
P vs time

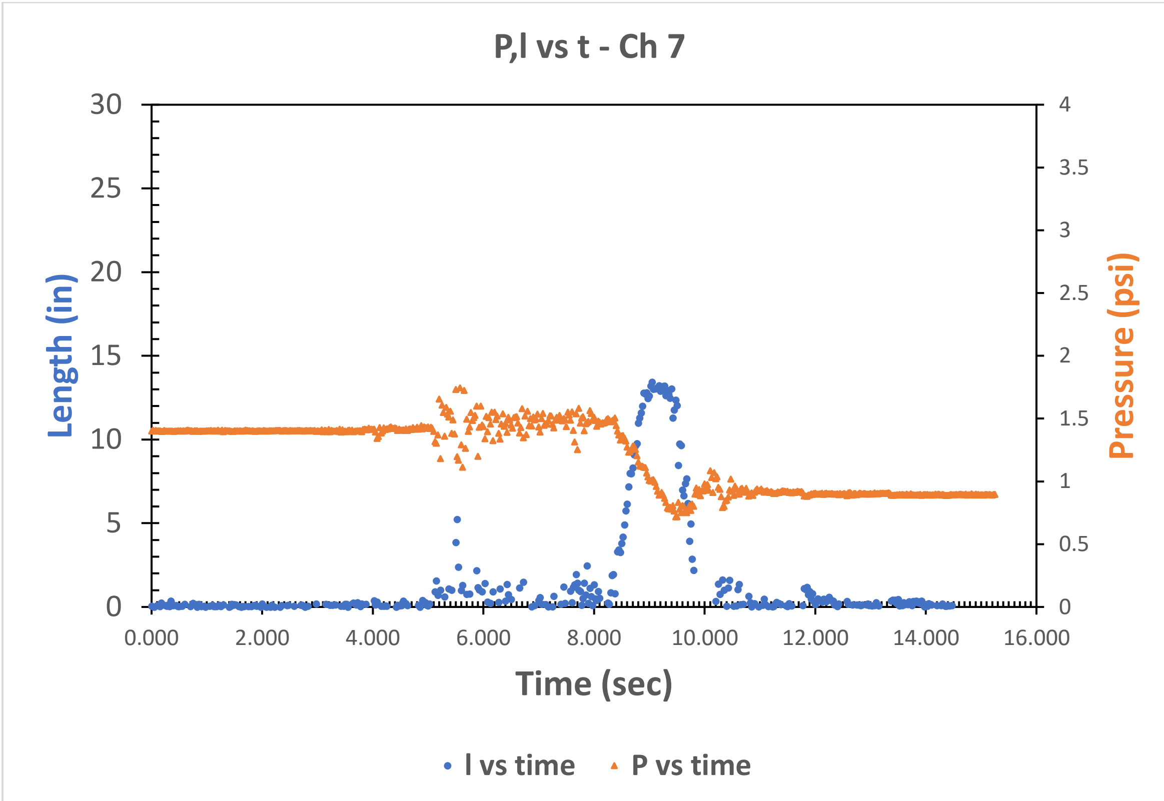
P,l vs t - Ch 7
30
25
20
15
10
5
0
Length (in)
4
3.5
3
2.5
2
1.5
1
0.5
0
Pressure (psi)
0.000
2.000
4.000
6.000
8.000
10.000
12.000
14.000
16.000
Time (sec)
l vs time
P vs time

Slurry – Air Experiment 3

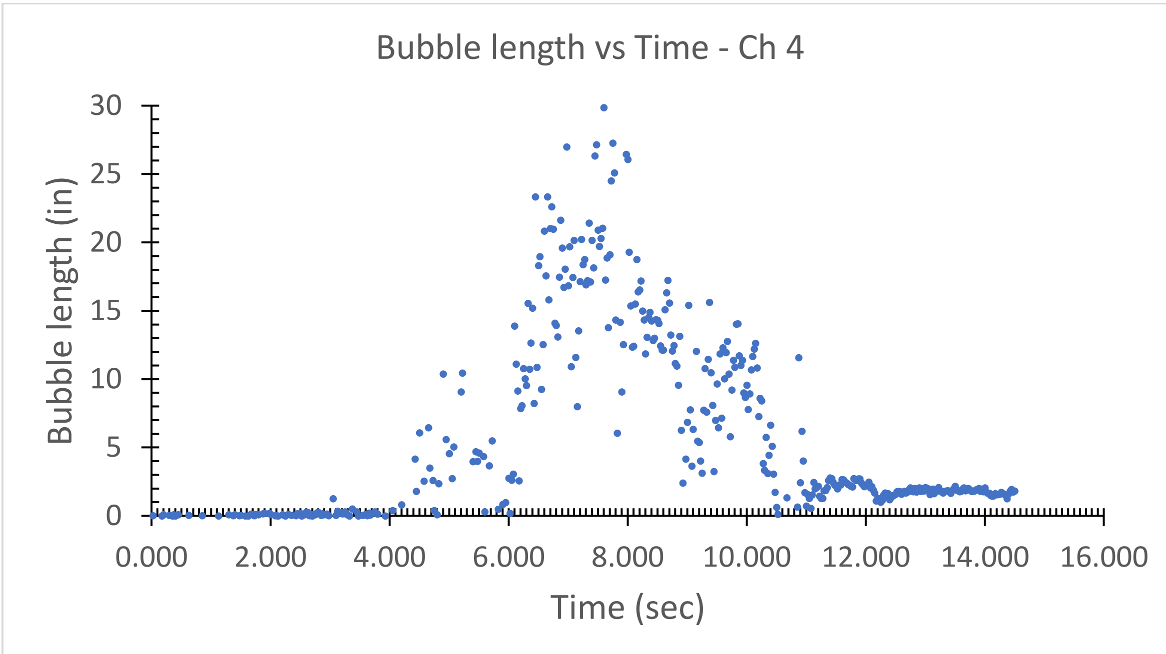

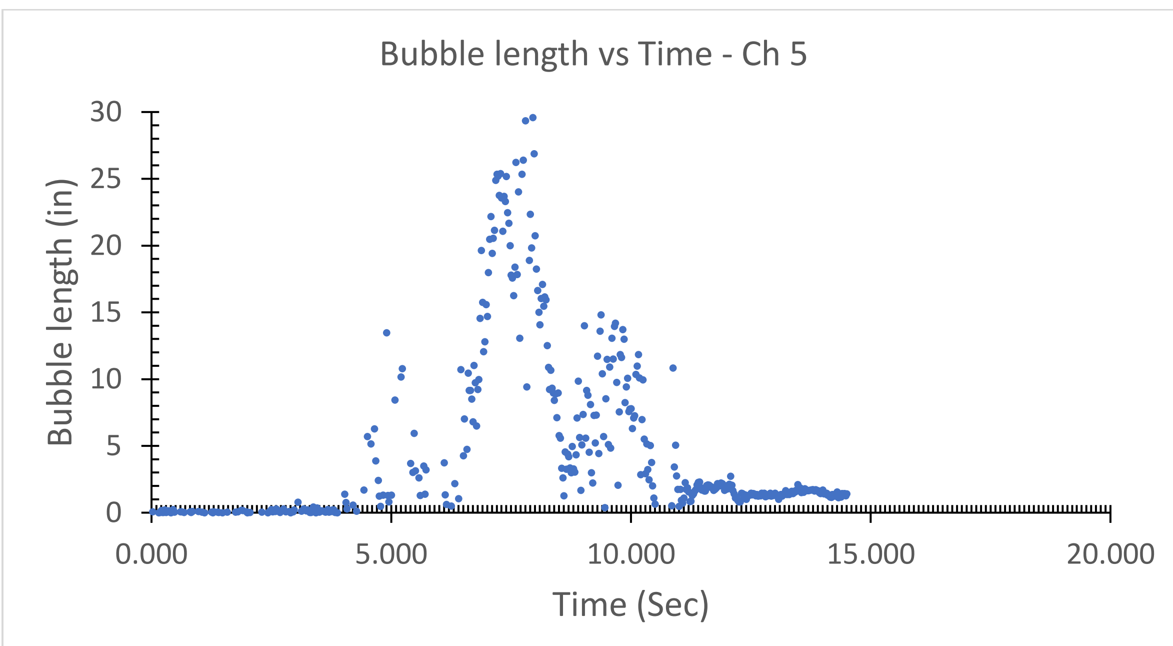

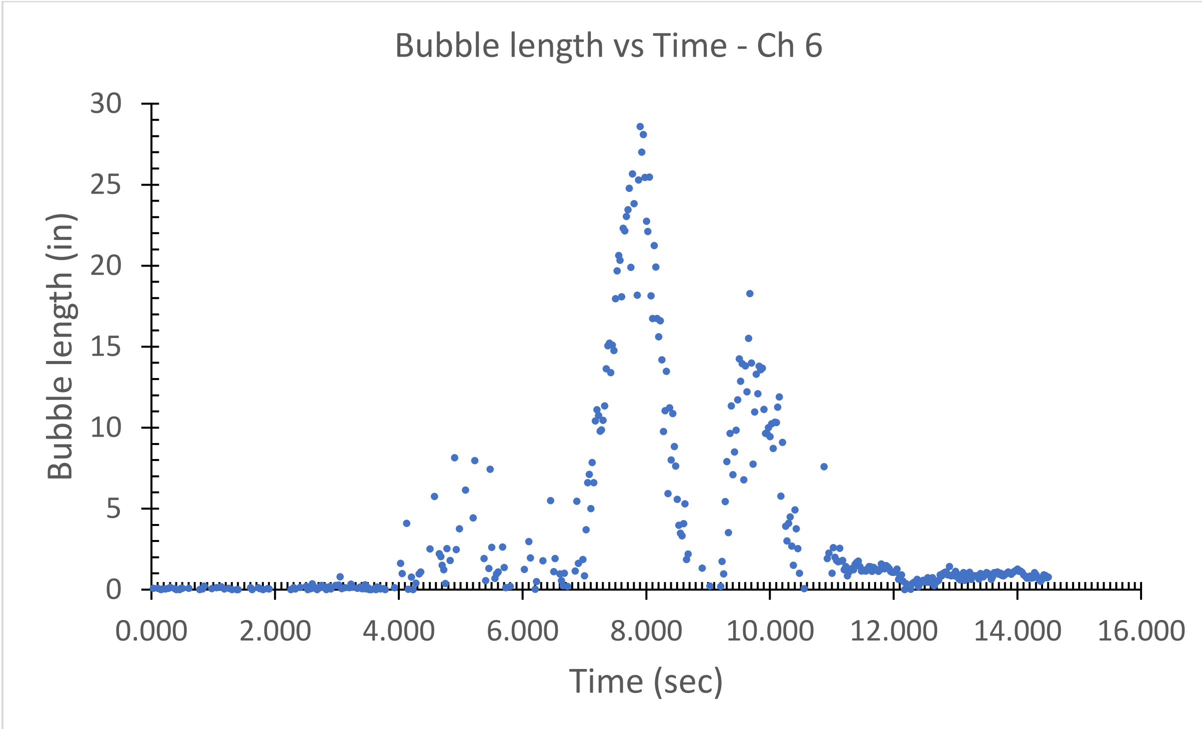
Bubble length vs Time - Ch 6
Bubble length (in)
30
25
20
15
10
5
0
0.000
2.000
4.000
6.000
8.000
10.000
12.000
14.000
16.000
Time (sec)

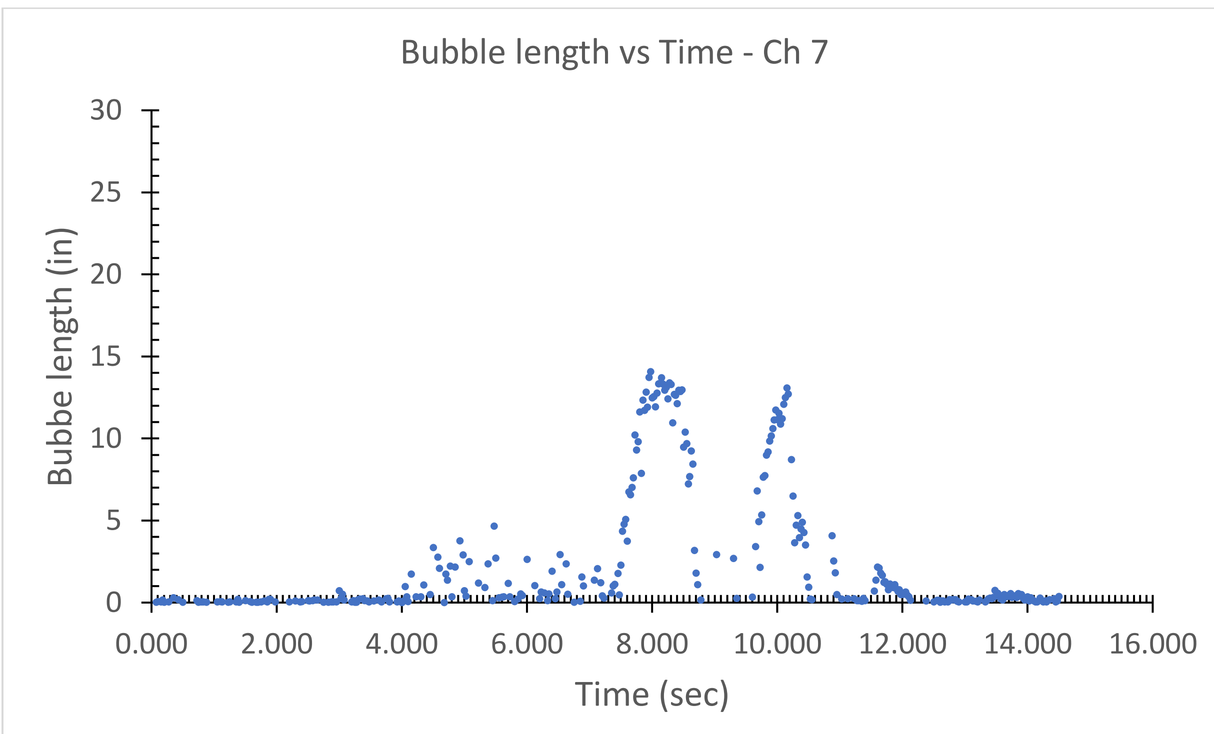
Bubble length vs Time - Ch 7
Bubbe length (in)
30
25
20
15
10
5
0
0.000
2.000
4.000
6.000
8.000
10.000
12.000
14.000
16.000
Time (sec)

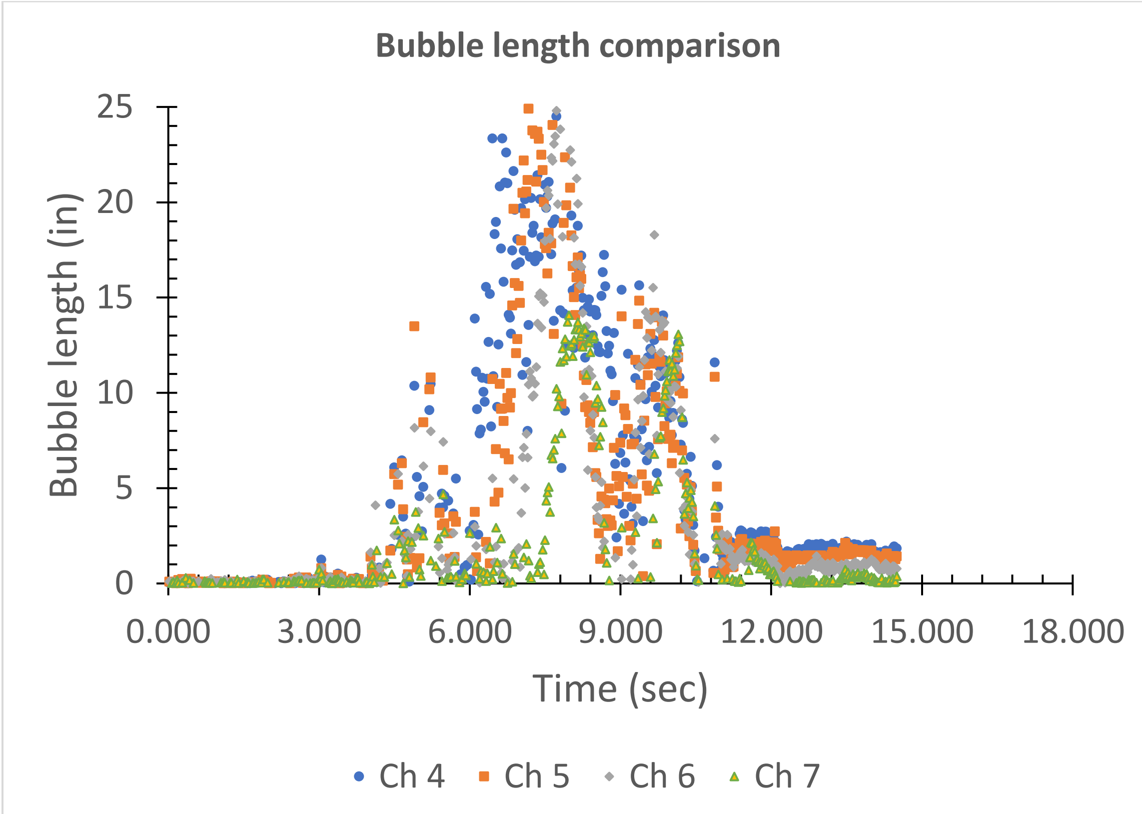
Bubble length comparison
Bubble length (in)
25
20
15
10
5
0
0.000
3.000
6.000
9.000
12.000
15.000
18.000
Time (sec)
Ch 4
Ch 5
Ch 6
Ch 7

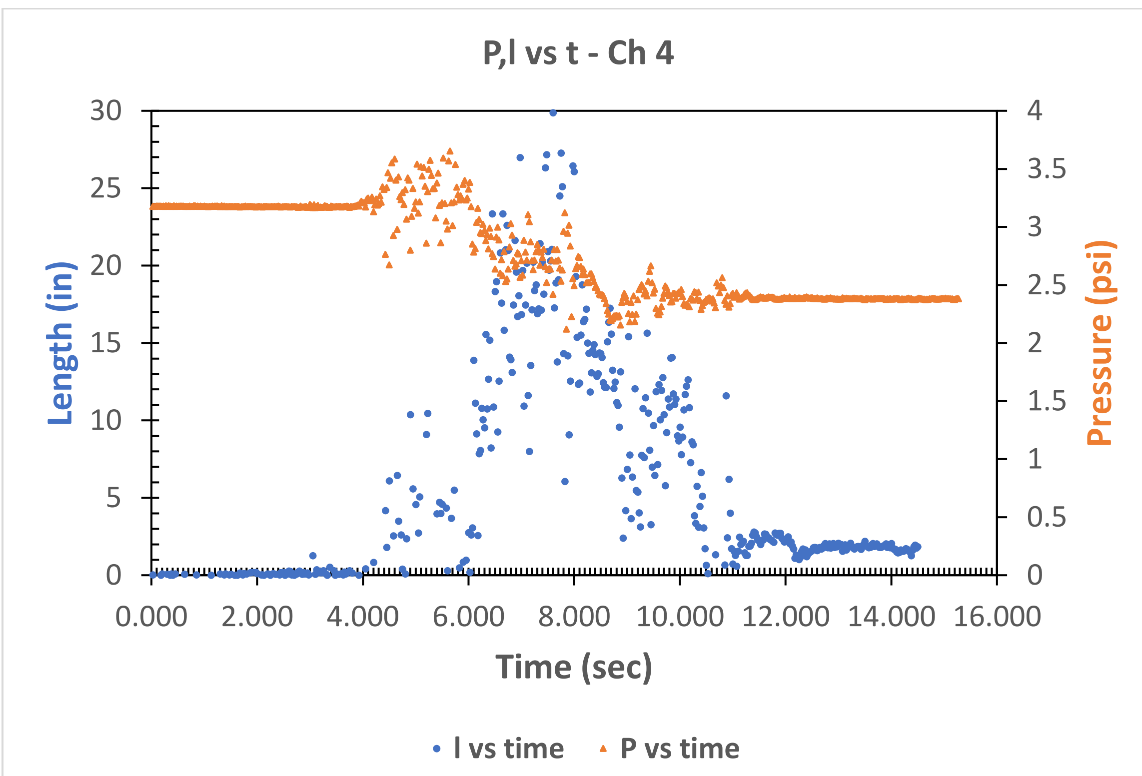
P,l vs t - Ch 4
Length (in)
Pressure (psi)
30
25
20
15
10
5
0
4
3.5
3
2.5
2
1.5
1
0.5
0
0.000
2.000
4.000
6.000
8.000
10.000
12.000
14.000
16.000
Time (sec)
l vs time
P vs time

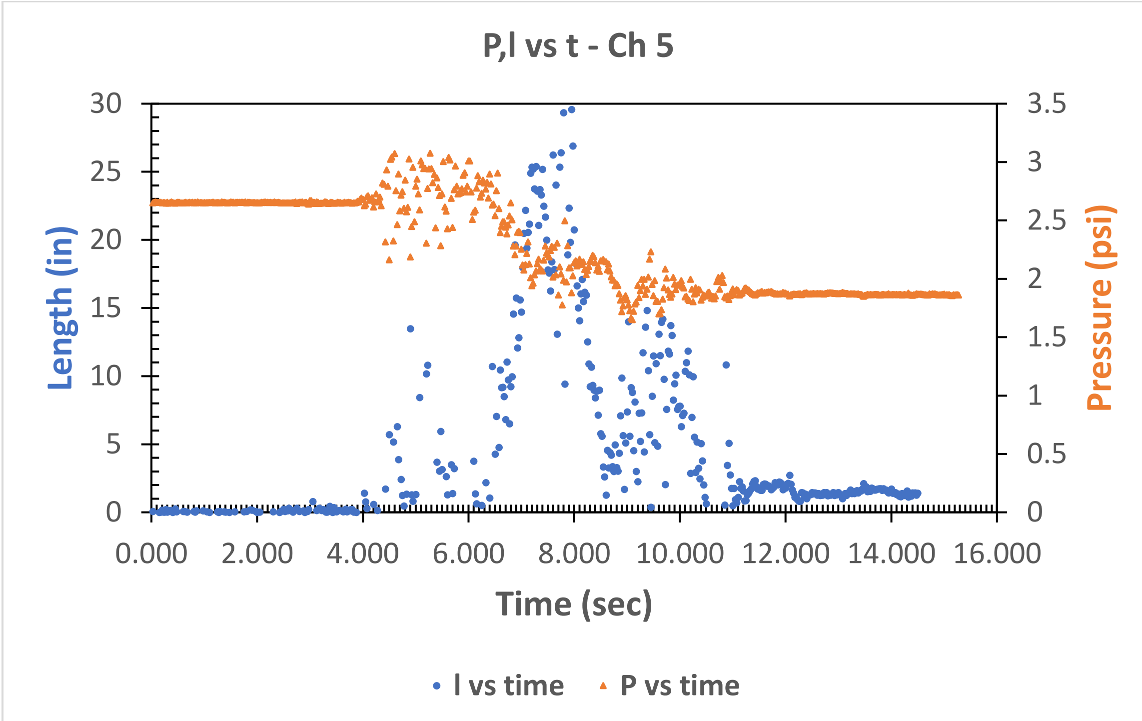

P,l vs t - Ch 5
Length (in)
Pressure (psi)
Time (sec)
0
5
10
15
20
25
30
0
0.5
1
1.5
2
2.5
3
3.5
0.000
2.000
4.000
6.000
8.000
10.000
12.000
14.000
16.000
l vs time
P vs time

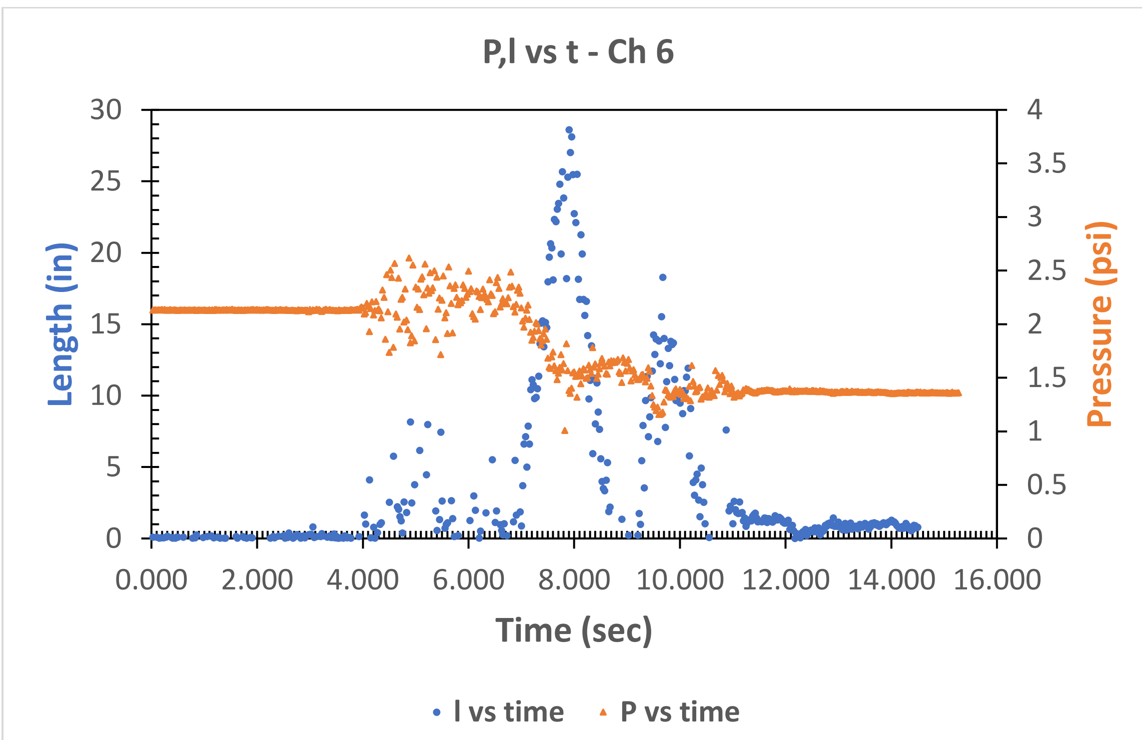

P,l vs t - Ch 6
Length (in)
Pressure (psi)
Time (sec)
0
5
10
15
20
25
30
0
0.5
1
1.5
2
2.5
3
3.5
4
0.000
2.000
4.000
6.000
8.000
10.000
12.000
14.000
16.000
l vs time
P vs time

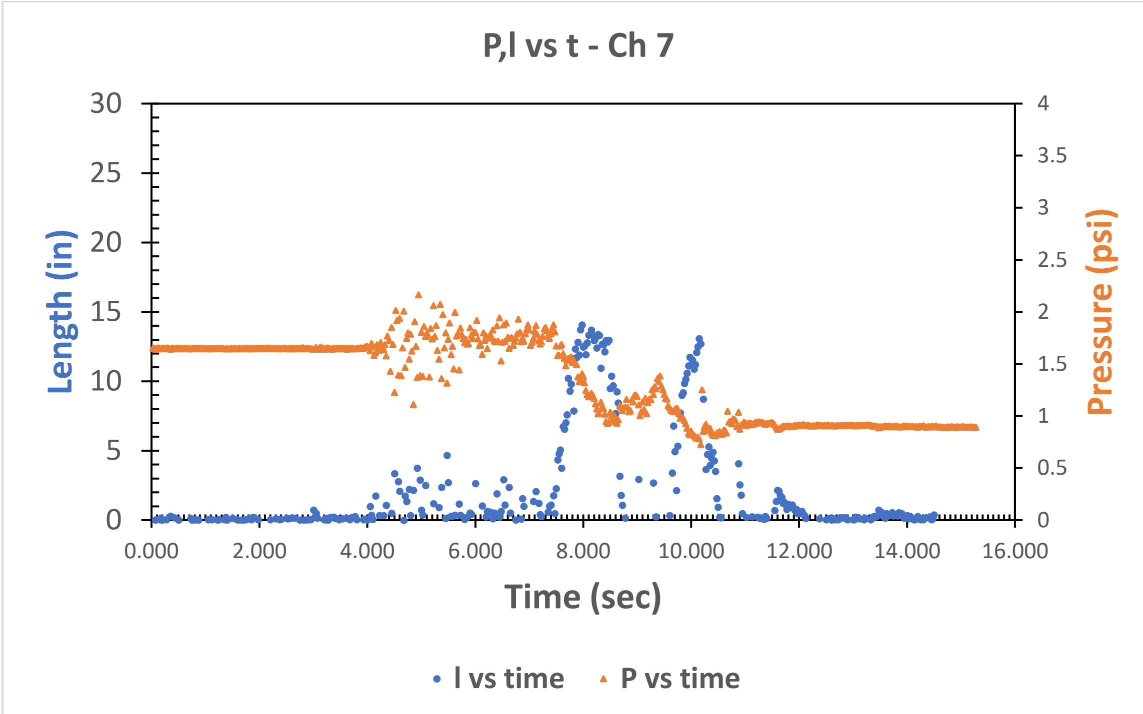

P,l vs t - Ch 7
Length (in)
Pressure (psi)
Time (sec)
l vs time
P vs time
0
5
10
15
20
25
30
0
0.5
1
1.5
2
2.5
3
3.5
4
0.000
2.000
4.000
6.000
8.000
10.000
12.000
14.000
16.000

Slurry– Air Experiment 4

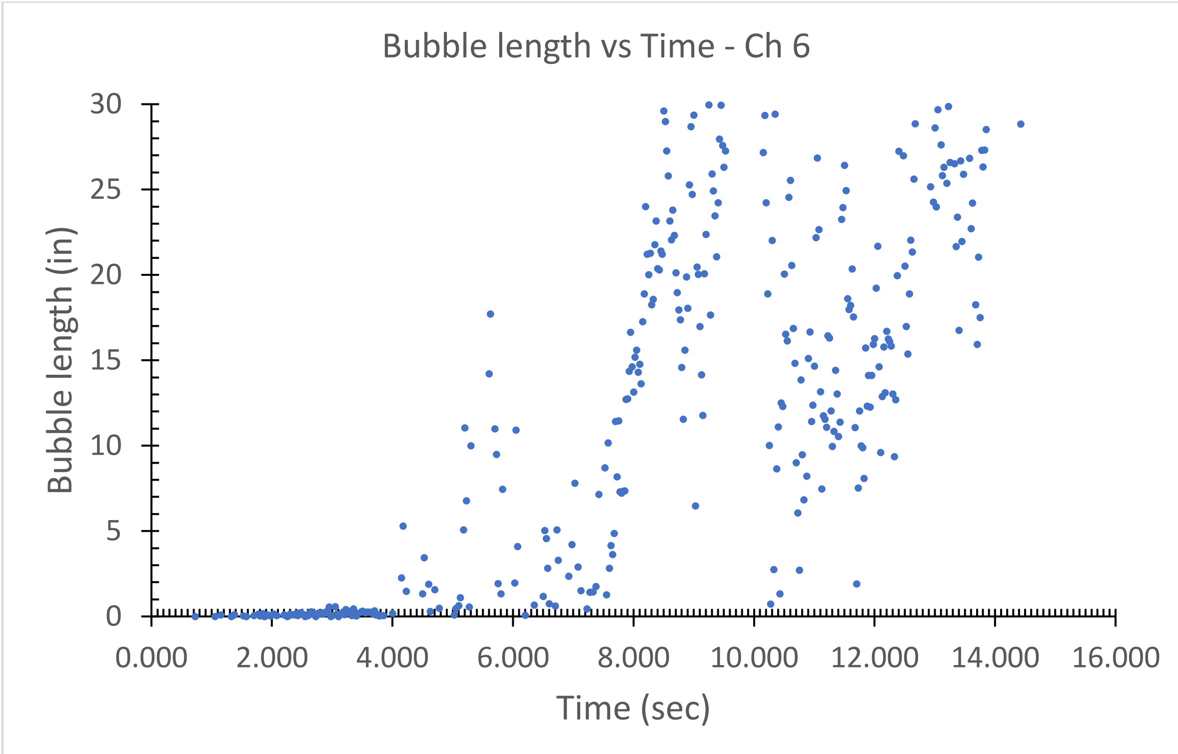

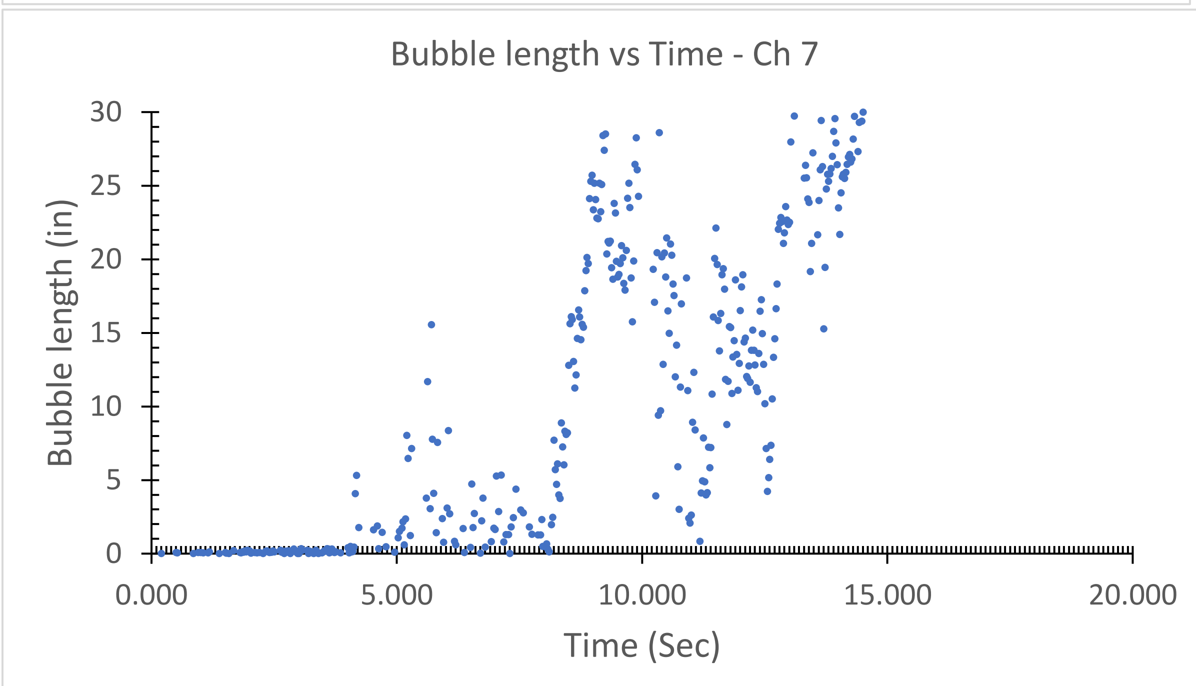

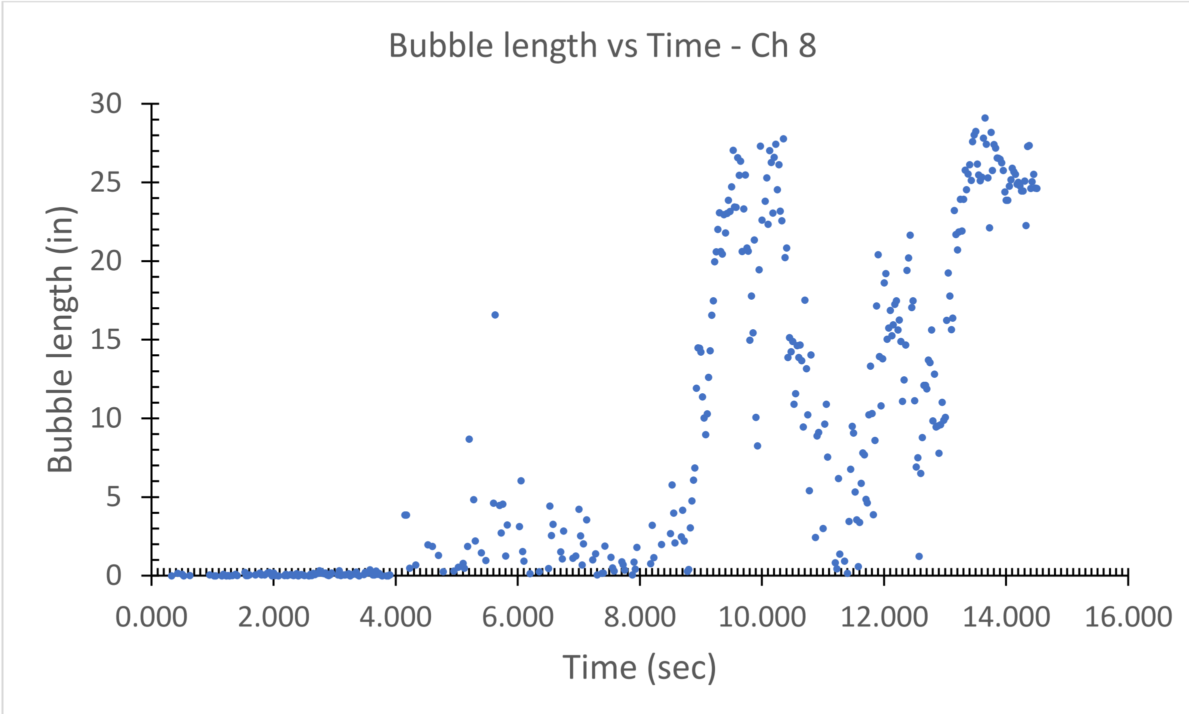
Bubble length vs Time - Ch 8
Bubble length (in)
30
25
20
15
10
5
0
0.000
2.000
4.000
6.000
8.000
10.000
12.000
14.000
16.000
Time (sec)

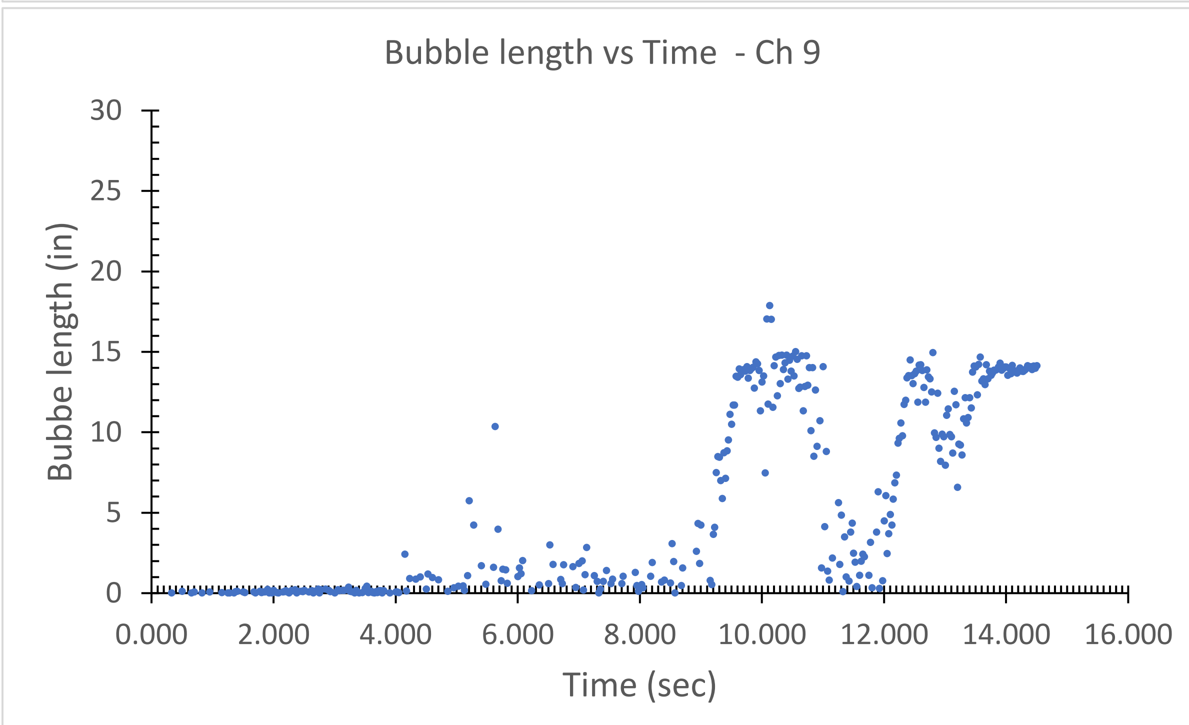
Bubble length vs Time - Ch 9
Bubbe length (in)
30
25
20
15
10
5
0
0.000
2.000
4.000
6.000
8.000
10.000
12.000
14.000
16.000
Time (sec)

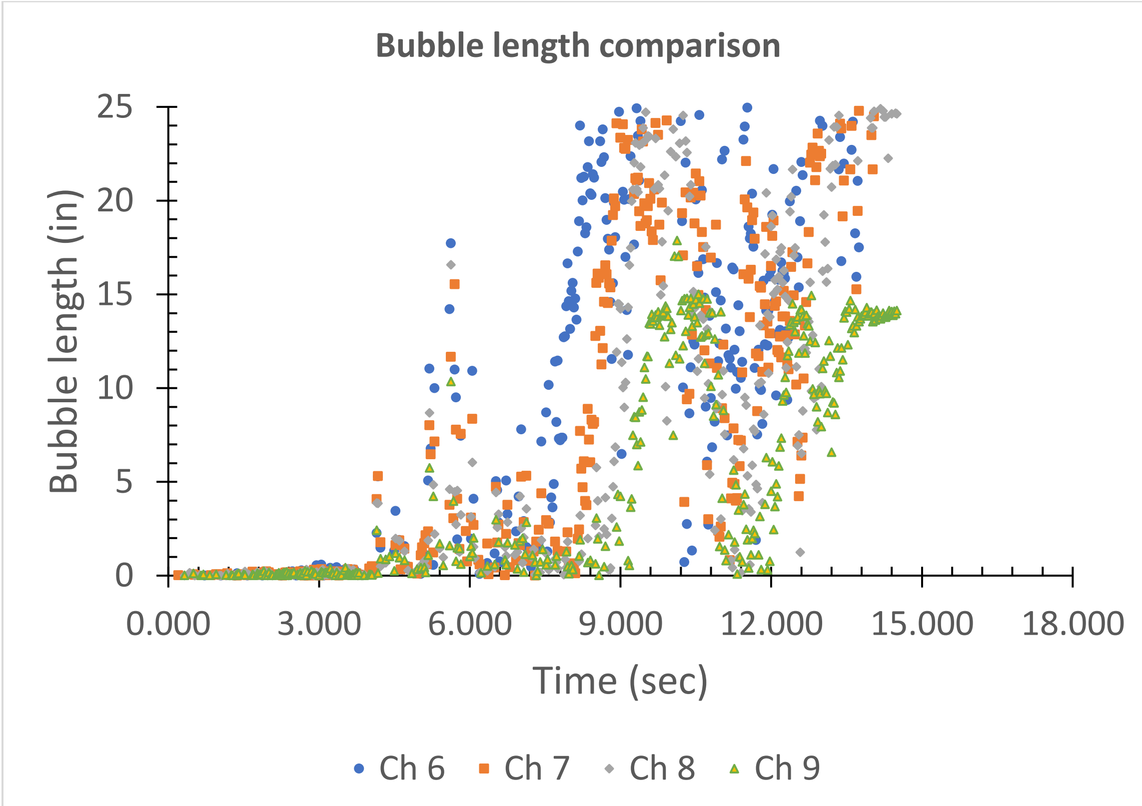

Bubble length comparison
25
20
15
10
5
0
Bubble length (in)
0.000
3.000
6.000
9.000
12.000
15.000
18.000
Time (sec)
Ch 6
Ch 7
Ch 8
Ch 9

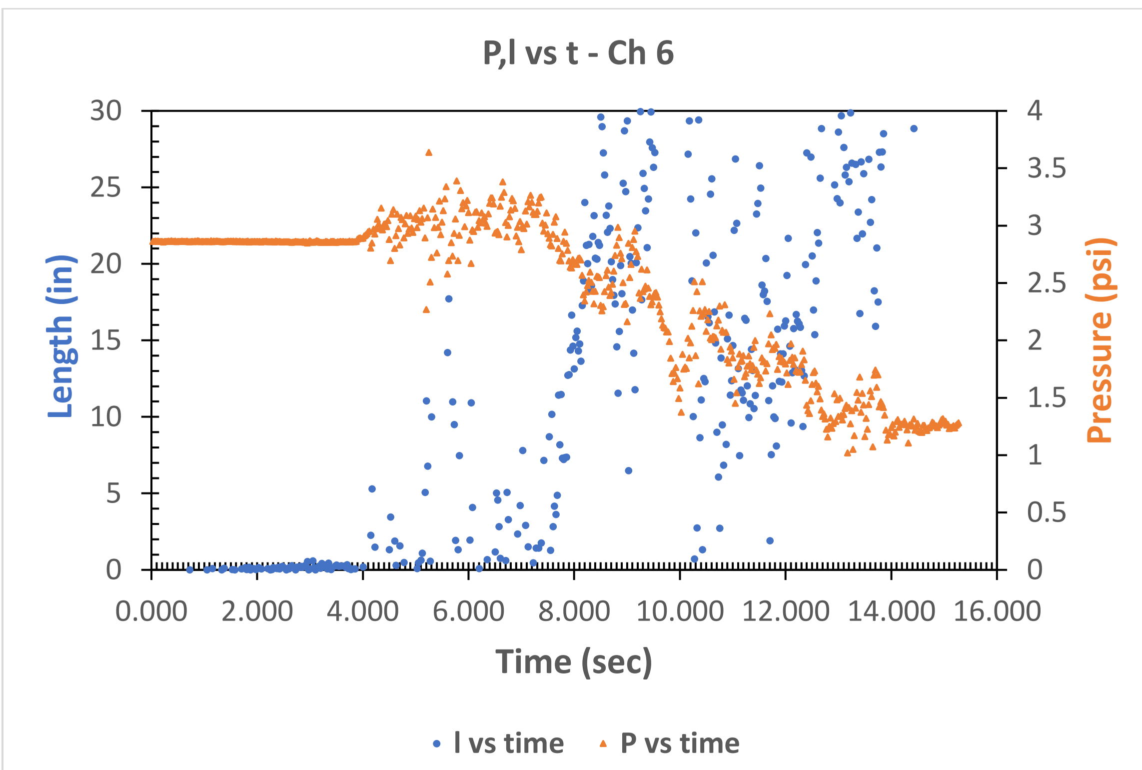

P,l vs t - Ch 6
30
25
20
15
10
5
0
Length (in)
4
3.5
3
2.5
2
1.5
1
0.5
0
Pressure (psi)
0.000
2.000
4.000
6.000
8.000
10.000
12.000
14.000
16.000
Time (sec)
l vs time
P vs time

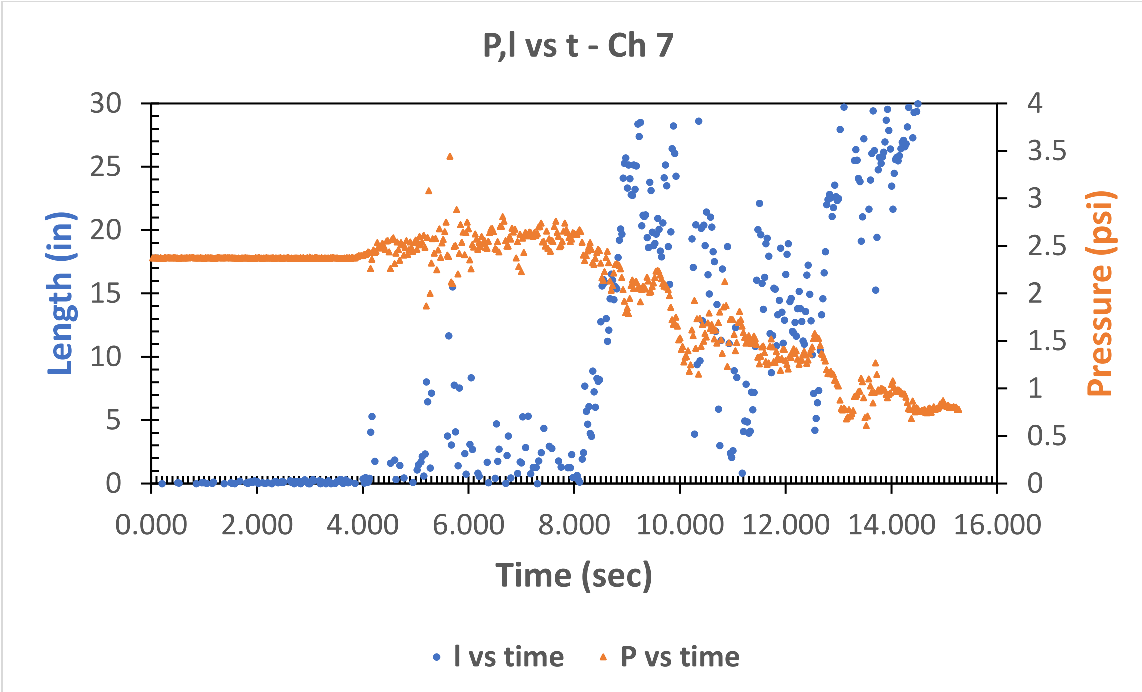
P,l vs t - Ch 7
Length (in)
Pressure (psi)
Time (sec)
0
5
10
15
20
25
30
0
0.5
1
1.5
2
2.5
3
3.5
4
0.000
2.000
4.000
6.000
8.000
10.000
12.000
14.000
16.000
l vs time
P vs time

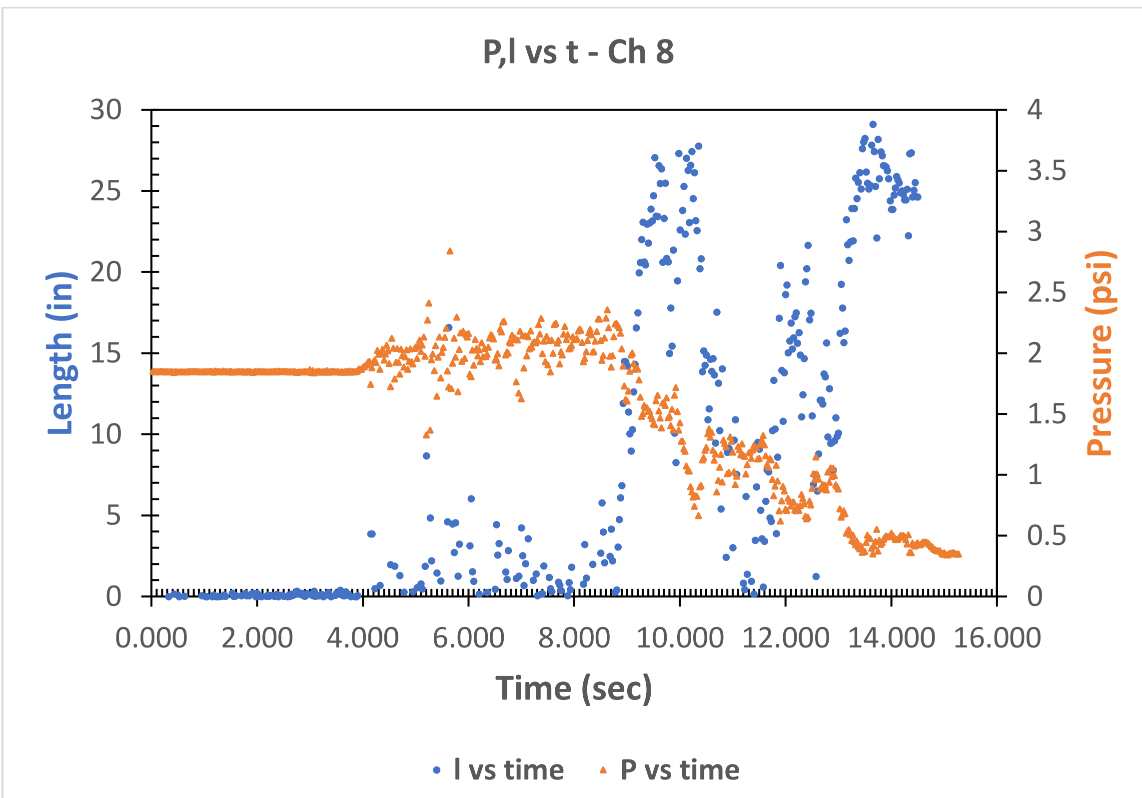
P,l vs t - Ch 8
Length (in)
Pressure (psi)
Time (sec)
0
5
10
15
20
25
30
0
0.5
1
1.5
2
2.5
3
3.5
4
0.000
2.000
4.000
6.000
8.000
10.000
12.000
14.000
16.000
l vs time
P vs time

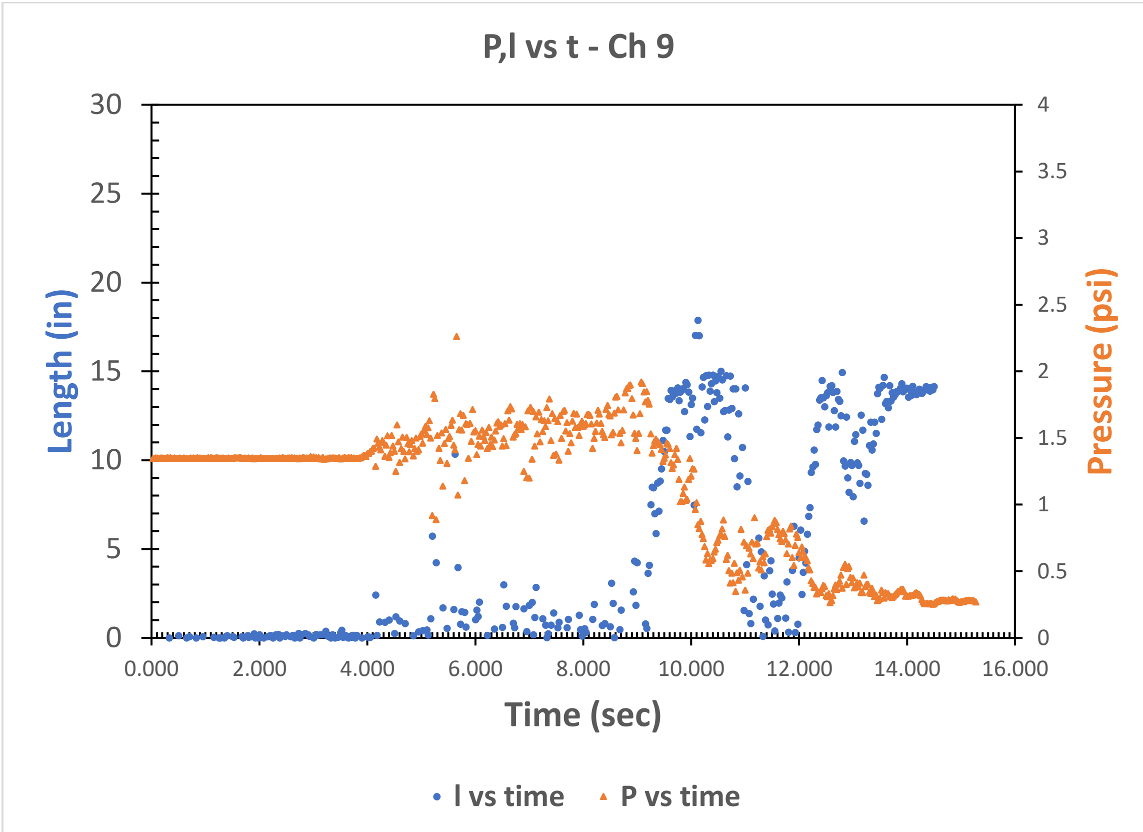

P,l vs t - Ch 9
Length (in)
Pressure (psi)
Time (sec)
l vs time
P vs time
0
5
10
15
20
25
30
0
0.5
1
1.5
2
2.5
3
3.5
4
0.000
2.000
4.000
6.000
8.000
10.000
12.000
14.000
16.000